THE UNIVERSITY OF QUEENSLAND

AUSTRALIA

The disulfide oxidative pathway in *Chlamydia trachomatis*

Signe Christensen

Master of Science, Bachelor of Science

A thesis submitted for the degree of Doctor of Philosophy at

The University of Queensland in 2018

Institute for Molecular Bioscience

Abstract

The disulfide oxidative pathway in bacteria is responsible for disulfide bond formation in secreted proteins including many virulence factors. The archetypal *Escherichia coli* DsbA and DsbB enzymes form a redox relay that catalyses disulfide bond formation and constitutes the oxidative folding pathway. DsbA orthologs from a broad range of bacteria have been characterised and while the enzymes have similar structural and biochemical characteristics they vary in redox chemistry and surface properties. An overview of the DsbA and DsbB enzymes from different bacteria is provided in Chapter 1. Chapter 1 also provides an overview of antibiotics with well-known and novel targets, including bacterial oxidative folding.

Chlamydia trachomatis is an obligate intracellular pathogen responsible for blinding trachoma and the sexually transmitted infection chlamydia that can lead to infertility and ectopic pregnancy. *C. trachomatis* has a biphasic developmental cycle that is dependent on coordinated disulfide bond formation and reduction for differentiation between the two distinct cell types: reticular body (RB) and elementary body (EB) (reviewed in chapter 1).

Chapter 2 presents a biochemical and structural characterisation of a truncated soluble form of DsbA from *C. trachomatis* (CtDsbA), which was published in *PLOS ONE*. CtDsbA is the first structurally characterised DsbA having two small, uncharged amino acids separating the two active site cysteines (Cys-Ser-Ala-Cys). Characterisation of CtDsbA shows that is has oxidase activity and is structurally similar to other DsbAs. However, CtDsbA is distinct in that it is the weakest oxidising DsbA so far described. This is consistent with the analysis of the 2.7 Å resolution crystal structure showing a lack of factors stabilising the nucleophilic thiolate anion of Cys38. CtDsbA is also distinguished from most other DsbAs by having a disulfide bond, linking helix 2 and helix 5, that has only been reported in three other structurally characterised DsbAs, including *Wolbachia pipientis* DsbA1 (WpDsbA1).

Chapter 3 describes my studies of the interaction between CtDsbA and CtDsbB. In the oxidative pathway of *E. coli,* DsbA (EcDsbA) is kept in its active, oxidised state by the integral membrane protein DsbB (EcDsbB) in a mechanism dependent on a quinone co-factor. A BLAST search identified a protein (CtDsbB) in the genome of *C. trachomatis* with 21% sequence identity to EcDsbB and a predicted secondary structure topology equivalent to EcDsbB. Chapter 3 presents the characterisation of the interaction between

CtDsbA and CtDsbB showing that crude membranes containing heterogeneously expressed CtDsbB are able to oxidize CtDsbA. However, purified, detergent solubilised CtDsbB is not able to oxidise CtDsbA in the presence of ubiquinone-1 suggesting that purified CtDsbB is inactive in detergent micelles or that ubiquinone-1 is not a suitable co-factor for CtDsbB. In contrast to what was found for *Wolbachia* DsbA1, the non-catalytic disulfide of CtDsbA does not regulate interaction with CtDsbB. Interestingly, mutating the cysteines forming the non-catalytic disulfide to serines has minimal effect on CtDsbA thermal stability, and only marginally decreases the difference in melting temperature between reduced and oxidised forms of the enzyme.

In Chapter 4, I report on my attempts to generate a *dsbA* loss-of-function mutant. As disulfide cross-linking of the outer membrane plays an important role in *C. trachomatis* development and infection, CtDsbA might play a specialised role to regulate the redox state of the cysteines that form cross-links in the outer membrane. This hypothesis is supported by the observation I made that CtDsbA expression correlates with RB to EB differentiation (Chapter 3). To pursue this further, I attempted to obtain a loss-of-function *dsbA* mutant by chemical mutagenesis with ethyl methanesulfonate (EMS). In a forward genetics approach, using sensitivity to dithiothreitol (DTT) as a phenotypic read out, approximately 2000 subpopulations of EMS treated *C. trachomatis* were screened. 14 subpopulations exhibited increased sensitivity towards DTT. Despite a hypothesis that a loss-of-function *dsbA* mutant would exhibit increased sensitivity to DTT, none of the 14 subpopulations had a mutation in the *dsbA* gene. In the reverse genetics approach approximately 14400 subpopulations were screened using Targeting Induced Local Lesions in Genomes (TILLING), but again no *dsbA* mutation was identified.

CtDsbA is the first DsbA to be characterised that has a catalytic dipeptide containing two small, uncharged amino acid residues. Characterisation revealed that CtDsbA is weakly oxidising with a mildly destabilising active site disulfide. Hence, characterisation of CtDsbA provides new insight into the diversity amongst DsbA proteins and supports the ongoing effort to develop inhibitors of DsbA enzymes. By comparison to *E. coli*, CtDsbB can form a redox-relay with CtDsbA. The forming of a functional redox relay was confirmed by the finding that crude membranes expressing CtDsbB facilitates CtDsbA activity. Despite screening more than 16000 subpopulations of EMS treated *C. trachomatis* LGV-2, no mutant was identified in the *dsbA* gene. Further experiments will be required to unpick the biological role of CtDsbA, and I discuss what these experiments could entail in Chapter 5.

Declaration by author

This thesis is composed of my original work, and contains no material previously published or written by another person except where due reference has been made in the text. I have clearly stated the contribution by others to jointly-authored works that I have included in my thesis.

I have clearly stated the contribution of others to my thesis as a whole, including statistical assistance, survey design, data analysis, significant technical procedures, professional editorial advice, financial support and any other original research work used or reported in my thesis. The content of my thesis is the result of work I have carried out since the commencement of my higher degree by research candidature and does not include a substantial part of work that has been submitted to qualify for the award of any other degree or diploma in any university or other tertiary institution. I have clearly stated which parts of my thesis, if any, have been submitted to qualify for another award.

I acknowledge that an electronic copy of my thesis must be lodged with the University Library and, subject to the policy and procedures of The University of Queensland, the thesis be made available for research and study in accordance with the Copyright Act 1968 unless a period of embargo has been approved by the Dean of the Graduate School.

I acknowledge that copyright of all material contained in my thesis resides with the copyright holder(s) of that material. Where appropriate I have obtained copyright permission from the copyright holder to reproduce material in this thesis and have sought permission from co-authors for any jointly authored works included in the thesis.

Publications during candidature

Structural and biochemical characterization of Chlamydia trachomatis DsbA reveals a cysteine-rich and weakly oxidising oxidoreductases Signe Christensen, Morten K. Grøftehauge, Karl Byriel, Wilhelmina M. Huston, Emily Furlong, Begoña Heras, Jennifer L. Martin and Róisín McMahon (2016). PLOS ONE 11(12): e0168485. doi:10.1371

Publications included in this thesis

Structural and biochemical characterization of Chlamydia trachomatis DsbA reveals a cysteine-rich and weakly oxidising oxidoreductases Signe Christensen, Morten K. Grøftehauge, Karl Byriel, Wilhelmina M. Huston, Emily Furlong, Begoña Heras, Jennifer L. Martin and Róisín McMahon (2016). PLOS ONE 11(12): e0168485. doi:10.1371

Contributor	Statement of contribution
Signe Christensen (Candidate)	Conception and design (22.5%) Analysis and interpretation (30%) Drafting and production (50%)
Morten Grøftehauge	Conception and design (22.5%) Analysis and interpretation (25%) Drafting and production (5%)
Karl Byriel	Conception and design (0%) Analysis and interpretation (5%) Drafting and production (0%)
Wilhelmina M. Huston	Conception and design (0%) Analysis and interpretation (5%) Drafting and production (10%)
Emily Furlong	Conception and design (0%) Analysis and interpretation (5%) Drafting and production (0%)
Begoña Heras	Conception and design (10%) Analysis and interpretation (5%) Drafting and production (0%)
Jennifer L. Martin	Conception and design (22.5%) Analysis and interpretation (10%) Drafting and production (10%)
Róisín M. McMahon	Conception and design (22.5%) Analysis and interpretation (15%) Drafting and production (25%)

Contributions by others to the thesis

Ms. Amba Lawrence - Generation of the Ethyl methanesulfonate (EMS) libraries of *C. trachomatis* LGV-2 and LGV-2*tmp.*

Statement of parts of the thesis submitted to qualify for the award of another degree

None.

Research Involving Human or Animal Subjects

No animal or human subjects were involved in this research.

Acknowledgements

I want to express my sincere appreciation to those who have contributed to this thesis and supported me in one way or the other.

First of all, I would like to thank Prof. Jenny Martin for giving me the opportunity to do my PhD under her leadership. It has been a truly exciting and rewarding adventure and I am grateful for her guidance and many valuable inputs to my thesis.

I am also grateful to Dr. Willa Huston for welcoming me in her group and opening my eyes to the world of microbiology. My stay in her laboratory brought a new and inspiring perspective to my thesis.

A special thanks to Dr. Róisín McMahon for her support throughout my PhD. Without her patient advice, continuously patient guidance and the many fruitful discussions my PhD would not have been the same.

I would also like to thank Dr. Amanda Carozzi and the rest of the Postgraduate team at IMB for excellent support from the very first contact with IMB and throughout my entire PhD.

Financial support

This research was supported by two NHRMC grants (GRT1061241 and GRT1099151), a Research Higher Degree Scholarship and UQI tuition fee award.

Keywords

Oxidative folding, Disulfide bond, DsbA, DsbB, anti-virulence, *Chlamydia trachomatis*

Australian and New Zealand Standard Research Classifications (ANZSRC)

ANZSRC code: 060199 Biochemistry and Cell Biology not elsewhere classified (55%)
ANZSRC code: 060112 Structural Biology (20%)
ANZSRC code: 060599 Microbiology not elsewhere classified (25%)

Fields of Research (FoR) Classification

FoR code: 0601, Biochemistry and Cell Biology, 75%
FoR code: 0605, Microbiology 25%

Table of contents

Table of figures

Chapter 1

Chapter 2

Chapter 3

Chapter 4

Table of tables

Chapter 1

Chapter 2

Chapter 3

Chapter 4

Abbreviations

3’CMP	3’-cytidinemonophospate
AbDsbA	*Acinetobacter baumannii* DsbA
AMP	Antimicrobial peptide
AMS	4-acetamido-4’-maleimidylstilbene-2,2’-disulfonic acid
B1-5	β-strand 1 to 5 in DsbA
BpsDsbA	*Burkholderia pseudomallei* DsbA
BpsDsbB	*Burkholderia pseudomallei* DsbB
BSA	Bovine serum albumin
BsDsbA	*Bacillus subtilis* DsbA
cCMP	cyclic-2’,3’-cytidinemonophosphate
CD	Circular Dichroism
COMC	Chlamydial outer membrane complex
CRISPRi	Clustered Regularly Interspaced Short Palindromic Repeats interference
CtDsbA	*Chlamydia trachomatis* DsbA
CtDsbB	*Chlamydia trachomatis* DsbB
CV	Column volumes
DAPI	4',6-diamidino-2-phenylindole
DDM	n-Dodecyl-beta-Maltoside
DHFA	Dihydrofolic acid
DMEM	Dulbecco Modified Eagle Media
DNA	Deoxyribonucleic acid
DOTA	tetraazacyclododecane-1,4,7,10-tetraaceticacid
DSB	Disulfide bond proteins
DsbA	Disulfide bonded protein A
DsbB	Disulfide bonded protein B
DsbG	Disulfide bonded protein G
DsbH	Disulfide bonded protein H
DsbI	Disulfide bonded protein I
DsbJ	Disulfide bonded protein J
DsbL	Disulfide bonded protein L
DTT	Dithiothreitol
E°	Redox potential

EB	Elementary body
ECL	Enhanced chemiluminescence
EcDsbA	*Escherichia coli* DsbA
EcDsbB	*Escherichia coli* DsbB
EcDsbC	*Escherichia coli* DsbC
EDTA	Ethylenediaminetetraacetic acid
EFTu	Elongation factor thermo unstable
EMS	Ethyl methanesulfonate
FCS	Fetal calf serum
FITC	Fluorescein isothiocyanate
FOV	Field of view
FRET	Fluorescent resonance energy transfer
FtDsbA	*Francisella tularensis* DsbA
GSSG	Glutathione (oxidised)
H1-8	α-helix 1 to 8 in DsbA
HRM	High Resolution Melting
IFN-ϒ	Gamma interferon
IFU	Inclusion forming unit
IMAC	Immobilised-metal affinity chromatography
L1-3	Loop 1 to 3 in DsbA
KpDsbA	*Klebsiella pneumoniae* DsbA
KpDsbB	*Klebsiella pneumoniae* DsbA
MES	2-(N-morpholino) ethanesulfonic acid
MK	Menaquinone
MOI	Multiplicity of infection
MOMP	Major outer membrane protein
MOPS	3-(N-morpholino) propanesulfonic acid
MtbDsbA	*Mycobacterium tuberculosis* DsbA
NmDsbA1-3	*Neisseria meningitidis* DsbA 1 to 3
NmDsbB	*Neisseria meningitidis* DsbB
NMR	Nuclear magnetic resonance
Ox	Oxidised
P1-2	Periplasmic region 1 and 2 in DsbB
PABA	*para*-aminobenzoic acid
PaDsbA1-2	*Pseudomonas aeruginosa* DsbA 1 and 2

PaDsbB1-2	*Pseudomonas aeruginosa* DsbB 1 and 2
PBS	Phosphate buffered saline
PDI	Protein disulfide isomerase
PmDsbA	*Proteus mirabilis* DsbA
PmDsbB	*Proteus mirabilis* DsbB
Pmp	Polymorphic membrane protein
PCR	Polymerase chain reaction
Q	Quinone
RB	Reticulate body
Red	Reduced
RFU	Relative fluorescence unit
RMSD	Root mean square deviation
RNA	Ribonucleic acid
SaDsbA	*Staphylococcus aureus* DsbA
ScRNase	Scrambled RNase
ScsB	Suppression of Copper Sensitivity protein B
SD	Standard deviation
SDS	Sodium dodecyl sulfate
SDS-PAGE	sodium dodecyl sulfate polyacrylamide gel electrophoresis
SeDsbA	*Salmonella enterica* Typhimurium DsbA
SeDsbB	*Salmonella enterica* Typhimurium DsbB
SPG	Sucrose-phosphate-glutamic acid
STI	Sexually transmitted infection
T3SS	Type III secretion system
TCA	Trichloroacetic acid
TCEP	Tris-(2-carboxyethyl)fosfin
THF	Tetrahydrofolate
TILLING	Targeting Induced Local Lesions IN Genomes
TM1-4	Transmembrane helix 1 to 4 in DsbB
T_m	Melting temperature
TP	Threonine-*cis*Proline
UQROCX	The University of Queensland Remote Operated Crystallisation X-ray Facility
UQ-x	Ubiquinone with x isoprenoid chain length
qPCR	Quantitative reverse transcription polymerase chain reaction

VcDsbA	*Vibrio cholerae* DsbA
VcDsbB	*Vibrio cholerae* DsbB
VKOR	Vitamin K epoxide reductase
VP	Valine-*cis*Proline
WpDsbA1	*Wolbachia pipientis* DsbA1
WpDsbB	*Wolbachia pipientis* DsbB
Wt	Wild type
XfDsbA	*Xylella fastidiosa* DsbA
XfDsbB	*Xylella fastidiosa* DsbB

Chapter 1: Introduction

1.1 Overview of introduction

The focus of this thesis is the oxidative folding pathway in the obligate, intracellular pathogen *Chlamydia trachomatis.* Characterisation of this pathway will broaden our knowledge of the diversity of the bacterial oxidative folding machinery, and of its application as a target for drug discovery. The recent rise in antibiotic resistance combined with a drying up of the antibiotic pipeline has led to a push to develop new antibiotics with novel methods of action. The proteins in the bacterial disulfide oxidative pathway are potential targets for a new class of antimicrobial drugs.

This introductory chapter gives a brief overview to the history of antibiotic discovery and resistance development, followed by a summary of potential strategies for new antibiotic discovery. This chapter also reviews what is known about the bacterial disulfide oxidative pathway, including a comparison of the DsbA-DsbB redox pair across different bacteria. In the final section, I review the treatment options and treatment failures of *C. trachomatis* infections, outline the unusual biphasic, disulfide dependent, developmental cycle of *C. trachomatis,* and summarise the aims and structure of the thesis.

1.1 The rise and fall of the golden age of antibiotics

In 1929 Sir Alexander Fleming discovered that the fungus *Penicillium notatum* inhibits the growth of the Gram-positive bacterium *Staphylococcus aureus* [1]. More than a decade later, the antibiotic penicillin was first prescribed to treat serious infections. Between 1935 and 1970, several classes of antibiotic drugs were marketed, including sulfonamides, β-lactams, tetracyclines, rifamycins and quinolones (Figure 1.1). The discovery of antibiotics is one of the greatest discoveries in modern medicine and has resulted in successful treatment of many diseases that were once lethal. One example is subcutaneous sulphanilamide, which decreased the mortality rate of meningococcal meningitis from 70-90 % to approximately 10 % [2]. However, even in the 1940s, less than a decade after introduction of the first sulfonamides, clinical resistance was observed (Figure 1.1). In fact, bacteria have developed resistance to all classes of clinical antibiotics, and infections by resistant bacteria were responsible for an estimated 8.6 million deaths globally in 2015 [3].

The classic antibiotics target a limited range of vital bacterial processes and pathways to kill or severely inhibit bacterial growth. Processes targeted by antibiotics include cell wall synthesis, protein synthesis, DNA synthesis, RNA synthesis and metabolism (Figure 1.2) (reviewed in [4]).

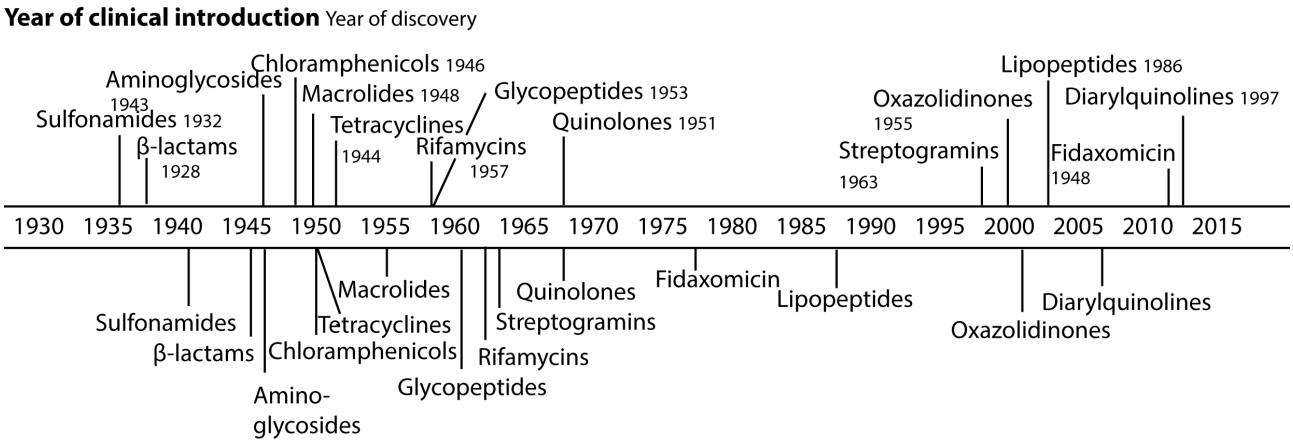

Figure 1.1 Timeline of antibiotic discovery and emergence of resistance.

For each class of antibiotic, clinical resistance (lower timeline) has been observed within 10 years of introduction of clinical use (upper timeline). Year of discovery is stated next to antibiotic class. Modified from [5].

The β-lactams are an example of a class of antibiotics targeting the cell membrane. The β-lactams target enzymes involved in synthesis of the bacterial cell wall thereby inhibiting growth [6].

Daptomycin is a cyclic lipoprotein targeting the cell membrane in most Gram-positive bacteria. Insertion of daptomycin into the bacterial cell membrane causes rapid membrane depolarisation and consequent efflux of potassium [7].

Several antibiotics, including rifampicin, inhibit RNA synthesis. Rifampicin binds at the β-subunit of the bacterial RNA polymerase thereby blocking the path of the elongating RNA when the transcript becomes two to three nucleotides long [8]. *para*-aminobenzoic acid (PABA) is required for formation of dihydrofolic acid (DHFA) production in bacteria; DHFA is a precursor of folic acid. Sulfonamides are structural analogues of PABA and consequently act as competitive antagonists of PABA thereby blocking synthesis of folic acid [9].

Tetracyclines inhibit protein synthesis by binding to the 30S ribosomal subunit in the mRNA translation complex thereby inhibiting the binding of aminoacyl-tRNA to the mRNA-ribosome complex [10, 11].

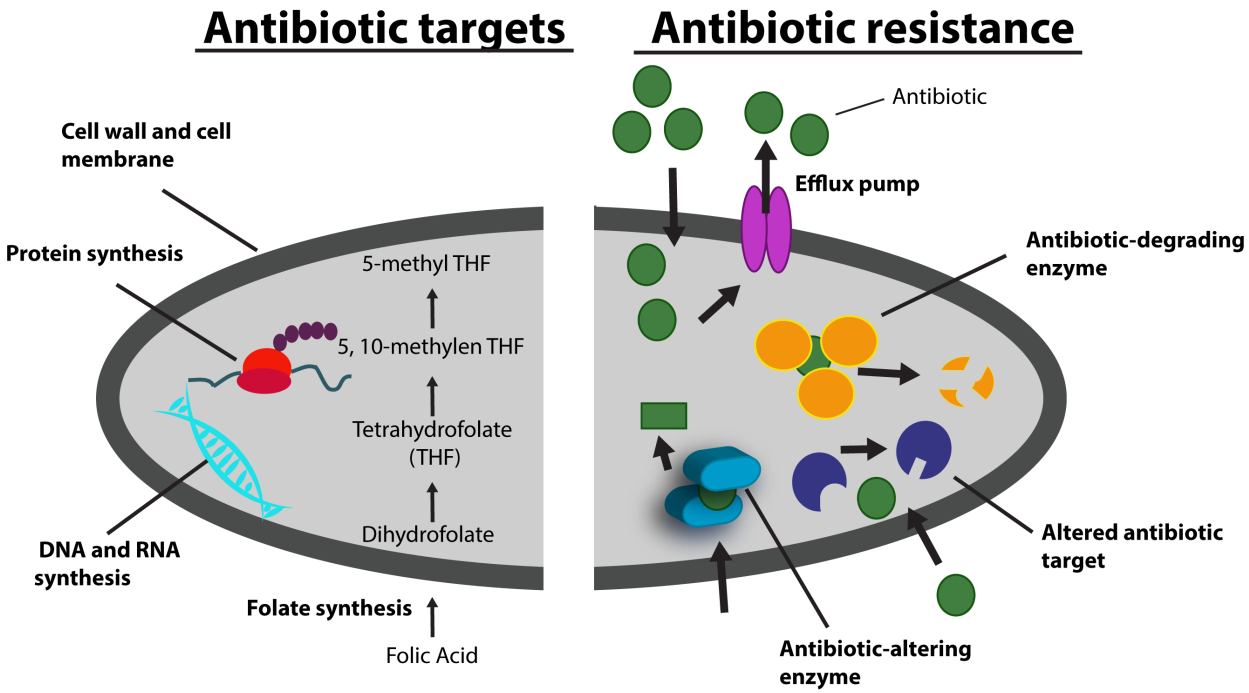

Figure 1.2 Bacterial targets for antibiotics and mechanism of resistance.

Traditional antibiotics target the cell wall and cell membrane, protein synthesis, metabolism (e.g. folate synthesis) and DNA and RNA synthesis (left). Bacteria utilise a range of mechanisms (right) to respond to antibiotics (green). This includes altering the antibiotic target (dark blue), efflux pumps (pink), antibiotic-altering enzymes (light blue) and antibiotic degrading enzymes (orange).

Targeting bacterial growth and viability induces a high degree of selective pressure for the development of antibiotic resistance. Consequently, bacteria have developed different mechanisms to deal with the threat of the antibiotics e.g. by pumping the antibiotic out of the cell or degrading the antibiotic (Figure 1.2). Other strategies involve altering the antibiotic target or enzymatic alteration of the antibiotic itself such that it is no longer effective (reviewed in [12]).

The bacterium *Klebsiella pneumoniae* has developed resistance to β-lactams by several mechanisms including production of β-lactamase that degrades β-lactams, altering the entry channel porins and increased expression of an efflux pump [13].

In addition to resistance to tetracyclines acquired by expression of efflux pumps, bacteria have also developed mechanisms to alter these antibiotics; acetylation of tetracyclines leads to inactivation of the antibiotic and is an example of antibiotic alteration [14, 15].

A major mechanism for resistance development to rifampicin is through mutations in the β-subunit of the bacterial RNA polymerase to prevent binding of the drug [16-18].

1.1.1 New strategies for developing antimicrobial drugs

Much effort has been directed towards identification of new classes of antibiotics as well as development of analogues of existing antibiotics. However, only six new classes of antibiotics have been marketed since the 1960s [19] (Figure 1.1). According to the Pew Trust [20] 39 antibiotics are in Phase I–III clinical trials as of March 2017, but the antibiotic pipeline is currently not efficient in getting new antibiotic drugs to the market. Historically only 33 % of antibiotics that reach clinical trials are marketed [21]. Further, most of the new antibiotics are not novel with respect to target or mechanism of action. Consequently, discovery of new antibiotics, especially antibiotics or antibacterials with novel mechanisms of action, are urgently needed. Several strategies are being taken including antimicrobial peptides, bacteriophages, therapeutic antibodies, potentiators of existing antibiotics and anti-virulence agents. These are discussed in turn below.

Antimicrobial peptides (AMPs) are oligopeptides consisting of five to more than a hundred amino acids, and are a part of the innate immune system of all classes of life. AMPs are inserted into the bacterial membrane causing displacement of lipids and alteration of membrane structure [22]. Due to their targeting of the bacterial membrane, AMPs are potentially active against a broad range of bacteria. In fact, they have been demonstrated to kill Gram-negative and Gram-positive bacteria as well as viruses and fungi [23]. Resistance to AMPs has developed through alteration of bacterial membrane composition, or lipid organisation, or destruction of the AMPs [24]. However, most AMPs lack recognition sites for proteases and membrane reorganisation is an energetically expensive solution for the bacteria [25]. Accordingly, AMPs are predicted to have a low risk of resistance development [25]. However, they can be toxic to eukaryotic cells [25, 26].

Bacteriophages are viruses with antibiotic activity due to their ability to lyse and kill bacteria [27]. Bacteriophages are highly host-specific and treatment with bacteriophages consequently decreases the risk of destroying commensal microbiota. However, bacteria can develop resistance against bacteriophages by digestion of the phage DNA, or by arresting bacteriophage infection by abortive infection, which promotes cell death and thus limits phage replication within the bacterial population before it produces virions [28].

Two types of **therapeutic antibodies** have activity against bacteria; one type binds the pathogen directly thereby making it susceptible to phagocytosis [29]. The other type neutralises toxins or other virulence factors produced by the bacteria [30]. As some therapeutic antibodies are already approved for clinical use in cancer treatment, many safety and pharmacokinetic concerns have already been addressed, which make them interesting for antibiotic development purposes. However, they are not

very cost-effective, and efficient diagnostic tools are yet to be developed to make the use of therapeutic antibodies feasible [26].

Potentiators of existing antibiotics reverse the resistance mechanism of the bacteria, or sensitise naturally resistant strains, allowing the antibiotic to work. A successful example is β-lactamase inhibitors that block the ability of bacterial enzymes to degrade β-lactam antibiotics [31]. Unfortunately resistance to these potentiators has also been reported [32].

1.1.2 Targeting virulence rather than viability as a strategy for drug development

Targeting virulence rather than bacterial growth or viability is a promising strategy for the development of new antimicrobial drugs with novel mechanisms of action [33-36]. Since the effect on viability of the pathogen may be minimised, anti-virulent antimicrobial drugs are hypothesised to limit resistance selection compared with traditional antibiotics, though this is yet to be confirmed [34]. High specificity for particular species potentially delays the occurrence of resistance in bacteria that are not dependent on the specific virulence factor targeted [34]. Further, high host-specificity limits the effect on the commensal microbiota, decreasing the risk of secondary infections and colonisation by drug-resistant bacteria [37]. Toxins [38], quorum sensing [37], biofilm production, secretion systems [39] and host cell adhesion [40] have all been explored as targets for anti-virulence drugs.

Another molecular target for anti-virulence therapy is oxidative protein folding. This step in protein folding is crucial for the assembly of a diverse range of bacterial virulence factors [41]. Consequently, targeting the disulfide bond machinery is a promising strategy for the development of an anti-virulence antimicrobial drug. Many virulence factors, including constituents of the type III and type IV secretion systems [42-47], flagella assembly [48] and several toxins [49-52], are dependent on the formation of disulfide bonds. Thus, inhibiting bacterial disulfide bond formation disrupts a broad range of virulence pathways, and leads to reduction or attenuation of virulence in many pathogens, including *Escherichia coli* [48], *Salmonella enterica* Typhimurium [46, 53], *Campylobacter jejuni* [54], *Yersinia pestis* [47], *Pseudomonas aeruginosa* [55, 56], *Vibrio cholerae* [50] and *Burkholderia pseudomallei* [57]. Due to the severe effect on virulence upon disruption of disulfide bond formation in many bacteria, the proteins involved in the oxidative pathway are of interest as targets for development of anti-virulent anti-microbial agents.

1.2 The disulfide oxidative pathway in bacteria

E. coli DsbA (EcDsbA) is the primary oxidase in the disulfide oxidative pathway of *E. coli* [58] and catalyses the introduction of disulfide bonds into folding proteins (Figure 1.3). By accepting electrons from the substrate protein, the active site cysteines of DsbA become reduced. In order to return to the active, oxidised state, DsbA is reoxidised in a reaction catalysed by the membrane protein partner DsbB - using quinones as electron acceptors - and ultimately delivering electrons to molecular oxygen via the respiratory pathway [59].

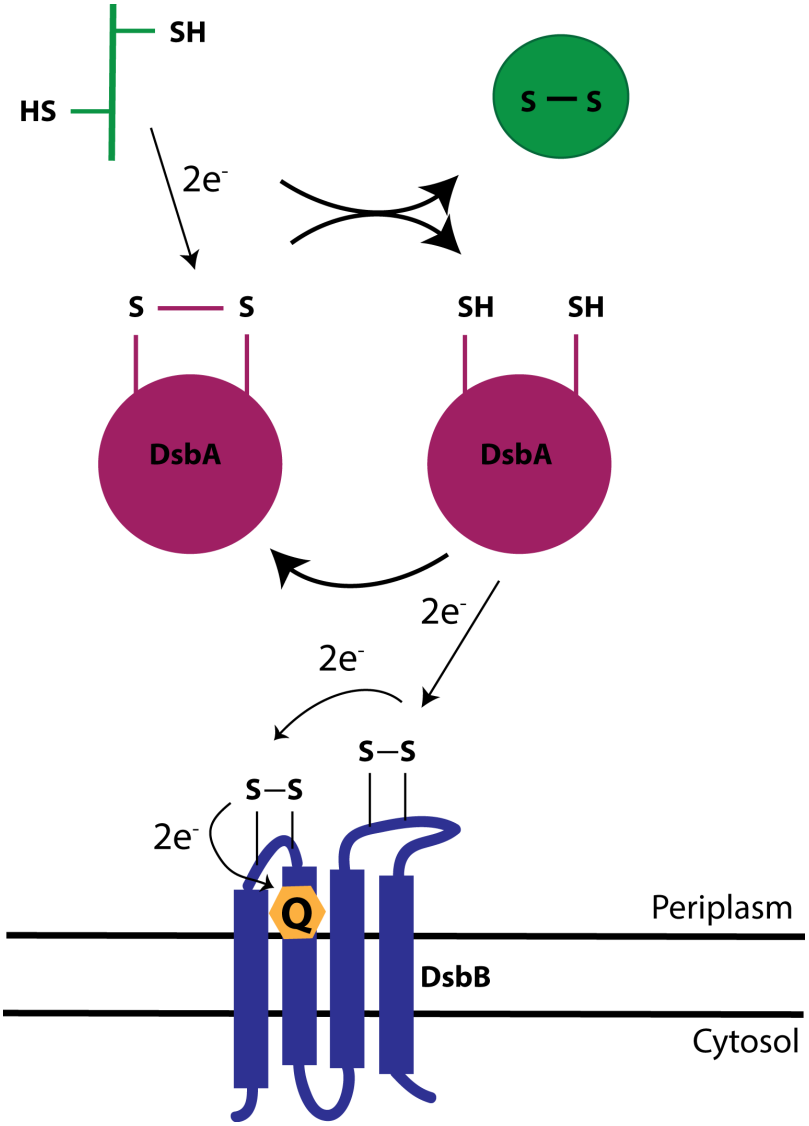

***Figure 1.3 Introduction of disulfide bonds in* E. coli.**

DsbA (pink) is a periplasmic protein that introduces disulfide bonds (S-S) into folding proteins (green) that have more than one cysteine. In turn, the active site disulfide bond of DsbA is reduced (SH). DsbA is regenerated to its active oxidised state by the membrane protein DsbB (blue) that donates electrons to quinone (Q) and ultimately to the electron transport chain [60].

1.2.1 Structure and function of the primary oxidase DsbA in *E. coli*

EcDsbA was the first DsbA enzyme to be structurally and functionally characterised and serves as the canonical model for DsbA enzymes [58, 61, 62]. The structure of EcDsbA consists of a thioredoxin domain (a five stranded β-sheet (B1-5) sandwiched between three α-helices (H1, H6 and H7)) and an inserted α-helical bundle domain (H2 to H5 and the N-terminal end of helix H6) [62, 63] (Figure 1.4A). The thioredoxin domain contains the active site with a Cys-Pro-His-Cys (CPHC) motif located at the N-terminal region of helix H1. A short sequence of three residues (Glu38-Val39-Leu40) is responsible for a kink in helix H1. Loop L1 links helix H1 and β-strand B3. Loop 2 links helix H6 and β-strand B4 and contains a *cis*Pro residue highly conserved in the thioredoxin fold [52]. The residue preceding the *cis*Pro residue in EcDsbA is a valine. A long loop (L3) connects helix H7 and B5. Hydrophobic residues from loop L3 and strand B1 form the base of a large hydrophobic groove on the catalytic surface of EcDsbA, and hydrophobic residues from loop L2 and helix H1 contribute to the roof of this groove. The hydrophobic groove and a hydrophobic patch on the catalytic surface of EcDsbA create a hydrophobic environment surrounding the surface exposed cysteine (Cys30) and allows for binding of unfolded protein substrates and the redox partner DsbB (Figure 1.4B) [47, 48, 62, 64-67].

The surface exposed Cys30 at the active site of EcDsbA has an unusually low pK_a value of 4.5 and is consequently present as a thiolate anion at physiological pH [68]. Several factors contribute to stabilising the thiolate anion including electrostatic stabilisation by His31 of the catalytic motif and the *cis*Pro in loop L2 that is in close proximity to the catalytic motif [68]. A major factor contributing to stabilisation of the thiolate anion in dithiol oxidoreductases is the helix dipole of helix H1 [69]. Due to stabilisation of the thiolate anion the reduced state is more stable than the oxidised state of the enzyme, evidenced by a melting temperature (T_m) of 350 K for the reduced state compared to 342 K for the oxidised state [70]. This destabilisation of the oxidised state provides a driving force for the highly oxidising redox potential of EcDsbA (-122 mV) [71].

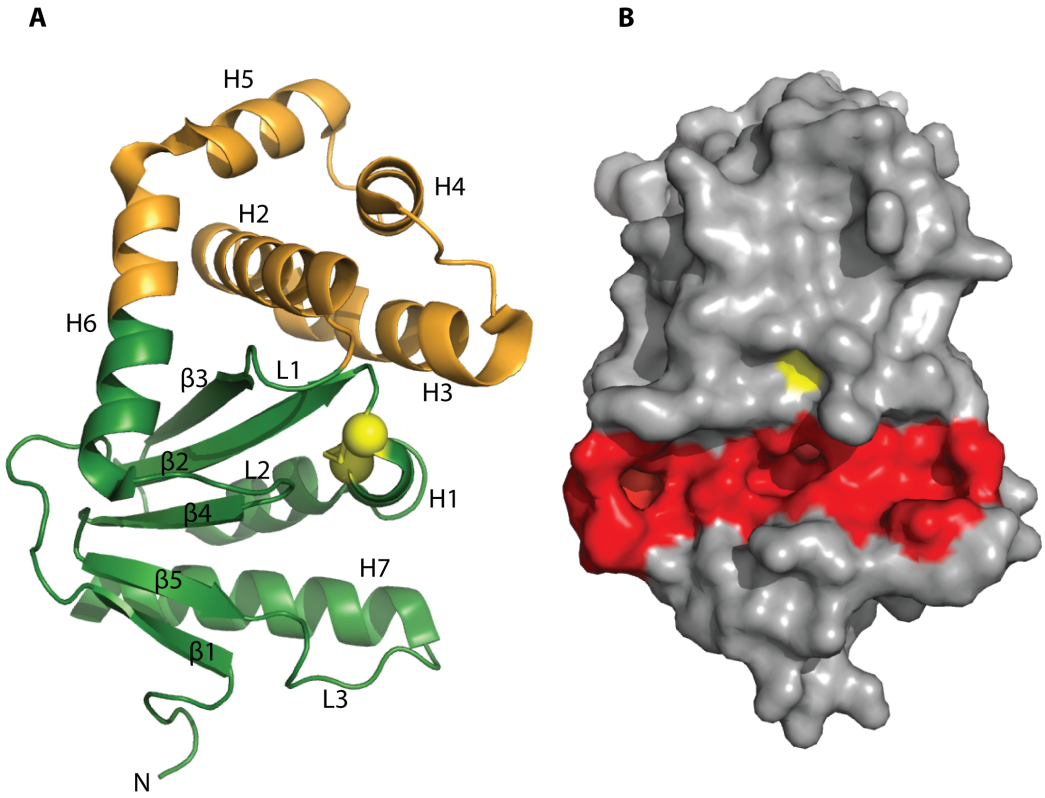

Figure 1.4 The structure of* E. coli *DsbA.

A) *EcDsbA (PDB code 1FVK) contains a thioredoxin domain (green) with a five stranded β-sheet (B1-5) sandwiched between three α-helices (H1, H6 and H7). The catalytic CPHC motif (cysteine sulfurs shown as yellow spheres) is located at the N-terminal region of the H1 helix. Helices H2 to H5 and the N-terminus of helix H6 make up the inserted helical domain (orange).* ***B)*** *Surface representation of EcDsbA (PDB code 1FVK) shows a large hydrophobic groove (red) close to the active site cysteines (yellow). Surface groove was identified by CastP [72] and images were generated in pymol [73].*

1.2.2 DsbA enzymes from different organisms have a broad spectrum of redox properties and surface features

Despite low sequence identity (generally 15 %-40 %) all DsbA orthologs that have been structurally characterised adopt a fold containing similar structural features to that of EcDsbA: a thioredoxin domain, a catalytic disulfide and an inserted helical domain [41, 57, 65, 74-81]. Structural variations to this core fold are responsible for differences in redox properties among the DsbA enzymes.

1.2.2.1 DsbA enzymes in Gram-negative bacteria

S. enterica Typhimurium DsbA (SeDsbA) [81], *K. pneumoniae* DsbA (KpDsbA) [74] and *Proteus mirabilis* DsbA (PmDsbA) [82], share 86 %, 81 % and 59 %, sequence identity with EcDsbA, respectively (Table 1.1). Both the catalytic CPHC motif and the Val-*cis*Pro (VP) motif are conserved in all three enzymes, and their structures and functional properties resemble closely those of EcDsbA. The pK_a value of the surface exposed cysteine is 4.2, 4.4 and 4.0 for SeDsbA, KpDsbA and PmDsbA, respectively. Also, the oxidising power is equivalent to EcDsbA with redox potentials between -129 mV and -116 mV. Like EcDsbA, the reduced state of each enzyme is more stable than the oxidised state: the difference in melting temperature is 9K, 12K and 10K for SeDsbA, KpDsbA and PmDsbA, respectively and is thereby in the same range as the 8 K difference in melting temperature seen in EcDsbA (Table 1.1).

Table 1.1 Comparison of structural and functional properties of DsbA orthologs

	Identity	CXXC	*Cis*-Pro	Second disulfide	T_m(K) Red	T_m(K) Ox	ΔT_m	pK_a	E° (mv)	Ref
EcDsbA	100 %	CPHC	VP		350	342	8	4.5	-122	[70] [72-73]
SeDsbA	86 %	CPHC	VP		351	342	9	4.2	-126	[81]
KpDsbA	81 %	CPHC	VP		347	335	12	4.0	-116	[74]
PmDsbA	59 %	CPHC	VP		348	338	10	4.0	-129	[82]
VcDsbA	40 %	CPHC	VP		357	346	11	5.1	-116	[76]
AbDsbA	32 %	CPHC	VP		-	-	-	-	-101	[83]
PaDsbA1	31 %	CPHC	VP		356	346	10	-	-94	[41]
BpsDsbA	26 %	CPHC	VP		-	-	-	2.8	-94	[57]
XfDsbA2	25 %	CPAC	TP		-	-	-	-	-100	[65]
NmDsbA2	25 %	CPHC	TP		343	326	17	3.3	-79	[77]
NmDsbA1	21 %	CPHC	TP		348	333	15	3.0	-79	[77]
NmDsbA3	21%	CVHC	TP		335	320	15	3.0	-81	[77]
PaDsbA2	21 %	CPFC	TP	X	-	-	-	-	-68	[75]
XfDsbA	19 %	CPHC	TP		-	-	-	-	-94	[65]
BsDsbA	18 %	CPSC	TP		-	-	-	-	-80	[79]
MtbDsbA	17 %	CPAC	TP	X	352	339	13	4.2	-99	[78]
SaDsbA	14 %	CPYC	TP		345	346	1	3.4	-131	[84]
WpDsbA1	10 %	CYHC	TP	X	337	331	6	4.7	-163	[80]
FtDsbA A	10 %	CMYC	TP		-	-	-	-	-132	[29]
FtDsbA B	10 %	CMYC	AP		-	-	-	-	-159	[29]

Properties are listed for DsbA from E. coli *(EcDsbA, PDB code 1FVK),* S. enterica *Typhimurium (SeDsbA, PDB code 3L9S),* K. pneumoniae *(KpDsbA, PDB code 4MCU),* P. mirabilis *(PmDsbA PDB code 4OCE),* V. cholerae *(VcDsbA, PDB code 4DVC),* A. baumannii *(AbDsbA, PDB code 4P3Y),* B. pseudomallei *(BpsDsbA, PDB code 4K2D),* P. aeruginosa *(PaDsbA1, PDB code 3H93 and PaDsbA2, PDB code 4N30),* X. fastidiosa *(XfDsbA, PDB code 2REM and XfDSbA2),* N. meningitidis *(NmDsbA1, PDB code 3DVW, NmDsbA2 and NmDsbA3, PDB code 3DVX),* M. tuberculosis *(MtbDsbA, PDB code 4K6X),* S. aureus *(SaDsbA, PDB code 3BCI),* B. subtilis *(BsDsbA, PDB code 3EU3),* W. pipientis *(WpDsbA1, PDB code 3F4R) and* Francisella tularensis *(FtDsbA A and FtDsbA B). Sequence identity to EcDsbA is calculated based on mature processed proteins. "-" not measured.*

V. cholerae DsbA (VcDsbA, also known as TcpG) shares 40 % sequence identity with EcDsbA, and also conserves the same catalytic motif (CPHC) and VP *cis*Pro motif [76]. However, the structure varies slightly from that of EcDsbA, SeDsbA, PmDsbA and KpDsbA. Specifically, the three-residue sequence in H1 is replaced by a proline residue, which results in helix H1 being less bent than in EcDsbA. Helix H7, which forms part of the hydrophobic groove in EcDsbA, is six residues shorter in VcDsbA than in EcDsbA resulting in a truncation of the hydrophobic groove [76] (Figure 1.5). Despite a higher pK_a of the solvent exposed cysteine (5.1), the difference in melting temperature (11 K) and the redox potential (-116 mV) are similar to those reported for EcDsbA (Table 1.1).

One of two DsbAs encoded in *P. aeruginosa* (PaDsbA1 (31 % sequence identity to EcDsbA)), as well as *B. pseudomallei* DsbA (BpsDsbA (26 % sequence identity to EcDsbA)) and *Xylella fastidiosa* DsbA (XfDsbA (19 % sequence identity with EcDsbA)) are less closely related to EcDsbA. The catalytic CPHC motif is conserved in all three of these DsbAs and the VP *cis*Pro motif is conserved in PaDsbA1 and BpsDsbA (Table 1.1). However, the residue preceding the *cis*Pro in XfDsbA is threonine rather than valine (TP motif) (Table 1.1). Like VcDsbA, PaDsbA1 [41], BpsDsbA [57] and XfDsbA [65] have a less pronounced bend in helix H1 than EcDsbA. Helix H7 is four residues longer in XfDsbA than in EcDsbA but the loop connecting strand B5 and helix H7 are six residues shorter resulting in a truncated hydrophobic groove. A similar pocket is seen in BpsDsbA and XfDsbA (Figure 1.5). Despite the structural similarities with VcDsbA, PaDsbA1, BpsDsbA and XfDsbA all have redox potentials of -94 mV and are therefore more oxidising than both EcDsbA and VcDsbA (Table 1.1). The pK_a of the solvent exposed cysteine has not been determined for PaDsbA1 or XfDsbA, but for BpsDsbA the thiolate anion is highly acidic with a pK_a of 2.8 [57]. The thermal stability of the different redox forms has not been determined for BpsDsbA and XfDsbA, but for PaDsbA1 the melting temperature of the reduced state is 10 K higher than for the oxidised state. *X. fastidiosa* encodes a second DsbA, XfDsbA2, with 41 % sequence identity to XfDsbA and 25 % sequence identity to EcDsbA. XfDsbA2 has not been structurally characterised, but its redox potential has been determined to -100 mV [65].

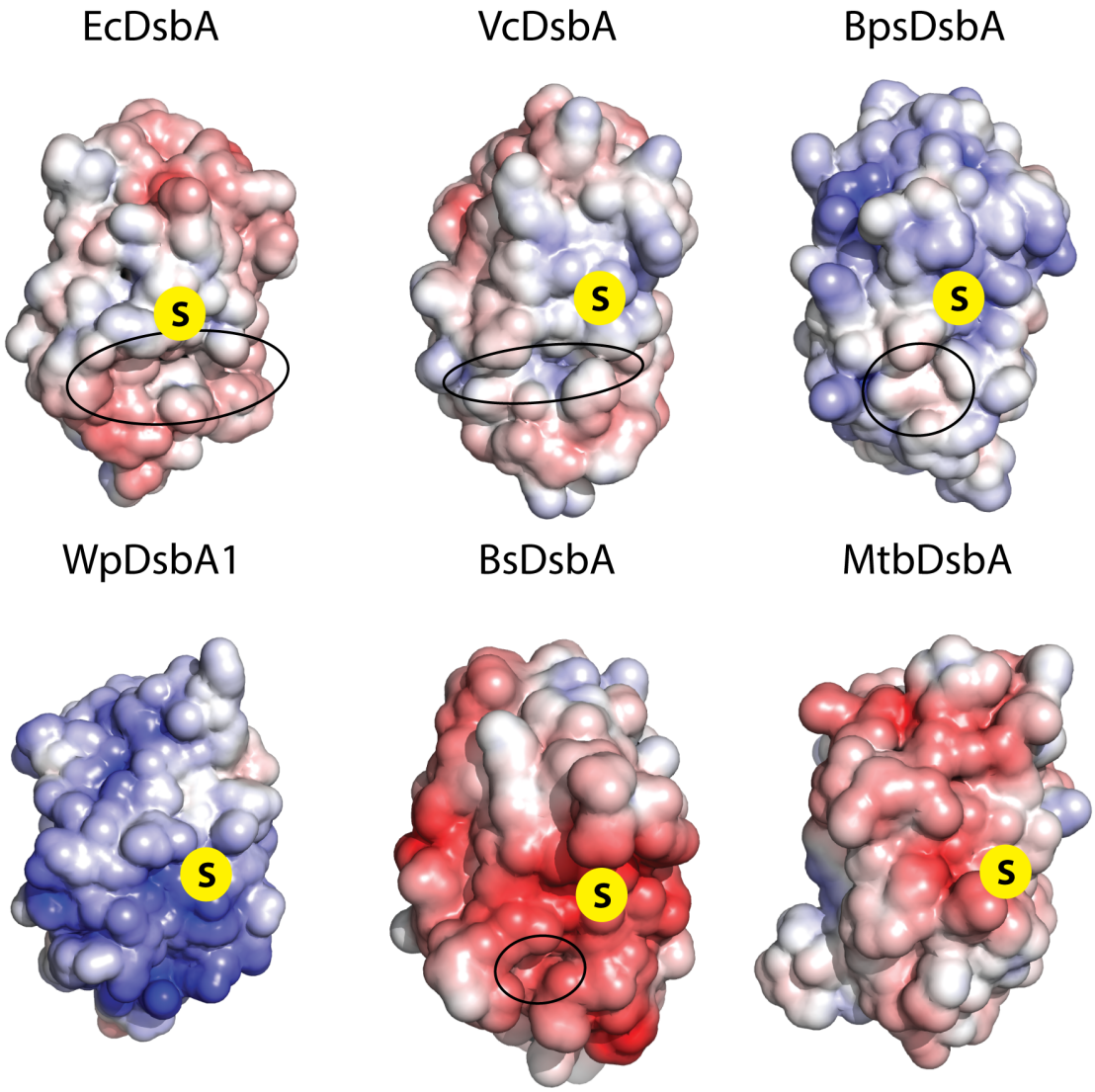

Figure 1.5 DsbA Surface properties.

Surface view of EcDsbA (PDB code 1fvk), VcDsbA (PDB code 4DVC), BpsDsbA (PDB code 4K2D), WpDsbA1 (PDB code 3F4R), BsDsbA (PDB code 3EU3) and MtbDsbA (PDB code 4K6X) showing the electrostatic surface potential and groove or pocket (black ring) close to the active site disulfide (yellow S). Electrostatic surface potential is plotted between -7.5 (red) and +7.5 (blue) and was calculated in ABPS [85] using the PARSE force field. Calculations are based on an ionic strength of 150 mM, with protein and solvent dielectric constants of 2 and 78, respectively. Pockets were identified by CastP [72] and images were generated in pymol [73].

The second DsbA encoded in the *P. aeruginosa* genome (PaDsbA2) shares 21 % sequence identity with EcDsbA and has a less bent helix H1 [75]. PaDsbA2 diverges from the previously described DsbAs by having an altered topology of the central β-sheet. Specifically, the B1 strand in PaDsbA2 is hydrogen bonded to the opposite end of the central β-sheet compared with EcDsbA. This β-sheet arrangement was first described for *Wolbachia pipientis* DsbA1 (WpDsbA1) [80] (Figure 1.6). Further, PaDsbA2 does not have a groove on the catalytic surface and the residues contributing to the

hydrophobic groove in EcDsbA are replaced with polar and charged residues in PaDsbA2. PaDsbA2 is the most oxidising of all the DsbA enzymes characterised to date with a redox potential of -68 mV and it contains an additional disulfide bond linking helix H2 and helix H5 [75].

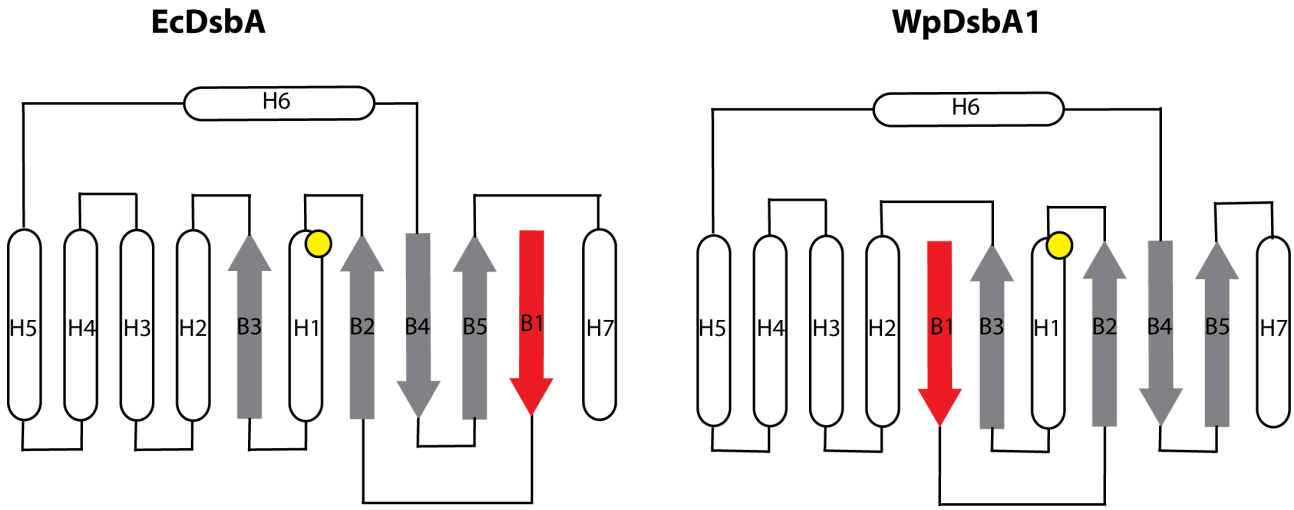

Figure 1.6 β-sheet topology of EcDsbA and WpDsbA1.
In EcDsbA (left) strand B1 (red) is hydrogen-bonded to strand B5 in the central β-sheet (grey) whereas strand B1 (red) is hydrogen-bonded to strand B3 in WpDsbA1 (right) resulting in different β-sheet topology in the two DsbA enzymes.

Acinetobacter baumannii (AbDsbA) shares 32 % sequence identity with EcDsbA, and 44 % sequence identity with PaDsbA1. Accordingly, AbDsbA is more closely related to PaDsbA1, BpsDsbA and XfDsbA. Like XfDsbA, AbDsbA has a conserved CPHC motif and a TP motif though with a slightly less oxidising redox potential (-101 mV) (Table 1.1). Interestingly, AbDsbA binds elongation factor thermo unstable (EFTu) non-covalently at a binding site different to the binding site for DsbB [83]. An avirulent strain of *A. baumannii* encodes a DsbA with a point mutation in the catalytic motif (H36L); this mutation results in a significant decrease in redox potential of the enzyme from -101 mV (wild-type) to -134 mV (mutant) [83].

The *Neisseria meningitidis* genome encodes three DsbA homologs; NmDsbA1, NmDsbA2 and NmDsbA3 that all share between 20 % and 25 % sequence identity with EcDsbA (Table 1.1). NmDsbA1 and NmDsbA2 are lipid-anchored to the inner membrane whereas NmDsbA3 is predicted to be soluble and localised to the periplasm [77]. All three *N. meningitidis* DsbAs have a TP motif, but the CPHC motif is conserved only in NmDsbA1 and NmDsbA2; NmDsbA3 has a Cys-Val-His-Cys (CVHC) catalytic motif. The structures of NmDsbA1 and NmDsbA3 have been reported and are similar to PaDsbA1 (RMSD 2.2 and 2.3 Å, respectively), though with differing surface properties [77]. Whereas the surface groove of NmDsbA3 is hydrophobic – similar to EcDsbA - the groove in

NmDsbA1 is more acidic [77]. The redox potentials of the three *N. meningitidis* DsbAs are -79 mV, -79 mV and -81 mV, respectively, all more oxidising than EcDsbA. This is also reflected in the more acidic surface exposed cysteines (pK_a = 3.0, 3.3 and 3.0) compared with EcDsbA, and a larger difference in melting temperature between the reduced and oxidised states of the enzymes (15K–17K compared to 8 K in EcDsbA) (Table 1.1).

WpDsbA1 shares just 10 % sequence identity with EcDsbA and is, except for NmDsbA3, the only structurally characterised DsbA that doesn't have a proline in the catalytic motif. In WpDsbA1 the proline in the catalytic motif is replaced with a tyrosine residue (CYHC). The *cis*Pro motif in WpDsbA1 is TP. WpDsbA1 has the alternate β-sheet topology also found in PaDsbA2, (Figure 1.6) [80] and also contains an additional disulfide that links helices H2 and H5. In addition, due to deletions in the sub-domain made up of strand B4 and B5 as well as helix H7, WpDsbA1, like PaDsbA2, does not have a catalytic surface groove. Additionally, the catalytic surface of WpDsbA1 is relatively basic (Figure 1.5). Further, the melting temperature of reduced WpDsbA1 is just 6 K higher than that of oxidised WpDsbA1, and the pK_a of the surface exposed cysteine (4.7) is less acidic than most other characterised DsbAs (except VcDsbA). Accordingly, the redox potential of WpDsbA1 (-163 mV) is significantly lower than that of EcDsbA (Table 1.1).

Francisella tularensis DsbA (FtDsbA) shares 10 % sequence identity with EcDsbA and is distinguished from other DsbA enzymes by being dimeric and harbouring both oxidase and isomerase activity [29]. Moreover, FtDsbA is anchored to the outer membrane [86]. FtDsbA has a Cys-Met-Tyr-Cys (CMYC) catalytic motif where neither the proline nor a histidine from EcDsbA is conserved. The *cis*Pro motif encodes a single polymorphism between type A and type B *F. tularensis*. Type A FtDsbA has a Thr-*cis*Pro motif and a redox potential of -159 mV, whereas type B FtDsbA has an Ala-*cis*Pro (AP) motif and a more oxidising redox potential of -131 mV (Table 1.1) [29].

1.2.2.2 DsbA enzymes in non-Gram-negative bacteria

Three DsbAs from non-Gram-negative bacteria have been characterised to date. These are the acid-fast bacteria *Mycobacterium tuberculosis* DsbA (MtbDsbA) and the two Gram-positive bacteria *S. aureus* DsbA (SaDsbA) and *Bacillus subtilis* DsbA (BsDsbA). Common to these three DsbAs is a TP *cis*Pro motif and a catalytic motif with only the proline conserved in the dipeptide separating the two cysteines (Table 1.1). Accordingly, the catalytic motif is CPSC, CPAC and CPYC in BsDsbA, MtbDsbA and SaDsbA, respectively. Additionally these DsbA enzymes share the β-sheet topology of WpDsbA1 and PaDsbA2 [78-79, 84].

BsDsbA has a redox potential of -80 mV and is therefore one of the strongest oxidases yet characterised. By contrast, SaDsbA with a redox potential of -131 mV is among the weakest DsbA oxidases. Interestingly, the reduced and oxidised states of SaDsbA are almost equally stable with the melting temperature of the reduced state just 1 K higher than that of the oxidised state (Table 1.1). With a redox potential of -99 mV the oxidase power of MtbDsbA lies between that of BsDsbA and SaDsbA. In contrast to SaDsbA the difference in melting temperature between reduced and oxidised MtbDsbA is 13 K (Table 1.1).

MtbDsbA is distinguished from other DsbA enzymes by having an additional eighth helix, H8, packing against helices H1 and H7, as well as a second disulfide like that of PaDsbA2 and WpDsbA1 [78]. Loop L3 is shorter in MtbDsbA than in EcDsbA and consequently doesn't have the distinct groove of the EcDsbA catalytic surface, but the hydrophobic nature is partly preserved in MtbDsbA (Figure 1.5) [78]. In contrast, the catalytic surface is primarily acidic in BsDsbA and SaDsbA (illustrated by BsDsbA in Figure 1.5). BsDsbA is the only of the characterised DsbA enzymes from Gram-positive bacteria that has a pocket at the surface close to the active site (Figure 1.5).

1.2.2.3 A second non-catalytic disulfide is present in some DsbAs

A disulfide bond that links helices H2 and H5 is present in three structurally characterised DsbAs: MtbDsbA, PaDsbA2 and WpDsbA1. Further the cysteines forming this disulfide are conserved across α-Proteobacteria [80]. In WpDsbA1 the disulfide is predicted to introduce local stress, which is associated with a functional rather than a structural role [87]. This is consistent with the observation that the presence of the second disulfide inhibits interaction with partner protein *W. pipientis* DsbB [80]. Disruption of this second disulfide has limited effect on the enzymatic properties, changing the redox potential minimally from -163 mV to -161 mV. In contrast, disruption of the second disulfide in PaDsbA2 leads to a significant change by decreasing the redox potential from -68 mV to -118 mV [75]. The role of the second disulfide in MtbDsbA has not been determined but has been suggested to play a structural role [78, 88].

1.2.2.4 Correlation of structure and function in DsbA enzymes

There is a general trend that DsbAs with a more acidic surface exposed cysteine (defined by pK_a), have a greater melting temperature difference between their reduced and oxidised states, and are more oxidising (defined by redox potential) (Table 1.1). Further, as a general rule, those DsbAs with a threonine rather than a valine in the *cis*Pro motif have higher redox potential values. In some cases, this is due to additional stabilisation of the thiolate anion by the threonine side-chain [65, 66, 77]. The exception to this is SaDsbA and WpDsbA1, which despite the enhanced oxidising properties of

the threonine in the *cis*Pro motif is amongst the least oxidising DsbAs characterised. However, the distance between threonine oxygen and cysteine sulfur in these two enzymes is 4.0-4.4 Å (compared with 3.0 to 3.5 Å for other DsbAs with a *cis*Pro-Thr motif). Consequently, the positioning of the threonine is critical to its ability to stabilise the thiolate anion and contribute to oxidising power.

A bioinformatic study of prokaryotic genomes reveals that the dipeptide separating the two cysteines in the catalytic motif are highly conserved in DsbA enzymes [89]; in 78 % of DsbA proteins the first residue of the dipeptide is a proline and in 87 % the second residue is either aromatic, polar or charged. This is interesting, as the dipeptide separating the two cysteines in the catalytic motif has been shown to greatly influence the redox properties of dithiol oxidoreductases [71]. In the two characterised DsbAs where the proline is not conserved, NmDsbA3 and WpDsbA1, the redox potential is slightly higher or significantly lower than in EcDsbA, respectively. Moreover, the redox potential is slightly higher than EcDsbA in XfDsbA2 and MtbDsbA - the two characterised DsbAs that do not have a basic, aromatic or polar residue in the second position of the CXXC motif [65, 78]. Likewise, mutating the histidine in the catalytic motif of AbDsbA to the small uncharged residue Leucine increases the redox potential from -101 mV to -134 mV [83]. FtDsbA represents the first biochemically characterised DsbA where neither of the amino acids in the EcDsbA catalytic motif are conserved. The two FtDsbA variants have redox potentials of -159 mV and -131 mV and are thereby among the least oxidising DsbA enzymes characterised.

Even though the difference in stability between reduced and oxidised EcDsbA contributes significantly to EcDsbA catalysis [71], SaDsbA has oxidising activity despite the active site disulfide not being destabilising. Curiously, the *S. aureus* genome does not encode a DsbB homolog suggesting that SaDsbA does not require a protein re-oxidation partner. The equivalent stabilities of the reduced and oxidised state of SaDsbA led Heras *et al.* to speculate that extracellular oxidants may be responsible for oxidation of SaDsbA to return it to the active state, although the mechanism for this remains unknown [84].

1.2.2.5 Substrate range of DsbA enzymes

Most DsbA enzymes display broad substrate specificity. In fact, EcDsbA has been estimated to interact with up to several hundred different substrates [48, 90] and more than 50 substrates are identified for FtDsbA (type B) [29]. Curiously, the surface of the active, oxidised, form of EcDsbA is more flexible than the reduced form [91]. This might allow for adaption to different substrates. The disulfide bonds introduced by EcDsbA are primarily buried in the protein core of the substrate [92]. Consequently, introduction of disulfide bonds into the substrate protein must occur in its unfolded

state. As the hydrophobic core will be exposed in the unfolded protein this is consistent with binding to the large hydrophobic groove in EcDsbA. The diversity in length, depth and electrostatic potential of the groove at the catalytic surface suggests that different DsbAs might have different substrate specificity.

Most DsbA proteins are soluble and localised to the periplasm; the exceptions are the two lipoproteins NmDsbA1 and NmDsbA2 as well as PaDsbA2 that has a predicted N-terminal transmembrane helix (predicted by TMHMM [93]). MtbDsbA has an N-terminal sequence that could be either a signal peptide or a transmembrane helix [78]. NmDsbA1 and NmDsbA2 have a different substrate range to that of the soluble periplasmic NmDsbA3. Specifically, NmDsbA1 and NmDsbA2, but not NmDsbA3, are required for correct folding of type IV pili and the protein PilQ that is required for DNA uptake [94]. PaDsbA2 cannot complement a PaDsbA1 mutant *in vivo* suggesting that the two DsbAs in *P. aeruginosa* also have different substrate specificities and thus different roles [75].

Of the more than 50 substrates that have been identified for the outer membrane located FtDsbA (type B) several are outer membrane proteins and known virulence factors [29, 95]. The formation of the correct native disulfide bonds in the proteins of the *F. tularensis* envelope is maintained by the oxidase and isomerase activity of FtDsbA. This has been suggested to provide additional protection against phagosomal reactive oxygen species for this intracellular pathogen [29].

1.2.2.6 A classification system for DsbA enzymes

A structural classification system for DsbA enzymes has been developed based on 13 DsbAs that have been extensively characterised structurally and functionally. On this basis, these 13 DsbAs were divided into two subclasses based on β-sheet topology [96]. DsbAs with the same β-sheet topology as EcDsbA are classified as DsbA-I and DsbAs with β-sheet topology resembling the topology in WpDsbA1 (Figure 1.6) are classified as DsbA-II (Table 1.2). DsbA-I enzymes are further divided into subclasses based on loop conformations. Specifically, the conformation of loop L2, which in DsbA-Ia enzymes faces the catalytic disulfide and points away from the catalytic disulfide in DsbA-Ib enzymes and the length of loop L3. The surface of the DsbA-II enzymes is generally less hydrophobic than the DsbA-I enzymes, and differences in electrostatic surface potential divides the DsbA-II enzymes into two subclasses (Table 1.2). The surface of enzymes in the DsbA-IIa class is more negatively charged (BsDsbA and MtbDsbA in Figure 1.5) whereas the surface of WpDsbA1, the only member of the DsbA- IIb class, is more positively charged (Figure 1.5).

Table 1.2 DsbA enzymes are divided into four subclasses

Class	DsbA	Seq. Identity to reference DsbA	RMSD to reference DsbA (Å)
DsbA – Ia	**EcDsbA**	100 %	0.9
	SeDsbA	86 %	1.0
	KpDsbA	81 %	1.2
	VcDsbA	40 %	0.9
DsbA – Ib	**BpsDsbA**	100 %	-
	PaDsbA1	44 %	1.8
	XfDsbA	30 %	1.9
	NmDsbA1	29 %	2.4
	NmDsbA3	27 %	2.6
DsbA – IIa	**MtbDsbA**	100 %	0.3
	SaDsbA	21 %	2.4
	BsDsbA	20 %	2.0
DsbA – IIb	**WpDsbA1**	100 %	-

Sequence identity and RMSD of a structural alignment (TM-align [97]) are listed compared to the reference DsbA in each subclass (bold text) [57]. SeDsbA (PDB code 3L9S), KpDsbA (PDB code 4MCU) and VcDsbA (PDB code 4DVC) were aligned with EcDsbA (PDB code 1FVK). PaDsbA1 (PDB code 3H93), XfDsbA (PDB code 2REM), NmDsbA1 (PDB code 3DVW) and NmDsbA3 (PDB code 3DVX) were aligned with BpsDsbA (PDB code 4K2D). SaDsbA (PDB code 3BCI) and BsDsbA (PDB code 3EU3) were aligned with MtbDsbA (PDB code 4K6X). WpDsbA1 (PDB code 3F4R) is the only DsbA classified as DsbA-IIb. RMSD for the two reference proteins EcDsbA and MtbDsbA is based on structural alignment of individual protomers A and B.

The enzymes within the DsbA-Ia class, and to a lesser extent the DsbA-Ib class, are more closely related to each other in sequence and structure than the DsbA-II enzymes (Table 1.2). This is also reflected in the redox properties for each class. The DsbA-Ia enzymes have redox potentials varying from -122 mV to -116 mV. The redox potential of the DsbA-Ib enzymes are all larger than this – varying from -94 mV to -79 mV. The DsbA-IIa class, however, includes one of the most oxidising DsbAs (BsDsbA with a redox potential of -80 mV) and one of the least oxidising DsbAs (SaDsbA with a redox potential of -131 mV) (Table 1.1). Identification of subclasses of DsbA enzymes with distinct structural and functional characteristic opens the possibility of developing drugs that target a specific subclass of DsbA.

1.2.3 EcDsbB oxidises EcDsbA via a quinone-dependent mechanism

The redox partner for DsbA in *E. coli* is the membrane protein DsbB (EcDsbB) [98]. EcDsbB has four transmembrane helices (TM1-4) arranged in a four-helix bundle and two periplasmic segments (P1 and P2) each containing two cysteine residues capable of forming disulfide bonds. Both disulfide bonds are required for EcDsbB catalysis [99]. The redox potentials for the two redox pairs Cys41/Cys44 and Cys104/Cys130 are -210 mV and -250 mV, respectively [100]. This is curious, as they are less oxidising than the substrate they oxidise, EcDsbA that has a redox potential of -122 mV. The EcDsbB-mediated oxidation of EcDsbA is thought to be driven by electron flow to the very much more oxidising ubiquinone (UQ) (+110 mV) under aerobic conditions, or menaquinone (MK) (-74 mV) under anaerobic conditions [60].

Two different mechanisms of EcDsbB mediated oxidation of EcDsbA have been proposed [101]; the slow and the rapid pathway (Figure 1.7). Both pathways are initiated by nucleophilic attack on the EcDsbB Cys104-Cys130 disulfide by EcDsbA Cys30 thiolate resulting in an intermolecular disulfide between Cys104 of EcDsbB and Cys30 of EcDsbA (Figure 1.7). In the slow pathway, an interloop disulfide is formed between Cys41 and Cys130 of EcDsbB prior to release of EcDsbA. In the rapid pathway, formation of the interloop Cys41-Cys130 disulfide bond in EcDsbB follows release of EcDsbA. In both pathways, the native Cys41-Cys44 and Cys104-Cys130 disulfide bonds of EcDsbB are re-established in an UQ-dependent manner leaving UQ reduced. The majority of EcDsbA is oxidised via the rapid pathway [101].

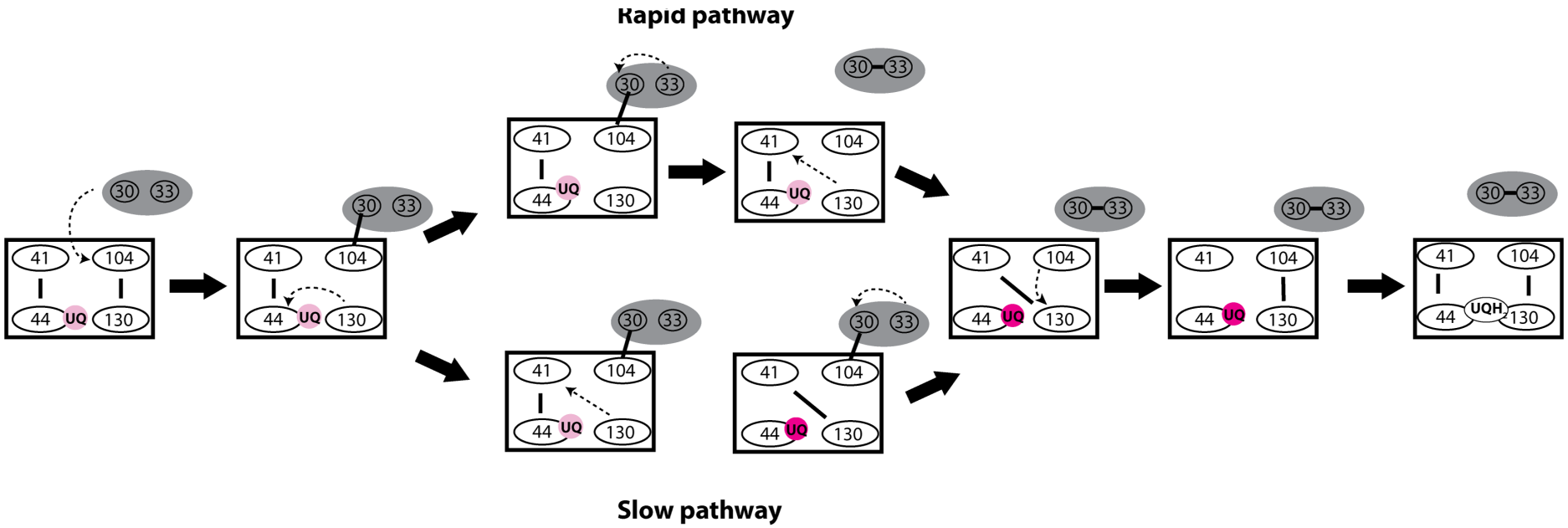

Figure 1.7 EcDsbB mediated oxidation of EcDsbA can proceed via two pathways.

In both pathways EcDsbA oxidation is initiated by a nucleophilic attack on the Cys104-Cys130 disulfide in the periplasmic region P2 of EcDsbB by the thiolate of Cys30 in EcDsbA resulting in an intermolecular disulfide bond between Cys104 of EcDsbB and Cys30 of EcDsbA. In the rapid pathway EcDsbA is released and an interloop Cys41-Cys130 disulfide is established. In the slow pathway an interloop disulfide is formed between Cys41 and Cys130 of EcDsbB followed by release of EcDsbA. Oxidation of Cys41-Cys44 and Cys104-Cys130 disulfide bonds is facilitated by UQ..

The structure of the membrane protein EcDsbB has been solved in three different conformations, capturing different steps of catalysis (Figure 1.8). The crystal structure of EcDsbB Cys41Ser is solved in complex with a monoclonal antibody Fab fragment (3.4 Å resolution) and represents the initial state of DsbB where a Cys104-Cys130 disulfide is present and available for nucleophilic attack by Cys30 of EcDsbA [101] (Figure 1.8A). In the crystal structure of the EcDsbA-EcDsbB complex (3.7 Å resolution), EcDsbB is locked in an intermediate state containing an intermolecular Cys30-Cys104 disulfide (Figure 1.8B) [101]. In the NMR-structure of the EcDsbB [CSSC] construct both Cys44 and Cys104 are mutated to serines (Figure 1.8C). The construct mimics the reaction intermediate containing the interloop disulfide between Cys41 and Cys130 [102] (Figure 1.8C).

Figure 1.8 Three EcDsbB structures represent different stages of EcDsbB catalysis. ***A)*** *Side and top view of EcDsbB C41S (PDB code 2ZUQ) that was co-crystallised with a monoclonal Fab antibody fragment (not shown). Residues Arg109-Trp113 lack electron density and were not modelled. The four transmembrane helices (TM1-TM4) form a four-helix bundle with a periplasmic region between TM1 and TM2 (P1) and between TM3 and TM4 (P2). Periplasmic region P1 contains a Cys41Ser mutation (red) and Cys44 (yellow). Periplasmic region P2 contains Cys104 and Cys130 (yellow). EcDsbB C41S mimics the initial state of EcDsbB catalysis (box diagram).* ***B)*** *Side and top view of the complex between EcDsbB C130S – EcDsbA C33A (PDB code 2ZUP) (only residues Phe28 to Gln35 of EcDsbA are shown (grey)). The EcDsbB structure is overall similar to that shown in A, but residues 116 to 120 adopt a short membrane-parallel helix separating periplasmic region P2 into two loops containing Cys104 and Cys130, respectively. Further, the distance between Cys104 (yellow) and Cys130Ser (red) is increased from 6.3Å in panel A to 8.9 Å in this structure. EcDsbB C130S – EcDsbA C33A represents the state of EcDsbB catalysis where EcDsbB is covalently bound through a disulfide bond between Cys104 in EcDsbB and Cys30 in EcDsbA (box diagram).* ***C)*** *In EcDsbB CSSC (PDB code 2K73) Cys44 and Cys104 are mutated to serines (red). The top and side views are generally similar to A and B. However, Cys130 (yellow) is 3 Å apart from to Cys41 (yellow) compared to 10 Å and 8.2 Å in A and B, respectively consequently this represents the catalysis intermediate containing an interloop disulfide bond between Cys41 and Cys130 (box diagram)*

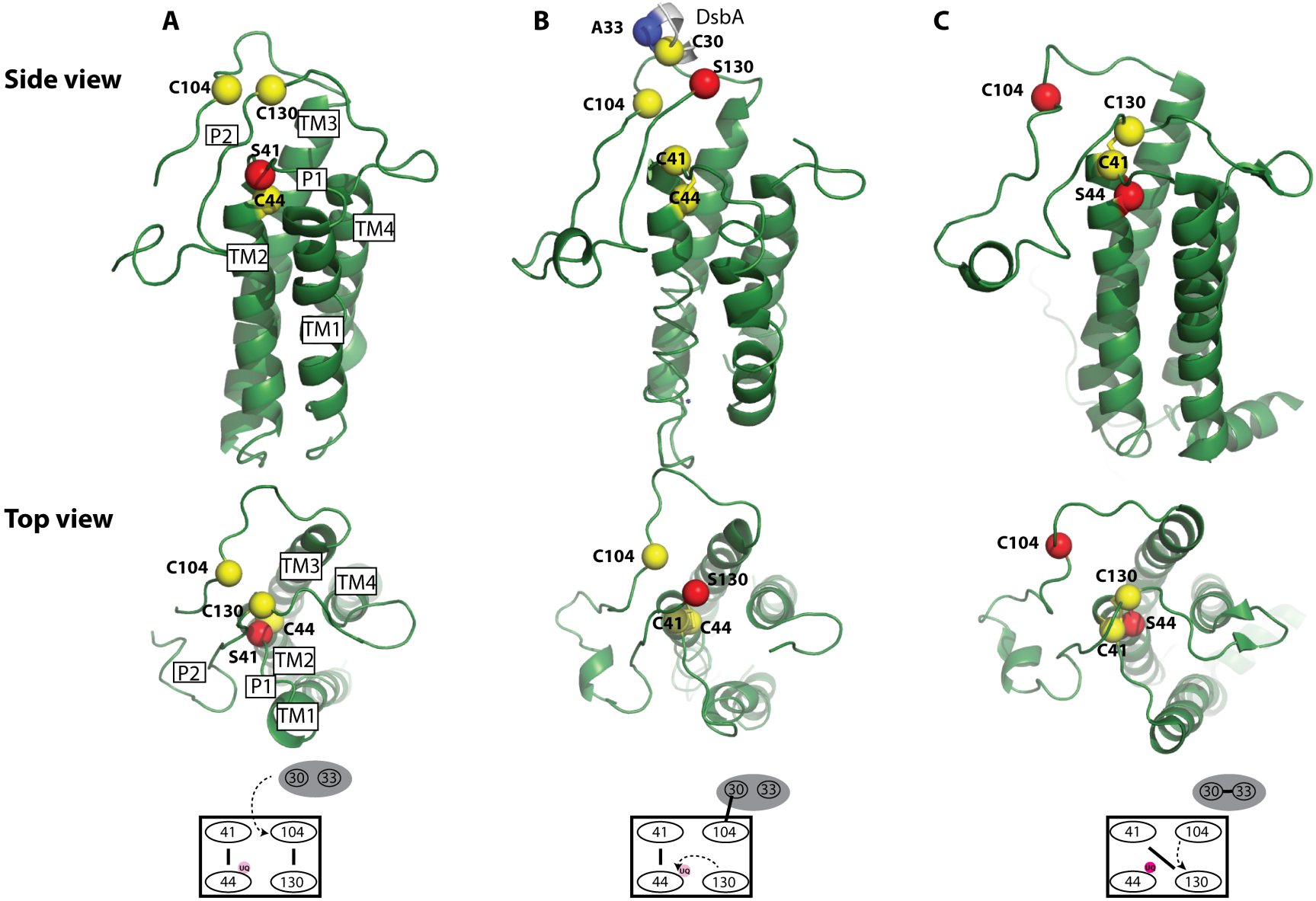
A
B
C
Side view
Top view
DsbA
A33
C30
S130
C104
C130
S44
C41
C44
TM1
TM2
TM3
TM4
P1
P2
S41
41
104
44
130
30
33
UQ

In all three structures EcDsbB adopts a four helix-bundle conformation consisting of four transmembrane helices (TM1-4) with periplasmic regions between helix TM1 and TM2 (P1) and between helix TM3 and TM4 (P2). Residues 116 to 120 in periplasmic region P2 form a short membrane parallel helix [101]. The amphipathic nature of the helix and the neighbouring residues are responsible for peripherally tethering the helix to the membrane; the hydrophobic residues Leu114, Leu116, Val120, Val123 and Phe125 are oriented towards the membrane, whereas Asp117, Lys118 and Gln122 face the periplasmic space. The membrane-tethered helix separates P2 into two loops; one containing Cys104 and one containing Cys130 allowing the two loops to undergo independent conformational changes and allows for the two cysteines to move independently (Figure 1.8B+C) [101].

Upon EcDsbB interaction with EcDsbA, Pro100-Phe106 (in periplasmic region P2) of EcDsbB binds to the hydrophobic groove of EcDsbA (Figure 1.9). The binding to EcDsbA induces a significant conformational change in P2 of EcDsbB; the Pro100 to Cys104 region shifts outward towards the four-helix bundle leading to separation of Cys104 and Cys130. In the EcDsbB-EcDsbA complex the distance between Cys104 and Cys130 is 8.9 Å (Figure 1.8B) compared to 6.3 Å in EcDsbB C41S-Fab (Figure 1.8A), that represents EcDsbB prior to interaction with EcDsbA. The physical separation of Cys104 and Cys130 hinders electron flow from EcDsbB to EcDsbA and is therefore essential for hindering reoxidation of the Cys104-Cys130 disulfide bond of EcDsbB, which is more energetically favoured than oxidation of the Cys30-Cys33 disulfide bond of EcDsbA [101].

In the structure of EcDsbB C41S, residue Cys130 is in close proximity to Cys104 forming an interloop disulfide bond (Figure 1.8A). In the EcDsbB-EcDsbA complex, the Asp129-Cys130 region of EcDsbB is adjacent to highly conserved Phe63-Gly65 segment of loop L1 in EcDsbA and is separated from Cys104 (Figure 1.8B) [101]. In contrast, Cys130 in EcDsbB CSSC approaches Cys41 in loop P1 to form an interloop disulfide bond (Figure 1.8C) [102]. The transient association of Cys130 of EcDsbB with loop L1 of EcDsbA separates Cys130 from Cys104 and Cys41, thereby allowing Cys33 of EcDsbA to attack the intermolecular disulfide, prior to the attack on Cys41 to Cys130. The resulting reduction of EcDsbA and subsequent release of EcDsbB is thought to increase flexibility in the Asp129-Cys130 region and allow Cys30 of EcDsbA to quickly approach the Cys41-Cys44 disulfide in EcDsbB to form a transient disulfide with Cys41. This mechanism has been suggested to be responsible for the dominance of the rapid pathway [101]. A smaller proportion of the EcDsbB catalysis enters the slow pathway when the flexible nature of the region allows Cys130 of EcDsbB to detach from loop L1 of EcDsbA and approach Cys41 of EcDsbB while EcDsbB is still attached to EcDsbA [101].

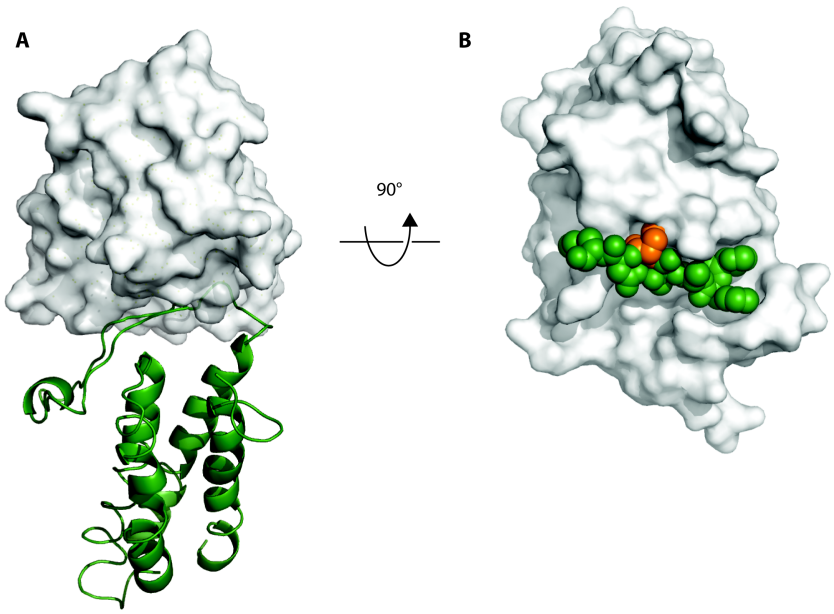

Figure 1.9 Pro100 to Phe106 of EcDsbB binds to the hydrophobic groove of EcDsbA.

A) *EcDsbB (green) binds to the hydrophobic groove of EcDsbA (grey) in the EcDsbB C130S – EcDsbA C33A complex (PDB code 2ZUP).* ***B)*** *EcDsbA (grey) is turned 90° around the horizontal axis compared to A. Only residues 100-106 of EcDsbB are shown as spheres (green). The segment spanning from Pro100 to Phe106 binds to the hydrophobic groove of EcDsbA where Cys104 of EcDsbB (orange) forms a disulfide bond with Cys30 of EcDsbA.*

1.2.3.1 Ubiquinone forms a charge-transfer complex with Cys44 in EcDsbB

UQ acts as an electron acceptor for EcDsbB and is required for the final steps in EcDsbB-mediated oxidation of EcDsbA (Figure 1.7). The UQ binding site is found at the periplasmic site of EcDsbB between TM1, TM2 and TM4 in the four-helix bundle with the isoprenoid tail running between TM1 and TM4 (Figure 1.10) [102]. The binding site for the 1,4-benzoquinone head group of UQ consists of Gln33 in the C-terminal region of TM1, residues 29 to 48 in the N-terminal region of TM2 and residues in loop P1. Especially Arg48, Gln33 and Met142 at the N-terminal end of helix TM2 are expected to be involved in binding of UQ [101-103]. The S atom of Cys44 is 3.1 Å away from C_1 of the quinone ring and a charge-transfer complex is formed between UQ and the thiolate anion of Cys44 [104] (Figure 1.10). The guanidinium moiety of Arg48 is 3.0 Å away from the S atom of Cys44 (Figure 1.10) potentially stabilising the charge-transfer complex by forming a hydrogen bond with the thiolate form of Cys44.

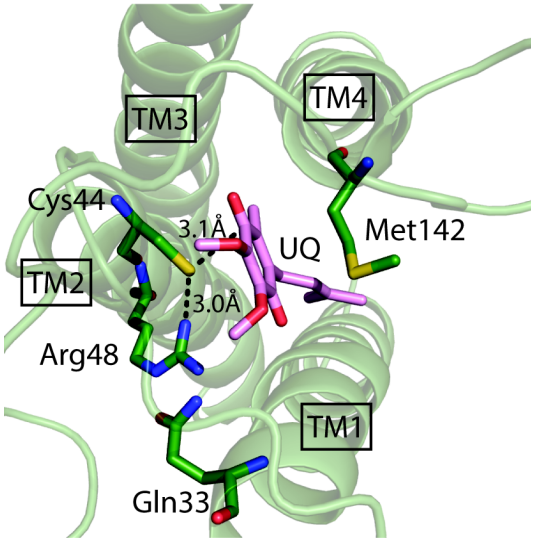

Figure 1.10 UQ forms a charge transfer complex with Cys44 of EcDsbB.

In the structure of EcDsbB C41S (PDB code 2ZUQ) UQ (pink) is bound at the N-terminal end of helix TM2 forming a charge-transfer complex with Cys44. The charge transfer complex is stabilised by the guanidinium moiety of Arg48. Gln33 and Met142 are also proposed to be involved in UQ binding

1.2.3.2 The UQ binding site and an amphiphilic segment is conserved in DsbB orthologs

With the exception of the DsbA-IIa enzymes from Gram-positive bacteria, all the organisms categorised with a DsbA belonging to the DsbA-I and DsbA-II subclasses encode at least one DsbB ortholog. *P. aeruginosa* encodes two DsbBs (PaDsbB1 and PaDsbB2) that both are capable of oxidising both PaDsbA1 and PaDsbA2 [75]. Sequence alignment of the DsbB orthologs reveals that they share the same overall topology with four membrane-spanning sections (TM1-4) and two periplasmic regions (P1 and P2) (Figure 1.11). The DsbBs that are predicted redox partners for the DsbAs in DsbA-I have identical membrane topology predictions. For other DsbBs, the membrane topology predictions (made using TMHMM [93]) are more diverse although the proteins are still predicted to have the same overall topology and periplasmic loops of generally similar length as EcDsbB. For example, in BpsDsbB, loop P1 is slightly longer than in EcDsbB whereas loop P2 is shorter. On the other hand, periplasmic loop P2 is eight and 11 residues longer in *N. meningitidis* DsbB (NmDsbB) and *X. fastidiosa* DsbB (XfDsbB), respectively. Considering the uncertainty of this topology prediction for helix termini, the findings on loop length should be taken with reservation.

The location of the two cysteines in the periplasmic region P2 is conserved at the N-terminal end and C-terminal end of P2, respectively in the aligned DsbB enzymes. However, the second cysteine in the P2 loop of *B. pseudomallei* DsbB (BpsDsbB) is in the predicted TM4 helix. This could indicate

that the shorter P2 loop of BpsDsbB is an artefact of the topology prediction. Interestingly, the amphiphilic pattern of residues 114-125 in periplasmic region P2 is conserved in all aligned DsbB enzymes (Figure 1.11) suggesting that the membrane tethered-helix is conserved and important for catalysis.

Arg48 – thought to be responsible for stabilising the charge-transfer complex between UQ and Cys44 - is conserved in all DsbBs in the alignment, whereas Gln33 - also suggested to be involved in UQ binding - is conserved in eight out of ten DsbBs. In the other two, WpDsbB and PaDsbB2, this residue is replaced by glutamic acid. Met142 is conserved in six out of ten DsbBs. Leucine or isoleucine is found at this position in the remaining four DsbBs suggesting that a hydrophobic residue in this position is required for UQ binding. The DsbA binding region from Pro100-Phe106 is partly conserved in *S. enterica* Typhimurium DsbB (SeDsbB), *K. pneumoniae* DsbB (KpDsbB) and *V. cholerae* (VcDsbB). Pro100-Phe101 and Tyr103-Cys104-Asp105 are conserved in all three DsbBs. Residues 102 and 106 vary amongst the three DsbBs, but except for a glutamine in position 102 in KpDsbB the hydrophobic nature of the residues are conserved. The predicted DsbA binding segments are not conserved in the remaining DsbBs, though the segment is predominantly hydrophobic. The lower degree of conservation of the DsbA binding segment compared to the UQ binding site and amphiphilic pattern in P2 is likely to reflect differences in the DsbB binding site in the corresponding DsbA.

The Gram-positive bacterium *M. tuberculosis* encodes no DsbB, but MtbDsbA is oxidised by the integral membrane protein vitamin K epoxide reductase (VKOR), proposed to be a functional homolog of DsbB. In contrast to DsbB enzymes, VKORs have five transmembrane helices. But equivalent to DsbB enzymes, VKORs have two periplasmic loops each containing two cysteines that are required for catalysis [81].

Figure 1.11 Sequence alignment of DsbB orthologs.
Sequence alignment using Clustal Omega [105] with manual alignment of cysteine residues in loop P2 of DsbB orthologs from E. coli, S. enterica Typhimurium *(SeDsbB),* K. pneumoniae *(KpDsbB),* V. cholerae *(VcDsbB),* B. pseudomallei *(BpsDsbB),* N. meningitidis *(NmDsbB),* X. fastidiosa *(XfDsbB),* P. aeruginosa *(PaDsbB1 and PaDsbB2) and* W. pipientis *(WpDsbB). Topology prediction in TMHMM [93] revealed that all orthologs have four transmembrane helices, TM1-4 (blue) and two periplasmic loops, P1 and P2 (green). Cysteines corresponding to the cysteines in the two periplasmic loops in EcDsbB are marked with a black box. Residues involved in UQ binding are marked with a pink box. The segment responsible for EcDsbA binding in EcDsbB as well as the segment forming*

the membrane-parallel helix in loop P2 in EcDsbB are labelled. "" indicates fully conserved residues. Conservation of residues with highly similar properties (above 0.5 in the Gonnet PAM 250 matrix) are marked with ":". Conservation of residues with weakly similar properties (below 0.5 in the Gonnet PAM 250 matrix) is marked with ".".*

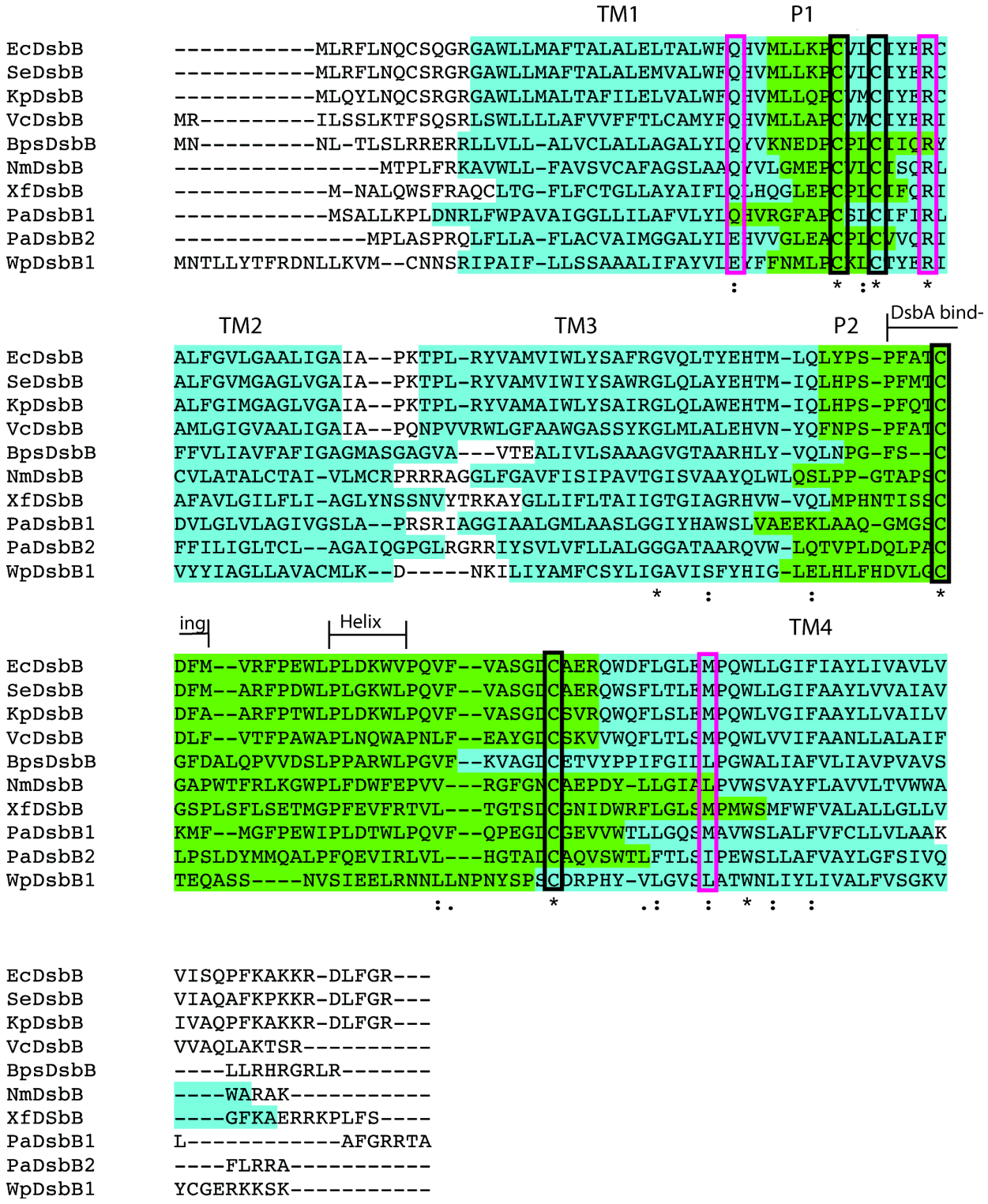

1.2.4 The oxidative pathway in *E. coli* is not conserved in all bacteria

Even though the oxidative pathway in *E. coli,* constituted by EcDsbA and EcDsbB, has served as the canonical model for oxidative folding in bacteria, the oxidative pathway is not conserved in all bacteria. Whereas most proteobacteria encode both DsbA and DsbB, many Gram-negative bacteria have an extended repertoire of Disulfide Bond (DSB) proteins. Additional to the DsbA-DsbB redox pair, the uropathogenic *E. coli* strain, CFT073, encodes another redox pair (DsbL and DsbI) responsible for the specific oxidative folding of aryl-sulphate sulphotransferase [106]. Another example is the periplasmic redox proteins DsbJ and DsbH [107] that are conserved in the *Chlamydia* phylum.

N. meningitidis, S. enterica Typhimurium*, P. aeruginosa* and *W. pipientis* all encode more than one DsbA. Indeed, a bioinformatics screen of DSB proteins revealed that out of 421 genomes, 51 had more than one DsbA-like protein encoded [89]. *N. meningitidis* and *W. pipientis* both encode a single DsbB homolog. WpDsbB only oxidises one of the *W. pipientis* DsbA orthologs, WpDsbA1 [108]. *P. aeruginosa,* on the other hand, encodes two DsbB homologs (PaDsbB1 and PaDsbB2) that are both capable of oxidising PaDsbA1 and PaDsbA2 [75].

In contrast, there were 156 bacterial genomes for which no DsbA was identified [89]. In particular, many Gram-positive bacteria have a limited suite of DSB proteins. For example *S. aureus, B. subtilis* and *Listeria monocytogenes* encode DsbA, but not DsbB [109]. Many bacteria that encode DsbA but lack DsbB, for example, *M. tuberculosis* and *Streptomyces coelicolor*, encode the DsbB analogue VKOR. Some bacteria, like *Streptococcus pyogenes*, encode neither DsbA nor DsbB and are proposed to utilise isopeptide bonds for stabilisation of secreted proteins rather than disulfide bonds [110].

1.2.5 Targeting the oxidative pathway as a strategy for development of anti-virulence drugs

Disruption of disulfide bond formation is a promising strategy for development of anti-virulence antimicrobials [33] and several components in the oxidative pathway have been targeted for inhibition. Many DsbA enzymes have a broad substrate range, and consequently, inhibiting DsbA oxidase activity will potentially disrupt a number of virulence pathways simultaneously.

Previous, EcDsbA inhibitors have been developed using a Fragment-Based Drug Discovery approach. Screening of a library of more than 1000 fragments identified 37 hits, from five different chemical classes, that bound non-covalently to EcDsbA [111]. Structure guided development of

analogues of one chemical class of these EcDsbA binding molecules resulted in two inhibitors with IC_{50} values of 185 ± 10 μM and 310 ± 16 μM, respectively. Treatment of *E. coli* K-12 cells with one compound led to reduced motility, with no effect on bacterial growth; a phenotype that is consistent with inhibition of EcDsbA. Inhibitors of EcDsbA have also been developed based on peptides mimicking the EcDsbB periplasmic loop segment that binds to EcDsbA [112]. This approach led to identification of a peptide that inhibits the activity of EcDsbA with an IC_{50} of 8.8 ± 1.1 μM. This peptide also binds to PmDsbA, an enzyme that is structurally closely related to EcDsbA [112], supporting the hypothesis that inhibitors can be developed to target DsbAs belonging to the same class of DsbA enzymes.

EcDsbB has also been explored as an anti-virulence target. In a Fragment-Based Drug Discovery approach [113] 93 initial hits were tested in an enzymatic assay for the ability of EcDsbB to reoxidise EcDsbA or reduce the cofactor UQ-5. Eight fragments significantly inhibited EcDsbB activity either by competing for quinone binding, or for binding of both EcDsbA and quinone to EcDsbB. Other inhibitors were developed by applying structure-activity relationship principles. In particular, one compound with an IC_{50} of 1.1 μM inhibited both EcDsbA and EcDsbB by covalent addition of a propionyl group to cysteines or lysines [114]. In a third example, screening of more than 51,000 compounds in a cell based assay identified six specific inhibitors of EcDsbB (that did not inhibit *M. tuberculosis* VKOR). One of these compounds inhibited binding of UQ, emphasising the important role of UQ in EcDsbB catalysis [115].

1.3 Targeting disulfide bond formation in *C. trachomatis*

In vitro and in cell studies of the disulfide bond formation in many bacteria has identified the oxidative pathway as a strategy for development of new antimicrobials for pathogens that are resistant to antibiotics. In this thesis, the oxidative pathway of *C. trachomatis* has been explored to provide fundamental knowledge that could underpin future efforts aimed at developing inhibitors of DSB enzymes.

1.3.1 Undiagnosed infections with *Chlamydia trachomatis* can have severe consequences for fertility and eye sight

Members of the *Chlamydia* phylum are intracellular obligate Gram-negative bacteria infecting eukaryotic cells. *Chlamydia trachomatis* is one of three *Chlamydialae* under the phylum *Chlamydia* that infects humans. Infection with serovars A to C leads to blinding trachoma, which is the leading cause of preventable blindness worldwide [116, 117]. Infection causes roughening of the inner surface of the eyelid. This can lead to pain in the eyes, breakdown of the outer surface or cornea,

visual impairment and, ultimately, blindness. The infection can be treated with antibiotics and surgery to prevent blindness after scarring has occurred. However, blindness caused by *C. trachomatis* is irreversible [118, 119].

The sexually transmitted infection (STI) Chlamydia is caused by infection with serovars D to K whereas serovars L1 to L3 lead to infection in the lymphatic system [117]. Chlamydia infections, especially in the female genital tract, are often asymptomatic and consequently are often underdiagnosed. An untreated infection carries a high risk of prolonged exposure of the epithelium of the fallopian tube to *C. trachomatis,* or its released antigens. This can lead to scarring and disruption of tubal integrity with severe consequences such as infertility, ectopic pregnancy and premature termination of pregnancy. Other consequences of genital tract infections include pelvic inflammatory disease, endometriosis, and perihepatitis [120].

1.3.2 The chlamydial developmental cycle is dependent on formation and degradation of disulfide bonds

All species in the chlamydial phylum, including *C. trachomatis*, have a biphasic developmental cycle alternating between two morphologically and functionally distinct cell types. These are the infectious extracellular elementary body (EB) and the intracellular replicating reticulate body (RB). The Chlamydial Outer Membrane Complex (COMC) is a network of highly disulfide cross-linked outer membrane and outer membrane-associated proteins formed in the EB (Figure 1.12) [121-125].

The Major Outer Membrane Protein (MOMP) comprises 60 % of the outer membrane protein mass [126]. Other constituents of the COMC are the two cysteine-rich proteins OmcA and OmcB, eight of the nine polymorphic membrane proteins (Pmp) found in *C. trachomatis* and components of the Type III Secretion System (T3SS) [124, 127-130]. Disulfide cross-linking of the COMC is required for the integrity of the EB, by conferring resistance to osmotic pressure and proteolysis [131, 132].

C. trachomatis infection is initiated by attachment of the EB form of the bacterium to the host cell. This is facilitated by a trimolecular bridge between bacterial adhesion molecules, host cell receptors and host heparin sulphate proteoglycans and involves OmcB, MOMP and the Pmps [125, 133-139]. Following attachment to the host cell, chlamydial effector proteins synthesised in the previous infection cycle and packed into the EB are translocated into the host cell by the T3SS where they promote internalisation and induce actin filament formation [140]. The EB is internalised to a membrane-derived vesicle called the inclusion body (Figure 1.13).

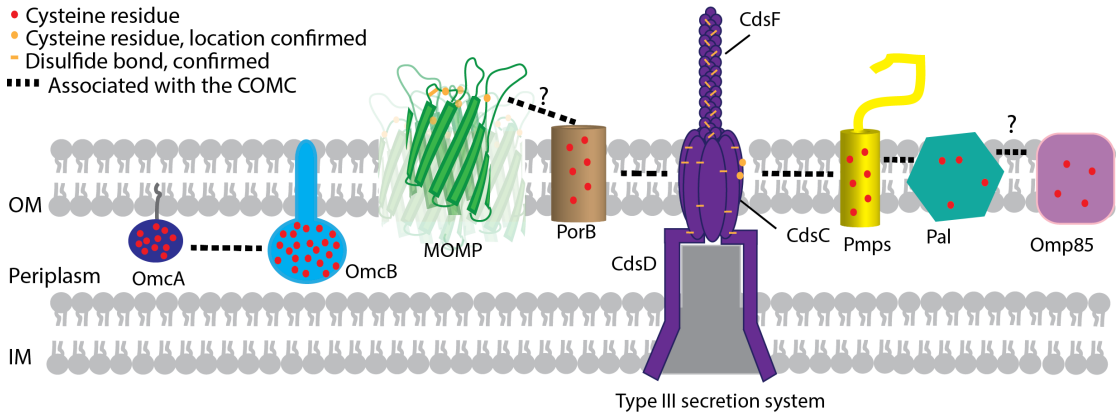

Figure 1.12 Composition of the Chlamydial Outer Membrane Complex.

The COMC consists of cysteine-rich outer membrane proteins and periplasmic proteins associated with the outer membrane. The location of cysteine residues and disulfide bonds with experimentally validated locations is shown in orange. Other cysteines are shown in red. Proteins associated with the COMC are linked with a dashed line. The structure of MOMP (green) is based on the model of Atanu et al. *[141]. MOMP are inserted in the membrane as trimers with all cysteines located in the predicted extracellular loops. For two of the three monomers (depicted as semi-transparent) in the MOMP trimer, the loops and disulfides are not labelled for visualisation purposes. It is still unclear if MOMP is disulfide linked to the other proteins of the COMC. OmcA (dark blue) has a cysteine content of ~15 % and is associated with the membrane via a lipid anchor. OmcB (light blue) has a cysteine content of 4-6 % with no cysteines in the membrane-spanning region. With the exception of PmpD, all Pmps have been identified in the COMC (yellow). PorB (brown) and Pal (turquoise) have also been identified as belonging to the COMC, whereas it is still uncertain if Omp85 (pink) is associated with the COMC. In the T3SS (purple) CdsF forms homomeric disulfide bonds. CdsC forms homomeric disulfide bonds as well as heteromeric disulfide bonds with CdsD. CdsC is also suggested to form intermolecular disulfide bonds with the COMC.*

Within the first two hours of infection the disulfide cross-links of the COMC are reduced [142-145]. Reduction of the COMC is associated with differentiation to RBs [131]. The increased fluidity of the membrane after disulfide bond reduction permits replication by binary fission. EB to RB differentiation also leads to an increase in size as well as decondensation of chromatin causing the genome to become transcriptionally active [131]. Proteins synthesised early (6-8 hours post-infection) in the replicative phase are responsible for remodelling of the inclusion membrane, redirection of exocytic vesicles to the inclusion and facilitating interaction with the host cell [146]. Shortly after, components of the COMC are synthesised, including MOMP, the T3SS needle protein, CdsF, as well as PmpE and PmpF [143, 144, 147-150]. Several dithiol oxidoreductases are synthesised during the replicative phase, including DsbA, DsbB, Suppression of Copper Sensitivity B (ScsB) [151] as well as DsbJ and DsbH [147].

After several rounds of replication, the RBs differentiate into EBs in an asynchronous manner and the disulfide cross-linking network is re-established (Figure 1.13). OmcA and OmcB expression is upregulated in the late stages of replication or early stages of RB to EB differentiation [143, 147-149]. Whereas MOMP is inserted in the outer membrane in the reduced thiol form, OmcA and OmcB are oxidised simultaneously with expression [143, 148]. MOMP as well as T3SS components are oxidised during RB to EB differentiation and are, at least partly, oxidised at the time of host cell lysis when new infectious progeny are released [143-145, 148, 152].

Stress caused by nutrient deprivation, exposure to host cytokines or β-lactam antibiotics can cause the RB to significantly alter its metabolism and gene transcription causing the RB to enter a persistent state where the bacteria cease to replicate but remain viable (Figure 1.13) [153-156]. The persistent state is reversed upon removal of the factor causing the stress and RB replication is resumed [157, 158].

The importance of disulfide cross-linking of the COMC in *C. trachomatis* is emphasised by the finding that treatment with the reducing agent dithiothreitol (DTT) prior to infection significantly reduces infectivity [131, 137, 142]. However, limited information is available about the processes responsible for redox regulation of the COMC. Host cell Protein Disulfide Isomerase (PDI) and intracellular glutathione are involved in reduction of the disulfide cross-linking of the COMC during internalisation [159-161]. However, a study [143] shows that inhibition of chlamydial protein synthesis inhibits reduction of MOMP whereas inhibition of host cell protein synthesis does not. This suggests that PDI and glutathione are not solely responsible for reduction of the COMC. No chlamydial proteins have been identified as redox regulators of the COMC, but given that DsbJ is exclusively found in members of the *Chlamydia* phylum, DsbJ has been proposed to be involved in regulating the redox state of the COMC proteins. For example, DsbJ may regulate the reducing activity of the periplasmic oxidase DsbH [145].

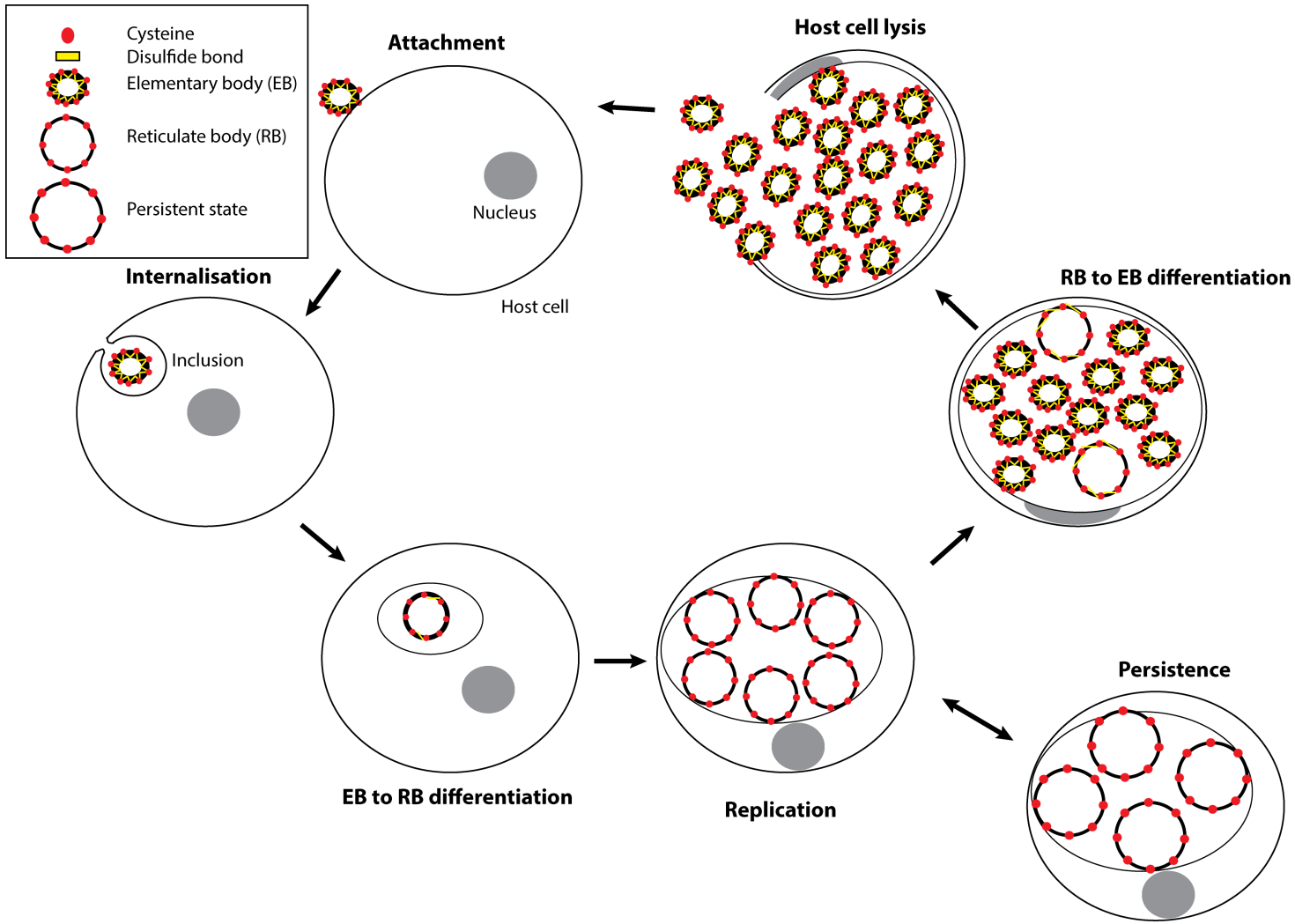

Figure 1.13 The* C. trachomatis *developmental cycle.

Infection is initiated by EB attachment to the host cell. The EB is internalised in a membrane-enclosed inclusion where the EB differentiates to RB. Following differentiation, the RB replicates by binary fission and these then differentiate to EBs. These are then released when the host cell lyses. In response to stress the RB can enter a reversible state of persistence. Cysteines are indicated as red dots and disulfide bonds as yellow lines.

1.3.3 Treatment and treatment failure of infections with *C. trachomatis*

C. trachomatis is routinely treated with azithromycin, doxycycline, erythromycin, levofloxacin or ofloxacin. These antibiotics are able to pass through lipophilic plasma membranes to reach the RB, which are more susceptible to antibiotics than EBs [162].

C. trachomatis has been shown to develop resistance *in vitro* against several classes of antibiotics including rifamycins and fluoroquinolones, such as azithromycin [87, 163-174]. Even though antibiotic resistance can be selected for *in vitro,* only 15 cases of resistant strains isolated from patients have been reported [175-179]. However, in 11 out of 15 reported cases the apparent antibiotic resistance was due to treatment failure and no resistant strains have been reported since 2000. Several factors can be responsible for the treatment failure e.g. reinfection, heterotypic resistance, persistence, and infection of anatomic sites where *C. trachomatis* is unavailable to antibiotics. In fact, treatment failure is a substantial problem with chlamydial infection; studies show treatment failure in up to 14 % of women despite no post-treatment sexual contact [180].

In heterotypic resistance, a subset of individual bacteria show reduced sensitivity to antibiotic treatment. All of the 15 reported cases of antibiotic resistance showed characteristics of heterotypic resistance where <1-10 % of the population were not susceptible to antibiotic treatment [175-179]. Due to the asynchronous RB to EB differentiation, a mid-stage inclusion will contain replicating RBs as well as non-replicating EBs. As EBs are less susceptible to antibiotics the asynchronous differentiation might ensure the survival of a subset of the population thereby causing heterotypic resistance [181].

Persistence can occur upon treatment with β-lactam antibiotics or in response to tryptophan starvation caused by the release of gamma interferon (IFN-ϒ) as part of the host immune response [182, 183]. The emergence of persistent *Chlamydia* has been linked to reduced sensitivity to antibiotics *in vitro* and might contribute to treatment failure [170, 181, 184-186].

Treatment of *Chlamydia* is further complicated by the common occurrence of co-infections with *Treponema pallidum* and *Neisseria gonorrhoeae* [187, 188]. Both *T. palladium* and *N. gonorrhoeae* are routinely treated with β-lactam antibiotics. Consequently, the treatment of *T. palladium* and *N. gonorrhoeae* could potentially induce persistence of *C. trachomatis.*

Antibiotic treatment of *C. trachomatis* infections can have severe effects on the native microbiota, and cause vaginal and gut dysbiosis. The bacterium, *Lactobacillus*, is the dominant species in the vaginal microbiota in most women of fertile age [189]. *Lactobacillus* inhibits *C. trachomatis* infectivity by producing antibacterial compounds such as hydrogen peroxide and lactic acid, causing co-aggregation, competitive exclusion, immunomodulation and potentially downregulation of toxin production by *C. trachomatis* [190, 191]. Antibiotic treatment can potentially deplete *Lactobacillus* populations thereby increasing the risk of reinfection with *C. trachomatis.*

Even though *C. trachomatis* is susceptible to many broad-spectrum antibiotics the high degree of treatment failure as well as the effect on the microbiota in the gut and, especially, in the vagina calls for new drugs targeting *C. trachomatis* with a narrower host range. Significantly, a BLAST search using DsbA sequences from *E. coli* and *C. trachomatis* against the Lactobacillus genomes (Taxid: 1578) identified no DsbA homologs suggesting that targeting CtDsbA will not have any off-target effects on lactobacillus.

1.4 Thesis objectives

The increase in antibiotic-resistant bacteria over the last decade underpins the need for development of antimicrobial drugs with new modes of action. Considering the requirement for oxidative folding of virulence factors in many pathogens, the proteins involved in the disulfide oxidative folding pathway have gained interest as potential targets for development of anti-virulence antimicrobial drugs. The diversity in redox activity and surface properties amongst DsbA proteins suggest that drugs can be developed that target a specific subset of DsbA enzymes.

The objective of the research reported in this thesis was to characterise the oxidative pathway in *C. trachomatis,* especially with a focus on the role of DsbA *in vitro* and *in vivo*. Characterising DsbA is done for two purposes, to provide: (i) new fundamental understanding that expands our knowledge of the diversity of DsbA enzymes and oxidative pathways in bacteria and (ii) a specific exploration of the oxidative pathway in *C. trachomatis* as a target for narrow spectrum anti-virulence inhibitor development. Considering the importance of disulfide bonds in infection and development in *C. trachomatis* the oxidative pathway might play a specialised role in *C. trachomatis* by regulating the redox state of the proteins in the chlamydial outer membrane complex.

To shed new light on the oxidative pathway in *C. trachomatis* three aims were investigated:

- Aim 1 (Chapter 2, published work) - characterise the structure and function of *C. trachomatis* DsbA (CtDsbA). Knowledge of differences and similarities between CtDsbA and other characterised DsbA enzymes contributes to building a structural library of DsbA enzymes to guide development of broad and narrow spectrum drugs targeting DsbA enzymes.

- Aim 2 (Chapter 3) - characterise the oxidative pathway in *C. trachomatis*. The goal was to explore similarities with, as well as deviations from, the oxidative pathways in *E. coli* by studying (i) the interaction between CtDsbA and *C. trachomatis* DsbB (CtDsbB) and (ii) UQ binding of CtDsbB. In addition, the determination of expression levels of CtDsbA was monitored during *C. trachomatis* infection of mouse fibroblasts (McCoy cells) to contribute to our understanding of the role of CtDsbA in *C. trachomatis* infection.

- Aim 3 (Chapter 4) - investigate approaches to generate a *dsbA* loss-of-function mutant in *C. trachomatis* for studying the impact on virulence. Genetic manipulation of *C. trachomatis* is challenging due to the biphasic lifecycle, so a random mutagenesis approach was taken in an effort to obtain loss-of-function mutations.

Chapter 5 summarises the results and broad conclusions of the three research chapters. Moreover, it discusses the potential of the results of this thesis to guide further development of antimicrobial drugs and explores the potential of targeting the oxidative pathway in *C. trachomatis* for development of drugs against *C. trachomatis*. The biological role of CtDsbA is reviewed based on the characterisation of CtDsbA and the interaction between CtDsbA and CtDsbB. I also outline further steps needed to address the biological function of the oxidative pathway in *C. trachomatis*.

Chapter 2: Structural and biochemical characterisation of *Chlamydia trachomatis* DsbA reveals a cysteine-rich and weakly oxidising oxidoreductase

The following chapter is a manuscript published in PLOS ONE with Dr. Morten Grøftehauge and myself as co-first authors. The manuscript addresses aim 1 of this thesis by presenting the structural and biochemical characterisation of CtDsbA thereby contributing to the structural library of DsbA enzymes.

Dr. Róisín McMahon and Dr. Morten Grøftehauge solved the structure of CtDsbA with assistance from Karl Byriel. Ms. Emily Furlong performed the initial attempt of the scrambled RNase assay and the remaining biochemical characterisation and analysis was performed by myself. I wrote the first draft of the paper, and the final manuscript was reviewed and edited by myself, Dr. Morten Grøftehauge, Dr. Wilhelmina M. Huston, Dr. Begoña Heras, Prof. Jennifer L. Martin and Dr. Róisín M. McMahon.

Please note that formatting is changed from the version published in PLOS ONE.

2.1 Authors

Signe Christensen*[1], Morten K. Grøftehauge*[1], Karl Byriel[1], Wilhelmina M. Huston[2], Emily Furlong[1], Begoña Heras[1], Jennifer L. Martin[1 %] and Róisín M. McMahon[1, %]

* These authors contributed equally to this work

[%] co-corresponding author

[1] Division of Chemistry and Structural Biology, Institute for Molecular Bioscience, University of Queensland, St. Lucia, Queensland 4072, Australia

[2]. School of Life Sciences, University of Technology Sydney, Broadway, NSW, 2007, Australia.

2.2 Current address

Begoña Heras: La Trobe Institute for Molecular Science, La Trobe University, Melbourne, VIC 3086, Australia

Morten Grøftehauge: School of Biological and Biomedical Sciences, Durham University, Durham DH1 3LE, UK

Jennifer L. Martin: The Eskitis Institute for Drug Discovery, Griffith University, Don Young Rd, Nathan QLD 4111, Australia

2.3 Abstract

The Gram-negative bacteria *Chlamydia trachomatis* is an obligate intracellular human pathogen that can cause pelvic inflammatory disease, infertility and blinding trachoma. *C. trachomatis* encodes a homolog of the dithiol oxidoreductase DsbA. Bacterial DsbA proteins introduce disulfide bonds to folding proteins providing structural bracing for secreted virulence factors, consequently these proteins are potential targets for antimicrobial drugs. Despite sharing functional and structural characteristics, the DsbA enzymes studied to date vary widely in their redox character. In this study we show that the truncated soluble form of the predicted membrane anchored protein *C. trachomatis* DsbA (CtDsbA) has oxidase activity and redox properties broadly similar to other characterised DsbA proteins. However CtDsbA is distinguished from other DsbAs by having six cysteines, including a second disulfide bond, and an unusual dipeptide sequence in its catalytic motif (Cys-Ser-Ala-Cys). We report the 2.7 Å crystal structure of CtDsbA revealing a typical DsbA fold, which is most similar

to that of DsbA-II type proteins. Consistent with this, the catalytic surface of CtDsbA is negatively charged and lacks the hydrophobic groove found in EcDsbA and DsbAs from other *enterobacteriaceae*. Biochemical characterisation of CtDsbA reveals it to be weakly oxidising compared to other DsbAs and with only a mildly destabilising active site disulfide bond. Analysis of the crystal structure suggests that this redox character is consistent with a lack of contributing factors to stabilise the active site nucleophilic thiolate relative to more oxidising DsbA proteins.

2.4 Introduction

Disulfide bond proteins (DSB) are thiol-disulfide oxidoreductases found in the periplasm of Gram-negative bacteria, which catalyse the oxidative folding of disulfide bond containing substrate proteins. The first DSB protein to be described was that of the primary oxidase DsbA from *Escherichia coli* (EcDsbA) [192]. EcDsbA is a highly oxidising protein with a redox potential of -122 mV [192] which introduces disulfide bonds into folding proteins resulting in its own active site reduction. EcDsbA is subsequently returned to its active oxidised state by interaction with an integral membrane partner protein EcDsbB. The structure of EcDsbA consists of a thioredoxin catalytic domain (containing the active site motif CPHC) with an inserted helical domain [62].

Extensive efforts over many years have yielded a structural library of over a dozen bacterial DsbA proteins. These have recently been classified into two groups (DsbA-I and DsbA-II) on the basis of structural and functional features [96]. DsbA-I and DsbA-II proteins are demarcated primarily on the basis of altered central β-sheet topology, a distinction that also approximately separates DsbA proteins from Gram negative and Gram-positive bacteria.

Each DsbA group can be further subdivided into two subclasses on the basis of surface features. Type DsbA-Ia and Ib groups are relatively well represented with four and five protein members respectively. By comparison, DsbA-II proteins are less well characterised; to date only three DsbA proteins have been classified as DsbA-IIa (DsbA from *Mycobacterium tuberculosis*, *Staphylococcus aureus* and *Bacillus subtilis*) whilst DsbA-IIb is solely represented by DsbA1 from the endosymbiont *Wolbachia pipientis*. Within DsbA-Ia and DsbA-Ib, member proteins have similar redox characteristics with redox potentials falling within a 10 mV or 15 mV range, respectively [70, 74, 76, 77, 84]. Among the DsbA-IIa proteins redox potentials are much more varied, ranging from -131 mV [84] to -80 mV [79].

It is well documented that pathways responsible for disulfide bond formation can vary markedly amongst different bacterial species [89]. In *C. trachomatis*, *in silico* analysis suggests that the disulfide oxidative pathway, and to some extent the isomerase pathway, resembles the canonical DSB pathways of *E. coli* K12. *C. trachomatis* possesses a gene predicted to be a homolog of the *E. coli* DsbA [89] hereafter referred to as CtDsbA. Immediately upstream of *dsbA C. trachomatis* also encodes a homolog of *E. coli* DsbB. This protein is predicted to be a transmembrane protein with four transmembrane helices and two cysteine-residue containing periplasmic loops. DsbB is presumably responsible for oxidising CtDsbA in a manner analogous to the *E. coli* DsbA-DsbB interaction. Notably *C. trachomatis* does not encode a homolog of the *E. coli* isomerase DsbC but has a gene with significant homology to *E. coli* DsbD, a membrane bound electron transporter and partner protein of *E. coli* DsbC. Drawing on recent extensive phylogenetic analysis of the DsbD superfamily in eubacteria [151], this gene is most likely a member of the sub-family ScsB. Finally *C. trachomatis* was found to contain homologs to genes coding for two periplasmic *C. pneumonia* proteins: DsbH and DsbJ. DsbH and DsbJ are suggested to play a role in maintaining a reducing periplasm, and have not yet been reported outside of chlamydial species [107].

Here we investigated the DsbA enzyme from *Chlamydia trachomatis*, responsible for human urogenital *Chlamydia* infections. This infection is among the most common sexually transmitted infections worldwide with an estimated 131 million urogenital cases reported globally in 2012 by the World Health Organization [193]. A common complication of genital chlamydial infection in women is pelvic inflammatory disease, which, if untreated, can lead to infertility. Furthermore, strains of *C. trachomatis* can also infect the ocular mucosa where it can cause blinding trachoma [194].

In the present study we confirm that CtDsbA has oxidising enzymatic activity and a structure similar to that of other DsbA-II type proteins that contain a second non-catalytic disulfide bond. We find that CtDsbA has a particularly weak oxidising potential for a DsbA enzyme, which appears to stem in part from its uncommon active site dipeptide motif of two uncharged amino acids. Characterisation of CtDsbA expands the DsbA structural library, provides further insight into the diversity of bacterial DsbA proteins and supports continued exploration of the potential for DsbA inhibitors with multi-species activity.

2.5 Materials and Methods

2.5.1 Protein expression and purification

The recombinant CtDsbA expressed and characterised in this study was generated using residues 34 to 238 of *C. trachomatis dsbA* (NCBI Gene with ID 5858475, currently annotated as DsbG). A variant form of the protein (called CtDsbA-SSS) was produced by mutating each of the three non-active site cysteines to a serine (C66S, C80S and C141S). Both constructs were synthesised and inserted into a modified pET21a vector by ligation independent cloning as described [195]. Both genes were codon-optimised for expression in *Escherichia coli*. The vector includes a N-terminal His_6-tag followed by a linker containing a recognition site for the tobacco-etch virus (TEV) protease. Design of the constructs was informed by bioinformatics analysis (HMMTOP [196, 197], and PSIPRED [198] to remove the predicted N-terminal transmembrane helix, and maximise solubility of the purified protein. Sequence verified plasmids were routinely amplified in *E. coli* TOP10 cells cultured at 37°C with orbital shaking (200 rpm) in LB broth supplemented with ampicillin (100 µg/mL), and subsequently isolated with a QIAprep Spin Miniprep Kit (QIAGEN).

For biochemical assays CtDsbA and CtDsbA-SSS were expressed in *Escherichia coli* BL21 (DE3) pLysS cells using ZYP-5052 autoinduction medium [199] in the presence of ampicillin (100 µg/mL) and chloramphenicol (34 µg/mL). Cultures were incubated at 30 °C, for 16 h with orbital shaking at 200 rpm. Harvested cells were re-suspended in a solution of 25 mM HEPES pH 7.5, 150 mM NaCl (Buffer 1), DNAse and protease inhibitors and lysed using a constant pressure cell disrupter. Clarified lysate was purified with Talon® resin (Clontech, Australia) washing with 25 mM HEPES pH 7.5, 500 mM NaCl, 2.5 mM imidazole and eluting with Buffer 1 and 500 mM imidazole. Purified protein was dialysed against Buffer 1 to remove imidazole prior to cleavage of the N-terminal His_6-tag by treatment with a His-tagged TEV protease. TEV cleaves leaving two non-endogenous amino acids (S -1 and N 0) at the N-terminus of the protein. Contaminating TEV protease and uncleaved CtDsbA were removed by a second immobilised metal affinity chromatography step prior to a final size exclusion step in Buffer 1 using a Superdex S75 column. As required CtDsbA and CtDsbA-SSS were reduced and oxidised by 20 fold molar excess of DTT or 100 fold molar excess of oxidised glutathione, respectively. The protein redox state was confirmed by Ellman's reagent [200].

For crystallisation experiments CtDsbA was prepared as described above with the following differences. Harvested cells were re-suspended in a solution of 50 mM Tris pH 7.6, 500 mM $(NH_4)_2SO_4$ (Buffer 2), 0.5 % Triton X-100, DNAse and protease inhibitors, and lysed by sonication. Immobilised-Metal Affinity Chromatography (IMAC) purification was performed with Profinity

resin (Biorad) equilibrated in Buffer 2 supplemented with 10 mM imidazole. Following wash steps (5 column volumes of Buffer 2), purified protein was eluted in Buffer 2 supplemented with 500 mM imidazole. Purified protein was dialysed against 50 mM HEPES pH 7.6, 500 mM $(NH_4)_2SO_4$ and 0.5 mM of the reducing agent tris-(2-carboxyethyl)fosfin (TCEP) prior to TEV cleavage and a second IMAC step. Protein purity (>95 %) was confirmed by SDS-PAGE analysis.

2.5.2 Insulin reduction assay

DsbA proteins catalyse the reduction of the disulfide bond formed between chain A and B of insulin. When the disulfide bond is reduced, chain B of insulin precipitates. This reaction can be monitored by an increase in absorbance at 650 nm [201]. Reaction mixtures were prepared in 1 mL cuvettes with 10 µM protein, 0.33 mM DTT and 2 mM EDTA in 100 mM NaH_2PO_4/ Na_2HPO_4 pH 7.0. The reaction was started by adding insulin (IO516, Sigma Aldrich, Australia) at a final concentration of 0.13 mM. Plotted data shows mean and standard deviation (SD) for three biological replicates.

2.5.3 Peptide oxidation assay

The redox activity of a disulfide bonded protein can be assessed by its ability to oxidatively fold the peptide CQQGFDGTQNSCK which has a N-terminal europium ion (Eu^{III}) in an amide-coupled tetraazacyclododecane-1,4,7,10-tetraaceticacid (DOTA) chelate and a C-terminal coumarin chromophore (AnaSpec, USA) [108, 202, 203]. Upon oxidative folding the two terminal tags come in close proximity resulting in a detectable fluorescent resonance energy transfer (FRET) effect. The assay was performed in a 384-well plate (Perkin Elmer, USA). A solution of 50 mM MES, 50 mM NaCl, 2 mM EDTA, pH 5.5, 2 mM GSSG and protein concentration of 80 nM (EcDsbA) or 320 nM (CtDsbA, MtbDsbA and αWpDsbA1) were added to the wells in 25 µL aliquots. Adding 25 µL peptide to a final concentration of 25 µM started the reaction. Change in fluorescence at 340 nm was followed using a Synergy H1 Multimode plate reader (BioTek, USA). Plotted data shows mean and SD for two biological replicates.

2.5.4 Scrambled-RNaseA assay

The ability of CtDsbA to isomerise disulfide bonds was evaluated by a scrambled RNaseA (ScRNaseA) assay. To generate scrambled RNaseA, disulfides were first reduced and unfolded by incubating RNaseA overnight in 50 mM Tris-HCl, pH 8 in the presence of 6 M GdmCl and 150 mM DTT at room temperature. The reduced and unfolded protein was acidified with 100 mM acetic

acid/NaOH pH 4 and purified over a GE-25 Sephadex desalting resin. The eight free thiols were confirmed by Ellman's reagent. To randomly oxidised disulfides, the reduced and unfolded RNaseA was diluted to 0.5 mg/ml in 50 mM tris-HCl, pH 8.5, 6 M GdmCl and incubated in a dark room at room temperature for at least 5 days. The randomly oxidised RNaseA (ScRNase) was concentrated, acidified and purified as described above, and oxidation of the disulfide bonds was confirmed by Ellman's reagent. Isomerase activity was evaluated by following the renaturation of ScRNaseA spectrophotometrically. RNase A with native disulfide bonds is able to cleave cyclic-2',3'-cytidinemonophosphate (cCMP) into 3'-cytidinemonophospate (3'CMP) resulting in an increase in absorption at 296 nm. EcDsbA, EcDsbC and CtDsbA (10 μM final concentration), were added to 100 mM sodium phosphate pH 7, 1 mM EDTA and 10 μM DTT and incubated for 5 min. To start the assay ScRNase was added at a final concentration of 40 μM. Native RNase and ScRNase (40 μM) were included as controls. At multiple time points from 0 to 360 min after initiation of the assay a 50 μL aliquot of each reaction was added to 150 μL of 3mM cCMP and the increase in absorbance at 296 nm was monitored every 10 second for 3 min. 3 biological replicates were performed for CtDsbA.

2.5.5 Motility assay

In order to investigate whether CtDsbA can complement EcDsbA, the *CtdsbA* gene was cloned into the expression vector pBAD33 [204] under the control of an arabinose inducible promoter and 3' of an *E. coli* specific signal peptide sequence. *EcdsbA* was likewise cloned into pBAD33 as a control. *E. coli* strains deficient in EcDsbA (JBC817) and EcDsbA and DsbB (JBC818) [58] were transformed with pBAD33-*CtDsbA* and pBAD33-*EcDsbA* and grown on LB agar. Liquid cultures (20 mL) were grown in M63 minimal media lacking cysteine and methionine. Each culture was normalised to an OD_{600} of 1.0. 2 μL culture containing ~10^7 cells was used to carefully inoculate M63 minimal media soft agar in the presence or absence of arabinose (1 mg/mL). Plates were incubated at 37 °C. The zone of motility was measured after approximately 7 h.

2.5.6 Relative stability of oxidised and reduced forms of DsbA

The thermal unfolding of reduced and oxidised CtDsbA was determined using a Jasco J-810 circular dichroism (CD) spectropolarimeter. Measurements were carried out with 10 μM protein in 100 mM NaH_2PO_4/Na_2HPO_4, 0.1 mM EDTA, pH 7.0 in a 1 mm quartz cuvette. The unfolding was monitored as a change in molar ellipticity at 220 nm with a heat rate of 0.5 K/min from 298 K to 398 K. Plotted data shows mean and SD for two biological replicates.

2.5.7 Determination of the redox potential

The standard redox potential of CtDsbA was determined following a shift in electrophoretic mobility upon reduction of the active site disulfide. Samples were prepared with fully oxidised CtDsbA-SSS in degassed 100 mM sodium phosphate pH 7.0, 1 mM EDTA and 20 mM oxidised DTT and varying concentration of DTT (0 µM-16 mM) and equilibrated at 30°C. After 24 hours the reaction was stopped by adding 1/5 of the reaction volume of 10 % 2,4,6-Trichloroanisole (TCA). The precipitated protein was collected by centrifugation at 13,300 g for 10 min at 4 °C. The pellets were washed with 200 µL ice cold 100 % acetone and dissolved in 10 µL 50 mM Tris-HCl pH 7.0, 1 % SDS, 2 mM AMS. The difference in migration between the reduced and oxidised CtDsbA-SSS was determined on a 12 % SDS Bis-Tris PAGE (Life Technologies, USA). The gel was stained and the intensity of the bands were analysed by ImageLab (BIO-RAD) The equilibrium constant K_{eq} and the redox potential E^0 were calculated as described previously [80]. Plotted data shows mean and SD for four biological replicates.

2.5.8 Determination of pK_a of Cys38 of CtDsbA

The pK_a of the nucleophilic active site cysteine, Cys38, of CtDsbA was determined by following the pH-dependent specific absorption of the thiolate anion at 240 nm. The pH-dependent absorbance at 240 nm was measured for the oxidised protein as a reference.

20 µM samples of reduced and oxidised CtDsbA were prepared in 10 mM K_2HPO_4, 10 mM boric acid, 10 mM sodium succinate, 200 mM KCl and 1 mM EDTA over a pH range of 1.6 – 8.0, in a total volume of 200 µL. Absorbance at 240 nm and 280 nm was measured in a Synergy H1 multimode plate reader (Biotek, USA). The pH-dependent absorbance of the thiolate anion was corrected for, buffer absorbance, non-specific absorption at 240 nm and variations in protein concentrations and fitted to the Henderson-Hasselbalch equation

2.5.9 Crystallisation of CtDsbA

CtDsbA was crystallised using The University of Queensland Remote Operated Crystallisation X-ray Facility (UQROCX), the vapour-diffusion method and hanging drops. 96-well plates (200 nL of protein and 200 nL of reservoir solution, against 75 µL reservoir solution) were set using a Mosquito crystallisation robot (TTP Labtech) against commercially available crystallisation screens. All crystallisation experiments were maintained at 298 K. Screening of commercially available

crystallisation screens with CtDsbA at a concentration of 26 mg/mL identified an initial condition (100 mM BisTris propane pH 9.0, 3.1 M potassium formate) that yielded both salt crystals as well as protein crystals. Subsequent investigation of additives was performed in 24-well plates with (2 µL protein and 2 µL crystallisation condition, against a 500 µL reservoir volume) and resulted in an optimised crystallisation condition of 100 mM BisTris propane pH 9.0, 3.1 M Sodium formate and 4 % Tacsimate™.

2.5.10 X-ray data collection, structure solution and refinement

Crystals were cryocooled in liquid nitrogen without additional cryoprotectant. X-ray data were collected at 100 K at UQROCX using a Rigaku FR-E Superbright X-ray generator and a Rigaku Saturn 944 CCD area detector. Data were collected over a 360° rotation at a wavelength of 1.54187 Å. Using the autoPROC software toolbox [205] the data were indexed and integrated with XDS [206], prior to further processing with Pointless and scaling with Aimless [207]. A high resolution limit of 2.7 Å was applied to the data following evaluation of the half-dataset correlation coefficient, R_{meas} and completeness values in Aimless. As a result of this prioritisation, the I/σI value in the highest resolution shell is high (5.9). The space group was determined to be $P2_12_12$ with two copies of CtDsbA in the asymmetric unit. We note that Xtriage analysis flagged L-test anomalies that may stem from data quality deficiencies. Merohedral and pseudo-merohedral twin laws are not possible in this lattice. All phasing and model refinement procedures were implemented within the Phenix software suite. The data were phased using molecular replacement methods with AutoMR using *Bacillus subtilis* BdbD (PDB ID, 3EU3, [79]) as a search model. The search model was prepared for molecular replacement using Sculptor, with additional trimming of predicted loop regions informed by inspection of sequence alignment analysis with CtDsbA. The resulting model was subject to automated building and rebuilding using AutoBuild followed by iterative rounds of refinement (phenix.refine [208]) - including refinement using hydrogen atoms using a riding model - and model building using COOT [209]. The quality of the final model was assessed with Molprobity [210] throughout the refinement process.

The electron density map supported building of an almost continuous model of residues in chain A from residue 6 – 203. There was insufficient density to model residues 133 – 135 inclusive in a loop connecting H4 and H5. Lys16 and Tyr17 on chain A are modeled as alanine as it was not possible to resolve the side chain atoms of either residue satisfactorily. Chain B extends from residues 3 to 203 with breaks from 110 - 111 and 133 - 134 inclusive in two separate loop regions. Both molecules in the asymmetric unit are structurally highly similar, and superpose with a RMSD of 1.08 Å (191

equivalent Cα atoms). Inspection of the structural alignment indicates that the main-chain atoms of all major secondary structure elements superimpose almost exactly. Structural differences between the two molecules are limited to the most N-terminal residues (residues 3 – 18) and several loop regions connecting: B1-B2 (residues 23-28), H2-H3 (residues 88-93), H3-H4 (residues 109-116 and H4-H5 (residues 132-136). As noted above the H4-H5 loop is incomplete in both chains, and the H3-H4 loop is incomplete in chain B. Additionally there are minor deviations in the position of the C-terminal end of H7. Notably the loops that constitute the catalytic surface – including the active site – are structurally equivalent. Further analysis of CtDsbA is restricted to chain B. All figures depict chain B.

There is additional electron density adjacent to the non-catalytic disulfide bridge (Cys 84-Cys 145) suggestive of a small molecule ligand. We attempted to identify this ligand by searching a library of 200 common ligands using the Ligand Identification module in Phenix. This relatively blind search strategy proposed succinic acid (a component of the crystallisation reagent Tacsimate™) as a potential ligand. Refinement of a model including succinic acid resulting in an acceptable fit to the electron density but an elevated R_{free} factor. For comparison we also modelled another potential ligand (2-oxoglutaric acid) identified by the search which we do not believe to have been present during protein purification or crystallisation, and this yielded a similar density fit and elevated R_{free} factor. User guided searching and modelling of other known crystallisation components did not yield a better fitting ligand. In light of the moderate resolution of the data and as we cannot identify a ligand with confidence, this density remains unmodelled.

Data-collection and refinement statistics are summarised in

Table 2.1. The final refined structure has been deposited in the Protein Data Bank (PDB ID 5KBC.) All structural figures were generated using Pymol (PyMOL Molecular Graphics System, version 1.6 Schrodinger, LLC, http://pymol.org) and Adobe Illustrator.

2.6 Results

2.6.1 The *Chlamydia trachomatis* genome encodes a DsbA with multiple cysteine residues.

C. trachomatis DsbA was first identified using a bioinformatic interrogation of all publicly available and complete prokaryotic genomes, using the Complete Microbial Resource at the Craig Venter

Institute and the DsbA sequences from *E. coli*, *S. aureus* and *W. pipientis* as query terms [89]. This analysis returned a single gene in *C. trachomatis* (strain: 434/Bu, serotype: L2) predicted to encode a DsbA-like protein (Gene ID 5858475; UniProt CTL0429) and hereafter referred to as CtDsbA. We note that this gene is currently annotated as DsbG in UniProt, but based on its 15 % sequence identity with EcDsbA, and 20 % and 21 % sequence identity with SaDsbA and *Mycobacterium tuberculosis* DsbA, respectively, we hypothesised that it is in fact a DsbA-like protein. Unlike EcDsbA or SaDsbA, but in common with MtbDsbA, *P. aeruginosa* DsbA2 and WpDsbA1, the predicted CtDsbA encodes additional cysteine residues outside of the active site motif. The full-length encoded CtDsbA protein has six cysteines in total. Bioinformatic analysis using multiple algorithms indicated that CtDsbA has a predicted transmembrane region from residues 11/12 - 28/29. From residue 29 onwards the protein sequence is predicted to face the outside of the cytoplasmic membrane (as described in Materials and Methods). We designed an expression construct restricted to the expected mature soluble CtDsbA protein starting at residue 34 to ensure no inadvertent inclusion of the predicted transmembrane helix. This construct has five cysteines.

2.6.2 CtDsbA catalyses the reduction of insulin

To investigate CtDsbA activity we first evaluated its redox activity in the classic insulin reduction assay. Isomerases such as EcDsbC catalyse this reaction very rapidly whereas oxidases, such as EcDsbA, catalyse the reaction much more slowly. We found that CtDsbA is able to catalyse the reduction of insulin more slowly than EcDsbA and EcDsbC (Figure 2.1A). The weak insulin reduction activity of CtDsbA relative to EcDsbC suggests that CtDsbA is more likely to be an oxidase than isomerase or reductase.

2.6.3 CtDsbA has oxidase activity in vitro

The oxidase activity of CtDsbA was further investigated by its ability to oxidise a fluorescently labelled peptide substrate containing two cysteine residues. Like EcDsbA, CtDsbA was able to oxidise the model peptide substrate but a similar response required a concentration of CtDsbA four times that of EcDsbA (Figure 2.1B). At equivalent concentrations, the activity of CtDsbA is similar to the DsbA-IIb protein, WpDsbA1 but markedly less than that of the DsbA-IIa protein MtbDsbA. These results indicate that CtDsbA has oxidase activity in this assay, but either is intrinsically less active than EcDsbA and the class IIa protein MtbDsbA or does not interact with the substrate as avidly as EcDsbA and MtbDsbA.

Figure 2.1 Biochemical characterisation of CtDsbA.

A) *Reduction of insulin (131 µM) was measured as increase in absorbance at 650 nm in 0.1 mM sodium phosphate buffer, pH 7, 2 mM EDTA. The reaction was performed in the absence (■) or presence of 10 µM EcDsbC (●), EcDsbA (♦) or CtDsbA (○). Representative data are shown for the absence and presence of 10 µM EcDsbA. Mean and SD are shown for two biological replicates (three biological replicates for CtDsbA).* ***B)*** *80 nM EcDsbA (▼) and 320 nM CtDsbA (●), MtbDsbA (■) and WpDsbA1 (▲) oxidise a fluorescently labeled protein in the presence of 2 mM GSSG. GSSG shows only limited oxidising activity in the absence of a DsbA protein (♦). The buffer only control (○) shows no oxidising activity. For MtbDsbA, WpDsbA1, EcDsbA and CtDsbA mean and SD of two biological replicates are shown (for each biological replicate, four technical replicates were performed). For the buffer and GSSG only controls, mean and SD for four technical replicates are shown.* ***C)*** *Isomerase activity was assessed as the ability to refold scrambled RNAseA. ScRNase (40 µM) was incubated in 0.1 M sodium phosphate buffer pH 7.0,1 mM EDTA, 10 µM DTT in the absence and presence of 10 µM EcDsbA (■), EcDsbC (○) and CtDsbA (●). RNase activity was monitored as the cleavage of cCMP which leads to an increase in absorbance at 296 nm. Mean and SD for three biological replicates is shown for CtDsbA. EcDsbC and EcDsbA is able to restore ~80 % and ~20 % of RNaseA activity, which is equivalent to what has been reported previously [84].* ***D)*** *Temperature induced unfolding of oxidised (○) and reduced (●) CtDsbA was determined by far UV CD spectroscopy. The thermal unfolding of CtDsbA results in an increase in molar ellipticity at 220 nm showing that the reduced form of CtDsbA is more stable than the oxidised form. Mean and SD are shown for two biological replicates.*

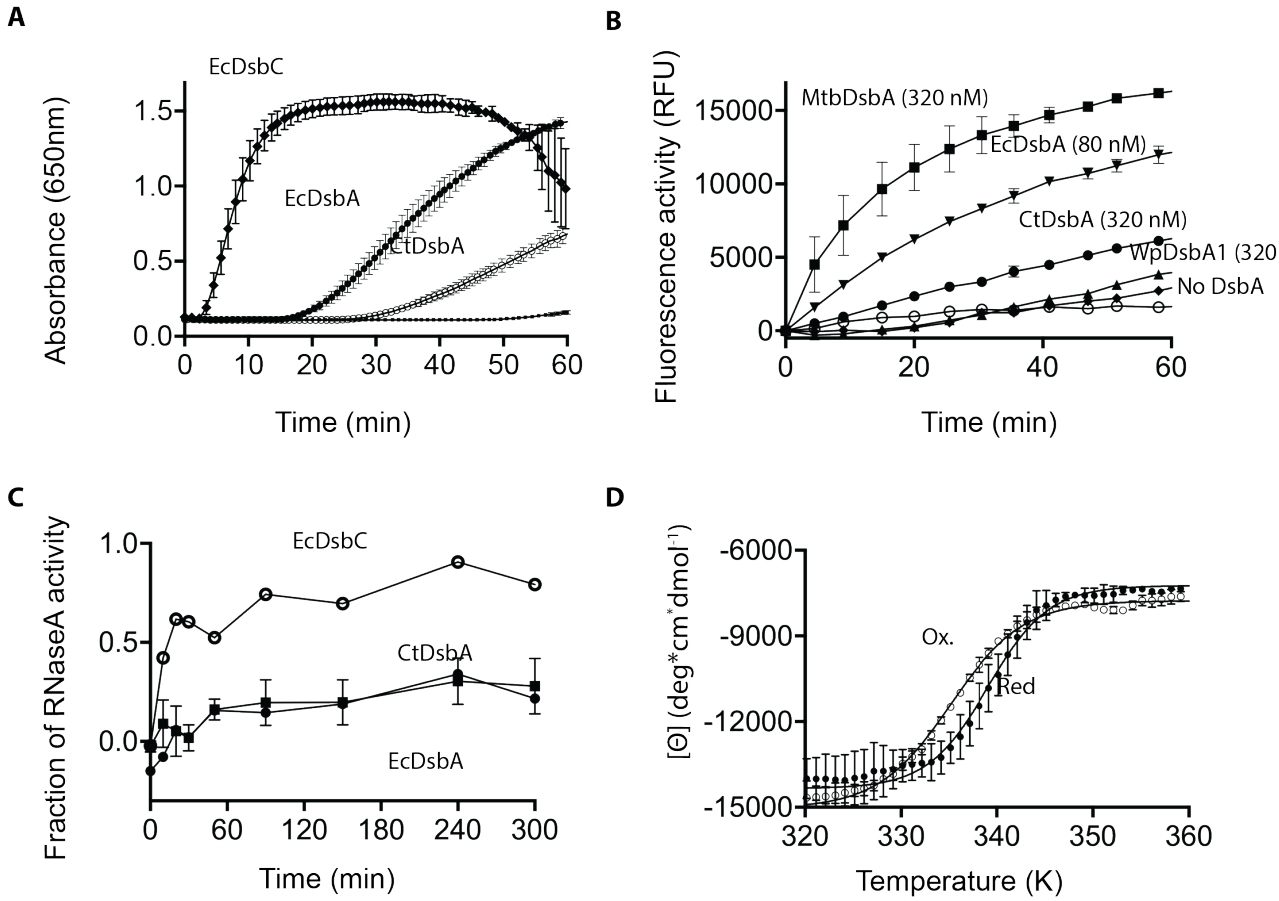

2.6.4 CtDsbA does not have isomerase activity in the scrambled RNase assay

To determine whether CtDsbA has disulfide isomerase activity we measured the ability of CtDsbA to isomerise the non-native disulfide bonds of scrambled RNaseA (ScRNaseA). Whereas the isomerase EcDsbC was able to restore about 80 % of RNaseA activity over the course of the experiment, CtDsbA was only able to restore approximately 20 % of RnaseA activity in this same time period (Figure 2.1C); this is comparable to the activity of the oxidase EcDsbA. Together these data indicate that CtDsbA does not have isomerase activity and behaves more like an oxidase in this assay.

2.6.5 The active site disulfide in CtDsbA is destabilising

The disulfide bond in DsbA proteins is typically destabilising, in contrast to most proteins where disulfide bonds generally confer stability. We found that CtDsbA also has a destabilising disulfide as the melting temperature (T_m) for the reduced form (339.1 K ± 0.2) is 4 K greater than the oxidised form (335.1 K ± 0.1) (Figure 2.1D).

2.6.6 CtDsbA is less oxidising than *E. coli* DsbA

The redox potential of CtDsbA in equilibrium with DTT was determined by monitoring the difference in electrophoretic mobility between the reduced and oxidised form (Figure 2.2). To measure the redox potential of the active site disulfide, we used the CtDsbA-SSS construct that only contains the two cysteines in the active site. We found a K_{eq} of $3.7 \pm 0.8 \times 10^{-4}$ M corresponding to a redox potential of -229 mV. This makes CtDsbA a much weaker oxidase than EcDsbA (E° -122 mV) and to our knowledge, the most reducing DsbA characterised to date.

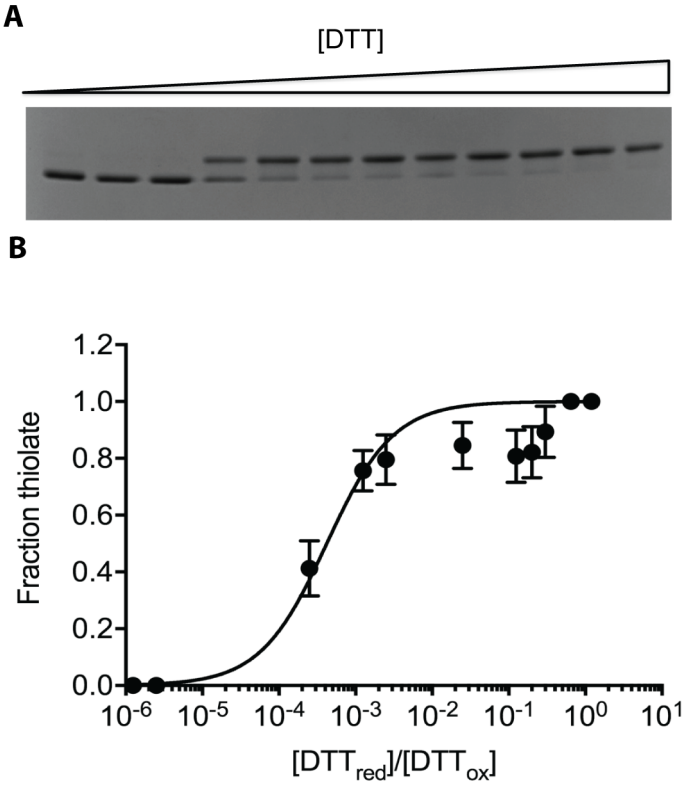

Figure 2.2 Redox potential determination for CtDsbA-SSS by electrophoretic motility shift.
A) *SDS-PAGE gel of oxidised CtDsbA (3 µM) incubated for 24 h with increasing concentration of DTT (0 µM -12 mM).* ***B)*** *The fraction of thiolate as a function of reduced DTT versus oxidised DTT is plotted. Fitting of the data revealed a Keq of 3.8 ± 0.8 x 10^{-4} M equivalent to a redox potential of -229 mV. Mean and SD calculated from 4 biological replicates are plotted.*

2.6.7 CtDsbA cannot rescue deletion of *dsbA* in *E. coli*

Deletion of the *dsbA* gene leads to pleiotropic phenotypes in *E. coli* [58]. One phenotype associated with DsbA-deficient *E. coli* is the loss of motility due to a failure to assemble functional flagella [211]. CtDsbA was expressed in Δ*dsbA* and Δ*dsbA/dsbB* backgrounds to determine if CtDsbA can complement EcDsbA. Exogenous expression of EcDsbA restored motility in Δ*dsbA E. coli* on soft

agar (zone of motility 21 mm in comparison to 6 mm in the uninduced control; Figure 2.3) but as expected could not rescue the phenotype in Δ*dsbA/dsbB* bacteria. Expression of CtDsbA did not restore motility in either the Δ*dsbA or* Δ*dsbA/dsbB* bacteria, suggesting that CtDsbA cannot complement EcDsbA deficiency in *E. coli.*

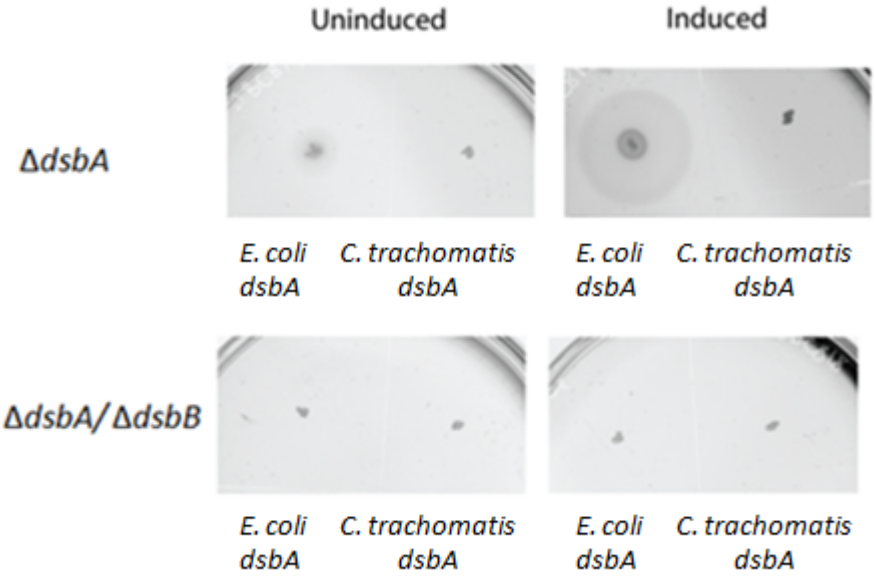

Figure 2.3 CtDsbA does not complement EcDsbA.

dsbA *null* E. coli *are unable to swarm on soft agar. Exogenous expression of EcDsbA under an arabinose inducible promoter is able to complement this non-motile phenotype as shown by the swarming halo around the original inoculation point (upper panel, EcDsbA induced). CtDsbA is not able to restore the phenotype. Neither EcDsbA nor CtDsbA is able to restore mobility in a ecdsbA/ecdsbB double null* E. coli *strain (lower panels) indicating the requirement for EcDsbB to maintain a pool of oxidised DsbA.*

2.6.8 The crystal structure of CtDsbA features an uncommon dipeptide catalytic motif

We solved the crystal structure of CtDsbA, which was determined to 2.7 Å resolution by using molecular replacement methods. The resulting model was refined to a final R_{factor} and R_{free} of 24.8 % and 28.2 %, respectively. Full details of data collection and refinement parameters, and additional model quality indicators can be found in Table 2.1.

Table 2.1 X-ray data measurement and refinement statistics for CtDsbA

Data collection and processing	
Wavelength (Å)	1.54187
Resolution range (Å)	43.3-2.7 (2.8-2.7)
Space group	P 2_1 2_1 2
Unit cell (Å, °)	92.2 98.1 44.8 90.0 90.0 90.0
Rmerge	0.101 (0.401)
Rmeas (within I+/I-)	0.110 (0.429)
Rmeas (all I+ & I-)	0.109 (0.432)
Total number of observations	82358 (737)
Total number unique	11646 (102)
Mean((I)/sd(I))	19.6 (5.9)
Mn(I) half-set correlation CC(1/2)	0.998 (0.880)
Completeness (%)	100 (86.4)
Multiplicity	7.1 (7.2)
Refinement and model quality	
Refinement	
R-factor (%)	24.76 (30.84)
R-free (%)	28.23 (38.54)
Number of atoms	6176
Macromolecules	3083
Ligands	
Water	22
Protein residues	390
R.M.S.D from ideal geometry	
RMS(bonds) (Å)	0.003
RMS(angles) (°)	0.69
Molprobity analysis	
Ramachandran favored (%)	96.84
Ramachandran outliers (%)	0.26
Clashscore*	6.36 (100^{th} percentile* (N=186, 2.706 Å ± 0.25Å))
Molprobity score**	1.74 (100^{th} percentile* (N=5290, 2.706 Å ± 0.25Å)
Average B-factor ($Å^2$)	45.90
Macromolecules	45.90
Solvent	44.20

Values in parentheses refer to the highest resolution shell

‡ $Rfactor = \sum_h \left| |F_{obs}|_h - |F_{calc}|_h \right| / \sum_h |F_{obs}|_h$, *where* h *defines the unique reflections*

§ R_{free} *calculated over 5.0 % of total reflections excluded from refinement*

** Clashscore: 100th percentile is the best among structures of comparable resolution; 0th percentile is the worst. For clashscore the comparative set of structures was selected in 2004, for MolProbity score in 2006*

*** MolProbity score combines the clashscore, rotamer, and Ramachandran evaluations into a single score, normalised to be on the same scale as X-ray resolution.*

Consistent with all structurally characterised DsbA proteins, CtDsbA comprises a thioredoxin domain into which a second helical domain is inserted (Figure 2.4A). The catalytic face of DsbA proteins is composed of a canonical Cys-Xaa-Xaa-Cys motif (where Xaa is any amino acid) positioned at the N-terminal end of H1, and three additional neighboring loops: Loop 1 (linking B3 and H2), the so-called *cis*Pro Loop 2 (linking H6 and B4) and Loop 3 (linking B5 and H7) (Figure 2.4A). Together these loops determine DsbA enzymatic activity, modulate redox character and govern interactions with both substrate proteins and the redox partner protein DsbB [195].

In CtDsbA, the active site motif is Cys-Ser-Ala-Cys (Figure 2.4B). Commonly the active site motif of DsbA proteins features a Pro at the X_1 position: 78 % of DsbA proteins identified in prokaryotic genomes have a Pro at this position [89]. Furthermore the active site motif commonly includes an aromatic, polar or positively charged side chain at position X_2 (just 13 % of DsbA proteins identified in prokaryotic genomes lack such a residue at this position [89]). Via extensive mutational and biochemical analyses it has been established that the dipeptide sequence is a very important – although not the sole - determinant of thiol-disulfide oxidoreductase potential and function [71, 212, 213]. CtDsbAs dipeptide sequence is notable in that it lacks a Pro at X_1 and has a non-polar aliphatic residue (Ala) at X_2. This is the first structural description of such an active site configuration. In the crystal structure Cys38 and Cys41 are oxidised, with a disulfide bond length of 2.03 Å (Figure 2.4B). This is unusual in that X-ray crystal structures of oxidised DsbA proteins often capture a radiation-induced reduced state (e.g. [57]). The electron density maps for CtDsbA clearly support the presence of the oxidised form (Figure 2.4C).

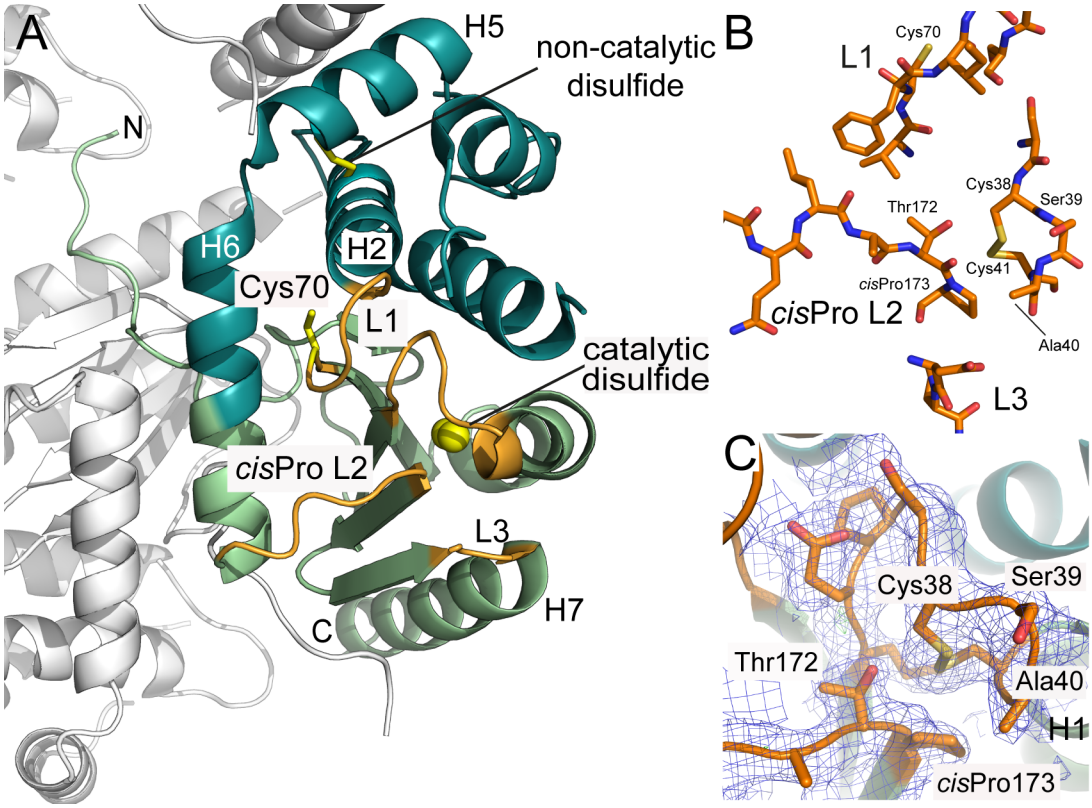

Figure 2.4 Crystal structure of CtDsbA.

A) *The crystal structure of CtDsbA contains a thioredoxin domain (light green) and a helical domain (dark green.) Loops on the catalytic surface that constitute the active site of CtDsbA and determine redox activity are colored orange and labeled. The active site catalytic disulfide is highlighted with sulfurs shown as yellow spheres. The non-catalytic disulfide (between Cys84 and Cys145) and the single thiol (Cys70) in L1 are shown in stick representation. The most N-terminal region of CtDsbA is unstructured. Crystal packing interactions with the second monomer in the asymmetric unit and a symmetry related molecule (shown in white) stabilise this region of the protein such that is well resolved in the electron density map.* ***B)*** *Close view of the four loops (L1, cisPro L2, L3 and the Cys-Ser-Ala-Cys motif) which constitute the active site surface of CtDsbA.* ***C)*** *In the crystal structure the active site cysteines are oxidised. Analysis of bond distances indicates that the Cys 38 thiolate could be stabilised by favorable bond interactions with Thr 172 (3.4 Å between Thr 172 OH and Cys 38 SG in the oxidised structure) of the neighboring cisPro L2 consistent with an oxidising protein character. The Cys 41 sulfur atom is 3.5 Å from the Thr 172 hydroxyl in the oxidised structure. 2Fo-Fc and Fo-Fc electron density maps for the active site and cisPro Loop 2 were generated from calculated phases using phenix.maps and are shown contoured at 1.0 σ and 3.0 σ respectively. The maps are shown within a 1 Å radius of each atom of each loop.*

Spatially close to the active site CSAC motif is the cisPro L2 loop (3) (Ala-Thr-*cis*Pro) connecting H6 and B4. This motif (typically Xaa-Val/Thr-cisPro, where Xaa is usually an aliphatic residue) is very highly conserved among DsbA homologs and is critical for activity. In the oxidised CtDsbA structure the Cys 38 sulfur atom is 3.6 Å from the carbonyl oxygen and 3.3 Å from the side chain hydroxyl of the cisPro-1 residue Thr 172 (Figure 2.4C). As with other DsbA proteins, it is conceivable that in the reduced form these atoms may facilitate hydrogen bond mediated stabilisation of the enzyme. We note that the Cys 38 sulfur is 3.3 Å from the side chain hydroxyl of Thr 172, which is within the range of observed atomic distances (3.1 – 4.6 Å) for DsbA proteins [96].

L1 and L3 play a role in partner protein interaction in other DsbA proteins. In CtDsbA L1 is 7 residues in length (Val-Cys-Phe-Ile-Arg-Gly-Ser) and is oriented towards the active site. Notably L1 contains an unpaired cysteine residue, which to our knowledge is the first structural report of an unpaired cysteine in a surface loop adjacent to the active site in DsbA (Figure 2.4). In EcDsbA, Loop 1 residues contribute to the binding interface with EcDsbB. In particular when Met 64, located in the middle of EcDsbA L1, is mutated to Ala the K_M of the DsbA-DsbB interaction is significantly increased [64]. In CtDsbA, Cys 70 is positioned at the C-terminus of the B3 strand, and directed towards Ser 75 and Met 76 of the adjacent H2; as the side chain of Cys 70 is relatively buried in comparison to Cys 38 it is unlikely to play a role in interaction with substrate or redox partner proteins unless this loop undergoes a significant conformational change during the catalytic cycle. Finally CtDsbA Loop 3, connecting B5 and H7 is short (Asp_{184}-Pro_{185}-Tyr_{186}) and adopts a tight turn facilitated in part by the central proline residue.

2.6.9 CtDsbA has a negatively charged catalytic surface without significant pockets

Unlike EcDsbA and other enterobacteriaciae DsbA proteins, CtDsbA does not have a pronounced groove along its active site surface, nor are there notable pockets adjacent to the active site (Figure 2.5A). Small discrete pockets are present on the non-catalytic face sandwiched between H1 and H3 (pocket 1), and formed between the long N-terminal extension and H6 (pocket 2) (Figure 2.5A). Inspection of the electrostatic potential of the active site surface indicates it to be predominantly acidic. Of particular note is the highly acidic patch immediately adjacent to the active site cysteines on the catalytic surface (Figure 2.5B).

Figure 2.5 Surface properties of CtDsbA.

A) *Surface representation for CtDsbA of the catalytic (left) and non-catalytic (right) faces. The active site residues Cys-Ser-Ala-Cys are colored yellow and the nucleophilic cysteine sulfur highlighted in orange. Pockets formed on the posterior face of the protein between H1 and H3 (pocket 1) and the N-terminal unstructured region and H6 (pocket 2) are labeled.* ***B)*** *Electrostatic surface representation of CtDsbA. Views are oriented as above. Electrostatic surface potential is contoured between -5 (red) and +5 (blue) kT/e. The nucleophilic cysteine is annotated with an S.*

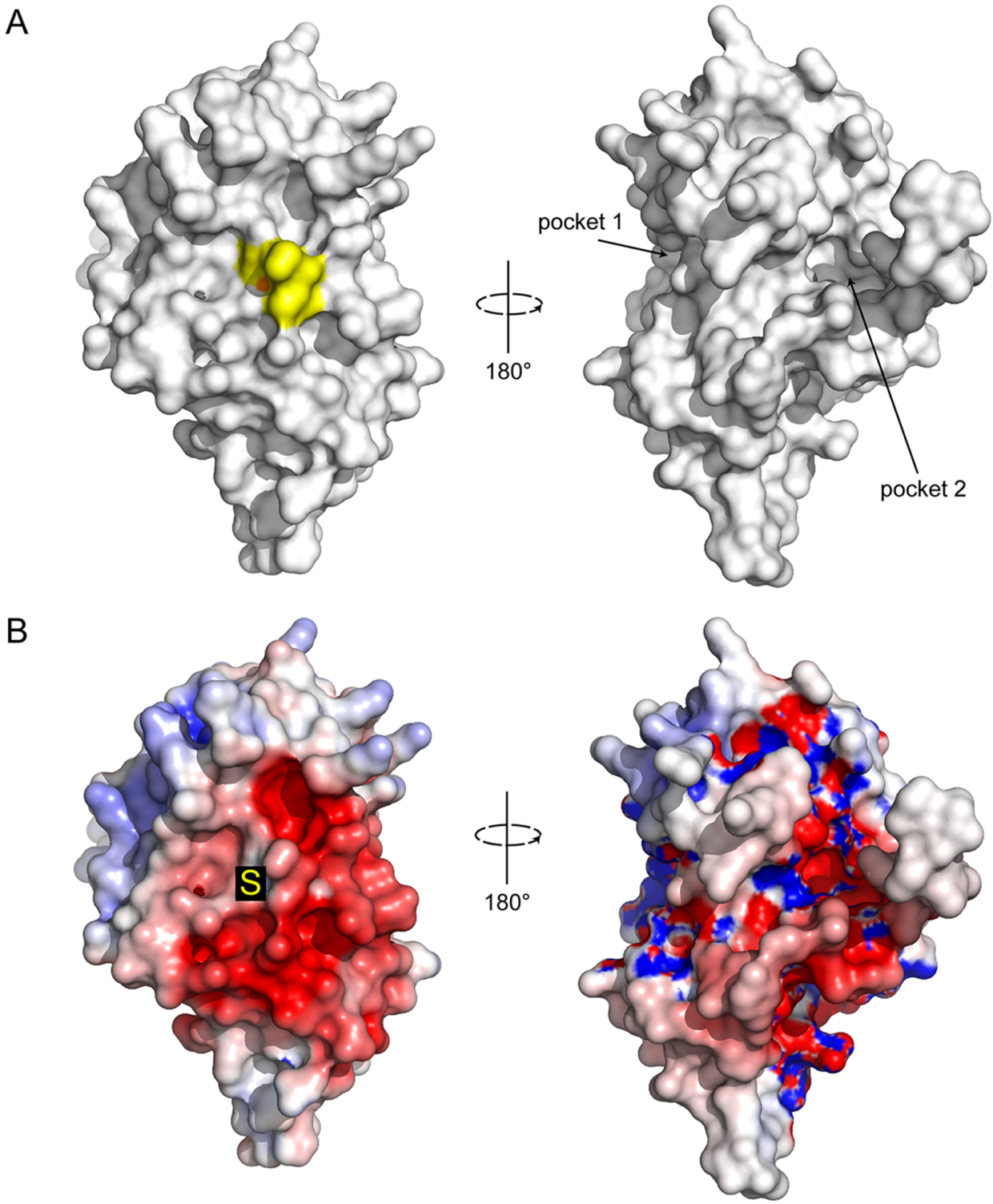

2.6.10 CtDsbA has a second non-catalytic disulfide bond

Notably CtDsbA has a second disulfide bridge formed between Cys 84 (H2) and Cys 145 (H5) stapling this helical bundle (Figure 2.4A and Figure 2.6). A similar non-catalytic disulfide has been observed previously in the structures of WpDsbA1 [80], MtbDsbA [78] and PaDsbA2 [75]. Superposition of these four structures reveals that the position of this non-catalytic disulfide is highly similar among these four structures in each case linking equivalent helices (Figure 2.6).

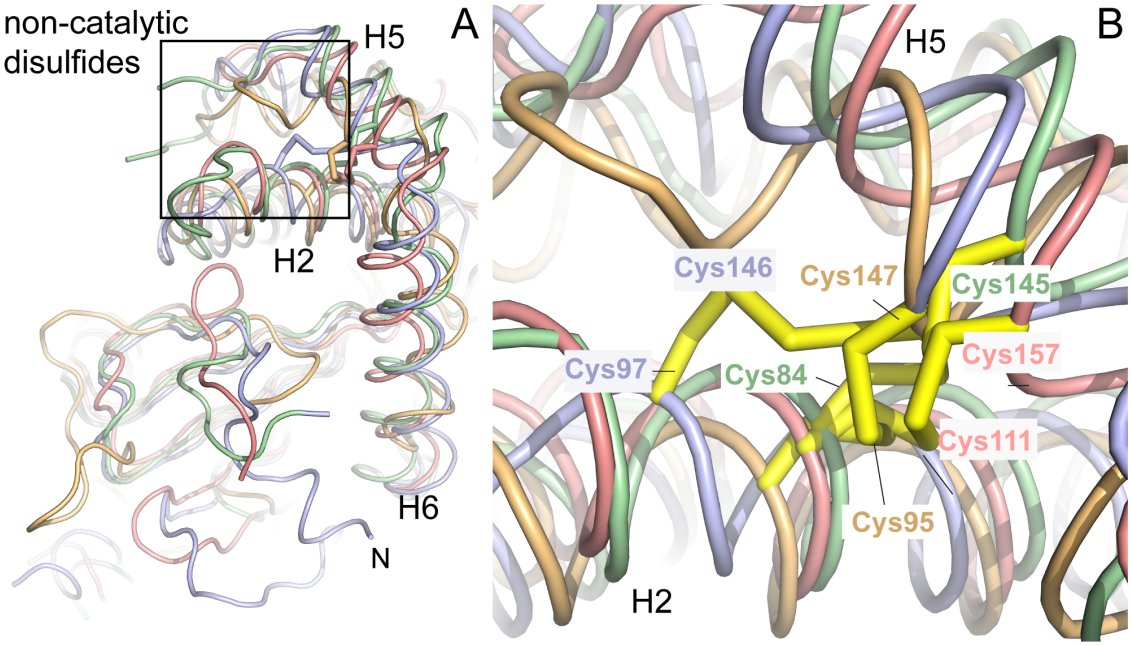

Figure 2.6 CtDsbA has a second non–catalytic disulfide bond.

A) *CtDsbA (green) is structurally most similar to WpDsbA1 (light blue), MtbDsbA (pink) and PaDsbA2 (orange) although it features an extended N-terminal unstructured region and lacks an additional eighth C-terminal helix present in MtbDsbA (not visible in this orientation.) Each of the four structures has a second non-catalytic disulfide bond which are very similarly positioned bracing H2 and H5 (or equivalent helices in PaDsbA2), the location of which is highlighted by a rectangular box. For clarity, depth cueing has been applied to focus on the foreground of the superimposed structures.* ***B)*** *Enlarged view of H2 and H5 and the non-catalytic disulfide bonds in each of the four superimposed structures. The view is oriented as in the rectangular box in panel A.*

CtDsbA is the fourth structure of a DsbA protein with a second (structural) disulfide bond, permitting a detailed examination of these enzymes as a group. Overall the sequence identity of CtDsbA, WpDsbA1, PaDsbA2 and MtbDsbA is modest (15-2 %; Figure 2.7, Table 2.2) The *cis*Pro Ala-Thr-Pro motif is conserved among the four proteins but the active site dipeptide is different in each and there is only limited sequence similarity in the residues immediately following the non-catalytic

cysteines. Structurally they are similar overall, superimposing on CtDsbA with a RMSD of 2.5 - 2.6 Å (for 163-176 equivalent Cα atoms) (Table 2.2) although MtbDsbA is distinct at its C-terminus where it has an additional and unique eighth helix. Aside from this, structural differences are confined to loop regions. CtDsbA has a particularly extended and disordered C-terminus and two elongated loop regions: residues 128-137 linking H4 and H5, and 88-94 linking H2 and H3 relative to the other proteins. These loops are aligned in a parallel manner adjacent to one another creating a horse shape protrusion on the back of the protein, encasing a number of small pockets.

2.6.11 Classification of CtDsbA

DsbA proteins have previously been segregated into distinct structural classes [96]. Assignment to one of the two major classes (DsbA-I and DsbA-II) is defined primarily by the β-sheet topology of the thioredoxin domain [96]. In the thioredoxin domain of CtDsbA, B1 hydrogen bonds to B3 to give a β-sheet topology of 1-3-2-4-5, assigning CtDsbA to the DsbA-II enzyme class. Previously identified members of DsbA-II include DsbA from the Gram positive species *S. aureus* and *B. subtilis*, the acid fast bacteria *M. tuberculosis* and the endosymbiont Gram negative species *W. pipientis*. Consistent with its assignment to DsbA-II, interrogation of the Protein Data Bank using DaliLite [214] identified that CtDsbA is structurally similar to the DsbA-II proteins *B. subtilis* BdbD (PDB ID 3EU3, 1.9 Å rmsd, 28 % sequence identity) and *W. pipientis* DsbA1 (PDB ID 3F4R, 2.3 Å rmsd, 20 % sequence identity) as well as PaDsbA2 (PDB ID 4N30, 2.6 Å rmsd, 15 % sequence identity) which although not previously classified also shares the β-sheet topology of other DsbA-II proteins and a second non-catalytic disulfide bond observed in 3 of the 4 previously assigned DsbA-II proteins (Figure 2.4, Table 2.2)

			Reference protein - CtDsbA						
			Identity	TM-score	RMSD (Cα)	CXXC	L1	cisPro L2	L3
Bacterium	DsbA	PDB ID							
C. trachomatis	CtDsbA	This study	-	-	-	EEPSCSAC	VCFIRGS	ITATP	DPT
P. aeruginosa	PaDsbA2	4N30	15	0.728	2.49 (168)	ADLECPFC	NMHG	ITATP	MAD
W. pipientis	WpDsbA1	3F4R	20	0.773	2.57 (176)	ASLTCYHC	FPLDY	ITATP	GGYK
M. tuberculosis	MtbDsbA	4K6X	21	0.699	2.63 (163)	EDFLCPAC	AILDSA	VHATP	IFNNG
E. coli	EcDsbA	1FVK	15	0.598	3.45 (153)	FSFFCPHC	NFMGGC	LRGVP	NPQGMDTSN

Table 2.2 CtDsbA is structurally similar to other DsbA proteins containing a second disulfide bond.

Structural comparison of CtDsbA to three other DsbA proteins that also contain a second disulfide bond (PaDsbA2, WpDsbA1 and MtbDsbA) and the canonical single disulfide containing EcDsbA. Structures were aligned to the reference CtDsbA protein using TM-align. The resulting template modeling score (TM-score) and root mean squared deviation (RMSD, for which the equivalent number of Cα atoms involved in the structural alignment is given in parenthesis) are tabulated. TM-score is a quantitative measure of similarity between two proteins independent of their length (a TM-score >0.5 generally corresponds to the same fold in SCOP; a score closer to 1.0 implies that they are highly similar.) Sequences of the catalytic motifs and loops on the catalytic face of each protein are also detailed. Note that the sequences of the highly variable L3 loop are not aligned.

2.7 Discussion

In the present study we demonstrate that the *C. trachomatis* encodes a DsbA protein (Gene ID 5858475 (UniProt CTL0429), which has oxidase activity and the structural features of a DsbA-II type protein. The weak activity of CtDsbA in the insulin reduction assay relative to EcDsbC, suggests that CtDsbA is a thiol disulfide oxidase and not an isomerase. Consistent with this, CtDsbA is able to oxidise the folding of a model peptide substrate *in vitro*, albeit less efficiently than the canonical oxidase EcDsbA. Our finding that CtDsbA is significantly less active than the isomerase EcDsbC in the ScRNase assay further supports the assertion that CtDsbA is an oxidase without disulfide isomerase activity.

Heterologous complementation studies shows that CtDsbA is not able to complement *EcDsbA* deficient *E. coli.* However this is not unprecedented among DsbA proteins. The DsbA-II proteins MtbDsbA and WpDsbA1, as well as the DsbA-Ib protein *N. meningitis* DsbA3 (NmDsbA3) are all DsbA proteins that are not able to complement EcDsbA deficiency. In common with CtDsbA these proteins are relatively structurally distinct from EcDsbA (RMSD between 2.76 and 3.71 Å, over 152-175 Cα atoms). Successful rescue of function relies upon an ability of the exogenous DsbA to interact with both the substrate flagella proteins and EcDsbB. The observed structural diversity may preclude one or both interactions and explain why they are not able to rescue DsbA activity in *dsbA* deficient *E. coli.*

Whilst DsbAs can be broadly very similar in their structure and function, the redox character of individual enzymes can vary considerably [195]. Like other DsbA proteins CtDsbA active site has a destabilising disulfide bond that lowers the melting temperature of the oxidised protein by 4 K relative to the reduced state. T_m differences between oxidised and reduced DsbAs range from 1 (SaDsbA) to 15 K (NmDsbA1) (Table 2.3). This puts CtDsbA at the lower end of the range of a destabilising disulfide placing it between SaDsbA, which, with a ΔT_m of 1 K has a melting temperature that is barely affected by oxidation [62], and WpDsbA1 with a ΔT_m of 6 K. Furthermore it suggests that the destabilising effect of oxidation in CtDsbA is relatively mild compared to that of the enterobacterial DsbAs (ΔT_m of 8 – 12 K for EcDsbA, SeDsbA and KpDsbA) or NmDsbA1 (ΔT_m 15 K). The redox potential of CtDsbA is -229 mV. This is substantially less oxidising than that of EcDsbA (-122 mV) and is to our knowledge, the most reducing redox potential reported for a DsbA protein. It is most similar to the redox potential of WpDsbA1 (-163 mV), and approaches that of the reducing enzyme thioredoxin (-270 mV, [215, 216].

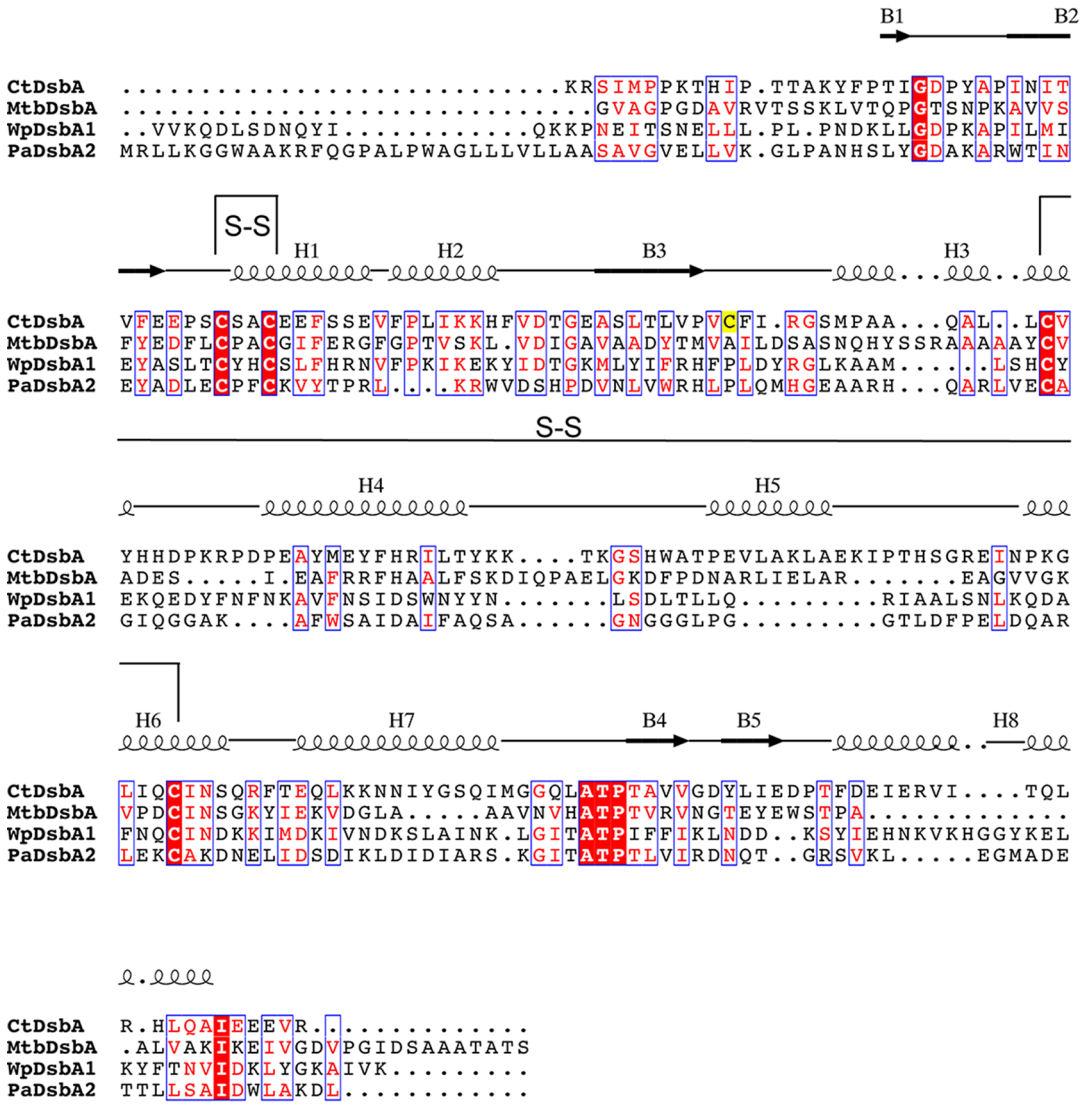

Figure 2.7 Sequence alignment of DsbAs with two disulfide bonds.

Sequence alignment of structurally characterised DsbAs with two disulfide bonds. Sequences were aligned using Clustal Omega and visualised using ESPript 3.0 [217]. Secondary structural elements are shown for the structure of CtDsbA. Disulfide bonds are indicated with black connecting lines and labeled S-S. The single unpaired cysteine C70 is highlighted in yellow.

The reactivity of DsbA proteins is greatly influenced by the pK_a of the nucleophilic active site cysteine. In reduced EcDsbA the thiol group of the surface exposed Cys 30 has a pK_a of 3.3 [192] which is notably lower than the typical value for a cysteine residue (~8.5). Preliminary experiments indicate that the pK_a of the nucleophilic cysteine in CtDsbA is slightly higher than that of EcDsbA. This observation is based on a single experiment (described in Methods) that could not be reliably repeated due to the instability of oxidised CtDsbA below pH 7. Thus the pK_a of the nucleophilic active site cysteine Cys38 in CtDsbA has not been determined. The interatomic distances suggests that the thiolate anion is somewhat stabilised by hydrogen bond interactions with the Cys41 amide N (2.8 Å in the oxidised structure) and the active site dipeptide X_2 Ala40 amide N (3.6 Å distance in

the oxidised structure, Figure 2.4C) as is observed in other DsbA proteins (summarised in [96]). However, the primary factor stabilising the nucleophilic thiolate in dithiol oxidoreductases is the N-helix dipole of H1 [71, 218], which is very sensitive to the microenvironment of the helix terminus.

Table 2.3 Comparison of melting temperatures, pK_a and redox potential of different DsbA proteins

	T_m(K) reduced	T_m (K) oxidised	p*K*a	K_{eq} (M)	E° (mV)
EcDsbA [70, 192]	350.9 ± 0.2	341.7 ± 0.2	3.3 ± 0.09	$8.1 \pm 0.2 \times 10^{-5}$	-122
SeDsbA [195]	351.2 ± 0.2	342.8 ± 0.4	3.3 ± 0.06	$12.8 \pm 0.3 \times 10^{-5}$	-126
KpDsbA [78]	347.1 ± 0.2	335.8 ± 0.3	3.2	$6.14 \pm 0.1 \times 10^{-5}$	-116
VcDsbA [76],[219]	357 ± 0.2	346 ± 0.2	5.1	$7.7 \pm 0.03 \times 10^{-5}$	-116
NmDsbA1 [77]	348 ± 2	333 ± 2	3.0	3.7×10^{-6}	-79
SaDsbA [84]	345.1 ± 0.08	345.6 ± 0.09	3.4 ± 0.07	$2.09 \pm 0.27 \times 10^{-4}$	-131
MtbDsbA [78]	ND	ND	4.2 ± 0.2	$17.37 \pm 0.1 \times 10^{-6}$	-99
WpDsbA1 [80]	337 ± 0.05	331 ± 0.05	4.7 ± 0.08	$2.2 \pm 0.27 \times 10^{-3}$	-163
CtDsbA	339 ± 0.2	335 ± 0.1	ND	$3.7 \pm 0.8 \times 10^{-4}$	-229

Errors are provided were available. ND Not determined.

Notably an uncharged aliphatic Ala at position X_2 of the active site dipeptide in CtDsbA would not destabilise the N-helix dipole as per His 32 in EcDsbA [218]. Nor can it offer direct electrostatic stabilisation of the thiolate anion as per a basic [63] or aromatic amino acid (via a sulfur-aromatic ring interaction [213] at this position). Similarly the lack of a helix breaking proline in the active site dipeptide removes enhancement of the H1 dipole proposed to occur in other more oxidising DsbA proteins [69, 213]. Together the apparent lack of factors in CtDsbA to destabilise the oxidised form of the protein, or conversely to stabilise the nucleophilic thiolate in the reduced state, is consistent with both the relatively small difference in T_m between oxidised and reduced CtDsbA, and the less oxidising redox potential relative to EcDsbA and other CPHC dipeptide containing DsbA proteins.

CtDsbA, WpDsbA1, PaDsbA2 and MtbDsbA all have a non-catalytic disulfide in the helical domain, in addition to the active site catalytic disulfide [75, 78, 80]. The functional consequence of the second disulfide bond in CtDsbA is unknown but in WpDsbA1 it may play a regulatory role by autoinhibiting its reoxidation by WpDsbB (25). In PaDsbA2 it is reported to influence the redox potential of the active site cysteines [75] as mutation of the second disulfide results in reduction of redox potential from -67 mV to -118 mV [75]. However, this is not the case in WpDsbA1 where deletion of the additional cysteines has a very modest effect on redox potential (-170 mV for wild-type and -163 mV for the mutant [80]), although it is associated with a small increase in the pK_a (pK_a of 4.7 for the wild-type and 5.0 for the mutant) of the nucleophilic cysteine [80]. MtbDsbA and wild-type PaDsbA2 have strongly oxidising redox potentials (-99 mV and -67 mV respectively) whereas WpDsbA1 and CtDsbA are the two most reducing DsbA proteins characterised to date. Together this suggests that the second disulfide is not a significant modifier of redox potential for enzymes containing two disulfides. Instead it is more likely that differences in redox character are a composite of contributing factors including the nature of the dipeptide sequence in the catalytic motif.

In the present study, we used a recombinant expression construct with five cysteines (one unpaired). In the full-length gene there is an additional cysteine in a predicted transmembrane region. In light of the predicted location of the additional cysteine, and the relative inaccessibility of the unpaired Cys 70 it appears unlikely that the N-terminal transmembrane cysteine and Cys 70 would interact with one another in the native protein. The high cysteine content is notable relative to other DsbAs, and may be a feature of chlamydial DSB proteins more generally; *Chlamydia pneumoniae* DsbH, a reducing dithiol oxidoreductase with structural similarity to thioredoxin and EcDsbDγ has seven cysteine residues, of which only two are engaged in a disulfide bond [107]. Interestingly the chlamydial proteome has striking cysteine and disulfide features more generally; for example, during its unique developmental cycle the bacteria adopt an extracellular infectious form called an

elementary body which is encapsulated by a highly complex envelope of disulfide cross linked proteins [146]. Upon infection of a host cell, these disulfide bonded proteins are reduced and the elementary body differentiates into reticulate bodies [146]. Additionally, a greater proportion of secreted proteins in *C. pneumoniae* have an unpaired number of cysteines (57 %) compared to that of *E. coli* (39 %*)*. This has led to a hypothesis that chlamydial species may maintain a particularly reducing periplasmic environment in order to prevent misfolding of cysteine rich proteins. If so, this may be supported in *C. trachomatis* by the relatively low redox potential of CtDsbA.

Based on its topology we assign CtDsbA to the DsbA-II class of enzymes. DsbA-II type enzymes can be further separated into two sub-divisions (DsbA-IIa and DsbA-IIb) on the basis of catalytic surface loop configurations and surface features. The archetypal DsbA-IIa protein is MtbDsbA in which Loop 1 is oriented towards the active site motif and the protein surface is decorated with negative potential [96]. Until now WpDsbA1 has been the single representative member of the DsbA-IIb subdivision distinguished primarily from DsbA-IIa by its strikingly positive electrostatic potential around the active site, and Gram negative origin. Notably the L1 configuration in DsbA-IIb also points towards the active site; and the same conformation is adopted in CtDsbA. Similar to currently identified DsbA-II proteins the surface of CtDsbA lacks the canonical grooves observed in DsbA-I (either along the catalytic surface (DsbA-Ia) or the posterior face of the protein (more typical of DsbA-Ib.) CtDsbA is strikingly charged near its active site with a pronounced patch of negative potential in this region. Taken together the structural features of CtDsbA and similarity to other DsbA-II proteins do not definitively assign CtDsbA to one of the two DsbA-II subclasses: whilst structurally more similar overall to DsbA-IIa's MtbDsbA with a similarly negatively charged catalytic surface, its Gram negative origin and more reducing redox potential is more consistent with that of WpDsbA1 and DsbA-IIb. It is possible that DsbA-II proteins represent a broader continuum of structural features not yet fully captured by the current repertoire of structures. We await further population of the DsbA-II class before definitively sub-categorising CtDsbA.

In conclusion, we have demonstrated that *C. trachomatis* encodes a DsbA protein with oxidase activity. The structure of CtDsbA yields new insight into the protein's relatively negative redox potential and our observation that the oxidised form of CtDsbA is only mildly destabilised relative to the reduced form. This characterisation of CtDsbA expands our understanding of the range of redox activities exhibited by DsbAs. Further it is a significant addition to a growing structural library of DsbA proteins, supporting ongoing exploration of the potential for development of narrow or broad spectrum antimicrobials against this important family of virulence-associated proteins [111], [112],[74],[96].

2.8 Acknowledgements

We acknowledge use of the University of Queensland Remote Operation Crystallisation and X-ray (UQ ROCX) Facility and thank Dr. Gordon King for his assistance and expertise.

Chapter 3: Characterisation of the oxidative pathway in *C. trachomatis*

3.1 Introduction

My studies of a soluble CtDsbA construct presented in Chapter 2 revealed that CtDsbA is a protein dithiol oxidase, though it is less oxidising than other characterised DsbAs. Identification of a homolog of EcDsbB in *C. trachomatis* (CtDsbB) suggests that CtDsbA and CtDsbB constitute a redox pair in the oxidative pathway of *C. trachomatis* thereby resembling the oxidative pathway in *E. coli* and other Gram-negative bacteria. Consequently, the role of CtDsbA would be to catalyse the formation of disulfide bonds in folding proteins. Considering the important role of disulfide cross-linking in chlamydial infection and its developmental cycle, it is possible that CtDsbA has a specialised role in *C. trachomatis.* For example, oxidising the cysteines in the Chlamydial Outer Membrane Complex (COMC). If CtDsbA is involved in disulfide formation of the COMC, regulation of CtDsbA oxidase activity might be important to ensure that oxidation of the COMC proteins occurs at the correct time in the developmental cycle.

Interestingly, CtDsbA is one of three characterised DsbAs with an extra disulfide *i.e.* additional to the active site disulfide. The effect of the second disulfide on redox properties has been characterised in WpDsbA1 and PaDsbA2. In WpDsbA1 the additional disulfide has been shown to inhibit the interaction with the partner protein WpDsbB, but has limited to no effect on intrinsic redox properties [108]. In contrast the second disulfide increases the redox potential of PaDsbA2 to -68 mV from -118 mV for a construct with only the active site cysteine present [75]. The additional disulfide of CtDsbA could potentially play a role in regulating CtDsbA activity or the interaction with CtDsbB. Alternatively, it might stabilise the fold of CtDsbA.

In this chapter the interaction between CtDsbA and CtDsbB is investigated to shed light on similarities as well as differences between the oxidative pathways in *E. coli* and *C. trachomatis*. To gain insight into the potential role of DsbA in regulating the redox state of the COMC proteins, the expression levels of CtDsbA are determined during replication, and during reticulate body (RB) to elementary body (EB) differentiation. Further, the role of the second disulfide in stability, as well as regulation of the interaction with CtDsbB, is studied.

3.2 Materials and methods

3.2.1 Expression and purification of soluble proteins

CtDsbA and CtDsbA-SSS were produced as described in Chapter 2 section 2.5.1

3.2.2 Expression, membrane preparation, solubilisation and purification of membrane proteins

CtDsbB SSCC was designed by mutating Cys36 and Cys39 in CtDsbB (NCBI Gene ID 471472) to serines. CtDsbB CCSS was designed by mutating Cys98 and Cys104 in CtDsbB to serines. CtDsbB and mutants were purchased as gBlocks (Integrated DNA technologies) with a 5' XhoI and a 3' NdeI restriction site for insertion to a pET21a vector. All constructs were expressed in *E. coli* C41 cells using PASM 5052 autoinduction media [199] containing ampicillin and grown at 30 °C for 18-24 h with orbital shaking at 200 rpm. Harvested cells were resuspended in 25 mM Tris pH 8.5, 150 mM NaCl and lysed using a cell disrupter (Constant Systems Ltd) (one passage at 28 Kpsi followed by a second passage at 30 Kpsi). Unbroken cells and debris were removed by centrifugation at 16,000 x rpm for 10 min. Membranes were harvested from the supernatant by ultracentrifugation (40,000 x rpm for one hour) at 4 °C. The pellet was resuspended in 25 mM Tris pH 7.5, 150 mM NaCl using a glass homogeniser. Membranes were solubilised in 137 mM, 10 mM phosphate, 2.7 mM KCl, pH 7.4 (PBS) with 1 % n-dodecyl-β-D-maltoside (DDM) by vigorous stirring at 4 °C. Solubilised membranes were ultracentrifuged for one hour at 40,000 x rpm at 4 °C. Protein purity, size and quantification were verified by NuPage 12% Bis-Tris SDS PAGE (Thermofisher). Solubilised membranes were loaded onto a 5 mL HisTrap™ HP column (GE Healthcare) equilibrated in 1 x PBS, 0.03 % DDM and 20 mM imidazole. The column was washed with the above buffer plus 40 mM imidazole (10 x column volume (CV)), 80 mM imidazole (10 x CV) and eluted with 160 mM imidazole (5 x CV). Eluted protein was further purified by size exclusion chromatography using a Superdex™ 200 16/60 column (GE Healthcare). Protein purity was evaluated on a NuPAGE 12% Bis-Tris SDS PAGE (Thermofisher) with MES running buffer (50 mM 2-(N-morpholino) ethanesulfonic acid (MES) pH 7.3, 50 mM Tris, 0.1 % sodium dodecyl sulfate (SDS) and 1 mM Ethylenediaminetetraacetic acid (EDTA).

3.2.3 Peptide oxidation assay

The peptide oxidation assay was performed as described in Chapter 2 section 2.5.3. Membranes containing CtDsbB, CtDsbB SSCC or CtDsbB CCSS (8 μM) were used instead of oxidised glutathione (GSSG).

3.2.4 Determination of redox state of CtDsbA, CtDsbA-SSS and EcDsbA

Reduced EcDsbA, CtDsbA or CtDsbA-SSS (30 μM) were mixed with EcDsbB or CtDsbB (50 nM) and UQ-1 (30 μM) in 50 mM NaPO4 pH 8.0, 100 mM NaCl, and 0.1 % DDM in a total volume of 100 μL. 5 μl samples were taken immediately after adding EcDsbB/CtDsbB, and then after 5, 20, 60 and 120 min incubation, before trichloroacetic acid (TCA) mediated precipitation and labelling with 4-acetamido-4'-maleimidylstilbene-2,2'-disulfonic acid (AMS) as described in Chapter 2 section 2.5.7.

3.2.5 Relative stability of oxidised and reduced forms of CtDsbA-SSS

The thermal stability of reduced and oxidised CtDsbA-SSS was determined by Circular Dichroism (CD) spectroscopy as described in Chapter 2 section 2.5.6.

3.2.6 Absorbance spectrum of DsbB proteins

Absorbance was measured on a Cary WinUV spectrophotometer (Agilent) between 800 nm and 300 nm with a scan speed of 300 nm/min. The absorbance spectrum for the CtDsbB constructs and EcDsbB were measured in 1 x PBS and 0.03 % DDM. The spectrum for BpsDsbB was measured in 1 x PBS, 0.3 % DM and 10 % glycerol. BpsDsbB SSCC and BpsDsbB CCSS were measured in 25 mM MES pH 6.5, 150 mM NaCl and 0.15 % Decyl Maltoside. Absorbance spectra were taken for the buffers alone as a baseline control. The plotted data shows the buffer subtracted spectra.

3.2.7 Investigation of CtDsbA expression levels by confocal microscopy

Coverslip cultures of *C. trachomatis* LGV-2 infected McCoy cells were fixed with 100 % methanol for 10 min after 20 h, 32 h and 44 h of infection and imaged using immunofluorescence with a Nikon A1 microscope. Cultures were stained with an anti-CtDsbA monoclonal antibody raised in rabbit and a secondary goat anti-rabbit IgG fluorescein isothiocyanate (FITC) antibody. The host cell nucleus

was stained with DAPI, and host cell cytoskeleton was stained with Alexa Fluor 594 Phalloidin. Coverslips were mounted on slides in Prolong Gold (Invitrogen) prior to visualisation.

3.3 Results

3.3.1 The *C. trachomatis* genome encodes a protein with 22 % sequence identity to EcDsbB

A BLAST search for EcDsbB against the *C. trachomatis* genome (NCBI Taxid: 813) revealed a protein of 136 amino acids with 22 % sequence identity with EcDsbB (Figure 3.1). This protein will be referred to as CtDsbB.

CtDsbB is predicted to have four transmembrane helices (TM1-4) and two periplasmic loops (TMHMM [93]) equivalent to the topology in EcDsbB. However, loop P2 is significantly shorter in CtDsbB than in EcDsbB (Figure 3.1).

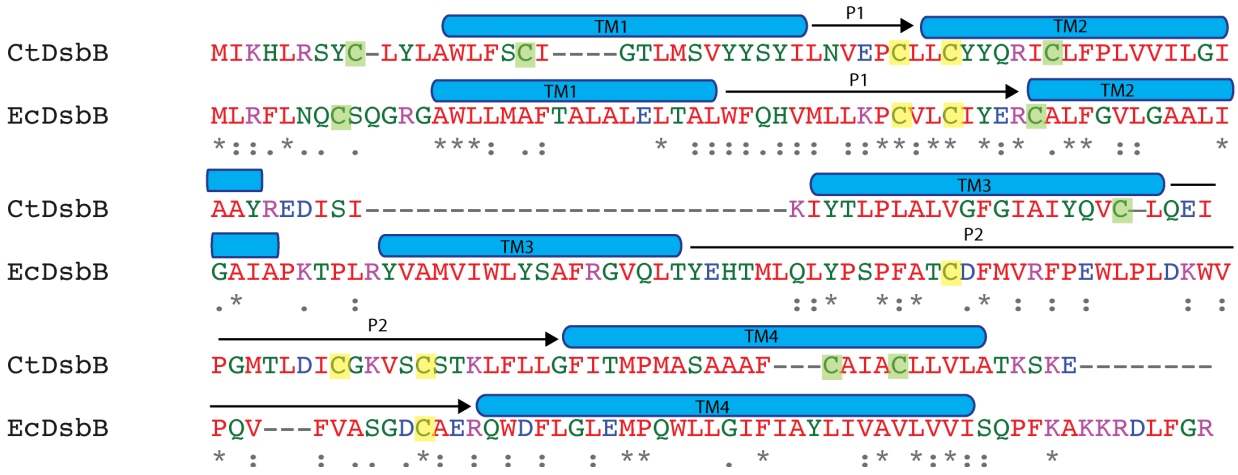

***Figure 3.1 Sequence alignment of DsbB from* E. coli *and* C. trachomatis.**

Sequence alignment of EcDsbB and CtDsbB performed in Clustal Omega [105]. Membrane topology prediction (TMHMM [93]) shows that CtDsbB, like EcDsbB, has four predicted transmembrane helices, TM1-4 (blue) and two predicted periplasmic regions, P1 and P2 (black arrow) each containing two cysteine residues (yellow). Other cysteines are highlighted in green. "" indicates fully conserved residues. Residues with highly similar properties (above 0.5 in the Gonnet PAM 250 matrix) are marked with ":". Residues with weakly similar properties (below 0.5 in the Gonnet PAM 250 matrix) are marked with ".".*

CtDsbB has ten cysteine residues compared to six cysteine residues in EcDsbB. Five of the cysteines in CtDsbB are embedded in the predicted transmembrane regions and one is located in the cytoplasmic N-terminal region. Similar to the arrangement of the catalytic cysteines in EcDsbB, the remaining four cysteines are located in the two periplasmic loops and at the N-terminal end of TM2. The location of Cys36 in loop P1 and Cys39 in the N-terminal of TM2 is equivalent to the location of the CXXC motif in EcDsbB. By comparison to EcDsbB, the periplasmic exposed cysteines Cys98 and Cys 104 are likely to be equivalent to the Cys104-Cys130 redox pair in loop P2 of EcDsbB (Figure 3.1). The similarity in sequence and topology with EcDsbB suggests that CtDsbB is a redox partner for CtDsbA. However, the difference in P2 loop length between CtDsbB and EcDsbB might influence the specific mechanism of CtDsbB catalysis. Loop P2 in EcDsbB contains a membrane parallel helix separating Cys104 and Cys130 of EcDsbB [101]. As Cys104 and Cys130 are 10 Å apart when the intermolecular disulfide bond between EcDsbA and EcDsbB are present, the physical separation of Cys104 and Cys130 prevents reoxidation of the Cys104-Cys130 disulfide. This ensures that oxidation of the active site disulfide of EcDsbA proceeds despite this reaction being less energetically favourable than reoxidation of the Cys104-Cys130 disulfide bond of EcDsbB [64]. Due to the short P2 loop in CtDsbB, a membrane-parallel helix is unlikely to be formed in CtDsbB. Secondary topology prediction of loop P2 by Jpred [220] supports the lack of a helix in loop P2 in CtDsbB. The proposed catalytic cysteines in loop P2 of CtDsbB, Cys98 and Cys104, are only separated by four residues compared to 25 residues separating Cys104 and Cys130 in EcDsbB. The short distance between Cys98 and Cys104 further impairs separation of the two cysteines. Considering the important role of loop P2 in separating the cysteines for EcDsbB catalysis, the shorter loop might suggest a modified mechanism of CtDsbB mediated oxidation of CtDsbA compared with that of EcDsbB and EcDsbA. Conservation of Arg48 and Met142, residues proposed to be involved in ubiquinone (UQ) binding in EcDsbB, suggests that CtDsbB is likewise capable of binding UQ.

Both periplasmic loop disulfides in EcDsbB are required for oxidation of EcDsbA. To investigate whether the mechanism of CtDsbA oxidation by CtDsbB is similar to that seen in *E. coli,* two CtDsbB mutants were designed with the cysteines in loop P1 and loop P2, respectively, mutated to serines (Figure 3.2). In CtDsbB SSCC Cys36 and Cys39 are mutated to serines. In CtDsbB CCSS Cys98 and Cys104 are mutated to serines.

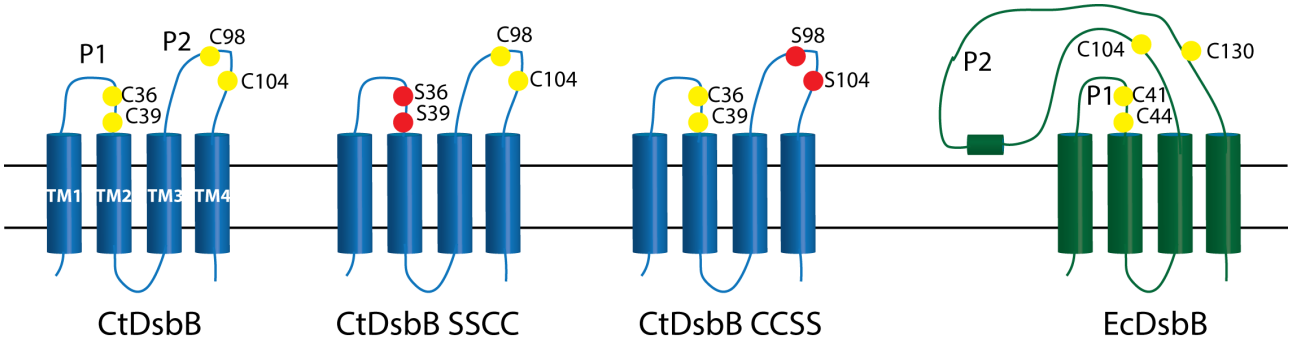

Figure 3.2 Design of CtDsbB periplasmic loop mutants.

CtDsbB (blue) is predicted to have four transmembrane helices (TM1-4) with two short periplasmic loops between TM1 and TM2 and between TM3 and TM4 respectively (P1 and P2). Each of the periplasmic loops contains two cysteines (yellow). In CtDsbB SSCC the cysteines in periplasmic loop P1 are mutated to serines (red). In CtDsbB CCSS the cysteines in periplasmic loop P2 are mutated to serines (red). EcDsbB (green) has four transmembrane helices and a periplasmic loop P1 of similar length to CtDsbA. Periplasmic loop P2 is significantly longer in EcDsbB and contains a short membrane parallel helix, which is likely absent in CtDsbB.

3.3.2 Membranes containing CtDsbB facilitate CtDsbA activity

E. coli membranes containing heterologously expressed CtDsbB, CtDsbB SSCC or CtDsbB CCSS were prepared and tested for their ability to facilitate CtDsbA oxidation of a synthetic fluorescently labelled peptide substrate (Figure 3.3). Adding membranes containing CtDsbB to CtDsbA gives rise to an increase in fluorescence as the peptide is oxidised. This indicates that the two proteins form a functional redox relay that enables CtDsbA to oxidise the cysteines in the peptide (Figure 3.3). However, the initial reaction rate is only 234±23 relative fluorescence unit (RFU)/s for CtDsbA and CtDsbB containing membranes (Table 3.1), compared to 2110 ±250 RFU/s for the redox relay formed between EcDsbA and membranes containing EcDsbB (Table 3.1). This suggests that CtDsbA is less active in the assay upon interaction with CtDsbB than the EcDsbA and EcDsbB counterparts. The initial rate for reactions containing only CtDsbA, or only membranes containing CtDsbB is 2.7±0.3 RFU/s and 9.5±0.2 RFU/s, respectively. These values are equivalent to the initial rate measured for the buffer only control (6.2±0.2 RFU/s) confirming that neither CtDsbA nor the membranes containing CtDsbB can significantly oxidise the synthetic peptide on their own (Figure 3.3 and Table 3.1).

Table 3.1 Initial rates, V_I, of peptide oxidation catalysed by DsbA upon interaction with DsbB constructs.

DsbA	DsbB	V_I (RFU/s)
None	None	6.2±0.2
EcDsbA	EcDsbB	2110±250
CtDsbA	None	2.7±0.3
	BpsDsbB SSSS	0.24±0.2
	CtDsbB SSCC	2.8±0.2
	CtDsbB CCSS	4.5±0.1
	CtDsbB	234±23
None	CtDsbB	9.5±0.2

Mean and SD for two biological replicates are presented

Adding membranes containing CtDsbB SSCC or CtDsbB CCSS to CtDsbA gives rise to initial rates of 2.8±0.2 RFU/s and 4.5±0.1 RFU/s, respectively (Figure 3.3B and Table 3.1). The fact that CtDsbA is significantly less active in the presence of CtDsbB SSCC and CtDsbB CCSS, than in the presence of CtDsbB suggests that the two disulfide bonds in the periplasmic loops are both required for complete oxidation of CtDsbA.

To exclude the possibility that other factors present in the *E. coli* membranes facilitate CtDsbA activity, a construct of a DsbB from another organism, *B. pseudomallei* (BpsDsbB) with all four cysteines in the two periplasmic loops mutated to serines (BpsDsbB SSSS) was included as a negative control. Replacing the cysteines in loop P1 and P2 with serines eliminates the ability of BpsDsbB to form a redox relay with any DsbA enzyme, including CtDsbA. This construct, rather than a cysteine-less mutant of CtDsbB, was chosen as a negative control as it was readily available and proven to be unable to facilitate BpsDsbA activity in the peptide oxidation assay [221].With an initial reaction rate of 0.24±0.2 RFU/s BpsDsbB SSSS containing membranes were not able to facilitate CtDsbA activity. Consequently, the observed CtDsbA activity arises from a specific interaction with CtDsbB, and other factors in the membrane preparation contribute minimally to CtDsbA activity.

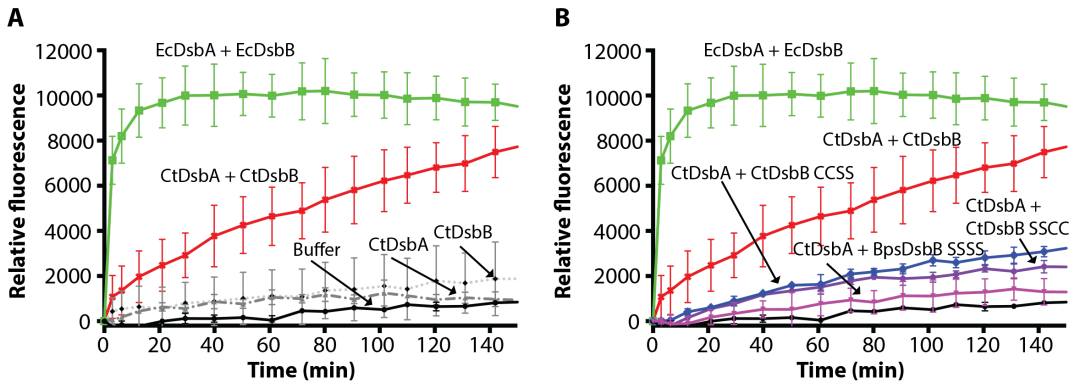

Figure 3.3 Both periplasmic disulfide bonds are required for CtDsbB to form a redox relay with CtDsbA.

An increase in fluorescence as a function of time is seen as a result of CtDsbA and CtDsbB catalysed oxidation of a fluorescently labelled peptide containing two cysteines. ***A)*** *A rapid increase in fluorescence is seen for 80 nM EcDsbA with membranes containing 8 µM EcDsbB (green). 640 nM CtDsbA with membranes containing 8 µM CtDsbB (red) gives a slower increase in fluorescence. Fluorescence only increases minimally for control reactions containing only CtDsbB (8 µM) membranes (grey dotted line), 640 nM CtDsbA (dashed line) or buffer only (black).* ***B)*** *The increase in fluorescence for 640 nM CtDsbA with membranes containing 8 µM CtDsbB CCSS (blue) and 640 nM CtDsbA with membranes containing 8 µM CtDsbB SSCC (purple) are significantly slower than 640 nM CtDsbA with membranes containing 8 µM CtDsbB (red), but marginally faster than 640 nM CtDsbA with membranes containing 8 µM BpsDsbB SSSS (pink) and buffer only (black). The curves for 80 nM EcDsbA with membranes containing 8 µM EcDsbB (green), 640 nM CtDsbA with membranes containing 8 µM CtDsbB (red) and buffer only (black) are the same as in A. Plotted data show mean and SD for two biological replicates.*

3.3.3 Purified, DDM-solubilised CtDsbB does not oxidise CtDsbA

To follow up on the hypothesis that the CtDsbA activity is due to oxidation by CtDsbB, the redox state of CtDsbA after incubation with purified detergent solubilised CtDsbB was studied in a gel shift assay. *In vivo* EcDsbB derives its oxidising power from a quinone cofactor and ultimately the electron transport chain [222]. For *E. coli, V. cholerae, W. pipientis* and *M. tuberculosis* systems, ubiquinone 1 (UQ-1) is able to accept electrons from DsbB in *in vitro* experiments [76, 78, 104, 108]. Thus UQ-1 was chosen as the quinone cofactor to use in CtDsbB *in vitro* experiments as well.

Initially a construct of the soluble CtDsbA in which the three cysteines outside of the active site were replaced with serine (CtDsbA-SSS) was chosen for this assay as the active site disulfide is the likely target for CtDsbB oxidation.

CtDsbA-SSS was incubated with UQ-1 in the presence or absence of purified, DDM-solubilised CtDsbB, and samples were taken after 0, 5, 20, 60 and 120 min (Figure 3.4A). The reaction was quenched by precipitation with TCA and samples were treated with AMS adding 0.5 KDa for every free cysteine. Consequently, the oxidation of CtDsbA-SSS can be monitored as a shift in electrophoretic motility on SDS-PAGE.

For CtDsbA-SSS incubated with CtDsbB and UQ-1, all of the protein migrates at a molecular weight corresponding to reduced CtDsbA-SSS up until 20 minutes after the reaction is started. At 60 and 120 minutes after the reaction is initiated, a small proportion of CtDsbA-SSS migrates at a molecular weight corresponding to oxidised CtDsbA-SSS indicating that the active site cysteines of CtDsbA are oxidised in the presence of CtDsbB and UQ-1 (Figure 3.4A). However, an equivalent proportion of CtDsbA-SSS becomes oxidised upon incubation with UQ-1 in the absence of CtDsbB (Figure 3.4A). This indicates that UQ-1 directly, rather than bound to CtDsbB, is responsible for the partial oxidisation of CtDsbA-SSS. No shift in migration of CtDsbA-SSS is observed upon incubation with CtDsbB in the absence of UQ-1 confirming that CtDsbB alone has no effect on the redox state of CtDsbA-SSS (Figure 3.4B). Without addition of CtDsbB or UQ-1 CtDsbA-SSS stays reduced over the course of 120 minutes confirming that CtDsbA-SSS does not spontaneously oxidise (Figure 3.4B).

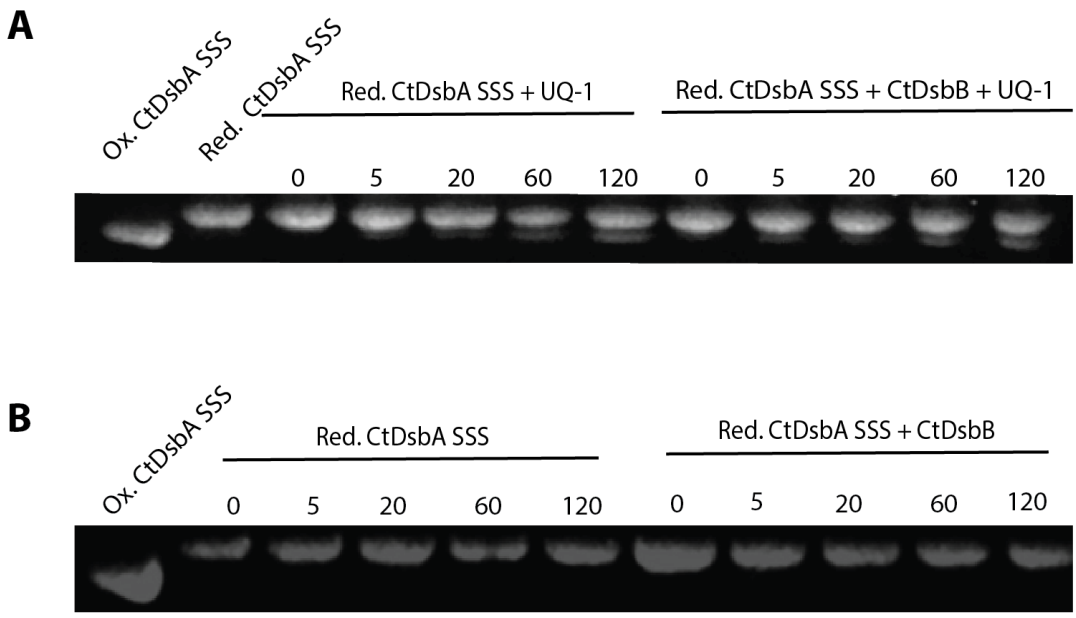

Figure 3.4 Purified and detergent solubilised CtDsbB does not fully oxidise CtDsbA-SSS.

The redox state of CtDsbA-SSS over time was monitored by a shift in electrophoretic mobility after treatment with the alkylating agent AMS that adds 0.5 kDa per reduced cysteine. ***A)*** *Reduced CtDsbA-SSS (30 μM) was incubated with UQ-1 (30 μM) in the absence or presence of purified detergent solubilised CtDsbB (50 nM) and incubated for 0, 5, 20, 60 and 120 min. CtDsbA-SSS is partly oxidised after 60 min both in the absence and presence of CtDsbB. Reduced and oxidised CtDsbA-SSS were included on the SDS-PAGE for reference.* ***B)*** *In the absence of UQ-1, CtDsbA-SSS does not change redox state over the course of 120 min in either the absence or presence of CtDsbB. Oxidised CtDsbA-SSS is included as a reference. Data shown represents one of three biological replicates.*

To determine whether oxidation of DsbA directly by UQ-1 is specific for CtDsbA-SSS, the ability of UQ-1 to oxidise EcDsbA was investigated. In contrast to what I found with CtDsbA-SSS reduced EcDsbA is partially oxidised immediately upon addition of EcDsbB and UQ-1, and fully oxidised after 5 min (Figure 3.5). This is consistent with what is reported in the literature [60]. In the absence of EcDsbB, EcDsbA is partly oxidised by UQ-1 after 20 min and gets slightly more oxidised at 60 min and 120 min. However, as also observed for CtDsbA-SSS, UQ-1 is not able to fully oxidise EcDsbA in the absence of EcDsbB (Figure 3.5).

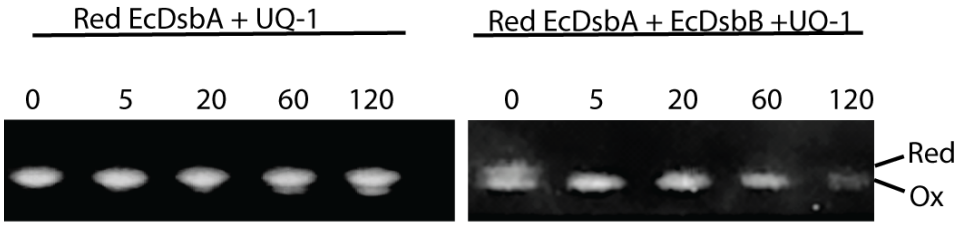

Figure 3.5 EcDsbA is partly oxidised by UQ-1 in the absence of EcDsbB.

The redox state of EcDsbA over time was monitored by a shift in electrophoretic mobility after treatment with the alkylating agent AMS that adds 0.5 kDa per reduced cysteine. Reduced EcDsbA (30 μM) was incubated with UQ-1 (30 μM) in the absence or presence of purified detergent solubilised EcDsbB (50 nM) and incubated for 0, 5, 20, 60 and 120 min. Data shown represents one of two biological replicates.

The second disulfide of CtDsbA might be important for the interaction with CtDsbB and could perhaps be responsible for the lack of oxidation of the CtDsbA-SSS mutant where this disulfide bond cannot form. Therefore the ability of CtDsbB to oxidise CtDsbA was investigated as well. Similar to the experiment using CtDsbA-SSS, no spontaneous oxidation of CtDsbA occurs over 120 minutes (Figure 3.6B). Neither does CtDsbB oxidise CtDsbA in the absence of UQ-1 (Figure 3.6B). Interestingly, no shift in migration is observed upon incubating of CtDsbA with UQ-1, neither in the absence or presence of CtDsbB (Figure 3.6A). In these experiments, CtDsbA, contrary to CtDsbA-SSS, is not oxidised by UQ-1 in a time course of 120 minutes.

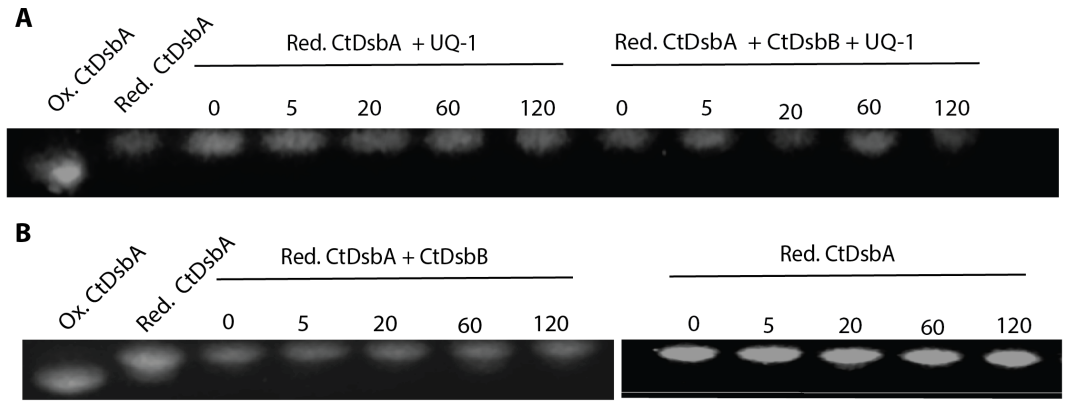

Figure 3.6 Purified and detergent solubilised CtDsbB is not able to oxidise CtDsbA.

The redox state of CtDsbA over time was monitored by a shift in electrophoretic mobility after treatment with the alkylating agent AMS that adds 0.5 kDa per reduced cysteine. Reduced and oxidised CtDsbA is included as reference. ***A)*** *The redox state of CtDsbA does not change after incubation with UQ-1 in the presence or absence of CtDsbB.* ***B)*** *Reduced CtDsbA is not oxidised in the absence or presence of CtDsbB in the course of 120 min. Data shown represents one of three biological replicates.*

UQ-1 facilitated CtDsbA activity was studied in the peptide oxidation assay to confirm that CtDsbA-SSS is oxidised by UQ-1. However, the increase in relative fluorescence over 140 minutes is the same for CtDsbA-SSS in the absence and presence of UQ-1 (Figure 3.7) indicating that UQ-1 is not able to oxidise CtDsbA sufficiently to support substrate oxidation in this assay. This is inconsistent with the observed shift in electrophoretic motility of CtDsbA-SSS upon incubation with UQ-1. As CtDsbA-SSS has intrinsically lower activity in the peptide oxidation assay compared to EcDsbA, the partial oxidation of CtDsbA-SSS observed in the gel shift assay is most likely insufficient to oxidise the peptide substrate. Consequently, any oxidation of CtDsbA-SSS is not reflected in an increase in fluorescence as the signal-to-noise ratio is too low.

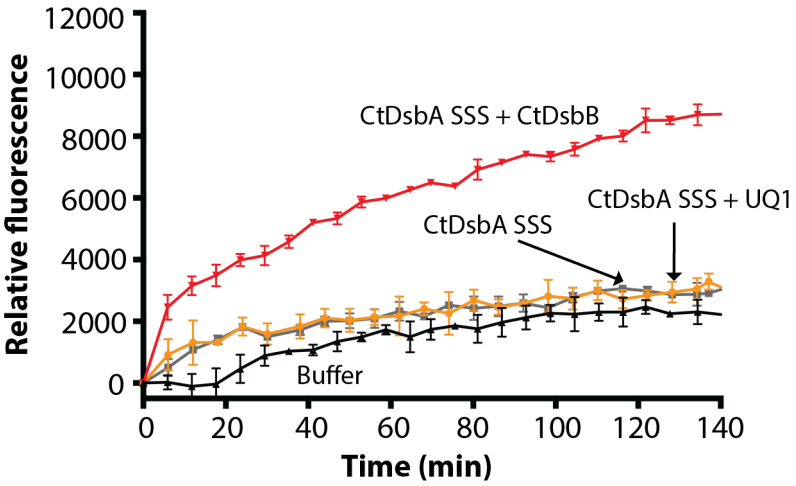

Figure 3.7 UQ-1 does not regenerate CtDsbA-SSS activity.

The increase in fluorescence with 640nM CtDsbA-SSS and UQ-1 (10 µM) is equivalent to that of CtDsbA-SSS alone, and of the buffer only control and significantly lower than when using CtDsbB containing membranes (8 µM) as a redox partner. Plotted data show mean and SD for two biological replicates.

3.3.4 CtDsbB binds UQ differently than EcDsbB

Two possible explanations for the observation that purified CtDsbB does not oxidise CtDsbA are (i) that CtDsbB is inactive in DDM micelles or (ii) that UQ-1 is not able to act as an electron acceptor for CtDsbB. To shed further light on the latter, the interaction with UQ was investigated further.

Reduced UQ (ubiquinol) is colourless, whereas oxidised UQ is yellow and gives rise to a peak in absorbance at 400 nm (Figure 3.8). Upon binding to EcDsbB the spectrum of UQ is red-shifted giving rise to a broad shoulder around 500 nm and a characteristic pink colour [104] (Figure 3.8). A charge-transfer complex between UQ and Cys44 of EcDsbB is responsible for the red-shift in UQ absorbance

[104] and the red-shift is more pronounced when EcDsbB is bound to EcDsbA [104]. Addition of the reducing agent dithiothreitol (DTT) to a preparation of UQ-bound DsbB results in the solution turning colourless due to reduction of UQ [104].

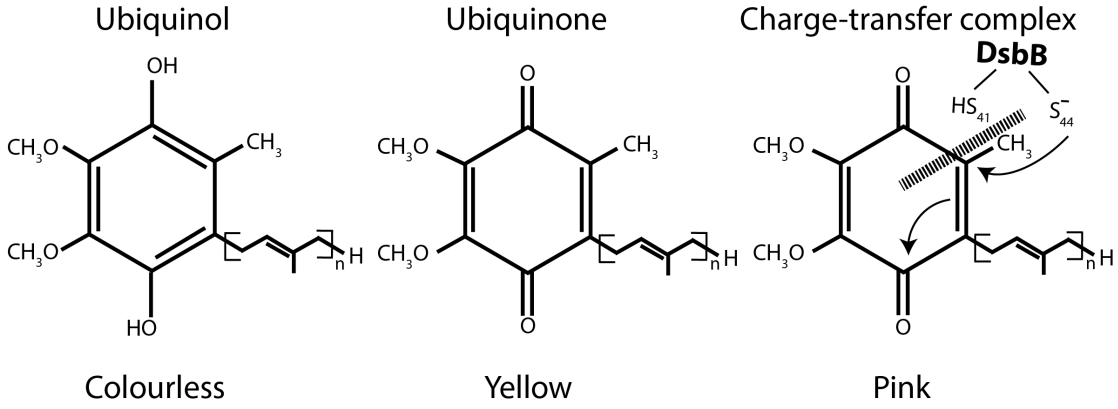

Figure 3.8 Colour of reduced and oxidised UQ and the charge-transfer complex formed between Cys44 of EcDsbB and UQ.

UQ consists of a 1,4 benzoquinone head group and an isoprenoid tail of varying length. Reduced ubiquinone (ubiquinol) is colourless whereas oxidised ubiquinone is yellow. Oxidised ubiquinone can form a charge-transfer complex with Cys44 of EcDsbB, which is characterised by a pink colour.

DsbB constructs from *E. coli, B. pseudomallei* and *C. trachomatis* were recombinantly expressed in *E. coli*, then detergent solubilised and purified. Detection of bound endogenous UQ acquired during expression in *E. coli* was studied by colour observations and absorbance spectrum properties.

Both EcDsbB and BpsDsbB have the characteristic pink colour of a charge-transfer complex formed between UQ and cysteine (Table 3.2). The spectra for EcDsbB and BpsDsbB also exhibit a peak at 410 nm and a shoulder around 500-550 nm in agreement with the spectra for a charge-transfer complex between UQ and DsbB as reported in the literature [104] (Table 3.2 and Figure 3.9). The protein solution of both BpsDsbB SSCC and BpsDsbB CCSS are faint yellow indicating potential binding of oxidised UQ (Table 3.2). The spectrum of BpsDsbB SSCC has no local maxima at 410 or 500 nm suggesting that UQ is bound in the reduced state or is not bound at all. The spectrum of BpsDsbB CCSS, on the other hand, is equivalent to BpsDsbB although lower in intensity. As the quinone binding site, by homology to EcDsbB, is intact in BpsDsbB CCSS, this most likely reflects limited binding of UQ in BpsDsbB CCSS, but no formation of a charge-transfer complex.

***Table 3.2 Colour and absorbance spectral properties of DsbB constructs from* E. coli, B. pseudomallei *and* C. trachomatis**

Protein	Colour	Local max 410 nm	Shoulder 500 nm
EcDsbB	Pink	Yes	Yes
BpsDsbB	Pink	Yes	Yes
BpsDsbB SSCC	Faint yellow	No	No
BpsDsbB CCSS	Faint yellow	Yes	Yes
CtDsbB	Orange	Yes	No
CtDsbB SSCC	Orange	Yes	No
CtDsbB CCSS	Orange	Yes	No

Interestingly, CtDsbB, CtDsbB SSCC and CtDsbB CCSS are all dark orange (Table 3.2). This can either be indicative of UQ binding, without formation of a charge-transfer complex with Cys38, or potentially binding of a metal [223-225]. CtDsbB turns colourless upon addition of DTT. As reduced UQ (ubiquinol) is colourless (Figure 3.8) this observation is consistent with binding of UQ to CtDsbB and its mutants.

Two factors could contribute to the orange colour of UQ bound to CtDsbB, CtDsbB SSCC and CtDsbB CCSS. One possibility is that oxidised ubiquinone binds without forming a charge-transfer complex with Cys36. Another possibility is that ubiquinone forms a quinhydrone-like charge-transfer complex with Tyr40 or Tyr41 that both are in close proximity to the predicted UQ binding site in CtDsbB. The charge-transfer complex with tyrosine gives rise to a brown-red colour [226]. Both theories are consistent with CtDsbB turning colourless upon addition of DTT, which would reduce bound UQ.

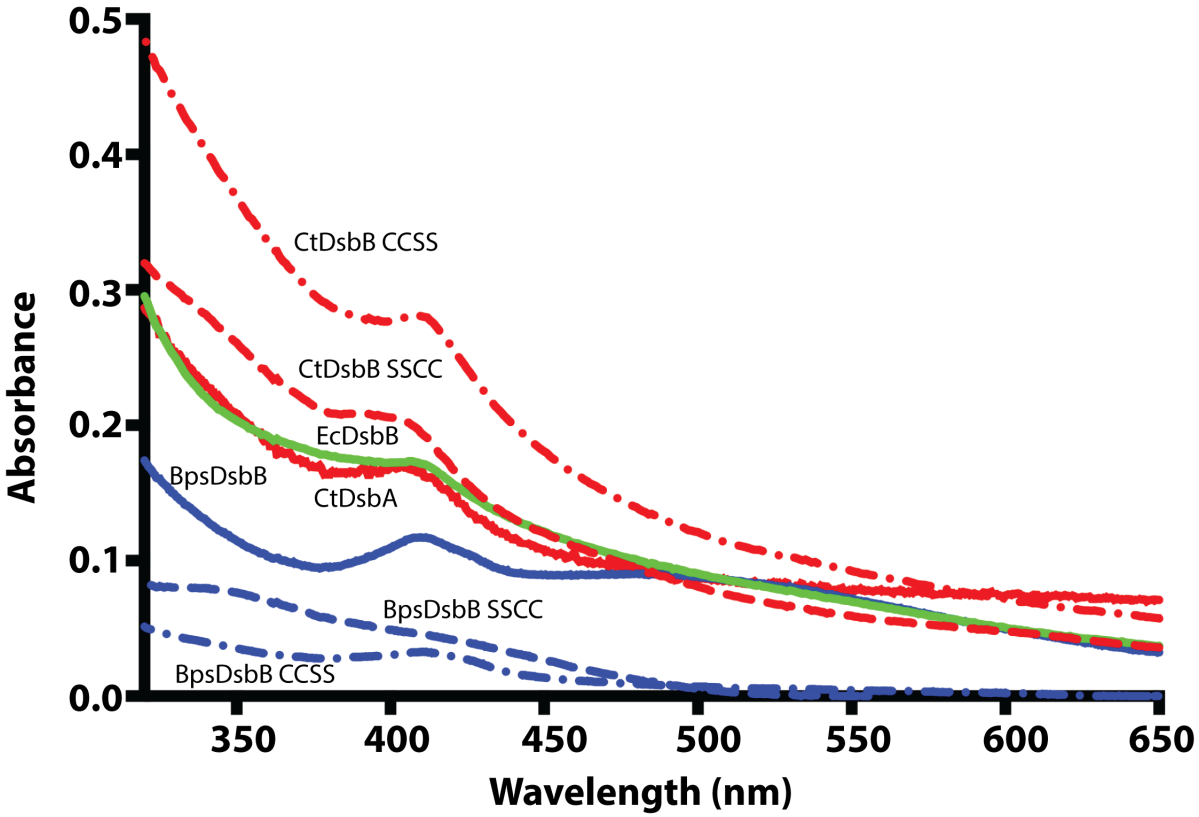

Figure 3.9 Absorbance spectrum of DsbB constructs.

Absorbance spectra were obtained for 1 mg/ml purified detergent solubilised EcDsbB (green) and 1.9 mg/ml purified detergent solubilised BpsDsbB (blue solid line), BpsDsbB SSCC (blue dashed line), BpsDsbB CCSS (blue dashed-dotted line), CtDsbB (red solid line), CtDsbB SSCC (red dashed line) and CtDsbB CCSS (red dashed-dotted line). A maximum at 410 nm indicates binding of ubiquinone in the oxidised state. A shoulder around 500 nm indicates presence of a charge-transfer complex between ubiquinone and cysteine. Data shown represent one of three repeats.

The absorbance spectra are equivalent for all three CtDsbB (Figure 3.9). This is consistent with the colour of the solution being the same for the three protein preparations. The spectra for the CtDsbB constructs exhibit a peak at 410 nm, but in contrast to the spectra for BpsDsbB and EcDsbB, does not have a shoulder at 500 nm. The spectra are consistent with binding of oxidised ubiquinone, but not with the presence of a ubiquinone-tyrosine quinhydrone-like charge-transfer complex as this complex would give rise to peaks at 360 nm and 455 nm [226]. Unlike EcDsbB and BpsDsbB, there is no evidence of a charge-transfer complex with cysteine in any of the spectra obtained for the three CtDsbB constructs indicating that CtDsbB may bind UQ differently to EcDsbB and BpsDsbB.

3.3.5 CtDsbA is expressed late in the *C. trachomatis* developmental cycle

To get an indication of the biological role of CtDsbA, I investigated at what point in the developmental cycle CtDsbA is expressed. An antibody against CtDsbA was raised in rabbit and used to monitor the expression levels of CtDsbA in *C. trachomatis* via confocal microscopy (Figure 3.10). McCoy cells were infected with *C. trachomatis* LGV-2 and the infected McCoy cells were harvested 20 hours, 32 hours and 44 hours post infection.

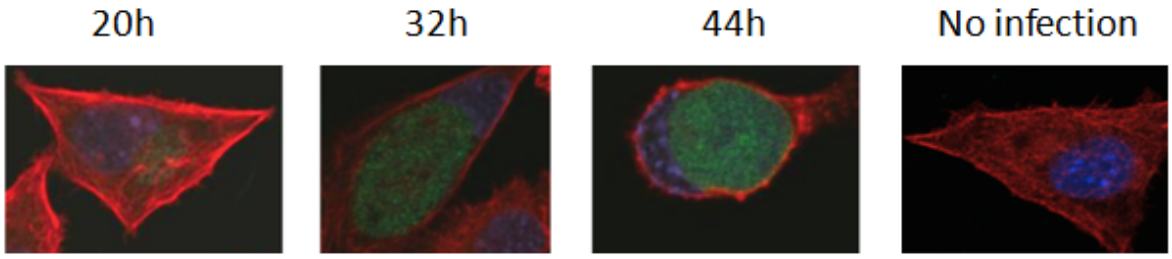

***Figure 3.10 Expression levels of CtDsbA in* C. trachomatis.**
Confocal images were obtained of C. trachomatis *LGV-2 infected McCoy cells harvested at 20 h, 32 h and 44 h post infection. A non-infected McCoy cell is included as a negative control. CtDsbA is stained with anti-CtDsbA antibody raised in rabbit with a secondary goat anti-rabbit IgG - Alexa Fluor 488 (green). The host cell nucleus is stained with the fluorescent dye DAPI (blue) that binds strongly to A-T rich regions in DNA. Host cell cytoskeleton is stained with Alexa Fluor 594 Phalloidin (red) that has high affinity for F-actin.*

The 20 h time point represents the middle to late replicative phase of the chlamydial life cycle. Confocal imaging with an anti-CtDsbA antibody coupled with a green fluorescent secondary antibody shows low levels of green fluorescently labelled protein at 20 h post infection suggesting that small amounts of CtDsbA are present in McCoy cells infected with *C. trachomatis* (Figure 3.10B). At 32 h post infection the expression of CtDsbA is significantly increased as judged by elevated amounts of green fluorescence in the confocal image of a *C. trachomatis* infected McCoy cell. These observations suggest that CtDsbA expression is upregulated between 20 h and 32 h post infection. It is noteworthy that at this point RB to EB differentiation has begun including oxidation of the cysteines in the COMC. Little to no additional increase in CtDsbA expression levels is observed between 32 hours and 44 hours.

3.3.6 The additional disulfide in CtDsbA contributes to a slight stabilisation of the oxidised state

A characteristic feature of CtDsbA is the presence of a second disulfide linking helix H2 and helix H5. An equivalent disulfide bond is found in MtbDsbA, PaDsbA2 and in DsbA proteins from alpha-proteobacteria such as WpDsbA1. The role of the second disulfide is not established for CtDsbA, but has different roles in WpDsbA1 and PaDsbA2 [75, 108]. To determine a possible role of the second disulfide in CtDsbA the effect of this second disulfide on thermal stability as well as interaction with CtDsbB was studied.

In Chapter 2 the melting temperature for reduced and oxidised CtDsbA was determined to be 339 ± 0.2 K and 335 ± 0.1 K, respectively. The melting temperature of reduced CtDsbA-SSS (336K ± 0.1) is also higher than its oxidised state (334K ± 0.2) (Figure 3.11A and Table 3.3). In the CtDsbA-SSS mutant the cysteines forming the disulfide bond between helix H2 and helix H5 as well as the free cysteine in the core of the protein (Cys70) are mutated to serines. Consequently oxidised CtDsbA-SSS only contains the active site disulfide bond compared to CtDsbA that has two disulfide bonds in the oxidised state. As the only difference between reduced CtDsbA and CtDsbA-SSS is the three cysteine-to-serine mutations (mimicking a state where the second disulfide is reduced) it was surprising that the melting temperature for reduced CtDsbA-SSS differs from the melting temperature of reduced CtDsbA (Table 3.3). This is most likely a reflection of the different biochemical properties of the serines compared to the cysteine residues that they are replacing. In particular, replacing the free cysteine (Cys70) in the core with the more polar serine residue might decrease the stability of CtDsbA-SSS and contribute to the decrease in melting temperature of reduced CtDsbA-SSS compared to reduced CtDsbA.

Table 3.3 Melting temperatures of CtDsbA and CtDsbA-SSS.

	CtDsbA	CtDsbA-SSS
T_m Reduced (K)	339 ± 0.2	336 ± 0.1
T_m Oxidised (K)	335 ± 0.1	334 ± 0.2

Melting temperatures for CtDsbA-SSS were obtained from Figure 3.11. Melting temperatures for CtDsbA are from Chapter 2 section 2.6.5. Mean and SD for three biological replicates are presented.

The difference in thermal stability between the reduced and oxidised states for CtDsbA-SSS is only 2 K compared to 4 K for CtDsbA suggesting that the second disulfide contributes to stabilising the active state of CtDsbA slightly (Figure 3.11A and Table 3.3).

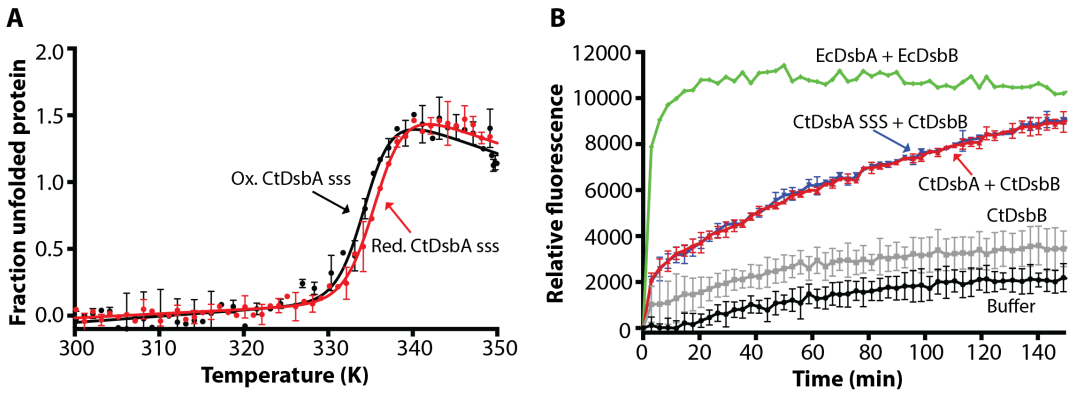

Figure 3.11 The second disulfide of CtDsbA has a small effect on protein stability, but does not appear to affect CtDsbA's interaction with CtDsbB.

A) *The thermal unfolding of reduced and oxidised CtDsbA-SSS was monitored by CD spectroscopy and the fraction of unfolded CtDsbA-SSS is plotted as a function of temperature. With a melting temperature of 336 K ± 0.1, reduced CtDsbA-SSS is slightly more stable than oxidised CtDsbA-SSS that has a melting temperature of 334 K ± 0.2. Plotted data show mean and SD for three biological replicates.* ***B)*** *An increase in fluorescence as a function of time is seen as a result of CtDsbA or CtDsbA-SSS catalysed oxidation of a fluorescently labelled peptide containing two cysteines. A rapid increase in fluorescence is seen for positive control 80 nM EcDsbA with membranes containing 8 μM EcDsbB (green). The activity of 640 nM CtDsbA (red) and 640 nM CtDsbA-SSS (blue) is equivalent upon interaction with membranes containing 8 μM CtDsbB. The activity of CtDsbB (grey) is only minimally higher than fluorescence for the buffer only control (black). Plotted data show mean and SD for three biological replicates, except for the EcDsbA + EcDsbB control where data from a single experiment was used.*

In the peptide oxidation assay (Figure 3.11B) the equivalent slope in fluorescence increase over time for CtDsbA and CtDsbA-SSS upon interaction with CtDsbB, indicates that CtDsbA and CtDsbA-SSS exhibit the same ability to oxidise a synthetic peptide upon interaction with CtDsbB containing membranes (Figure 3.11B). Consequently, the minor increase in stability of the oxidised state introduced by the second disulfide does not have an effect on CtDsbB-facilitated CtDsbA activity, at least not under these experimental conditions.

3.4 Discussion

3.4.1 Discrepancies in the CtDsbA-CtDsbB interaction suggests limitations in experimental design or purification

Despite the observation that crude membranes containing CtDsbB are able to facilitate CtDsbA oxidative folding activity, detergent solubilised purified CtDsbB was unable to oxidise CtDsbA in the presence of UQ-1. Considering the homology to the EcDsbA-EcDsbB redox pair, the inability of CtDsbB/UQ-1 to form an active redox relay with CtDsbA most likely reflects limitations in the experimental set-up or CtDsbB being inactivated in the purification protocol used, rather than CtDsbA and CtDsbB not being a genuine redox pair. This is supported by the ability of crude membranes containing CtDsbB to facilitate CtDsbA oxidative folding activity.

3.4.1.1 UQ binding diverting from EcDsbB might influence CtDsbB catalysis

Even though residues involved in UQ binding in EcDsbB are conserved in CtDsbB, CtDsbB is not able to oxidise CtDsbA in the presence of UQ-1. This might be a reflection of the observed difference in binding of endogenous UQ from *E. coli.* The peptide oxidation assay and the gel shift assay utilises two different UQs; in the gel shift assay UQ-1 is added, whereas in the peptide oxidation assay endogenous UQ from *E. coli* is present in the crude membranes. Despite the indications that CtDsbB is able to bind oxidised endogenous UQ expressed in *E. coli,* the difference in binding mechanisms might hinder binding of UQ-1 to EcDsbB. The main ubiquinone in *E. coli* is UQ-8, although smaller amounts of UQ 1-7 are also synthesised [227]. Even though most organisms use a highly specific ubiquinone, in many microorganisms the organism-specific UQ can be replaced with UQs with variable side chain length. For example, UQ-5-10 are able to replace UQ-6 in *S. cerevisiae in vivo* [228]. Further UQ-1 has successfully replaced ubiquinone with longer side chains in *in vitro* biochemical assays [76, 83, 104, 108, 229, 230] suggesting that UQ-1 would also be an appropriate cofactor for CtDsbB. However, small changes in side-chain length have also proven detrimental in other *in vitro* and *in vivo* studies [231, 232]. Interestingly, neither of the two DsbBs encoded in *P. aeruginosa* are able to oxidise PaDsbA2 to completion in a time course of an hour in the presence of the UQ analogue decylubiquione, further emphasising that the UQ side chain has potential impact on activity [75]. Potentially the endogenous UQ in *E. coli* is a more suitable cofactor for CtDsbB than UQ-1. This would explain the activity I observed in the peptide oxidation assay where endogenous *E. coli* UQ is used, and the lack of activity in the gel shift assay where UQ-1 was used. Although a potential UQ biosynthesis pathway has been identified in *C. trachomatis* [233, 234] the side-chain length of UQ has not been determined. To investigate whether the lack of CtDsbB catalysed oxidation

of CtDsbA is due to the inability of UQ-1 to act as electron acceptor for CtDsbB, different UQ molecules should be screened. CtDsbB's ability to oxidise CtDsbA in the presence of UQ can also be studied in a UQ reduction assay by monitoring a decrease in absorbance at 275 nm following reduction of UQ. As CtDsbB has been shown to facilitate CtDsbA activity in the presence of endogenous UQ from *E. coli,* UQ-8 would be a good starting point, as it is the dominant UQ in *E. coli*. However, UQ molecules with shorter and longer side-chains should be considered too. Menaquinone (MK) is the electron acceptor for EcDsbB under anaerobic conditions [230] and many Gram-negative and Gram-positive bacteria rely on MK entirely [234, 235]. Genomic sequencing of *C. trachomatis* identified four enzymes common to UQ and MK biosynthesis pathways [233]. Moreover, an intermediate in the futolosine pathway for MK biosynthesis has been identified and characterised structurally as well as functionally [234]. Accordingly, the possibility of CtDsbA oxidation by CtDsbB in the presence of MK should be explored too.

3.4.1.2 Optimising solubilisation conditions might improve activity of CtDsbB

When working with membrane proteins it is essential to provide an environment in which the protein is folded, active and solubilised outside the lipid bilayer. Detergents are often used for this purpose as they mimic the hydrophobic environment of the lipid bilayer. Whereas ionic detergents effectively solubilise most membrane proteins, they can also disrupt protein-protein interactions and therefore can sometimes denature the target protein [236-239]. Non-ionic detergents, such as DDM, primarily disrupt lipid-lipid interactions and are less denaturing of proteins [240-243]. A further potential complication is that an excessive presence of a micellar phase can interfere with many assay techniques [244]. Consequently, choosing the right detergent, as well as optimisation of detergent concentration and protein-to-detergent ratio is important for identifying the best condition for membrane protein stability and activity.

In this work CtDsbB was extracted from crude *E. coli* membranes by the non-ionic detergent DDM, which is generally considered a mild and non-denaturing detergent [244]. However, the detergent micelles may lack lipids that could be important for activity of the membrane protein, as seen for e.g. Na^+, K^+-ATPase [245, 246], the cytochrome *b6f* complex [247] and G protein-coupled signalling [248].

To obtain active solubilised CtDsbB the purification and solubilisation protocol should be further optimised. Screening of different detergents, as well as adjusting the protein-to-detergent ratios could potentially identify better detergent conditions for CtDsbB. However, introducing an environment that more closely resembles the membrane of *C. trachomatis* might have a greater effect on CtDsbB

activity. *C. trachomatis* produces lipids required for the formation of the inner and outer membrane [249], and the membrane mimics the bilayer of the eukaryotic host [250-256]. Consequently, a more native-like environment might be accomplished by including lipids such as phosphatidylcholine, phosphatidylinositol, sphingomyelin, or cholesterol, which are present in the chlamydial membrane [250-254, 256].

Nanodiscs (discoidal lipid bilayers that are stable and soluble in aqueous solutions) [257] might provide a better environment for CtDsbB than detergent micelles as they better control the oligomeric state of the target protein than detergent micelles. Moreover, CtDsbB is expressed with a His-tag, which allows for selection of nanodiscs containing CtDsbB. Purifying out empty nanodiscs will limit assay interference [258].

3.4.2 The potential role of CtDsbA in chlamydial infection

The observations presented in section 3.3.5 suggest that the CtDsbA protein expression onset occurs between 20 h and 32 h post infection. This is inconsistent with the onset of gene expression reported by a transcriptional profiling study in which CtDsbA expression (referred to as *DsbG* in the study) occurs 8 hours post infection [147]. This discrepancy could arise from the use of *C. trachomatis* serovar D (strain UW3/dx) in the transcriptional study compared to *C. trachomatis* LGV-2 here, but more likely reflects a difference in methodology. Confocal imaging reports on the protein levels whereas transcriptional profiling using quantitative reverse-transcription PCR (qPCR) reports expression levels of mRNA. Due to factors such as mRNA stability, transcription, and translation rates as well as protein degradation, the mRNA expression levels can differ by up to 60 % from the observed protein levels in both eukaryotes and prokaryotes [259, 260].

The Major Outer Membrane Protein (MOMP) in *C. trachomatis* is synthesised early in the replicative phase but is not oxidised until the onset of RB to EB differentiation [143, 145, 147-149, 152]. In contrast, the two cysteine-rich proteins, OmcA and OmcB are synthesised late in the replicative phase simultaneous with their oxidation [143, 145, 147-149]. The correlation between CtDsbA expression and onset of oxidation of the COMC proteins is interesting in terms of a potential role for CtDsbA in the redox regulation of the COMC. Although the role of CtDsbA in chlamydial infection is to be determined, the correlation between CtDsbA expression and oxidation of the COMC proteins suggests the intriguing possibility that CtDsbA is involved in the redox regulation of the chlamydial developmental cycle.

The disulfide bond formed between helices H2 and H5 is conserved in DsbAs from alpha-proteobacteria including *W. pipientis* [108]. It is also found in the DsbA from the acid-fast *M. tuberculosis* [78] and one of the two DsbAs (PaDsbA2) encoded by *P. aeruginosa* [75]. However, in two of the characterised DsbAs the second disulfide influences the interaction with the redox partner or the intrinsic redox properties, respectively [75, 108]. I found no apparent effect of the second disulfide on CtDsbA catalysis in the peptide oxidation assay. I also found that CtDsbA-SSS is partly oxidised by UQ-1 in the gel shift assay whereas no oxidation of CtDsbA is observed, suggesting that the second disulfide might influence the redox properties of CtDsbA. This might be a reflection of the small decrease in thermal stability between the reduced and oxidised state in CtDsbA-SSS compared to CtDsbA. This is consistent with what is seen for SaDsbA that does not have a destabilising active site disulfide and can be oxidised by extracellular oxidants [84]. A potential inhibitory effect on the interaction with CtDsbB could be followed directly in a UQ reduction assay as described above, assuming the appropriate UQ cofactor for CtDsbB can be identified. The redox potential of the active site disulfide in the absence of the second disulfide was determined in Chapter 2, section 2.6.6. Determining the redox potential of the active site disulfide with the second disulfide present might give important insight to the impact of the second disulfide on the intrinsic redox properties of CtDsbA.

The potential effect of the second disulfide on the redox properties of CtDsbA leaves an open question of the relevance of the second disulfide *in vivo*. If CtDsbA, as proposed in section 1.4, is involved in oxidation of the COMC proteins, regulation of CtDsbA oxidase activity is crucial for chlamydial infection. The second disulfide might be involved, somehow, in regulation of CtDsbA activity either by influencing the interaction with CtDsbB or modifying the interaction with substrates. AMS labelling of samples taken immediately upon infection with *C. trachomatis* as well as during EB to RB differentiation, replication, and RB to EB differentiation, followed by western blotting with anti-CtDsbA antibody could give important information about potential developmental stage specific regulation of CtDsbA. This technique has previously proven successful for determining the *in vivo* redox state of PaDsbA1 [75].

3.5 Conclusion

The identification of a DsbB homolog in *C. trachomatis* and the observation that CtDsbB is capable of facilitating CtDsbA activity in a mechanism dependent on the cysteines in both periplasmic loops indicates that the oxidative pathway in *C. trachomatis* resembles that of *E. coli* in some respects. However, the lack of oxidation of CtDsbA in the gel shift assay and the apparent differences in binding of UQ calls for further investigation of the interaction between CtDsbA and CtDsbB as the redox pair in the oxidative pathway of *C. trachomatis*. The role of the second disulfide in regulating CtDsbA activity also needs further investigation. The impact of the second disulfide is an important step in elucidating the role of the oxidative pathway of *C. trachomatis* infection. Further investigations, especially of the role of CtDsbA in *C. trachomatis* infection are required to explore the theory that the oxidative pathway is involved in oxidation of the COMC.

Chapter 4: Towards studying the biological role of CtDsbA

4.1 Introduction

The oxidase DsbA is important for the oxidative folding of virulence factors in many pathogens such as *E. coli* [48], *S. enterica* Typhimurium [46, 53], *C. jejuni* [54], *Y. pestis* [47], *P. aeruginosa* [55, 56], *Vibrio cholerae* [50] and *B. pseudomallei* [57]. However, the role of CtDsbA in *C. trachomatis* has not been explored. The characterisation of CtDsbA presented in Chapter 2 reveals that CtDsbA has oxidase activity, although weak, and adopts the same overall structure as other DsbA enzymes. The structural and functional similarities between CtDsbA and DsbA in other organisms suggest that CtDsbA might be important for oxidative folding of virulence factors in *C. trachomatis*. Further, the correlation between CtDsbA expression and onset of oxidation of the chlamydial outer membrane complex (COMC) presented in Chapter 3 suggests a specialised role for CtDsbA in *C. trachomatis* virulence. Creation of a *C. trachomatis* strain with a disruption in the *dsbA* gene would allow a more direct study of the role of CtDsbA in *C. trachomatis* infection and development.

The impermeable nature of *Chlamydia* hinders DNA uptake, stable DNA integration and bacterial propagation and selection [261]. Consequently, *Chlamydia* was, until recently, considered refractory to routine genetic manipulation tools such as shuttle plasmids, transposons and transducing phages [261]. The inaccessible nature of *C. trachomatis* arises from the biphasic life cycle of this obligate intracellular pathogen. The two cell types in the chlamydial life cycle - the elementary body (EB) and the reticulate body (RB) - can both be considered targets for DNA uptake. However, the outer membrane of the extracellular, infectious EB is highly cross-linked with disulfide bonds making the EB extremely rigid and consequently difficult to permeabilise [131]. Upon EB to RB differentiation the disulfide cross-linking of the membrane is reduced making the RB less rigid than the EB. However, as the RBs replicate within a membrane-enclosed inclusion inside the host cell, the chromosomal DNA is enclosed by the host cell membrane, the inclusion membrane and the outer and inner bacterial membrane. Accordingly, directing DNA to the target compartment is challenging. Electroporation has been explored as a strategy for insertion of DNA to the EB, and has been successful in two reported cases [262, 263]. However, due to low plasmid stability and poor transformation efficiency this is not an optimal strategy for introducing DNA into the EB. The first stable transformation of plasmid DNA into *Chlamydia* was achieved by the use of a shuttle vector. This method led to the development of expression vectors expressing *Chlamydia* open reading frames [264, 265], exogenous glycogen synthase kinase [81], as well as reporter proteins such as, green- and cyan- fluorescent proteins [266].

Despite the advances in stable DNA transformation, only a few examples of genetic manipulation of *Chlamydia spp.* have been reported in the literature; e.g. insertion of a group II intron has been used to induce gene disruption [267], but this technique is limited to sites where integration is evaluated to be efficient and requires the use of proprietary software.

The most successful strategy for genetic manipulation of *Chlamydia spp* to date combines the introduction of random mutations by chemical mutagenesis with whole genome sequencing. This has gained interest as a way of studying the effect of gene products with critical functions [261, 268]. *Chlamydiaceae,* the chlamydial family to which *C. trachomatis* belongs, lack an effective polymerase V error-prone repair system, a defect which typically increases mutation rate [269]. As *Chlamydia* species have a high gene density, an inefficient proofreading system increases the mutation frequency and consequently increases the ratio of gene disruption caused by point- or frame-shift mutations. Consequently, chemical mutagenesis is a valuable tool for studying gene functions in *Chlamydia* even though it does not offer the option to selectively inactivate individual genes. Chemical mutagenesis combined with whole genome sequencing has proven successful for identifying virulence factors using both a reverse and forward genetic approach [268, 270, 271].

In this chapter I report on this approach to study the role of CtDsbA in *C. trachomatis*. *C. trachomatis* was treated with the carcinogenic compound ethyl methanesulfonate (EMS) that introduces G to A and C to T base mutations in DNA [272] to create a library of EMS mutants. Both a forward and a reverse genetic approach were used to search for possible mutations introduced into the *dsbA* gene (Figure 4.1).

Figure 4.1 Screening of the EMS mutation libraries of* C. trachomatis *LGV-2 or* C. trachomatis *LGV-2* tmp *in a reverse and forward genetic approach.

C. trachomatis *LGV-2 or* C. trachomatis *LGV-2tmp were treated with EMS, which introduces randomly positioned base pair (G:C to A:T) mutations thereby creating a library of EMS mutants. In the reverse genetics approach (right) McCoy cells are infected with 15 inclusion-forming units (IFU) per well of the EMS library and grown continuously for eight days without passaging the infected cells. After eight days the* dsbA *genes were amplified with* dsbA *specific primers and treated with the endonuclease Cel-1 that cleaves specifically at base pair mismatches. If a base pair mismatch is identified the PCR products obtained from that specific well are sequenced with* dsbA *specific primers. In the forward genetic approach (left) McCoy cells are infected with 2 IFU per well of the EMS library. The infected cells are passaged every 48 h for eight days and then harvested. One third of the harvest was treated with 10 mM dithiotrethreitol (DTT) and used to infect a fresh monolayer*

of McCoy cells. As a control McCoy cells were infected with harvest that had not been treated with DTT. Wells with an altered phenotype upon DTT treatment were subjected to sequencing.

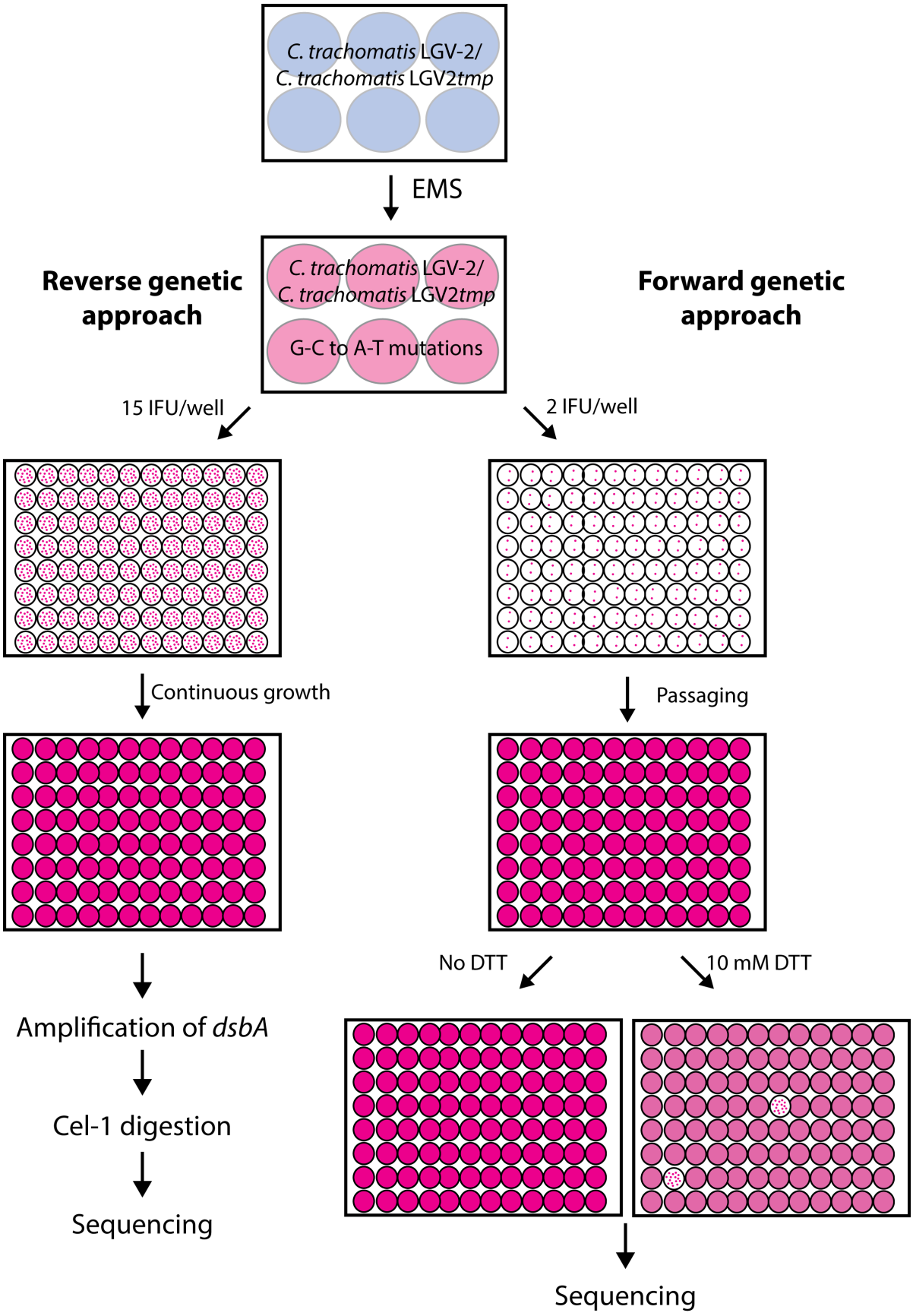

In the forward genetics approach, an EMS library was screened for increased sensitivity to the reducing agent dithiotrethreitol (DTT) (Figure 4.1). Treatment of EBs with DTT decreases infectivity significantly [131]. I hypothesised that mutations in a gene encoding a redox protein are therefore likely to result in altered sensitivity to DTT treatment. As such, a mutation will interfere with the formation of disulfide bonds. Reduction of the disulfide bonds in the extracellular EB decreases infectivity as shown by Hackstadt *et al.* [131]. Consequently, if CtDsbA is involved in oxidation of the COMC proteins, loss of CtDsbA activity might cause increased sensitivity to DTT as the disulfide bond cross-linking cannot be re-established. Even though increased DTT sensitivity might be observed for mutations in genes other than *dsbA,* this phenotypic screening approach was anticipated to significantly decrease the pool of potential mutants from which to identify a *dsbA* mutation.

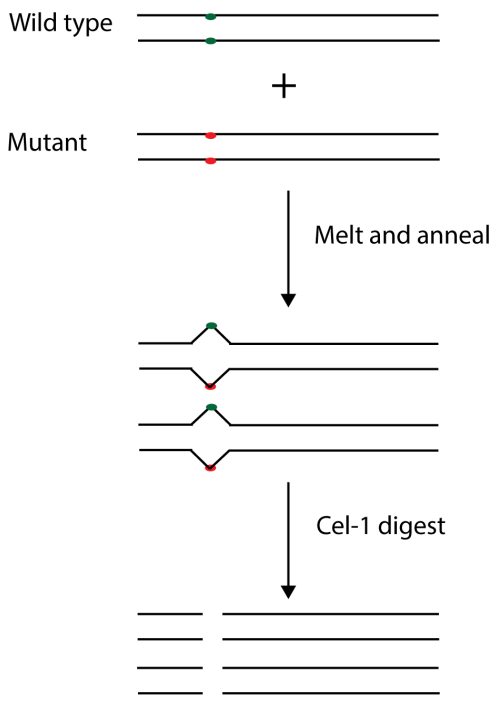

Figure 4.2 Schematic representation of TILLING.

A DNA heteroduplex with one base pair mismatch is created by melting and then annealing two PCR products, one of which is wild type (green) and one of which contains a point mutation (red). Cel-1 cleaves at the site of the base pair mismatch.

Targeting Induced Local Lesions IN Genomes (TILLING) was used to screen the library of EMS mutants in the reverse genetics approach (Figure 4.1). TILLING relies on the formation of a DNA heteroduplex between a native DNA strand and a strand with a single point mutation (Figure 4.2). The mismatch between the two strands creates a "bubble" that is recognised by the endonuclease Cel-1. Cel-1 can be easily extracted from celery making the approach cost-effective. Following Cel-1

digestion the DNA is separated by agarose gel electrophoresis to identify those samples that have been susceptible to Cel-1 activity.

4.2 Materials and methods

4.2.1 Cel-1 extraction from celery

Cel-1 was extracted from celery by ammonium sulphate precipitation [273]. Fresh clean celery stalks with the leaves removed were juiced at 4 °C using a household juicer and filtered through cloth. 1 M Tris-HCl pH 7.7 with protease inhibitor (1/1000 dilution of Merck Millipore inhibitor cocktail set III, EDTA free) was added to the celery juice to a final concentration of 0.1 M Tris-HCl. The celery juice was centrifuged at 4 °C, 2600 × g for 15 minutes. Solid $(NH_4)_2SO_4$ was added slowly to the supernatant with agitation to 25 % saturation (144 g/L). Following incubation with agitation at 4 °C for 30 minutes, the solution was centrifuged (4 °C at 15,000 × g for one hour) to remove protein of low solubility. $(NH_4)_2SO_4$ was added slowly to the supernatant under agitation to 80 % saturation (390 g/L). Following incubation with agitation at 4 °C for 30 minutes the solution was centrifuged 4 °C at 15,000 × g for one hour. The resulting pellet was resuspended in 1/10 of the starting volume of 0.1 M Tris-HCl pH 7.7 with protease inhibitor, and dialysed against 0.1 M Tris-HCl pH 7.7 with protease inhibitor. The buffer was exchanged hourly, seven times. After centrifugation at 20,000 × g for 20 minutes at 4 °C, the supernatant was aliquoted and stored at -20 °C.

4.2.2 Test of Cel-1 endonuclease activity of celery extract

A DNA heteroduplex was created between two PCR products encoding wt *bpsdsbA* and *bpsdsbA* carrying a single C to A point mutation resulting in the mutation of Lys133 to Met (*bpsdsbA L133M*). The heteroduplex was created by mixing the PCR products in 1:1 molar ratio and subjecting the mix to series of denaturing and annealing temperature conditions. Firstly, the products were heated to 99 °C for 10 minutes followed by a gradual decreasing temperature ramp (initial temperature of 70 °C, decreasing 0.3 °C each cycle for a total of 70 cycles of 20 seconds with a final temperature of 49 °C.) As a control, a homoduplex of *bpsdsbA* was subjected to the same treatment. Cel-1 endonuclease activity was tested by mixing 10 µL homo- or heteroduplex product with 100 mM HEPES pH 7.5, 100 mM KCl, 100 mM $MgSO_4$, 0.02 % Triton X-100 and 2 µg/mL BSA with varying volumes (0.5 µL to 8 µL) of celery extract at a final volume of 20 µL [273]. Cel-1 activity was confirmed by cutting at mismatch in heteroduplex. Cel-1 activity was confirmed by cutting of the mismatch in the DNA heteroduplex, and no cutting of the matched DNA homoduplex.

4.2.3 Test of primer specificity

Primers specific for the *dsbA* gene (Forward: 5'GACTCATAAGAAGTCTGAGAG and reverse: 5' CATAAGCGTTCCTATACAAG) were synthesised by Integrated DNA Technologies. Primer specificity was tested by amplifying the *dsbA* gene from heat-inactivated genomic DNA purified from *C. trachomatis* LGV-2. In a final volume of 50 µL, 50 ng of DNA was mixed with 0.2 µM of forward and reverse primer and 25 µL of JumpStart RedTaq Readymix (Sigma-Aldrich) containing JumpStart Taq DNA polymerase, 99 % pure deoxynucleotides and buffer.

4.2.4 Routine maintenance of McCoy cultures

Dulbecco Modified Eagle Media (DMEM) enriched with 10 % heat-inactivated Fetal Calf Serum (FCS), 2 % Glutamax^{TM}, 100 µg/mL streptomycin and 50 µg/mL gentamycin were used for all cell suspensions and infections.

Unless otherwise noted, infected and non-infected cells were incubated at 37 °C/5 % CO_2 in a humidified incubator.

McCoy cells were cultured in T75 culture flasks. Confluent cells were harvested by treatment with 1 mL of a 0.05 % trypsin/0.02 % EDTA solution and incubated 10 minutes at room temperature. Cells were dislodged by gentle tapping and resuspended in 9 mL fresh media. Cell density was determined by mixing a 10 µL cell suspension with 10 µL tryphan blue and counting using a haemocytometer under a microscope with a 10x objective. The resulting cell suspension was used to seed new T75 culture flasks, 6-well plates (1,500,000 cells/well) or 96-well plates (20,000 cells/well).

4.2.5 Infection of McCoy cells with *C. trachomatis*

24 h after seeding 6-well or 96-well plates with McCoy cells, the cells were infected with *C. trachomatis* LGV-2 or *C. trachomatis* LGV-2*tmp.* For infection, bacterial cells were diluted to the appropriate multiplicity of infection (MOI) in media. Bacteria were applied to McCoy cells and centrifuged at 28 °C at 500 × g for 30 min. After four hours incubation, the media was replaced with fresh media containing 1 µg/mL cyclohexamide and incubated for another 44 h. Unless otherwise stated infected McCoy cells were passaged every 48 h.

4.2.6 Passaging of infected McCoy cells

Infected McCoy cells grown in 96-well plates were passaged every 48 h by removing media from wells and harvested in 100 µL cold sucrose-phosphate-glutamic acid (SPG). The 100 µL SPG harvest was used to infect a fresh monolayer of McCoy seeded 96-well plates.

4.2.7 Continuous growth of infected McCoy cells

Infected McCoy cells were grown in 96-well plates with a media change four hours post infection. The infected cells were grown without passaging for eight days, but media was replaced with fresh media after four days.

4.2.8 Methanol fixing of infected McCoy cells

Media was removed from the wells, and the cells washed one time with 200 µL 137 mM NaCl, 2.7 mM KCl, 10 mM Na_2HPO_4, 1.8 mM KH_2PO_4, pH 7.4 (PBS). Cells were fixed by filling each well to the top of the well with 100 % methanol and incubating at room temperature for 10 min. Subsequently each well was washed twice with PBS. Plates were stained immediately, or stored in PBS for staining at a later stage.

4.2.9 HtrA and DAPI Antibody staining

In a 96-well plate containing *C. trachomatis* LGV-2 or *C. trachomatis* LGV-*2tmp* infected McCoy cells, the cells were permeabilised by adding 100-200 µL 0.5 % Triton X-100 in PBS to each well, followed by incubation for 15 min at room temperature. Permeabilisation buffer was removed and the infected cells were blocked with 1% Bovine Serum Albumin (BSA) in PBS for one hour at room temperature. After this point plates were kept in the dark by covering the plates with aluminium foil. The host cell nuclei were stained with 4',6-Diamidine-2'-phenylindole dihydrochloride (DAPI) antibody (1:40,000 dilution in 1 % BSA in PBS). The chlamydial inclusion was stained first with the primary antibody anti-HtrA rabbit sera (1:500 in 1 % BSA in PBS) and then with a secondary antibody: goat anti-rabbit IgG (H+L) – Alexa Fluor 488 (1:600 in 1 % BSA in PBS) [274-276]. Plates were imaged on IN Cell Analyzer 2200 (GE Healthcare) in the 2D acquisition mode. HtrA was imaged using the Fluorescein isothiocyanate (FITC) channel (excitation filter: 475/28x and emission filter 512/23m). DAPI was imaged using the DAPI channel (excitation filter: 590/18x and emission

filter 432/48m). Infectivity was calculated as the number of host cell nuclei with an associated chlamydial inclusion.

4.2.10 Titration of *C. trachomatis* infection

In a 96-well plate seeded with McCoy cells, individual wells were infected with 25 µl of *C. trachomatis* SPG stock in dilutions from 10^{-1} to 10^{-6} in duplicates. Infected cells were methanol-fixed, stained with anti-HtraA and DAPI. The number of inclusions was counted in four fields of view (FOV) per well (0.556 mm^2) using the multipoint tool in ImageJ. Titre (Inclusion forming Units (IFU) per mL) was calculated by multiplying the average number of inclusions per FOV with the total FOV/well (54.29 FOV per one well in a 96-well plate, instrument specific) and adjusting for the dilution and the volume of infection.

4.2.11 Establishment of mutation frequency

Six-well plates were seeded with 1.2 x 10^6 McCoy cells and infected with *C. trachomatis* LGV-2 in enriched DMEM media containing 0 µg/mL, 0.025 µg/mL, 0.05, µg/mL 0.1 µg/mL, 0.3 µg/mL or 0.5 µg/mL rifampicin to establish the lethal concentration of rifampicin. Following infection, the inoculum was removed and the cell layers overlayed with 2 mL 0.55 % agar in enriched DMEM. After the agarose had solidified, the infected McCoy cells were overlayed with enriched DMEM media containing 0 µg/mL, 0.025 µg/mL, 0.05 µg/mL, 0.1 µg/mL, 0.3 µg/mL or 0.5 µg/mL rifampicin and incubated with a change of the non-agarose overlay every third day. After 14 days, plaque formation was evaluated. The lethal concentration was determined as the concentration were plaque formation is absence. The experiment was performed in duplicate.

To determine mutation frequency, six-well plates seeded with 1.2 x 10^6 McCoy cells were infected with 5 mg/mL or 6 mg/mL *C. trachomatis* LGV-2 or *C. trachomatis* LGV-2 *tmp* libraries in enriched DMEM media containing the lethal dose of rifampicin identified above. Following infection, the inoculum was removed and the cell layers overlayed with 2 mL 0.55 % agar in enriched DMEM. After the agarose had solidified, infected McCoy cells overlayed with enriched DMEM media containing the lethal dose of rifampicin were incubated with change of the non-agarose overlay every third day. After 14 days, plaque forming was evaluated. This experiment was performed in duplicate.

4.2.12 Generation of EMS treated *C. trachomatis* library

McCoy cells were infected with *C. trachomatis* LGV-2 or *C. trachomatis* LGV-2*tmp* at an MOI of 5 in 6-well plates. 19 h post infection, infected cells were treated with concentrated EMS in enriched DMEM media (1:10 v/v dilution) to give final concentrations of 0, 2, 3, 4, 5, 6, 7 and 8 mg/mL. The plates were incubated at 37 °C for one hour, before replacing with fresh media containing 1 µg/ml cyclohexamide. 44 h post infection the cells were harvested in 1 mL cold SPG. The EMS libraries were titrated to determine IFU/well.

4.2.13 Comparison of passaging and continuous growth of infected McCoy cells

McCoy cells were infected with 2 IFU/well, 5 IFU/well, 10 IFU/well or 15 IFU/well of *C. trachomatis* LGV-2 in triplicates. After four hours the media was replaced with fresh media containing 1 µg/mL of cyclohexamide. Subsequently the plates were incubated for eight days, with a media change after four days. As a control McCoy cells were infected with 2 IFU/well, 5 IFU/well, 10 IFU/well or 15 IFU/well *C. trachomatis* LGV-2 in triplicate and passaged every 48 h for eight days. Both plates were fixed with methanol and stained with anti-HtraA and DAPI. Inclusions were counted using the multi-point selection tool in ImageJ and a student's T-test for two independent mean were calculated.

4.2.14 Initial investigation of *C. trachomatis* LGV-2 sensitivity towards DTT

24 h after infecting McCoy cells with *C. trachomatis* LGV-2 (MOI: 0.5) each well was harvested in 100 µL cold SPG. 50 µL of SPG harvested cells was treated with a final DTT concentration of 10 mM, 25 mM or 100 mM in PBS and was incubated for two hours. Subsequently the DTT treated SPG harvest was used to infect a fresh layer of McCoy cells. After one hour the media was replaced with fresh media containing 1 µg/ml of cyclohexamide and incubated for another 30 h. Cells were fixed with methanol and stained with DAPI and a HtrA specific antibody.

4.2.15 Screening of EMS library for increased DTT sensitivity

24 h after seeding, McCoy cells were infected with 2 IFU/well of the 5 mg/mL EMS treated *C. trachomatis* LGV-2 library with a media change after four hours. After eight days of passaging every 48 h, the infected cells were harvested in 100 µL SPG. 30 µL of SPG suspended cells were treated with 10 mM DTT as described in section 4.2.13 and used to infect a fresh monolayer of McCoy cells. As a control, 30 µL of SPG suspended cells were used to infect a fresh monolayer of McCoy cells

without DTT treatment. The remaining 40 µL of SPG suspended cells was frozen at -80 °C. Incubated cells were incubated for six days with passaging every 48 h. Cells were fixed with methanol and stained with DAPI and a HtrA specific antibody. Wells with an altered phenotype upon DTT treatment were subjected to Sanger sequencing outsourced to Australian Genome Research Facility and samples were prepared as per their recommendations.

4.2.16 EMS library screen using TILLING

In a 96-well plate, McCoy cells were infected with 15 IFU/well of 6 mg/mL EMS treated *C. trachomatis* LGV-2 or *C. trachomatis* LGV-2*tmp* chlamydial library with a media change after four hours. After eight days of continuous growth, with a media change after four days, each well was harvested with 80 µl SPG. 1 µl SPG harvested cells was amplified by PCR using CtDsbA specific oligonucleotides at a final volume of 10 µL and subjected to Cel-1 treatment. Wells with a potential mutation in the *dsbA* gene, as evaluated by Cel-1 cleavage, were subjected to Sanger sequencing outsourced to Australian Genome Research Facility and samples were prepared as per their recommendations.

4.3 Results

4.3.1 Introduction of random mutations by EMS

Treatment with the carcinogenic organic compound EMS introduces randomly positioned mutations in DNA. The ethyl group of EMS reacts with guanine in DNA resulting in the formation of O^6-ethylguanine. O^6-ethylguanine frequently pairs with thymine, rather than cytosine, which is the natural partner of guanine. Consequently, following EMS exposure, the original G:C is replaced with an A:T pair after several rounds of replication [272].

The full-length *C. trachomatis dsbA* gene has 237 codons. Of these, 189 contain a guanine or cytosine base and can therefore be mutated upon treatment with EMS (Table 4.1). However, EMS mutagenesis is only an appropriate strategy for obtaining a loss-of-function *dsbA* mutant if EMS is capable of introducing nonsense mutations in the *dsbA* gene. Alternatively, introduction of missense mutations in the cysteine codons can potentially give insight into the importance of these particular residues for CtDsbA activity. Analysis of the *dsbA* gene reveals that the number of possible mutations is 285, of which 210 are non-synonymous and 66 are synonymous and therefore silent (Table 4.1).

Table 4.1 Potential for EMS induced mutations in CtDsbA and their effect.

Codons	Codons with mutations	Mutations	Synonymous mutations	Non-synonymous mutations	Nonsense mutations	Non-synonymous mutations in Cys codons
237	**189**	**285**	**66**	**210**	**9**	**6**

There are 237 codons in the full-length dsbA gene in C. trachomatis *of which 189 have the potential to be mutated by EMS. Out of 285 possible mutations 66 are synonymous, 210 are non-synonymous and nine are nonsense mutations. All six cysteine residues are potential targets for EMS mutation.*

There are nine options for nonsense mutations in the *dsbA* gene (Table 4.1). The full-length *dsbA* gene contains six codons for cysteines, all of which can potentially be mutated to tyrosine upon treatment with EMS (Table 4.1). As shown in Chapters 2 and 3 the truncated, soluble construct of CtDsbA has oxidase activity in the absence of the non-catalytic disulfide and the unpaired Cys70. Consequently, only disruption of the two codons corresponding to the active site cysteines is likely to result in loss of function of CtDsbA.

4.3.2 Establishment of EMS library

McCoy cells infected with *C. trachomatis* LGV-2 or *C. trachomatis* LGV-*2tmp* were treated with 2 mg/mL to 8mg/mL of EMS to create a library of EMS mutants. However, treatment with EMS concentration above 7 mg/mL resulted in a complete loss of infectivity and no bacteria could be harvested (Figure 4.3). To enhance the probability of obtaining a loss-of-function mutation in the *dsbA* gene, the libraries obtained from treating with 5 mg/mL and 6 mg/mL of EMS were screened.

Efforts were made to establish the mutation frequency of EMS treatment, by evaluating the frequency of acquired rifampicin resistance in EMS-treated cells. The lethal dose of rifampicin was determined to be 0.3 mg/mL as evaluated by the absence of plaques at this concentration. Unfortunately, evaluation of acquired rifampicin resistance failed due to disruption of the soft agar overlay. Due to time pressure this experiment was not repeated. The protocol has previously been used successfully in the laboratory of Dr. Wilhelmina Huston, where this experiment was performed. In previous experiments the mutation frequency was established to be 0.9 mutations for the *C. trachomatis* D UW-3/Cx genome treated with 2 mg/mL EMS [277]. Another study by Kari *et al.* showed that treating *C. trachomatis* D UW-3/Cx with 5 mg/mL EMS leads to a mutation frequency of approximately 2.5 mutations per chlamydial genome [271]. As there are 4.3×10^5 possible mutation sites in *C. trachomatis* and 11 possible mutation sites in the *dsbA* gene that result in a loss-of-function mutation,

an estimated 16,300 subpopulations should be screened to identify one loss-of function mutation in the *dsbA* gene.

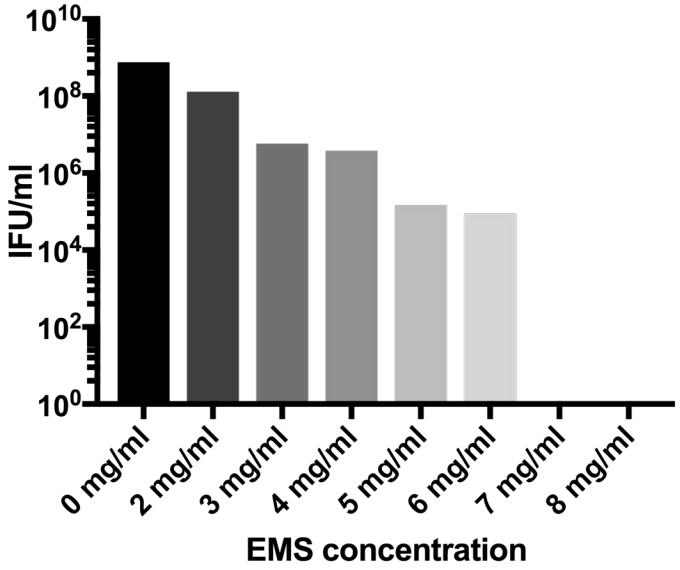

Figure 4.3 Titration of EMS libraries.

To establish the titre of the EMS library, McCoy cells were infected with C. trachomatis *LGV-2 treated with 0, 2, 3, 4, 5, 6, 7 or 8 mg/mL EMS. 30 h post infection the cells were fixed with methanol and host cell nuclei were stained with the fluorescent dye DAPI that binds strongly to A-T rich regions in DNA. Chlamydial inclusions were stained for the chlamydial inclusion protein HtrA with an anti-HtrA antibody with secondary antibody goat anti-rabbit IgG (H+L) – Alexa Fluor 488. The titre (IFU/mL) of each library was established by calculating the number of inclusions in each well and adjusting for the volume used to infect.*

4.3.3 Test of Cel1 activity

Identification of a *dsbA* mutation in the TILLING screen of the EMS library requires extraction of active Cel-1 from celery. Cel-1 was extracted from fresh celery by ammonium sulfate precipitation. The Cel-1 endonuclease activity of the celery extract was tested by assessing its ability to cleave at a base pair mismatch in a DNA heteroduplex (Figure 4.4). The heteroduplex was formed between PCR products of *bpsdsbA* wt and *bpsdsbA* carrying a single C to A point mutation resulting in a Lysine to Methionine mutation (*bpsdsbA L133M*). The heteroduplex was formed by subjecting *bpsdsbA* and *bpsdsbA* L133M to several rounds of melting and annealing conditions. The heteroduplex has a size of 636 bp and cleaving at the base pair corresponding to the C-A mismatch results in two fragments of 400 bp and 236 bp, respectively. The heteroduplex was treated with between 0.5 µL and 8 µL of celery extract for 15 minutes at 45 °C and analysed by 2 % agarose gel electrophoresis (Figure 4.4).

A homoduplex of *bpsdsbA* was included as a negative control and treated with 8 µL celery extract. Only a band corresponding to the uncleaved heteroduplex (~600bp) is present upon treatment with 0.5 µL celery extract (Figure 4.4). Treatment with 2 µL celery extract results in a faint band at approximately 400 bp corresponding to the larger of the cleaved fragments, however the smaller fragment is not visible (Figure 4.4). Three bands are present upon treatment with 4 µL celery extract. The band at 600 bp represents the uncleaved heteroduplex, whereas the presence of two bands at approximately 400 bp and 200 bp are in agreement with cleaving at the C-A mismatch by Cel-1 (Figure 4.4). The intensity of the two smaller bands increases with treatment with 6 µL and 8 µL celery extract indicating that a greater fraction of the heteroduplex is cleaved (Figure 4.4). For the homoduplex of *bpsdsbA* wt, only a band at approximately 600 bp is present after treatment with 8 µL celery extract confirming that Cel-1 is present and cleaves specifically at the mismatch (Figure 4.4).

A smear is present in all lanes of the agarose gel. Despite the smear, treatment with 4 µL celery extract led to easy recognition and good separation of the two bands corresponding to Cel-1 digestion. Therefore 4 µL was used in the TILLING screen.

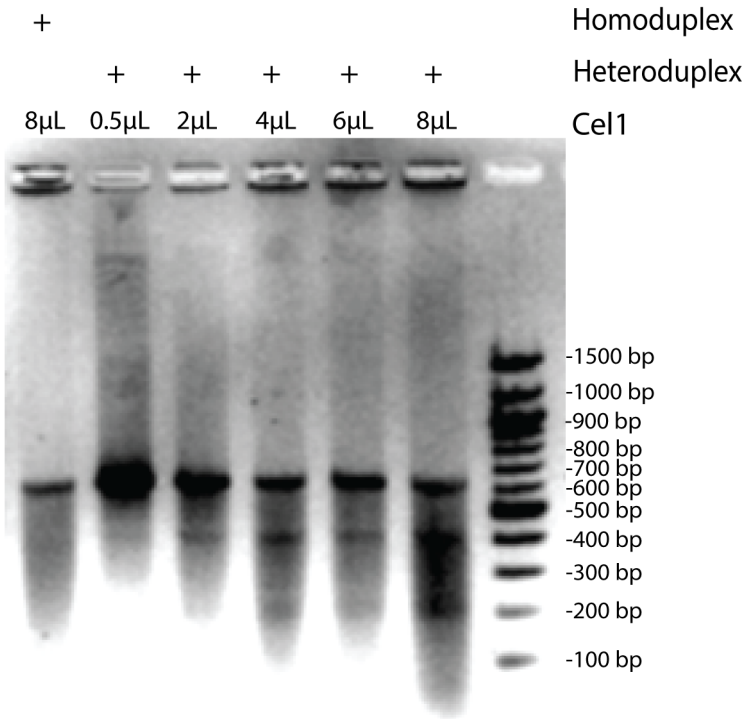

Figure 4.4 Test for Cel-1 endonuclease activity of celery extract.

Cel-1 endonuclease activity was confirmed by testing the ability of increasing volumes of celery extract (0.5 µL to 8 µL) to cut at mismatches in DNA heteroduplex formed between bpsdsbA wt *and* bpsdsbA L133M *containing a single base pair mismatch. A* bpsdsbA wt *homoduplex was included as a negative control. Both the heteroduplex and homoduplex are 636 bp long. Cel-1 cleavage of the heteroduplex results in two additional bands at ~400 bp and ~ 200 bp.*

4.3.4 Initial screen of *C. trachomatis* LGV-2 sensitivity towards DTT

DTT sensitivity was chosen as a phenotypic readout for a potential mutation in the *dsbA* gene in the forward genetics approach. Upon prior treatment of *C. trachomatis* LGV-434 with 10 mM DTT, infection of HeLa cells with the bacteria decreases to 22 % of the infection achieved in the absence of DTT [131]. If the EMS library contains a loss-of-function mutation in the *dsbA* gene this mutant is likely to show increased sensitivity to treatment with DTT. To identify an appropriate DTT concentration to use in the screen, *C. trachomatis* LGV-2 infected McCoy cells were treated with 0, 5, 10, 25 or 100 mM DTT (Figure 4.5).

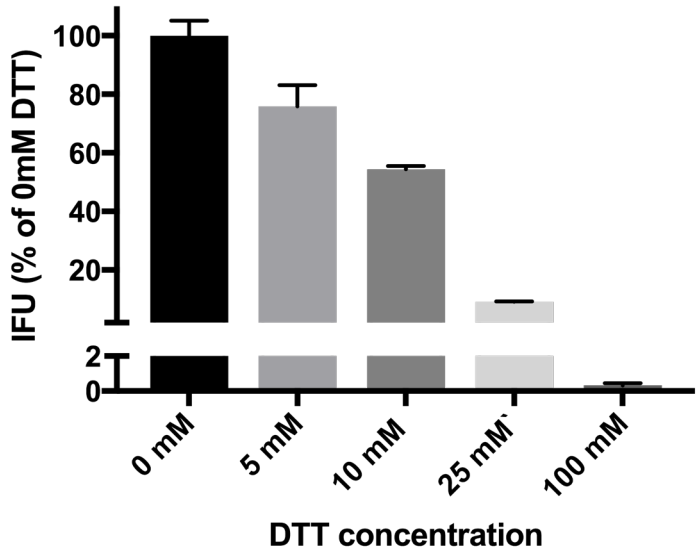

Figure 4.5 Effect of DTT on infectivity.

McCoy cells were infected with C. trachomatis LGV-2 *and treated with 0, 5, 10, 25 or 100 mM DTT in triplicate. 30 h post infection the cells were fixed with methanol and host cell nuclei were stained with the fluorescent dye DAPI. Chlamydial inclusions were stained for the chlamydial inclusion protein HtrA with an anti-HtrA antibody with secondary antibody goat anti-rabbit IgG (H+L) – Alexa Fluor 488. The titre (IFU/mL) of each DTT treated infection was established by calculating the number of inclusions in each well and adjusting for the volume used to infect. The titre is indicated as % of the titre of the infection treated with 0 DTT. Mean and standard deviation of three individual experiments are shown.*

Treatment with 5 mM DTT resulted in 25 ± 7 % decrease in IFU compared to the untreated control (Figure 4.5). Due to the relatively limited effect on infection observed upon treatment with 5 mM DTT this condition was not used further in the DTT sensitivity screen of the EMS library. For 25 mM and 100 mM DTT the IFU count was decreased by 90 ± 1 % and 99 ± 0.1 %, respectively (Figure

4.5). As infectivity was almost abolished after treatment with 25 mM DTT, and completely abolished with 100 mM DTT, a further decrease of infection would be difficult to evaluate. Upon treatment with 10 mM DTT the IFU count was 46 ± 1 % of the untreated control (Figure 4.5). This is a significant decrease in infectivity, but would also allow observation of further decrease in infectivity resulting from a mutant with increased sensitivity to DTT.

High DTT concentrations can potentially directly influence the host cell in addition to affecting the infectivity of *C. trachomatis*. Therefore, the effect of DTT on the monolayer of infected McCoy cells was tested (Figure 4.6).

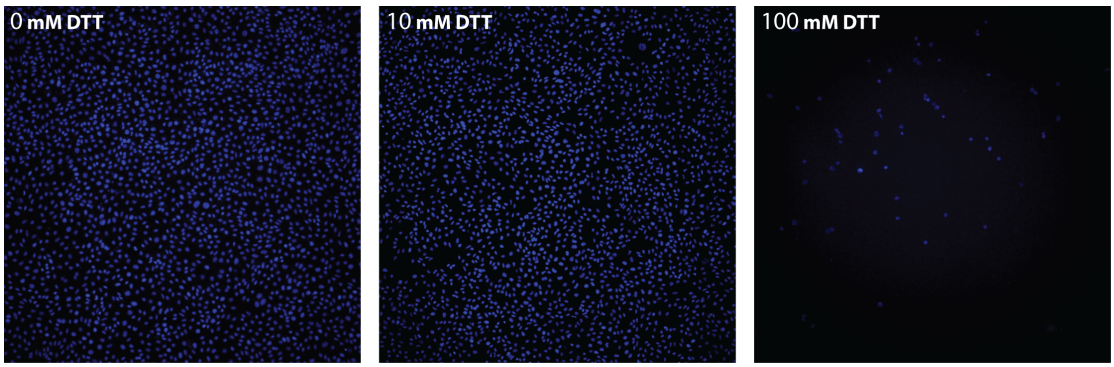

Figure 4.6 The effect of DTT on the McCoy cell monolayer.
C. trachomatis *LGV-2 infected McCoy cells were treated with 0, 10 and 100 mM DTT and the host cell nucleus (blue) was stained with DAPI.*

The condition of the McCoy cell monolayer was evaluated by staining DTT treated *C. trachomatis* LGV-2 infected McCoy cells with the fluorescent dye DAPI. As DAPI binds strongly to A-T rich regions in DNA, each blue spot in Figure 4.6 represents a host cell nucleus. Consequently, the number of host cells surviving the DTT treatment can be visualised. Treatment with 100 mM DTT has a significant effect on the monolayer as judged by the severe disruption of the monolayer. In contrast, the number of nuclei after treatment with 10 mM DTT is equivalent to the untreated control (Figure 4.6), suggesting that treatment with 10 mM DTT has limited or no effect on the host cell viability. As treatment with 10 mM DTT leads to an appropriate decrease in infectivity of *C. trachomatis* but does not affect host cell viability, 10 mM DTT was chosen for screening the EMS library for increased DTT sensitivity.

4.3.5 Comparing suitability of continuous growth vs. passage of infected McCoy cells for screening

In the forward and reverse genetic approach McCoy cells were infected with a limited number of IFUs and grown for eight days to increase the number of McCoy cells infected by the EMS mutants. This allows observation of decreased infectivity as a result of increased DTT sensitivity in the forward genetics approach or amplification of the *dsbA* gene in the reverse genetics approach, respectively. In the DTT sensitivity screen, McCoy cells were infected with 2 IFU/well in a 96-well plate. 2 IFUs were chosen as this number allows for observation of a decrease in infectivity compared to the untreated control. Infecting with more than 2 IFUs increases the possibility that a healthy subpopulation without a mutation in the *dsbA* gene might outgrow the subpopulation containing a mutation in the *dsbA* gene, thereby making observation of a decrease in infectivity challenging. Evaluation of decreased infectivity would be simpler if infecting with 1 IFU/well, however infecting with 2 IFU/well doubles the number of subpopulations screened in each well without significantly interfering with evaluation of the effect of DTT treatment. 2 IFU/well was thus chosen for experimental efficiency.

As the TILLING approach does not select for a specific phenotype of the McCoy cells, it allows for infection with a higher IFU. However, infecting with more than 15 IFU could potentially complicate identification of a mutant by sequencing. As each well would contain more than 15 subpopulations, of which only one is likely to contain a specific point mutation, the ratio of wild type (wt) to mutant base is potentially too small to identify the mutation.

To minimise handling it would be advantageous if the number of infected McCoy cells can be increased by continuous growth rather than passaging every 48 h. To identify an appropriate IFU for continuous growth, McCoy cells were infected with *C. trachomatis* at an IFU of 2 IFU/wells, 5 IFU/wells, 10 IFU/wells or 15 IFU/wells and grown continuously for eight days with a media change after four days. Control infections with 2 IFU/wells, 5 IFU/wells, 10 IFU/wells or 15 IFU/wells were passaged every 48 h by harvesting in SPG and using the SPG harvest to infect a fresh monolayer of McCoy cells. After eight days, the cells were fixed and the chlamydial inclusion protein HtrA was stained with an anti-HtrA antibody and secondary goat anti-rabbit IgG (H+L) – Alexa Fluor 488 antibody to identify chlamydial inclusions (Figure 4.7).

There are on average 6.3 ± 1.5 inclusions per FOV when imaging the wells containing McCoy cells infected with 2 IFU/well and cultured continuously for eight days (Figure 4.7A). In comparison wells that had been passaged every 48 h had on average 236 ± 73 inclusions per FOV (Figure 4.7B). When comparing the passaged and continuously cultured cells infected with 2 IFU/well in a students t-test for comparison of two independent means, a p-value of 0.005 is obtained. Similar results are found for infections of 5 IFU/well (p=0.002) (Figure 4.7C+D). When McCoy cells are infected with 10 IFU/well the yield after eight days of continuous growth without passaging (Figure 4.7E) is approximately half of the yield compared to when the cells are passaged every 48 h for eight days (Figure 4.7F), but the difference is not statistically significant (p=0.1). Infecting with 15 IFU/well gives approximately the same yield of chlamydial inclusions (p=0.2) after eight days of continuous growth as passaging every 48 h (Figure 4.7G+H). Consequently, it was decided to infect with 2 IFU/well and to passage the infected cells when assessing the EMS library for DTT sensitivity. When assessing the library using the TILLING approach the cells can be infected with 15 IFU/well and grown continuously without passaging.

Figure 4.7 Yield of chlamydial inclusions eight days post infection after continuous growth compared to passaging.

The chlamydial inclusion protein, HtrA (green), is stained with anti-HtrA antibody with secondary antibody goat anti-rabbit IgG (H+L) – Alexa Fluor 488 and imaged using an IN Cell Analyzer 2200. Each green spot represents a single chlamydial inclusion. McCoy cells infected with 2 IFU/well had a significantly lower (p=0.005) yield of inclusions after 8 days of continuous growth (A) than when passaged every 48 h (B). McCoy cells infected with 5 IFU/well had a significantly lower yield (p=0.002) of inclusions after 8 days of continuous growth (C) than when passaged every 48 h (D). McCoy cells infected with 10 IFU/well had a slightly lower yield of inclusions after 8 days of continuous growth (E) than when passaged every 48 h (F), but this was not statistically significant (p=0.1). McCoy cells infected with 15 IFU/well had a similar yield of inclusions (p=0.2) after 8 days of continuous growth (G) as when passaged every 48 h (H).

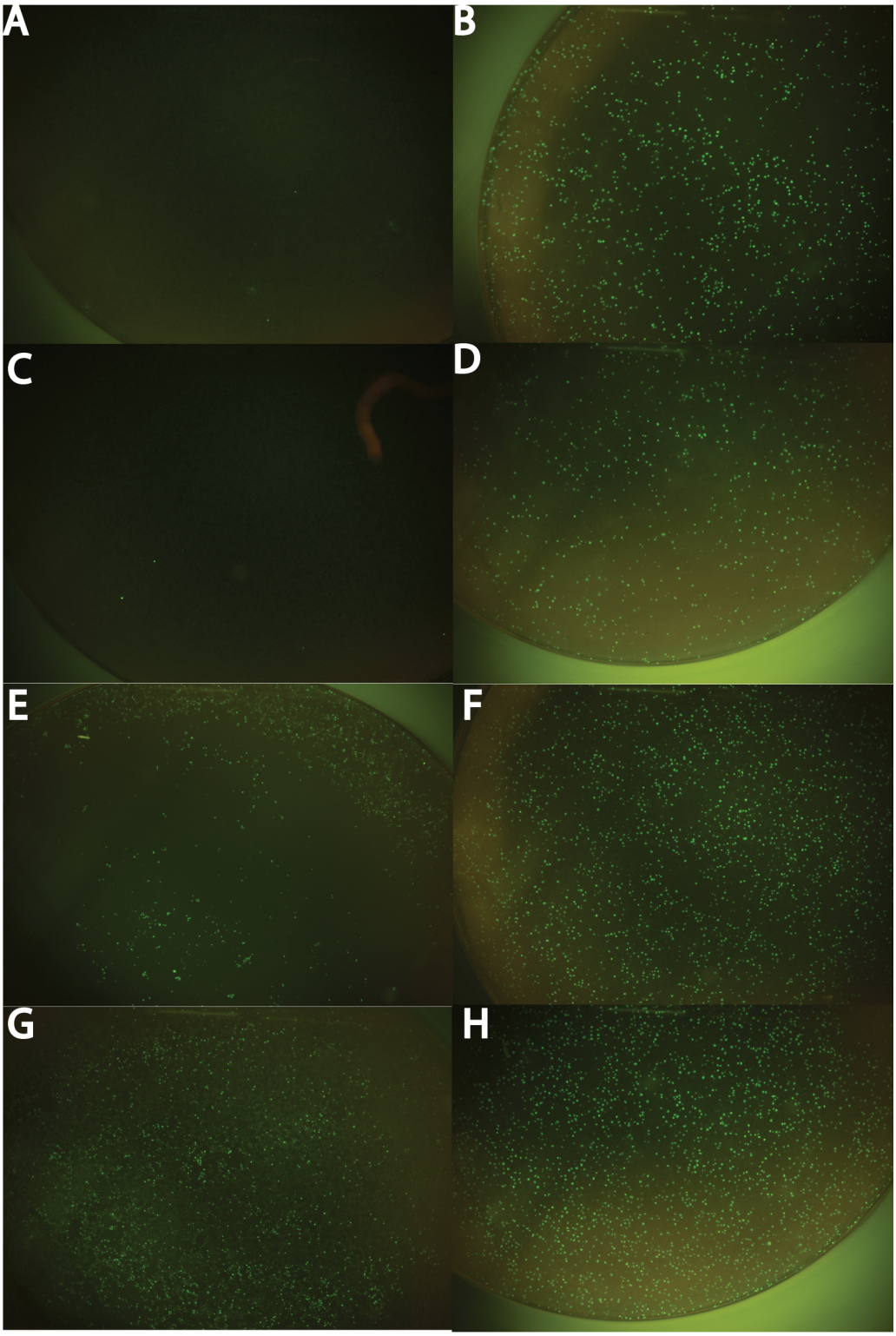
A
B
C
D
E
F
G
H

4.3.6 Forward genetics approach of screening EMS library for increased DTT sensitivity

In the forward genetics approach the EMS library was screened for increased sensitivity to DTT to decrease the pool of potential EMS mutants with a loss-of-function mutation in the *dsbA* gene.

McCoy cells in 96-well plates were infected with the 5 mg/mL EMS-treated library of *C. trachomatis* LGV-2 at 2 IFU/well and passaged every 48 h for eight days. After harvesting in SPG, one third of the harvest was treated with 10 mM DTT and used to infect a fresh monolayer of McCoy cells. As a control, another third of the harvest was used to infect McCoy cells without prior treatment with DTT. Both DTT treated and control infections were passaged for six days before cells were fixed and stained. The host cell nucleus was stained with DAPI and the inclusions were stained with an antibody specific for the inclusion protein HtrA with a secondary antibody goat anti-rabbit IgG (H+L) – Alexa Fluor 488 antibody. Infectivity was calculated as the number of host cell nuclei (blue) associated with a chlamydial inclusion (green) (Figure 4.8).

Treating *C. trachomatis* LGV-2 with 10 mM DTT led to a 46 % decrease in infectivity (Figure 4.5). The hypothesis is that a loss-of-function mutation in the *dsbA* gene will lead to increased sensitivity to DTT treatment and consequently decreased infectivity. In this screen infections showing more than 60 % decrease in infectivity upon DTT treatment were regarded as hits for increased DTT sensitivity.

Four different phenotypes were observed upon treatment of the EMS library with 10 mM DTT; (i) a decrease in infectivity upon treatment of the EMS library with DTT equivalent to the 46 % decrease in infectivity observed for DTT treatment of *C. trachomatis* LGV-2 wt (Figure 4.8A); (ii) a decrease in infectivity greater than 60 % of the DTT treated infections compared to the untreated controls (Figure 4.8B); (iii) an increase in infectivity of DTT treated infections compared to the untreated control (Figure 4.8C); (iv) a decrease in inclusion size in the DTT treated infections compared to the untreated control (Figure 4.8D).

Figure 4.8 Four different phenotypes were observed upon treatment of EMS library with 10 mM DTT.

McCoy cells were infected with the 5 mg/mL EMS treated library of C. trachomatis *LGV-2 at 2 IFU/well and passaged every 48 h and harvested in SPG. One third of the harvest was treated with 10 mM DTT and used to infect a fresh monolayer of McCoy cells. As a control, another third of the harvest was used to infect McCoy cells without prior treatment with DTT. Infections were cultured for six days with passaging every 48 h. After fixing the cells with methanol the host cell nucleus (blue) was stained with DAPI. The chlamydial inclusion protein HtrA (green) was stained with anti-HtrA antibody with secondary antibody goat anti-rabbit IgG (H+L) – Alexa Fluor 488 and imaged on IN Cell Analyzer 2200.* ***A)*** *DTT treatment of one well of the EMS library results in decrease in infectivity of 51 % compared to the corresponding untreated well. This is equivalent to a decrease in infectivity of 46 % observed for* C. trachomatis *LGV-2 treated with 10 mM DTT.* ***B)*** *DTT treatment of one well of the EMS library leads to a decrease in infectivity of 70 % compared to the untreated control.* ***C)*** *DTT treatment of one well of the EMS library leads to an increase in infectivity compared to an untreated control.* ***D)*** *DTT treatment of one well of the EMS library leads to a decreased inclusion size compared to the untreated control. For ease of comparison the host cell nucleus is omitted from this image.*

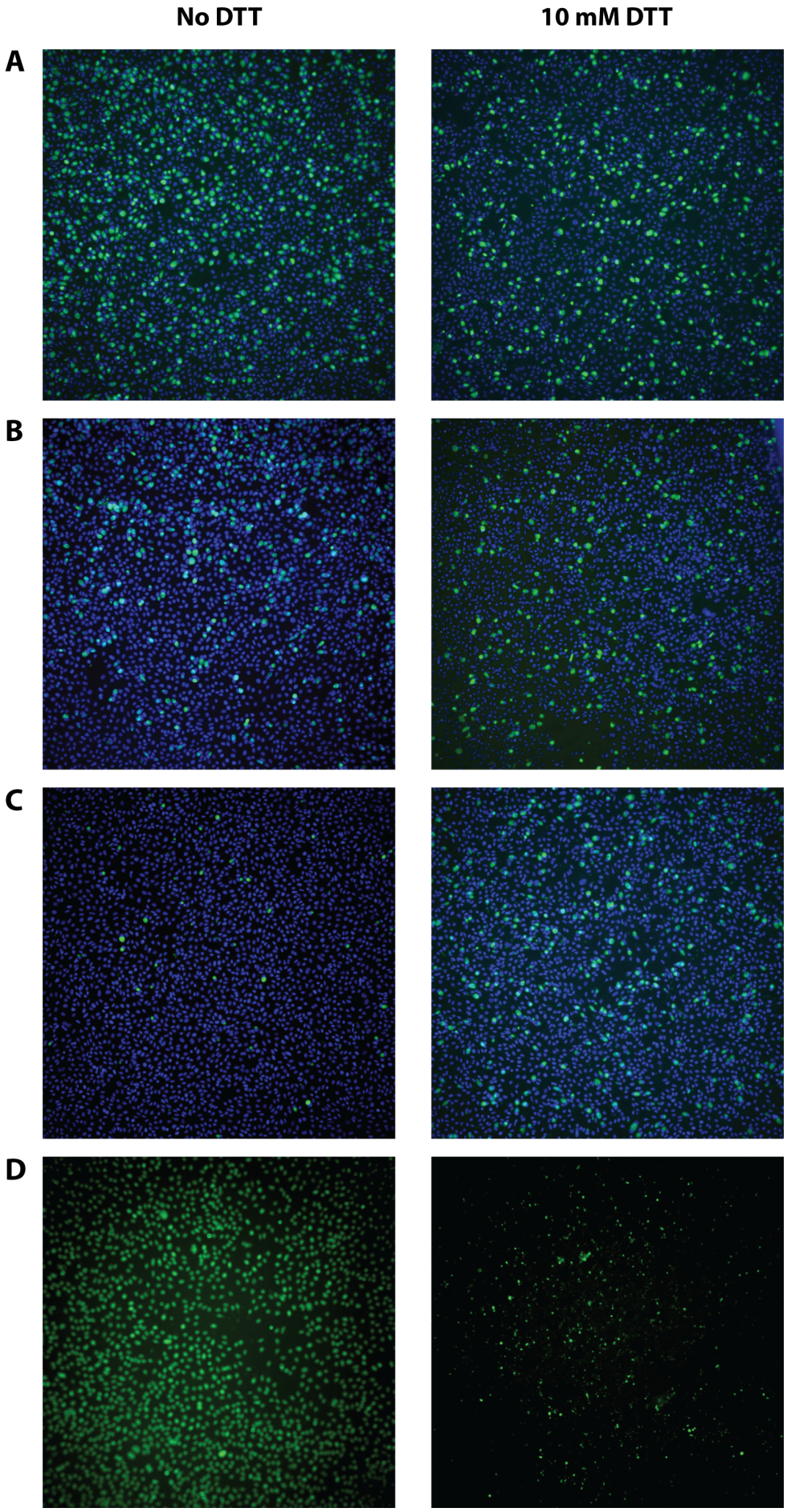
No DTT
10 mM DTT
A
B
C
D

Out of 963 wells screened, 927 wells showed no significant change in DTT sensitivity of the EMS library compared to control *C. trachomatis* LGV-2 (Table 4.2). An example of this is shown in Figure 4.8A, where treatment with DTT led to a decrease in infectivity of 51 % compared to the untreated control, which is roughly equivalent to the 46 % decrease observed upon DTT treatment of *C. trachomatis* LGV-2 (Figure 4.5). 36 wells showed altered phenotype upon treatment with DTT compared to the untreated control (Table 4.2). Increased sensitivity for DTT was observed in 28 wells as evaluated by a decrease in infectivity greater than 60 % upon DTT treatment (Table 4.2), including one well where the infectivity decreased by 70 % upon DTT treatment compared to the untreated control (Figure 4.8B). In one of five wells with ***increased*** infectivity, the infectivity of the DTT treated control is 51 % higher than in the untreated control (Figure 4.8C). Figure 4.8D shows one example out of three infections that exhibited reduced inclusion size compared to the untreated control (Table 4.2).

Table 4.2 EMS treated* C. trachomatis *LGV-2 library phenotypes observed upon DTT treatment.

Phenotype	Observations	Confirmation of Phenotype
No difference	927	-
Decrease in infectivity	28	14
Increase in infectivity	5	0
Decrease in inclusion size	3	0

To investigate the robustness of the phenotype, DTT treatment was repeated for the 36 wells showing an altered phenotype. The phenotype was confirmed for 14 of the 36 infections showing altered phenotype in the original screen (Table 4.2). All cases of confirmed phenotype in the screen of the 5 mg/mL EMS treated library of *C. trachomatis* LGV-2 showed a decrease in infectivity upon DTT treatment larger than the 60 %. The 14 infections with a confirmed phenotype were subjected to Sanger sequencing with *dsbA* specific primers, but none contained *C. trachomatis* with a mutation in the *dsbA* gene.

4.3.7 Reverse genetics approach for screening of EMS Library using TILLING

McCoy cells were infected with 15 IFU/well of the EMS libraries derived from treating *C. trachomatis* LGV-2 or *C. trachomatis* LGV-*2tmp* with 6 mg/mL EMS. As per the previously described experiment (Section 4.3.5) the number of McCoy cells infected with 15 subpopulations of EMS mutants were increased by continuous growth for eight days and harvested. The harvested cells were heat-inactivated and the *dsbA* gene was amplified with primers specific for the *dsbA* gene. As only one subpopulation out of 15 in each infection is likely to have a specific mutation in the *dsbA* gene, a heteroduplex will form after melting and annealing of the 15 subpopulations if any of the

subpopulations harbours a mutation in the *dsbA* gene. A potential mutation can subsequently be identified by treatment with celery extract with Cel-1 endonuclease activity.

The specificity of the primer set was tested by amplifying the *dsbA* gene from heat-inactivated *C. trachomatis* LGV-2 EBs by PCR. Different annealing temperatures were investigated to identify the correct annealing temperature for the PCR reaction. Annealing temperatures from 40-50 °C resulted in a single band on a 2 % agarose gel corresponding to the length of the PCR product of *dsbA* (733 bp) (Figure 4.9). 41.9 °C was chosen as the annealing temperature to use for amplifying *dsbA* from the EMS library by TILLING as this temperature resulted in the highest quantity of PCR product as indicated by the intensity of the band (Figure 4.9).

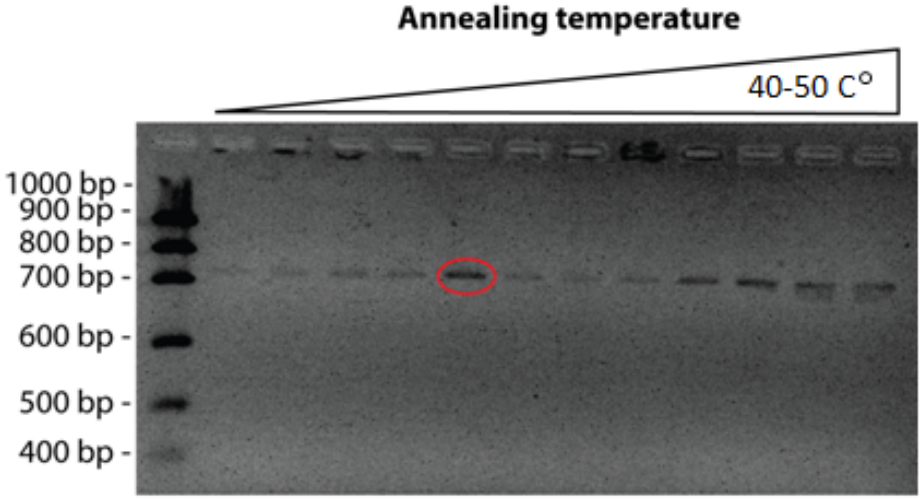

Figure 4.9 Control of amplification specificity of* dsbA *primers.
Heat-inactivated C. trachomatis *LGV-2 EBs were subjected to PCR with annealing temperature ranging from 40 °C to 50 °C. The band circled in red corresponds to an annealing temperature of 41.9 °C.*

Ten 96-well plates of McCoy cells infected with 15 IFU per well were screened by TILLING after eight days of continuous growth. The *dsbA* gene was isolated by PCR with primers specific for the *dsbA* gene. Subsequently the PCR products from each infection were subjected to several rounds of melting and annealing conditions creating a pool of DNA homo- and heteroduplexes. Homo-and heteroduplexes of the *dsbA* gene were isolated by PCR. Cel-1 digestion was used to identify potential heteroduplexes of the *dsbA* gene. Cel-1 digested PCR products were run on agarose gels to identify lower molecular weight bands corresponding to Cel-1 digestion at a point mutation. However *dsbA* was not amplified for all infections and evaluation of Cel-1 digestion was complicated by the appearance of a smear on the agarose gel for most of the PCR products (Figure 4.10).

Out of 960 wells screened only eight pools of DNA duplexes had what appeared to be a very faint band resulting from Cel-1 cleavage. The pool of DNA duplexes from these eight infections was Sanger sequenced with both the forward and reverse *dsbA* specific primers, resulting in a total 16 reads. For 5 of the 16 reads the sequence quality was too poor to evaluate potential mutations. For one well (pool of duplexes), both the forward and reverse sequencing was of poor quality, but for three others wells the sequencing with only the reverse primer was of poor quality. However, even the remaining 11 high quality reads (with sequence information for 7 pools of duplexes) did not reveal any mutations in the *dsbA* gene. In conclusion seven pools of duplexes with an apparent mutation as judged by Cel-1 digestion were false positives as sequencing identified no mutation in the *dsbA* gene. In the remaining pool of duplexes the sequencing quality was too poor to be conclusive.

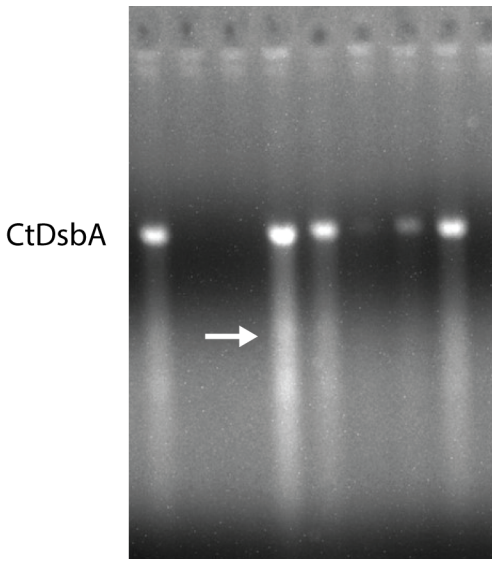

Figure 4.10 Cel-1 digest of* dsbA *PCR products.
McCoy cells infected with mutants from the EMS library were harvested and subjected to PCR with dsbA specific primers. The PCR product was treated with celery extract and Cel-1 digestion was evaluated on 2 % agarose gel. The white arrow indicates the appearance of a faint band corresponding to a lower molecular weight than the dsbA *gene (CtDsbA).*

4.4 Discussion

A *C. trachomatis* strain with a disruption in the *dsbA* gene would be a valuable tool for gaining insight into the role of CtDsbA in *C. trachomatis* virulence. Random mutagenesis by EMS was chosen as a strategy to obtain a loss-of-function mutation in the *dsbA* gene of *C. trachomatis*. A library of EMS mutants was created by treating *C. trachomatis* LGV-2 and *C. trachomatis* LGV-2*tmp* with EMS and EMS concentrations of 5 and 6 mg/mL were chosen as that gave the highest mutation frequency

without suppressing infectivity significantly. As EMS libraries obtained by treating *C. trachomatis* D UW-3/Cx with 5 to 6 mg/mL EMS have approximately 2.5 mutations per genome, a subpopulation with a loss-of-function mutation in the *dsbA* gene is also likely to have at least one more mutation elsewhere in the genome. However, as approximately one third of all mutations introduced by EMS in the genome of *C. trachomatis* are synonymous and less than 10 % are nonsense mutations [270] it is unlikely that a loss-of-function mutation in the *dsbA* gene would be accompanied by a mutation in another gene severely influencing infection. Consequently, a mutation rate of 2.5 mutations per genome increases the likelihood of obtaining a loss-of-function mutation in the *dsbA* gene with minimal risk of creating a severe disruption of an additional critical gene. However, *C. trachomatis* D UW-3/Cx and *C. trachomatis* LGV-2 exhibit different susceptibility to antibiotics. Consequently the frequency of acquired rifampicin resistance, and thus mutation frequency, determined for *C. trachomatis* D UW-3/Cx might not accurately reflect the mutation frequency in *C. trachomatis* LGV-2 although treated with the same concentration of EMS. Therefore, the mutation frequency of the EMS treated *C. trachomatis* LGV-2 library should be determined to confirm the mutation rate in this specific library.

A total of approximately 16,000 EMS treated subpopulations of *C. trachomatis* LGV-2 and *C. trachomatis* LGV-2*tmp* were screened in the TILLING approach and the DTT sensitivity screen combined. With 2.5 mutations per genome and 4.3 x 10^5 mutations sites in the genome of *C. trachomatis*, in theory one of 16,300 subpopulations from the EMS library should contain a loss-of-function mutation in the *dsbA* gene. Unfortunately, even though 16,000 subpopulations out of the estimated 16,300 subpopulations were screened, no mutations in the *dsbA* gene were identified either in the forward or reverse genetic approach. As 16,300 is an estimation of the subpopulation needed to screen to obtain one loss-of-function mutation in the *dsbA* gene, it might be that EMS random mutagenesis resulted in no mutations in *dsbA* in the screened subpopulations. Alternatively, a mutation did occur in the *dsbA* gene but was not detected in either of the two screens. As there are 289 potential mutation sites in the dsbA gene screen, approximately 25 point mutations should have been introduced into the *dsbA* gene in the 16,000 subpopulations screened. Synonymous mutations as well as non-disruptive non-synonymous point mutations in the *dsbA* gene would not show up in the DTT sensitivity screen, but would still be recognised by Cel-1 digestion and should consequently be detected when sequencing the *dsbA* gene. Approximately 14,000 of the 16,000 subpopulations screened were screened using the TILLING approach and accordingly about 22 mutations in the *dsbA* are likely to be present in the subpopulations screened. The failure to identify any mutations in the *dsbA* gene suggests that either the mutation frequency is significantly lower than anticipated or the TILLING approach is not sensitive enough to report the mutations.

To test whether the assumption of 2.5 mutations per genome is correct, the mutation frequency of the screened EMS libraries should be experimentally determined. The mutation rate can be determined by finding the frequency of acquired rifampicin resistance in the EMS library. There is a total of 37 points that can introduce nonsense mutations to the *trpBA* operon and thus introduce rifampicin resistance [271]. Accordingly, one in approximately 5,000 subpopulations would gain resistance to rifampicin with a mutation frequency of 2.5 mutations. The rifampicin resistance frequency of an EMS library is established by infecting a monolayer of McCoy cells with the EMS library at a known MOI. Infected McCoy cells are treated with a lethal dose of rifampicin and the number of subpopulations that survive the treatment is determined.

4.4.1 Evaluation of the TILLING screen

Alternatively, the lack of identification of a mutation in the *dsbA* gene could be due to the weaknesses in detection of mutations in the TILLING approach. This is further emphasised by the high ratio of false positives in the Cel-1 digestion. The identification of bands corresponding to Cel-1 digestion products was challenging due to the smear on the agarose gel. Although the smear is also present on the agarose gel testing for endonuclease activity of the celery extract, the smear did not interfere with identification of digestion products. However, in the TILLING screen, the PCR product of *dsbA* is derived from 15 subpopulations, where it is expected that one subpopulation potentially contains a mutation in the *dsbA* gene. Accordingly, the bands corresponding to the digestion products will be very faint and more difficult to distinguish on a smeared gel. As the observed digested bands are extremely faint, it is possible that they may be artefacts arising from the presence of smear. Similarly, it is highly likely that bands corresponding to Cel-1 digestion products in other reactions are not recognised on the gel due to the smear. Reducing the number of IFUs screened per well may solve the issue of detection of digestion products. Smearing is a common occurrence when running Cel-1 digested PCR products on agarose gel [273]. Optimising the ratio of Cel-1 to target DNA can potentially reduce the smear. Alternatively, Cel-1 can be replaced with a different endonuclease digesting specifically at base pair mismatches. The endonuclease Guide-it Resolvase does reduce the occurrence of smear and is also less sensitive to buffers used in the PCR reaction, according to the manufacturer (TaKaRa). In High Resolution Melting (HRM) analysis, a mutation in a PCR product can be identified by change in melting temperature and this offers a high-throughput alternative to evaluating mutations by endonucleases. Although the method is reliable, the sensitivity decreases with amplicon length and the impact on melting temperature of a single mutation in PCR products larger than 300 bp is close to zero [278]. Furthermore, the sensitivity of the method is highest when

50 % of the population contains the mutant, but the difference in melting temperature can still be detected with around 5 % of mutant DNA in the population [278]. Considering the length of the *dsbA* PCR product (636 bp) and a frequency of mutation of 6.7 % (i.e. if one of 15 subpopulations contains a mutation) the sensitivity of HRM is likely too low to be a suitable method for identifying a mutant in the *dsbA* gene.

The high ratio of false positives in the TILLING screen could also arise from failure to identify the base pair mismatch in the manual evaluation of the Sanger sequencing reads. In recent years, sequencing by next generation sequencing platforms have gained popularity as a high-throughput, deep sequencing alternative to Sanger sequencing. The most common and suitable option for an application such as this would be the Illumina miSeq using a PCR amplicon sequencing approach. However, read lengths are limited to 2x300 bp [278]. Consequently, the *dsbA* gene (636 bp) pushes the limit on read length by this method, or two separate amplicons would be needed for each well. The newest Illumina platform, Illumina HiSeq, and the benchtop sequencer, Illumina MiSeq, both have error rates of ~0.3 error per 100 bp [279], which give on average 1.9 misreads in the *dsbA* gene. Given the low representation of mutants with wild-type in the pools, this error rate is higher than the dsbA mutation rate in the population. So, although this is a promising strategy the limitations in read length and the relatively high error rate mean that this method is not yet compatible with the TILLING screen for mutations in the *dsbA* gene.

4.4.2 Evaluation of the screen for increased DTT sensitivity

In the DTT sensitivity approach, 960 wells each containing two subpopulations of the EMS library were screened. Out of 36 wells exhibiting an altered phenotype upon DTT treatment, the phenotype was confirmed for 14 wells. In all confirmed cases the wells contain subpopulations that exhibit decreased infectivity upon DTT treatment suggesting that these wells contain a subpopulation with increased sensitivity to DTT. Sequencing of the *dsbA* gene in the subpopulations with increased sensitivity to DTT did not reveal any mutations in the *dsbA* gene. The DTT sensitivity screen was developed based on the hypothesis that infection would be reduced upon treatment with DTT of *C. trachomatis* lacking the DsbA oxidase activity. An EMS mutant harbouring a loss-of-function mutation in the *dsbA* gene might potentially cause complete loss of infection upon DTT treatment. Consequently, the amount of DNA arising from this subpopulation is minimal compared to the healthy subpopulation in the well and the signal-to-noise ratio might be too low to identify the mutation. As *C. trachomatis* is highly dependent on the redox regulation of the disulfide bonds in the outer membrane [81, 131] it is possible that disruption of oxidase activity could abolish infection

completely. Further it is possible that the increased sensitivity to DTT treatment arises from disruption of an alternative redox protein. Consequently the 14 wells should be subjected to whole-genome sequencing to identify which gene is responsible for the increased sensitivity to DTT.

4.4.3 Future directions for studying the biological role of CtDsbA

Obtaining a loss-of-function mutation in the *dsbA* gene of *C. trachomatis* was not possible using the approaches and conditions reported here. Unfortunately, this delays our understanding of the potential role of CtDsbA in *C. trachomatis* infection and development. More effort should be put towards obtaining a loss-of-function mutation in the *dsbA* gene. In addition to the undirected approach presented in this thesis, directed approaches could be attempted to obtain a loss-of-function mutation in the *dsbA* gene e.g by site-specific inactivation of the *dsbA* gene by insertion of a group II intron using the TargeTron^{TM} approach which has proven successful in *C. trachomatis* LGV-2 [267]. A recent paper discusses the feasibility of using Clustered Regularly Interspaced Short Palindromic Repeats interference (CRISPRi) to create knockout mutants in *Chlamydia.* Although creation of a single plasmid system for CRISPR, targeting the inclusion membrane protein *incA* (dCas9) was succesfull, it failed to knockout expression of *incA*. Reversible inhibition of *incA* was, however, accomplished by inducing dCas9 in the presence of guide RNA (gRNA) targeting the 5' UTR of *incA* [281]. The succesfull inhibition of *incA* expression shows that CRISPRi is promising strategy for creating knockout mutations in *Chlamydia* and should be explored as an alternative strategy for creating a knockout mutation of the *dsbA* gene. However, for the method to be suitable, issues with low plasmid stability and leaky expression of the tet promoter and low efficiency of transformation would need to be addressed.

Until a loss-of-function mutation for dsbA has been created characterisation of CtDsbA in *C. trachomatis* could contribute to the understanding of the role of CtDsbA without directly studying the effect of a lack of CtDsbA oxidase activity on *C. trachomatis.* Most importantly, the subcellular localisation of CtDsbA has not yet been determined. Whereas most Gram-negative DsbA enzymes are located in the periplasm, CtDsbA has a putative transmembrane region and localisation software tools predict CtDsbA to be either membrane-anchored or periplasmic (Section 2.6.1). The subcellular localisation of CtDsbA could be determined by cell fractionation in which the periplasmic compartment is separated from the cytosol and membrane fraction by centrifugation at 8,000 x g. Subsequently the cytoplasmic and membrane fractions can be separated by ultracentrifugation [282]. The fraction containing CtDsbA can be identified by western blotting with an antibody specific for CtDsbA.

Two of the three DsbAs in *N. meningitidis* are lipid proteins anchored to the membrane and inactivation of these (NmDsbA1 and NmDsbA2) have a greater effect on sensitivity towards reducing agents as well as proteins involved in adhesion compared to inactivation of the periplasmic NmDsbA3 [283]. Similarly, PaDsbA2, which is predicted to be membrane-anchored, is thought to have a different substrate range to that of periplasmic PaDsbA1 [75]. Consequently, membrane anchoring of CtDsbA could indicate a different substrate range than periplasmic DsbAs. Considering the disulfide-cross linking of the outer membrane in *C. trachomatis,* a different substrate range of CtDsbA compared to periplasmic DsbAs might be linked to a role in regulating the redox state of the outer membrane proteins. However, even if CtDsbA is membrane-anchored and interacts with proteins in the chlamydial outer membrane complex (COMC) it is not most likely directly involved in the COMC as it has not been identified in a previous analysis of the isolated COMC proteins [130].

4.5 Conclusions

Although no *dsbA* mutation was identified in the subpopulations screened, chemical mutagenesis remains the most promising strategy for obtaining a loss-of-function CtDsbA mutation. Whereas the reverse genetic approach using TILLING to identify mutations in the *dsbA* gene allows for screening of more IFU per infection, false positives in Cel-1 digestion products and a failure to identify true positive bands complicates the identification of a *dsbA* mutant. In the forward genetics approach, screening for increased DTT sensitivity can potentially lead to identification of redox protein mutants other than *dsbA* mutants. As fewer subpopulations are screened in each well this is a more cumbersome approach. However, since other redox sensitive proteins are likely to be affected by treatment with DTT the forward genetics approach can potentially identify other proteins important for the redox regulation of *C. trachomatis.*

Chapter 5: Discussion & Conclusion

The goal of this thesis was to characterise the oxidative pathway of the obligate intracellular pathogen *C. trachomatis,* specifically to investigate the structure and function of the putative primary oxidase CtDsbA and the interaction between CtDsbA and its predicted redox partner CtDsbB.

As a member of the *Chlamydia* phylum, *C. trachomatis* has a biphasic developmental cycle alternating between the infectious extracellular EB and the replicating intracellular RB. Differentiation from EB to RB is dependent on reduction of the disulfide cross-linking network of the chlamydial envelope [143-145, 148]. Conversely, restoration of the disulfide cross-linking network is required for RB to EB differentiation at the late stages of *C. trachomatis* infection [145, 284]. This developmental cycle led to the hypothesis that the oxidative pathway in *C. trachomatis* may play a specialised role in oxidising the outer membrane and outer membrane associated proteins.

5.1 Expansion of the structural library of DsbA enzymes

The first aim of this thesis was to structurally and functionally characterise CtDsbA to shed new light on the diversity amongst DsbA enzymes. I found that the truncated soluble construct of CtDsbA is structurally and functionally similar to other characterised DsbA proteins, but is distinguished by being the least oxidising DsbA characterised to date and by having an active site disulfide that is only mildly destabilising (Chapter 2). Further, CtDsbA has an unusually high number of cysteines. The soluble construct of CtDsbA has, apart from the active site cysteines, a disulfide bond linking helix H1 and helix H5 and an unpaired cysteine (Cys70) in loop L1. An additional cysteine is found in the predicted transmembrane helix of the predicted full-length translated CtDsbA enzyme. The crystal structure of CtDsbA represents the first structural characterisation of a DsbA having two small uncharged amino acids in the dipeptide motif separating the catalytic cysteines.

The catalytic site dipeptide has been shown to modulate the redox properties of thioredoxin enzymes [71]; the proline residue found in position X_1 in the CX_1X_2C catalytic motif of EcDsbA favours electrostatic stabilisation of the thiolate anion by the helix dipole of helix H1. The serine in the equivalent position in CtDsbA does not offer this stabilisation, which is consistent with the low redox potential of CtDsbA. Other DsbAs that lack a proline in position X_1 include WpDsbA1 [108] and FtDsbA type A and type B [29]. These also have low redox potentials. WpDsbA1 contains a histidine in position X_2 (as does EcDsbA) that offers stabilisation of the thiolate anion. FtDsbA (type A and B) contains a tyrosine residue in position X_2 that would also be able to offer direct electrostatic stabilisation of the thiolate anion, which is consistent with a redox potential equivalent with that of WpDsbA1. However, as the structure of FtDsbA has not been determined the spatial arrangement of

the residues has not been determined. NmDsbA3 has a valine rather than a proline in position X_1 [65] and yet has a relatively high redox potential. In addition to the lack of a proline residue in position X_1, the alanine in position X_2 of CtDsbA offers no equivalent electrostatic stabilisation of the thiolate anion to that provided by the histidine in EcDsbA. The lack of factors contributing to stabilisation of the thiolate anion in CtDsbA is consistent with the low redox potential of the protein, and with the observation by Huber-Wünderlich and co-workers that the dipeptide separating the active site cysteines are pivotal for determination of redox properties [71].

Structurally, CtDsbA is most closely related to PaDsbA2, WpDsbA1 (DsbA-IIb) and BsDsbA (DsbA-IIa). On the basis of its β-sheet topology, CtDsbA belongs in the DsbA-II class with WpDsbA1, BsDsbA, MtbDsbA and SaDsbA. The surface of CtDsbA has no pockets adjacent to the active site, but several smaller pockets on the posterior face of the protein. Similar to the Gram-positive members of the DsbA-IIa subgroup, the surface of CtDsbA is predominantly negatively charged. In particular, the surface surrounding the active site is highly acidic. Characterisation of CtDsbA expands the number of structurally characterised DsbA enzymes with a charged catalytic surface and no identifiable pocket at the catalytic surface (Chapter 2).

5.2 Exploration of the oxidative pathway in *C. trachomatis*

The second goal of this thesis was to explore the potential similarities and differences between the oxidative pathway in *C. trachomatis* and the canonical oxidative pathway of *E. coli* (Chapter 3). The overall similarities between CtDsbA and other DsbA enzymes, as well as the identification of a DsbB homolog in *C. trachomatis* indicates that the oxidative pathway in *C. trachomatis* resembles the canonical DSB oxidative pathway of *E. coli* (Chapter 2 and 3). This is supported by the observation that crude membranes containing CtDsbB facilitate the oxidase activity of CtDsbA (Chapter 3, section 3.3.2). In contrast to this finding, purified detergent-solubilised CtDsbB was not able to oxidise truncated CtDsbA in the presence or absence of ubiquinone-1 (UQ-1) (Chapter 3, section 3.3.3). This is most likely due to CtDsbB being inactive in the *n*-Dodecyl β-D-maltoside (DDM) micelles used to prepare detergent-solubilised protein. Alternatively, UQ-1 may not be a suitable co-factor for CtDsbB. This would be in contrast to what is observed for other DsbB enzymes, where UQ-1 is able to facilitate DsbB mediated oxidation of DsbA from *E. coli, V. cholerae, W. pipientis* and *M. tuberculosis* [76, 78, 108, 230]. However, it might be explained by the difference in UQ binding observed between CtDsbB and EcDsbB (Chapter 3, section 3.3.4).

5.2.1 The role of the second disulfide of CtDsbA in the interaction with CtDsbB

CtDsbA contains a second disulfide bond linking helix H2 and helix H5. A similarly placed disulfide is present in three other structurally characterised DsbA enzymes: WpDsbA1, PaDsbA2 and MtbDsbA and appears to be conserved in DsbAs from alpha-proteobacteria [80]. In WpDsbA1, the second disulfide has an inhibitory effect on the interaction with WpDsbB, but no effect on redox potential [108], whereas it reduces the oxidase activity of PaDsbA2 significantly [75]. In MtbDsbA, the second disulfide is believed to play a structural role [78, 88]. The effect of the second disulfide on the interaction with the cognate redox partner (PaDsbB1 or VKOR, respectively) has not been investigated for PaDsbA2 and MtbDsbA.

Curiously I found that the second disulfide of CtDsbA does not have an inhibitory effect on its interaction with CtDsbB and has only a minimal effect on protein stability (Chapter 3, section 3.3.6). However, the second disulfide did contribute slightly to stabilisation of the active, oxidised state over the reduced state. Thus it is possible that the second disulfide of CtDsbA might influence the intrinsic redox properties of CtDsbA.

5.3 Forward and reverse genetics approaches to obtain a loss-of-function mutant of the *dsbA* gene in *C. trachomatis*

The third aim was to explore a forward and a reverse genetics approach to obtain a loss-of-function mutation in the *dsbA* gene in *C. trachomatis* (Chapter 4). Considering the importance of disulfide bonds in *C. trachomatis* infection and development, I hypothesised that CtDsbA is involved in oxidation of at least some of the proteins in the Chlamydial Outer Membrane Complex (COMC). The finding in Chapter 3, section 3.3.5 that CtDsbA expression correlates with the onset of oxidation of the COMC proteins supports the hypothesis that CtDsbA is involved in the oxidation of the COMC proteins. Obtaining a loss-of-function mutant of CtDsbA would enable investigation of the effect of the loss of CtDsbA activity on *C. trachomatis* infection and development, and provide insight into the role of CtDsbA *in vivo.* Altered dithiothreitol (DTT) susceptibility was verified as a phenotypic marker in the forward genetics approach (Chapter 4, section 4.3.6). Out of 1920 subpopulations screened, 14 exhibited reproducible sensitivity to DTT, but sequencing revealed no mutations in the *dsbA* gene. In the reverse genetic approach, approximately 14,000 subpopulations were screened for mutations in the *dsbA* gene (Chapter 4, section 4.3.7). Potential mutations in *dsbA* were searched by digestion with the endonuclease Cel-1 that cleaves specifically at base-pair mismatches followed by PCR amplification of the gene. Despite identification of Cel-1 cleavage of *dsbA* for eight infections

sequencing identified no mutations in the dsbA gene. The failure to obtain a loss-of-function CtDsbA mutant delays our understanding of the role of CtDsbA in chlamydial infections.

5.4 Future perspectives for developing antimicrobial drugs targeting DsbA enzymes

DsbA enzymes introduce disulfide bonds to a broad range of virulence factors. Consequently, inhibition of DsbA will lead to attenuation of virulence, while the bacteria remain viable. The structural library of DsbA enzymes that has been assembled, now including CtDsbA, provides a foundation for structure-guided drug development for an antimicrobial drug targeting virulence. DsbA homologs have been identified in commensal bacteria, such as *Streptococcus gordonii* [285] and commensal *Neisseriae* [94]. Consequently, targeting DsbA could potentially have off-target effects on the commensal microbiome. However, the structural library of DsbA enzymes shows that the active site pocket varies in length and depth and the electrostatic surface potential at the catalytic surface is different in DsbA-I and DsbA-II enzymes. The diverse characteristics of the DsbA enzymes potentially allows for development of highly specific DsbA inhibitors, which might limit the effect on the commensal microbiome. Furthermore, even if commensal bacteria are affected by an anti-DsbA compound they could still persist after such treatment, whereas this is not the case for antibiotic treatment. Disrupting DsbA activity has the potential to disrupt processes such as motility, adhesion and secretion without affecting bacterial growth as seen for compounds identified Adams *et al.* [111]. Consequently, clearing of an infection upon treatment with anti-DsbA compounds would also be dependent on the host cell immune system. Pathogenic bacteria trigger a strong immune response causing the host cell immune system to clear the infection, whereas commensal bacteria do not trigger an immune response to nearly the same degree [286,287]. This discrimination between pathogenic and commensal bacteria might potentially mean that anti-DsbA compounds can facilitate clearance of infections with pathogenic bacteria while the commensal microbiome persists.

Whereas the hydrophobic groove or pocket of EcDsbA and other members of the DsbA-I subgroup contributes to the druggable nature of the DsbA-I enzymes, CtDsbA and PaDsbA2 as well as the majority of the type II enzymes lack a binding pocket at the catalytic surface which could be challenging for developing inhibitors targeting DsbA. However, inhibitors containing a cysteine have been developed against EcDsbA [112]. As covalent linking, rather than hydrophobic contacts with the residues at the protein surface, facilitates binding of a cysteine containing inhibitor, inhibitors for DsbA enzymes could potentially be developed despite the lack of an identifiable binding pocket. In fact, a cysteine-containing peptide developed based on the sequence of the redox partner, VKOR, of

MtbDsbA has been shown to bind to the catalytic surface of MtbDsbA in a cysteine dependent manner with a K_D of 2.9 μM [78]. However, the rapid turnover of the substrate-DsbA disulfide bond due to the reactivity of the thiolate anion, as seen for EcDsbA [288] represents a challenge for development of a potent drug with binding of high specificity and affinity.

The inhibitory binding of EFTu to the non-catalytic surface of AbDsbA [82] presents the possibility of developing allosteric inhibitors that don't bind to the catalytic surface. This is a promising strategy for development of drugs for proteins such as CtDsbA that have no apparent pocket at the catalytic surface, but two pockets on the posterior surface.

Alternatively, development of inhibitors for the redox partner DsbB offers a mechanism to target oxidative folding by hindering recycling of active DsbA. As 60 % of marketed drugs target membrane proteins [289], this might represent a promising strategy, and indeed inhibitors have been developed against EcDsbB in fragment-based drug discovery approaches [113, 114] and a cell-based high-throughput screen [115]. However, the technical difficulties of working with membrane proteins outside of their native lipid environment represent a challenge. Further, apart from the thorough structural characterisation of EcDsbB [64, 101, 102], structural information is lacking for other DsbB enzymes making it a less ideal target for a structure-guided drug discovery approach. Screening for a phenotypic read-out, such as gain of β-galactosidase activity upon inhibition of EcDsbB [115], offers a way of screening compounds for specific inhibition of DsbB mediated oxidative folding without extracting DsbB from the native lipid environment. An equivalent cell-based high throughput screen might be a valuable approach for initial identification of inhibitors for DsbB lacking structural characterisation.

5.4.1 Development of drugs targeting the oxidative pathway in *C. trachomatis*

Due to the high degree of treatment failure and off-target effects on the gut and vaginal microbiome, new drugs for treating infections with *C. trachomatis* are needed. As the oxidative pathway has proven a promising target for development of drugs against *E. coli,* targeting the oxidative pathway might also serve as a strategy for development of drugs against *C. trachomatis*.

The correct redox state of the COMC is not only crucial for infection, but also pivotal for progression through the biphasic life cycle of *C. trachomatis* [131, 145, 148, 284]. If CtDsbA is, in fact, involved in regulating the redox state of the COMC it is likely that inhibition of CtDsbA will not just attenuate infection, but will compromise the viability of *C. trachomatis*. This doesn't prevent a CtDsbA

inhibitor from being a potent antibacterial drug, but it will not necessarily possess the advantages of an anti-virulence drug. One advantage of targeting virulence rather than viability is the potentially limited effect on the commensal microbiome. *Lactobacillus,* the predominant species in the vaginal microbiome [189], reduces the infectivity of *C. trachomatis.* Consequently, abolishing the *Lactobacilli* subpopulation in the vagina is associated with a higher risk of reinfection [190, 191]. Whereas antibiotics currently used for treating infections with *C. trachomatis* affects the viability of *Lactobacilli* [290], *Lactobacilli* do not encode a *dsbA* homolog and loss of CtDsbA activity is therefore not likely to affect the *Lactobacilli* subpopulation. This represents an advantage of a drug targeting CtDsbA compared to the drugs currently used to treat infections with *C. trachomatis* as it potentially reduces the risk of reinfection.

Another issue with treating *C. trachomatis* infections is the risk of inducing persistence and thereby creating a subpopulation that is able to escape treatment. Cysteine-depletion of *C. trachomatis* leads to disruption of RB to EB differentiation and consequently persistence [284]. If CtDsbA is involved in oxidation of the COMC, inhibition of CtDsbA is likely to affect RB to EB differentiation in a similar manner to cysteine depletion. Consequently, targeting CtDsbA might lead to persistence.

Knowledge of the structure and function of CtDsbA provides a foundation for development of inhibitors of CtDsbA in a fragment-based drug discovery approach. Especially, the possibility of allosteric inhibition should be explored considering the two pockets at the posterior surface of CtDsbA. As CtDsbA has no identifiable pocket at the catalytic surface the most attractive strategy for development of inhibitors is design of peptides capable of covalently binding to Cys38 e.g. based on the sequence of the interacting region for CtDsbB. This strategy has proven successful for identification of a peptide with inhibitory effect on MtbDsbA that, similar to CtDsbA, lacks an apparent binding pocket at the catalytic surface [78].

Targeting the oxidative pathway by disrupting the ability of CtDsbB to oxidise CtDsbA offers an alternative approach too and has proven successful for EcDsbB [115]. Targeting CtDsbB gives rise to the same challenges discussed for DsbB enzymes generally (Chapter 5, section 5.4). The molecular nature of the interaction between CtDsbA and CtDsbB is still poorly characterised, which makes evaluation of the structure-activity relationship challenging.

As an alternative for a Fragment-Based Drug Discovery approach guided by structural information about the target enzymes, inhibitors of *C. trachomatis* oxidative folding can be identified in cell-based assays. Little is known about the substrate range of CtDsbA in *C. trachomatis* and the biphasic

developmental cycle impairs genetic engineering. Consequently, development of a cell-based assay, like the β-galactosidase activity screen used for screening inhibitors of EcDsbB [115] is difficult as there is no distinguishable phenotypic read-out for lack of CtDsbA activity in *C. trachomatis*. However, if CtDsbB is able to complement a *dsbB*-null strain of *E. coli,* screening for inhibitors of CtDsbB may be possible in *E. coli.* Neither MtbDsbA nor CtDsbA rescue lack of EcDsbA in *E. coli*, but VKOR does rescue lack of EcDsbB activity [90]. Further, DsbB homologs from *A. baumannii, K. pneumoniae, V. cholerae, P. aeruginosa, S. enterica* Typhimurium (SeDsbB and DsbI) and from the distantly related *F. tularensis* and *Haemophilus influenzae* also complement a *dsbB* null strain in *E. coli* [115]. This suggests that CtDsbB may also do the same. Accordingly, if CtDsbB can be shown to complement EcDsbB null mutants, compounds could be screened for inhibition of CtDsbB in *E. coli.* Alternatively, CtDsbA and CtDsbB can both be recombinantly expressed in a *dsbA/dsbB* double mutant strain of *E. coli* and used for screening of inhibition of oxidative folding with a β-galactosidase activity read-out. Inhibition of the CtDsbA/CtDsbB activity can also be screened in the peptide oxidation assay, which is already established. However, the low signal-to-noise ratio in this assay for CtDsbA makes it difficult to detect the potential effect of an inhibitor.

5.5 Future perspectives for studying disulfide bond formation in *C. trachomatis*

Considering the important role of disulfides in the infection of *C. trachomatis,* more information is required to establish the role of the oxidative pathway in the regulation of the COMC redox state. Currently, whole genome sequencing of mutant libraries generated by chemical mutagenesis is the gold standard of genetic manipulations of *C. trachomatis* [270, 291]. Accordingly, more information should be directed towards screening of EMS libraries to identify a loss-of-function mutation of *dsbA* to study the effect of loss of oxidase activity. The forward genetics approach using DTT sensitivity as a phenotypic read-out did not lead to identification of *dsbA* mutants, so an alternative phenotypic marker could be explored. Under the assumption that the disulfide cross-linking network is compromised in *C. trachomatis* with a loss-of-function mutation in the *dsbA* gene, Machiavello stain could be used as a phenotypic marker. RBs stain blue with Machiavello screen whereas EBs stain red. However, it has been shown that upon disrupting the COMC disulfide cross-linking EBs stain blue with Machiavello stain [131]. As both RBs as well as EBs with a disrupted COMC will stain blue with Machiavello stain, the asynchronous differentiation from RB to EB complicates the phenotypic read-out but it should be possible to identify mutants with careful inspection and controls. Moreover, it is not established that CtDsbA does, in fact, oxidise the COMC. Even if CtDsbA does not oxidise the COMC cysteines, it is highly likely that CtDsbA is responsible for disulfide bond

formation in virulence factors as seen in e.g. *E. coli* [48], *S. enterica* Typhimurium [46, 53], *C. jejuni* [54], *Y. pestis* [47], *P. aeruginosa* [55, 56] and *V. cholerae* [50]. Consequently, a decrease in infectivity can be used as a phenotypic read out. However, as mutations in many other proteins is expected to be associated with a decrease in infectivity, this will still require sequencing of a large number of subpopulations to identify a mutation in the *dsbA* gene. The advantage of this approach is that other proteins important for virulence could be identified. As very few virulence factors in *C. trachomatis* have been identified this could aid the understanding of *C. trachomatis* infections.

As the reverse genetics approach allows for more subpopulations to be screened in each well this approach offers an alternative to the forward genetics approach where more subpopulations can be screened with less handling. However, optimisation of the TILLING screen is required for this to be a suitable strategy. Firstly, reduction of smear after gel electrophoresis is essential for identification of an endonuclease digestion product. Using purified Cel-1, rather than celery extract containing Cel-1, might reduce the smear. Alternatively, using a different endonuclease such as Guide-it Resolvase (TaKaRa) might solve the problem. Secondly, reducing the number of subpopulations screened in each well from 15 to 10 will allow for clearer identification of a mutation upon sequencing as discussed in Chapter 4 section 4.4.1.

As genetic manipulation of *C. trachomatis* is notoriously difficult, other approaches might need to be utilised for unpicking the biological role of CtDsbA. Development of a potent inhibitor for CtDsbA *in vitro,* e.g. by a Fragment-Based Drug Discovery approach, potentially allows for the study of the role of CtDsbA in the infection and development of *C. trachomatis.* The EcDsbB inhibitors identified by Landeta *et al* also had inhibitory effect on the DsbB enzyme in nine other Gram-negative bacteria: *A. baumannii, K. pneumoniae, V. cholerae,* F. tularensis, *H. influenzae,* two DsbB homologs from *P. aeruginosa* and two DsbB homologs from *S. enterica* Typhimurium [115]. Consequently, these inhibitors might also have an inhibitory effect on CtDsbB and if so would inhibit the recycling of oxidised CtDsbA. In that case, this inhibitor could be used for studying the effect of loss of CtDsbA oxidase activity on *C. trachomatis* infection and progression through the biphasic life cycle of this pathogen.

5.5.1 Studying the biological role of CtDsbA

Despite the unfruitful efforts to create a strain of *C. trachomatis* harbouring a loss-of-function mutation in the *dsbA* gene, my characterisation of CtDsbA has provided information about its redox character (Chapter 2), as well as expression levels of CtDsbA *in vivo* (Chapter 3), that allow for reflection on the biological relevance of CtDsbA oxidase activity.

The redox potential of CtDsbA (-229 mV) approaches the redox potential of the dithiol reductase thioredoxin (-270 mV) [216]. The weak oxidising power of CtDsbA challenges the view of CtDsbA as an oxidase *in vivo*. However, an EcDsbA construct containing mutations that make it highly reducing, still functions as an oxidase *in vivo* as long as the overall rate-limiting step in oxidation of the folding substrate, and recycling of oxidised EcDsbA is not significantly altered [292]. Consequently, CtDsbA may indeed function as an oxidase *in vivo* for cysteine containing substrates if it is recycled to the active oxidised state e.g. by CtDsbB.

Whereas the periplasm of Gram-negative bacteria is generally oxidising, the periplasmic space of *C. trachomatis* is highly reducing in the early stages of infection and oxidised later in the infection cycle [145]. DsbH and DsbJ (unique to the *Chlamydia* phylum) are two periplasmic oxidoreductases. It has been suggested that the periplasmic reductase DsbH contributes to keeping the periplasm reduced in a process regulated by DsbJ [145]. CtDsbB and ScsB (suppressor of copper sensitivity protein B) are both predicted to be integrated into the inner membrane and CtDsbA is predicted to be located in the periplasm, and potentially anchored to the inner membrane. The remaining oxidoreductases identified in *C. trachomatis* [147] are cytoplasmic. Based on the role of the well-studied *Caulobacter crescentus* ScsB, which is involved in a peroxide reduction pathway in the cell envelope [151], chlamydial ScsB is more likely to be involved in the reduction of peroxide than the regulation of the redox state of the disulfide bonds in the COMC. This would leave the oxidative pathway – the introduction of disulfide bonds - to CtDsbA and CtDsbB.

CtDsbA is expressed late in the infection cycle, according to confocal microscopy analysis with CtDsbA specific antibodies (Chapter 3, section 3.3.5). Therefore, CtDsbA is a possible candidate responsible for contributing to the shift in the redox environment of the periplasm, and the outer membrane from reducing to oxidising. The Major Outer Membrane Protein (MOMP) are inserted in the membrane in the reduced state and oxidised later in the developmental cycle [143, 145, 148]. As the cysteines in MOMP are predicted to be located at the external side of the outer membrane [293], it is unlikely that CtDsbA is able to oxidise MOMP. But CtDsbA might oxidise the two membrane-

anchored periplasmic cysteine-rich proteins OmcA and OmcB and the membrane bound polymorphic membrane proteins (Pmps) and Type III secretion system (T3SS). The predicted anchoring of CtDsbA to the inner membrane could potentially hinder oxidation of the proteins associated with the outer membrane. However, NmDsbA1 and NmDsbA2 are both anchored to the inner membrane and both are involved in oxidation of the outer membrane protein PilQ [94]. In contrast to MOMP, cross-linking of OmcA and OmcB is observed shortly after onset of expression [148] and also unlike MOMP, OmcA and OmcB are not inserted in the membrane as monomers [143]. Consequently, CtDsbA-catalysed oxidation of OmcA and OmcB might occur after secretion to the periplasm, but before these two proteins are inserted into the outer membrane, which would explain how inner membrane-anchored CtDsbA could oxidise the outer membrane proteins of COMC.

Traditionally, substrates for enzymes in the thioredoxin family, including FtDsbA, have been identified by trapping the substrate in an intermolecular disulfide bond by using a mutant with a CXXS catalytic motif [77, 294, 295]. Due to the *C.* trachomatis being refractory genetic manipulation, this is not a feasible strategy for CtDsbA. One way to circumvent the issues with genetic manipulation of *C. trachomatis* is to study the interaction between recombinantly expressed CtDsbA and potential substrates such as e.g. the COMC proteins OmcA or OmcB *in vitro*. This could be done by determining the redox state of OmcA/OmcB by AMS labelling and gel electrophoresis. Considering the general promiscuous nature of DsbA catalysis [48, 77, 90] this may involve the risk of identifying substrates that are not biologically relevant.

If a loss-of-function mutation in the *dsbA* gene could be obtained or, alternatively, an inhibitor for CtDsbA developed, it would allow study of the effect on CtDsbA activity on the redox state of the COMC proteins. One approach would be to utilise the different staining properties of *C. trachomatis* dependent on whether the disulfide cross-linking is present or not. If CtDsbA activity is required for disulfide cross-linking of the COMC a loss of CtDsbA activity will result in *C. trachomatis* staining blue with Machiavello stain. The redox state of the COMC proteins can also be identified using immunoblotting after isolation of the membrane fraction. This has previously been done to study the redox state of MOMP [145].

5.6 Conclusions

Characterisation of CtDsbA expanded the structural library of DsbA enzymes; CtDsbA represents the first structural characterisation of a DsbA enzyme with a catalytic dipeptide sequence with two small uncharged amino acids and more than four cysteines. As a consequence of the lack of factors contributing to stabilisation of the thiolate anion of Cys38, CtDsbA is the weakest oxidase characterised to date, and in contrast to other DsbA enzymes the active site disulfide is only mildly destabilising. Consequently, these findings have provided new insights into the diversity of redox character amongst DsbA enzymes.

The oxidative pathway of *C. trachomatis* awaits further study, but the finding that crude *E. coli* membranes containing recombinantly expressed CtDsbB can facilitate CtDsbA activity suggests that CtDsbA and CtDsbB constitute a functional redox relay. Accordingly, the oxidative pathway in *C. trachomatis* is likely to resemble the oxidative pathway in *E. coli.*

Despite screening more than 16,000 subpopulations of EMS treated *C. trachomatis* for mutations in the *dsbA* gene, no *dsbA* mutation was obtained. This was disappointing as the failure to obtain a loss-of-function mutation in the *dsbA* gene delays our understanding of the role of CtDsbA in *C. trachomatis* virulence. However, development of a phenotypic screen for DTT sensitivity of EMS mutants combined with the traditional reverse genetics approach using TILLING provides an excellent starting point for further efforts to obtain a loss-of-function mutant.

This thesis has expanded our knowledge of the structural and functional diversity of DsbA enzymes. Moreover, data I presented herein suggests that CtDsbA and CtDsbB form a functional redox relay resembling the oxidative pathway in *E. coli* to some extent. The oxidative pathway in *C. trachomatis* is an attractive target for development of an antimicrobial drug with less impact than current treatments on the commensal vaginal microbiome. However, more information about the substrate range in *C. trachomatis* is required before this potential can be further explored. Overall, this thesis provides the foundation for studying the biological role of CtDsbA in *C. trachomatis* infection and development.

References

1. Fleming, A., *On the Antibacterial Action of Cultures of a Penicillium, with Special Reference to their Use in the Isolation of B. influenzæ.* Br J Pathol., 1929(10): p. 226-236.
2. Schwentker, F.F., S. Gelman, and P.H. Long, *Landmark article April 24, 1937. The treatment of meningococcic meningitis with sulfanilamide. Preliminary report. By Francis F. Schwentker, Sidney Gelman, and Perrin H. Long.* JAMA, 1984. **251**(6): p. 788-90.
3. Collaborators, G.M.a.C.o.D., *Global, regional, and national life expectancy, all-cause mortality, and cause-specific mortality for 249 causes of death, 1980-2015: a systematic analysis for the Global Burden of Disease Study 2015.* Lancet, 2016(388): p. 1459-544.
4. Kohanski, M.A., D.J. Dwyer, and J.J. Collins, *How antibiotics kill bacteria: from targets to networks.* Nat Rev Microbiol, 2010. **8**(6): p. 423-35.
5. Clatworthy, A.E., E. Pierson, and D.T. Hung, *Targeting virulence: a new paradigm for antimicrobial therapy.* Nat Chem Biol, 2007. **3**(9): p. 541-8.
6. Bycroft, B.W. and R.E. Shute, *The molecular basis for the mode of action of Beta-lactam antibiotics and mechanisms of resistance.* Pharm Res, 1985. **2**(1): p. 3-14.
7. Silverman, J.A., N.G. Perlmutter, and H.M. Shapiro, *Correlation of daptomycin bactericidal activity and membrane depolarization in Staphylococcus aureus.* Antimicrob Agents Chemother, 2003. **47**(8): p. 2538-44.
8. Campbell, E.A., et al., *Structural mechanism for rifampicin inhibition of bacterial rna polymerase.* Cell, 2001. **104**(6): p. 901-12.
9. Henry, R.J., *The Mode of Action of Sulfonamides.* Bacteriol Rev, 1943. **7**(4): p. 175-262.
10. Chopra, I., P.M. Hawkey, and M. Hinton, *Tetracyclines, molecular and clinical aspects.* J Antimicrob Chemother, 1992. **29**(3): p. 245-77.
11. Schnappinger, D. and W. Hillen, *Tetracyclines: antibiotic action, uptake, and resistance mechanisms.* Arch Microbiol, 1996. **165**(6): p. 359-69.
12. Munita, J.M. and C.A. Arias, *Mechanisms of Antibiotic Resistance.* Microbiol Spectr, 2016. **4**(2).
13. Jacoby, G.A., D.M. Mills, and N. Chow, *Role of beta-lactamases and porins in resistance to ertapenem and other beta-lactams in Klebsiella pneumoniae.* Antimicrob Agents Chemother, 2004. **48**(8): p. 3203-6.
14. Speer, B.S. and A.A. Salyers, *Characterization of a novel tetracycline resistance that functions only in aerobically grown Escherichia coli.* J Bacteriol, 1988. **170**(4): p. 1423-9.
15. Speer, B.S. and A.A. Salyers, *Novel aerobic tetracycline resistance gene that chemically modifies tetracycline.* J Bacteriol, 1989. **171**(1): p. 148-53.

16. Rabussay, D. and W. Zillig, *A rifampicin resistent rna-polymerase from E. coli altered in the beta-subunit.* FEBS Lett, 1969. **5**(2): p. 104-106.
17. Heil, A. and W. Zillig, *Reconstitution of bacterial DNA-dependent RNA-polymerase from isolated subunits as a tool for the elucidation of the role of the subunits in transcription.* FEBS Lett, 1970. **11**(3): p. 165-168.
18. Halling, S.M., K.C. Burtis, and R.H. Doi, *Reconstitution studies show that rifampicin resistance is determined by the largest polypeptide of Bacillus subtilis RNA polymerase.* J Biol Chem, 1977. **252**(24): p. 9024-31.
19. Lewis, K., *Platforms for antibiotic discovery.* Nat Rev Drug Discov, 2013. **12**(5): p. 371-87.
20. Talkington, A., C. Dantoin, and R. Durrett, *Ordinary Differential Equation Models for Adoptive Immunotherapy.* Bull Math Biol, 2017.
21. Stern, S., C., Franken, L., Voller, S., Rentmaister, H. and Grosch, B., *A call for concerted Action on Antibiotics Redearch and Development.* The boston Consulting Group, Berlin, 2017.
22. Matsuzaki, K., K. Sugishita, and K. Miyajima, *Interactions of an antimicrobial peptide, magainin 2, with lipopolysaccharide-containing liposomes as a model for outer membranes of gram-negative bacteria.* FEBS Lett, 1999. **449**(2-3): p. 221-4.
23. Reddy, K.V., R.D. Yedery, and C. Aranha, *Antimicrobial peptides: premises and promises.* Int J Antimicrob Agents, 2004. **24**(6): p. 536-47.
24. Andersson, D.I., D. Hughes, and J.Z. Kubicek-Sutherland, *Mechanisms and consequences of bacterial resistance to antimicrobial peptides.* Drug Resist Updat, 2016. **26**: p. 43-57.
25. Zasloff, M., *Antimicrobial peptides in health and disease.* N Engl J Med, 2002. **347**(15): p. 1199-200.
26. Fernebro, J., *Fighting bacterial infections-future treatment options.* Drug Resist Updat, 2011. **14**(2): p. 125-39.
27. O'Flaherty, S., R.P. Ross, and A. Coffey, *Bacteriophage and their lysins for elimination of infectious bacteria.* FEMS Microbiol Rev, 2009. **33**(4): p. 801-19.
28. Stern, A. and R. Sorek, *The phage-host arms race: shaping the evolution of microbes.* Bioessays, 2011. **33**(1): p. 43-51.
29. DiGiandomenico, A., et al., *A multifunctional bispecific antibody protects against Pseudomonas aeruginosa.* Sci Transl Med, 2014. **6**(262): p. 262ra155.
30. Bebbington, C. and G. Yarranton, *Antibodies for the treatment of bacterial infections: current experience and future prospects.* Curr Opin Biotechnol, 2008. **19**(6): p. 613-9.
31. Drawz, S.M. and R.A. Bonomo, *Three decades of beta-lactamase inhibitors.* Clin Microbiol Rev, 2010. **23**(1): p. 160-201.

32. Buynak, J.D., *Understanding the longevity of the beta-lactam antibiotics and of antibiotic/beta-lactamase inhibitor combinations.* Biochem Pharmacol, 2006. **71**(7): p. 930-40.
33. Smith, R.P., et al., *Targeting Bacterial Dsb Proteins for the Development of Anti-Virulence Agents.* Molecules, 2016. **21**(7).
34. Escaich, S., *Novel agents to inhibit microbial virulence and pathogenicity.* Expert Opin Ther Pat, 2010. **20**(10): p. 1401-18.
35. Zucca, M., S. Scutera, and D. Savoia, *New antimicrobial frontiers.* Mini Rev Med Chem, 2011. **11**(10): p. 888-900.
36. Cegelski, L., et al., *The biology and future prospects of antivirulence therapies.* Nat Rev Microbiol, 2008. **6**(1): p. 17-27.
37. Rasko, D.A. and V. Sperandio, *Anti-virulence strategies to combat bacteria-mediated disease.* Nat Rev Drug Discov, 2010. **9**(2): p. 117-28.
38. Hung, D.T., et al., *Small-molecule inhibitor of Vibrio cholerae virulence and intestinal colonization.* Science, 2005. **310**(5748): p. 670-4.
39. Felise, H.B., et al., *An inhibitor of gram-negative bacterial virulence protein secretion.* Cell Host Microbe, 2008. **4**(4): p. 325-36.
40. Aberg, V., et al., *Pilicides regulate pili expression in E. coli without affecting the functional properties of the pilus rod.* Mol Biosyst, 2007. **3**(3): p. 214-8.
41. Heras, B., et al., *Structural and functional characterization of three DsbA paralogues from Salmonella enterica serovar typhimurium.* J Biol Chem, 2010. **285**(24): p. 18423-32.
42. Pugsley, A.P., N. Bayan, and N. Sauvonnet, *Disulfide bond formation in secreton component PulK provides a possible explanation for the role of DsbA in pullulanase secretion.* J Bacteriol, 2001. **183**(4): p. 1312-9.
43. Miki, T., et al., *DsbA directs efficient expression of outer membrane secretin EscC of the enteropathogenic Escherichia coli type III secretion apparatus.* Microb Pathog, 2008. **44**(2): p. 151-8.
44. Watarai, M., et al., *Disulfide oxidoreductase activity of Shigella flexneri is required for release of Ipa proteins and invasion of epithelial cells.* Proc Natl Acad Sci U S A, 1995. **92**(11): p. 4927-31.
45. Menard, R., P.J. Sansonetti, and C. Parsot, *Nonpolar mutagenesis of the ipa genes defines IpaB, IpaC, and IpaD as effectors of Shigella flexneri entry into epithelial cells.* J Bacteriol, 1993. **175**(18): p. 5899-906.

46. Miki, T., N. Okada, and H. Danbara, *Two periplasmic disulfide oxidoreductases, DsbA and SrgA, target outer membrane protein SpiA, a component of the Salmonella pathogenicity island 2 type III secretion system.* J Biol Chem, 2004. **279**(33): p. 34631-42.
47. Jackson, M.W. and G.V. Plano, *DsbA is required for stable expression of outer membrane protein YscC and for efficient Yop secretion in Yersinia pestis.* J Bacteriol, 1999. **181**(16): p. 5126-30.
48. Hiniker, A. and J.C. Bardwell, *In vivo substrate specificity of periplasmic disulfide oxidoreductases.* J Biol Chem, 2004. **279**(13): p. 12967-73.
49. Stenson, T.H. and A.A. Weiss, *DsbA and DsbC are required for secretion of pertussis toxin by Bordetella pertussis.* Infect Immun, 2002. **70**(5): p. 2297-303.
50. Peek, J.A. and R.K. Taylor, *Characterization of a periplasmic thiol:disulfide interchange protein required for the functional maturation of secreted virulence factors of Vibrio cholerae.* Proc Natl Acad Sci U S A, 1992. **89**(13): p. 6210-4.
51. Wulfing, C. and R. Rappuoli, *Efficient production of heat-labile enterotoxin mutant proteins by overexpression of dsbA in a degP-deficient Escherichia coli strain.* Arch Microbiol, 1997. **167**(5): p. 280-3.
52. Foreman, D.T., et al., *TolC and DsbA are needed for the secretion of STB, a heat-stable enterotoxin of Escherichia coli.* Mol Microbiol, 1995. **18**(2): p. 237-45.
53. Agudo, D., et al., *A proteomic approach to study Salmonella typhi periplasmic proteins altered by a lack of the DsbA thiol: disulfide isomerase.* Proteomics, 2004. **4**(2): p. 355-63.
54. Raczko, A.M., et al., *Characterization of new DsbB-like thiol-oxidoreductases of Campylobacter jejuni and Helicobacter pylori and classification of the DsbB family based on phylogenomic, structural and functional criteria.* Microbiology, 2005. **151**(Pt 1): p. 219-31.
55. Barbieri, J.T. and J. Sun, *Pseudomonas aeruginosa ExoS and ExoT.* Rev Physiol Biochem Pharmacol, 2004. **152**: p. 79-92.
56. Ha, U.H., Y. Wang, and S. Jin, *DsbA of Pseudomonas aeruginosa is essential for multiple virulence factors.* Infect Immun, 2003. **71**(3): p. 1590-5.
57. Ireland, P.M., et al., *Disarming Burkholderia pseudomallei: structural and functional characterization of a disulfide oxidoreductase (DsbA) required for virulence in vivo.* Antioxid Redox Signal, 2014. **20**(4): p. 606-17.
58. Bardwell, J.C., K. McGovern, and J. Beckwith, *Identification of a protein required for disulfide bond formation in vivo.* Cell, 1991. **67**(3): p. 581-9.
59. Kadokura, H., F. Katzen, and J. Beckwith, *Protein disulfide bond formation in prokaryotes.* Annu Rev Biochem, 2003. **72**: p. 111-35.

60. Bader, M.W., et al., *Disulfide bonds are generated by quinone reduction.* J Biol Chem, 2000. **275**(34): p. 26082-8.
61. Kamitani, S., Y. Akiyama, and K. Ito, *Identification and characterization of an Escherichia coli gene required for the formation of correctly folded alkaline phosphatase, a periplasmic enzyme.* EMBO J, 1992. **11**(1): p. 57-62.
62. Martin, J.L., J.C. Bardwell, and J. Kuriyan, *Crystal structure of the DsbA protein required for disulphide bond formation in vivo.* Nature, 1993. **365**(6445): p. 464-8.
63. Guddat, L.W., et al., *The uncharged surface features surrounding the active site of Escherichia coli DsbA are conserved and are implicated in peptide binding.* Protein Sci, 1997. **6**(6): p. 1148-56.
64. Inaba, K., et al., *Crystal structure of the DsbB-DsbA complex reveals a mechanism of disulfide bond generation.* Cell, 2006. **127**(4): p. 789-801.
65. Rinaldi, F.C., A.N. Meza, and B.G. Guimaraes, *Structural and biochemical characterization of Xylella fastidiosa DsbA family members: new insights into the enzyme-substrate interaction.* Biochemistry, 2009. **48**(15): p. 3508-18.
66. Paxman, J.J., et al., *The structure of the bacterial oxidoreductase enzyme DsbA in complex with a peptide reveals a basis for substrate specificity in the catalytic cycle of DsbA enzymes.* J Biol Chem, 2009. **284**(26): p. 17835-45.
67. Jacob-Dubuisson, F., et al., *PapD chaperone function in pilus biogenesis depends on oxidant and chaperone-like activities of DsbA.* Proc Natl Acad Sci U S A, 1994. **91**(24): p. 11552-6.
68. Hennecke, J., C. Spleiss, and R. Glockshuber, *Influence of acidic residues and the kink in the active-site helix on the properties of the disulfide oxidoreductase DsbA.* J Biol Chem, 1997. **272**(1): p. 189-95.
69. Kortemme, T. and T.E. Creighton, *Ionisation of cysteine residues at the termini of model alpha-helical peptides. Relevance to unusual thiol pKa values in proteins of the thioredoxin family.* J. Mol. Biol., 1995. **253**(5): p. 799-812.
70. Zapun, A., J.C. Bardwell, and T.E. Creighton, *The reactive and destabilizing disulfide bond of DsbA, a protein required for protein disulfide bond formation in vivo.* Biochemistry, 1993. **32**(19): p. 5083-92.
71. Huber-Wunderlich, M. and R. Glockshuber, *A single dipeptide sequence modulates the redox properties of a whole enzyme family.* Fold Des, 1998. **3**(3): p. 161-71.
72. Dundas, J., et al., *CASTp: computed atlas of surface topography of proteins with structural and topographical mapping of functionally annotated residues.* Nucleic Acids Res, 2006. **34**(Web Server issue): p. W116-8.
73. Pymol, *The PyMOL Molecular Graphics System, Version 2.0 Schrödinger, LLC.*

74. Kurth, F., et al., *Comparative sequence, structure and redox analyses of Klebsiella pneumoniae DsbA show that anti-virulence target DsbA enzymes fall into distinct classes.* PLoS One, 2013. **8**(11): p. e80210.
75. Arts, I.S., et al., *Dissecting the machinery that introduces disulfide bonds in Pseudomonas aeruginosa.* MBio, 2013. **4**(6): p. e00912-13.
76. Walden, P.M., et al., *The 1.2 A resolution crystal structure of TcpG, the Vibrio cholerae DsbA disulfide-forming protein required for pilus and cholera-toxin production.* Acta Crystallogr D Biol Crystallogr, 2012. **68**(Pt 10): p. 1290-302.
77. Lafaye, C., et al., *Biochemical and structural study of the homologues of the thiol-disulfide oxidoreductase DsbA in Neisseria meningitidis.* J Mol Biol, 2009. **392**(4): p. 952-66.
78. Premkumar, L., et al., *Rv2969c, essential for optimal growth in Mycobacterium tuberculosis, is a DsbA-like enzyme that interacts with VKOR-derived peptides and has atypical features of DsbA-like disulfide oxidases.* Acta Crystallogr D Biol Crystallogr, 2013. **69**(Pt 10): p. 1981-94.
79. Crow, A., et al., *Crystal structure and biophysical properties of Bacillus subtilis BdbD. An oxidizing thiol:disulfide oxidoreductase containing a novel metal site.* J. Biol. Chem., 2009. **284**(35): p. 23719-23733.
80. Kurz, M., et al., *Structural and functional characterization of the oxidoreductase alpha-DsbA1 from Wolbachia pipientis.* Antioxid Redox Signal, 2009. **11**(7): p. 1485-500.
81. Wang, X., et al., *Membrane topology and mutational analysis of Mycobacterium tuberculosis VKOR, a protein involved in disulfide bond formation and a homologue of human vitamin K epoxide reductase.* Antioxid Redox Signal, 2011. **14**(8): p. 1413-20.
82. Kurth, F., et al., *Crystal structure of the dithiol oxidase DsbA enzyme from proteus mirabilis bound non-covalently to an active site peptide ligand.* J Biol Chem, 2014. **289**(28): p. 19810-22.
83. Premkumar, L., et al., *Structure of the Acinetobacter baumannii dithiol oxidase DsbA bound to elongation factor EF-Tu reveals a novel protein interaction site.* J Biol Chem, 2014. **289**(29): p. 19869-80.
84. Heras, B., et al., *Staphylococcus aureus DsbA does not have a destabilizing disulfide. A new paradigm for bacterial oxidative folding.* J Biol Chem, 2008. **283**(7): p. 4261-71.
85. Jurrus, E., et al., *Improvements to the APBS biomolecular solvation software suite.* Protein Sci, 2018. **27**(1): p. 112-128.
86. Huntley, J.F., et al., *Characterization of Francisella tularensis outer membrane proteins.* J Bacteriol, 2007. **189**(2): p. 561-74.

87. Wouters, M.A., R.A. George, and N.L. Haworth, *"Forbidden" disulfides: their role as redox switches.* Curr Protein Pept Sci, 2007. **8**(5): p. 484-95.

88. Chim, N., et al., *Structural and biochemical characterization of the essential DsbA-like disulfide bond forming protein from Mycobacterium tuberculosis.* BMC Struct Biol, 2013. **13**: p. 23.

89. Heras, B., et al., *DSB proteins and bacterial pathogenicity.* Nat Rev Microbiol, 2009. **7**(3): p. 215-25.

90. Dutton, R.J., et al., *Inhibition of bacterial disulfide bond formation by the anticoagulant warfarin.* Proc Natl Acad Sci U S A, 2010. **107**(1): p. 297-301.

91. Couprie, J., et al., *Investigation of the DsbA mechanism through the synthesis and analysis of an irreversible enzyme-ligand complex.* Biochemistry, 2000. **39**(22): p. 6732-42.

92. Kadokura, H. and J. Beckwith, *Mechanisms of oxidative protein folding in the bacterial cell envelope.* Antioxid Redox Signal, 2010. **13**(8): p. 1231-46.

93. Krogh, A., et al., *Predicting transmembrane protein topology with a hidden Markov model: application to complete genomes.* J Mol Biol, 2001. **305**(3): p. 567-80.

94. Sinha, S., P.R. Langford, and J.S. Kroll, *Functional diversity of three different DsbA proteins from Neisseria meningitidis.* Microbiology, 2004. **150**(Pt 9): p. 2993-3000.

95. Straskova, A., et al., *Proteome analysis of an attenuated Francisella tularensis dsbA mutant: identification of potential DsbA substrate proteins.* J Proteome Res, 2009. **8**(11): p. 5336-46.

96. McMahon, R.M., L. Premkumar, and J.L. Martin, *Four structural subclasses of the antivirulence drug target disulfide oxidoreductase DsbA provide a platform for design of subclass-specific inhibitors.* Biochim Biophys Acta, 2014. **1844**(8): p. 1391-401.

97. Zhang, Y. and J. Skolnick, *TM-align: a protein structure alignment algorithm based on the TM-score.* Nucleic Acids Res, 2005. **33**(7): p. 2302-9.

98. Missiakas, D., C. Georgopoulos, and S. Raina, *Identification and characterization of the Escherichia coli gene dsbB, whose product is involved in the formation of disulfide bonds in vivo.* Proc Natl Acad Sci U S A, 1993. **90**(15): p. 7084-8.

99. Jander, G., N.L. Martin, and J. Beckwith, *Two cysteines in each periplasmic domain of the membrane protein DsbB are required for its function in protein disulfide bond formation.* EMBO J, 1994. **13**(21): p. 5121-7.

100. Inaba, K. and K. Ito, *Paradoxical redox properties of DsbB and DsbA in the protein disulfide-introducing reaction cascade.* EMBO J, 2002. **21**(11): p. 2646-54.

101. Inaba, K., et al., *Dynamic nature of disulphide bond formation catalysts revealed by crystal structures of DsbB.* EMBO J, 2009. **28**(6): p. 779-91.

102. Zhou, Y., et al., *NMR solution structure of the integral membrane enzyme DsbB: functional insights into DsbB-catalyzed disulfide bond formation.* Mol Cell, 2008. **31**(6): p. 896-908.
103. Kadokura, H., et al., *Roles of a conserved arginine residue of DsbB in linking protein disulfide-bond-formation pathway to the respiratory chain of Escherichia coli.* Proc Natl Acad Sci U S A, 2000. **97**(20): p. 10884-9.
104. Inaba, K., et al., *Critical role of a thiolate-quinone charge transfer complex and its adduct form in de novo disulfide bond generation by DsbB.* Proc Natl Acad Sci U S A, 2006. **103**(2): p. 287-92.
105. Sievers, F., et al., *Fast, scalable generation of high-quality protein multiple sequence alignments using Clustal Omega.* Mol Syst Biol, 2011. **7**: p. 539.
106. Grimshaw, J.P., et al., *DsbL and DsbI form a specific dithiol oxidase system for periplasmic arylsulfate sulfotransferase in uropathogenic Escherichia coli.* J Mol Biol, 2008. **380**(4): p. 667-80.
107. Mac, T.T., et al., *Insight into disulfide bond catalysis in Chlamydia from the structure and function of DsbH, a novel oxidoreductase.* J Biol Chem, 2008. **283**(2): p. 824-32.
108. Walden, P.M., et al., *The alpha-proteobacteria Wolbachia pipientis protein disulfide machinery has a regulatory mechanism absent in gamma-proteobacteria.* PLoS One, 2013. **8**(11): p. e81440.
109. Kouwen, T.R., et al., *Thiol-disulphide oxidoreductase modules in the low-GC Gram-positive bacteria.* Mol Microbiol, 2007. **64**(4): p. 984-99.
110. Kang, M.S., et al., *Effect of Leuconostoc spp. on the formation of Streptococcus mutans biofilm.* J Microbiol, 2007. **45**(4): p. 291-6.
111. Adams, L.A., et al., *Application of fragment-based screening to the design of inhibitors of Escherichia coli DsbA.* Angew Chem Int Ed Engl, 2015. **54**(7): p. 2179-84.
112. Duprez, W., et al., *Peptide inhibitors of the Escherichia coli DsbA oxidative machinery essential for bacterial virulence.* J Med Chem, 2015. **58**(2): p. 577-87.
113. Fruh, V., et al., *Application of fragment-based drug discovery to membrane proteins: identification of ligands of the integral membrane enzyme DsbB.* Chem Biol, 2010. **17**(8): p. 881-91.
114. Halili, M.A., et al., *Small molecule inhibitors of disulfide bond formation by the bacterial DsbA-DsbB dual enzyme system.* ACS Chem Biol, 2015. **10**(4): p. 957-64.
115. Landeta, C., et al., *Compounds targeting disulfide bond forming enzyme DsbB of Gram-negative bacteria.* Nat Chem Biol, 2015. **11**(4): p. 292-8.
116. Numazaki, K., *Current problems of perinatal Chlamydia trachomatis infections.* J Immune Based Ther Vaccines, 2004. **2**(1): p. 4.

117. Resnikoff, S., et al., *Global data on visual impairment in the year 2002.* Bull World Health Organ, 2004. **82**(11): p. 844-51.
118. Thylefors, B., et al., *A simple system for the assessment of trachoma and its complications.* Bull World Health Organ, 1987. **65**(4): p. 477-83.
119. Hu, V.H., M.J. Holland, and M.J. Burton, *Trachoma: protective and pathogenic ocular immune responses to Chlamydia trachomatis.* PLoS Negl Trop Dis, 2013. **7**(2): p. e2020.
120. Witkin, S.S., et al., *Chlamydia trachomatis: the Persistent Pathogen.* Clin Vaccine Immunol, 2017. **24**(10).
121. Hatch, T.P., I. Allan, and J.H. Pearce, *Structural and polypeptide differences between envelopes of infective and reproductive life cycle forms of Chlamydia spp.* J Bacteriol, 1984. **157**(1): p. 13-20.
122. Hatch, T.P., M. Miceli, and J.A. Silverman, *Synthesis of protein in host-free reticulate bodies of Chlamydia psittaci and Chlamydia trachomatis.* J Bacteriol, 1985. **162**(3): p. 938-42.
123. Sun, G., et al., *Structural and functional analyses of the major outer membrane protein of Chlamydia trachomatis.* J Bacteriol, 2007. **189**(17): p. 6222-35.
124. Tanzer, R.J. and T.P. Hatch, *Characterization of outer membrane proteins in Chlamydia trachomatis LGV serovar L2.* J Bacteriol, 2001. **183**(8): p. 2686-90.
125. Su, H., et al., *Chlamydia trachomatis-host cell interactions: role of the chlamydial major outer membrane protein as an adhesin.* Infect Immun, 1990. **58**(4): p. 1017-25.
126. Caldwell, H.D., J. Kromhout, and J. Schachter, *Purification and partial characterization of the major outer membrane protein of Chlamydia trachomatis.* Infect Immun, 1981. **31**(3): p. 1161-76.
127. Birkelund, S., et al., *Analysis of proteins in Chlamydia trachomatis L2 outer membrane complex, COMC.* FEMS Immunol Med Microbiol, 2009. **55**(2): p. 187-95.
128. Vandahl, B.B., et al., *The expression, processing and localization of polymorphic membrane proteins in Chlamydia pneumoniae strain CWL029.* BMC Microbiol, 2002. **2**: p. 36.
129. Tan, C., et al., *Variable expression of surface-exposed polymorphic membrane proteins in in vitro-grown Chlamydia trachomatis.* Cell Microbiol, 2010. **12**(2): p. 174-87.
130. Liu, X., et al., *Identification of Chlamydia trachomatis outer membrane complex proteins by differential proteomics.* J Bacteriol, 2010. **192**(11): p. 2852-60.
131. Hackstadt, T., W.J. Todd, and H.D. Caldwell, *Disulfide-mediated interactions of the chlamydial major outer membrane protein: role in the differentiation of chlamydiae?* J Bacteriol, 1985. **161**(1): p. 25-31.
132. Hatch, T.P., *Disulfide cross-linked envelope proteins: the functional equivalent of peptidoglycan in chlamydiae?* J Bacteriol, 1996. **178**(1): p. 1-5.

133. Zhang, J.P. and R.S. Stephens, *Mechanism of C. trachomatis attachment to eukaryotic host cells.* Cell, 1992. **69**(5): p. 861-9.
134. Fechtner, T., et al., *Characterization of the interaction between the chlamydial adhesin OmcB and the human host cell.* J Bacteriol, 2013. **195**(23): p. 5323-33.
135. Fadel, S. and A. Eley, *Chlamydia trachomatis OmcB protein is a surface-exposed glycosaminoglycan-dependent adhesin.* J Med Microbiol, 2007. **56**(Pt 1): p. 15-22.
136. Su, H., et al., *A recombinant Chlamydia trachomatis major outer membrane protein binds to heparan sulfate receptors on epithelial cells.* Proc Natl Acad Sci U S A, 1996. **93**(20): p. 11143-8.
137. Su, H., et al., *Differential effect of trypsin on infectivity of Chlamydia trachomatis: loss of infectivity requires cleavage of major outer membrane protein variable domains II and IV*. Infect Immun, 1988. **56**(8): p. 2094-100.
138. Jiwani, S., et al., *Chlamydia trachomatis Tarp cooperates with the Arp2/3 complex to increase the rate of actin polymerization.* Biochem Biophys Res Commun, 2012. **420**(4): p. 816-21.
139. Mehlitz, A. and T. Rudel, *Modulation of host signaling and cellular responses by Chlamydia.* Cell Commun Signal, 2013. **11**: p. 90.
140. Clifton, D.R., et al., *A chlamydial type III translocated protein is tyrosine-phosphorylated at the site of entry and associated with recruitment of actin.* Proc Natl Acad Sci U S A, 2004. **101**(27): p. 10166-71.
141. Atanu, F.O., E. Oviedo-Orta, and K.A. Watson, *A novel transport mechanism for MOMP in Chlamydophila pneumoniae and its putative role in immune-therapy*. PLoS One, 2013. **8**(4): p. e61139.
142. Raulston, J.E., et al., *Surface accessibility of the 70-kilodalton Chlamydia trachomatis heat shock protein following reduction of outer membrane protein disulfide bonds.* Infect Immun, 2002. **70**(2): p. 535-43.
143. Hatch, T.P., M. Miceli, and J.E. Sublett, *Synthesis of disulfide-bonded outer membrane proteins during the developmental cycle of Chlamydia psittaci and Chlamydia trachomatis*. J Bacteriol, 1986. **165**(2): p. 379-85.
144. Betts-Hampikian, H.J. and K.A. Fields, *Disulfide bonding within components of the Chlamydia type III secretion apparatus correlates with development.* J Bacteriol, 2011. **193**(24): p. 6950-9.
145. Wang, X., et al., *Developmental stage oxidoreductive states of Chlamydia and infected host cells.* MBio, 2014. **5**(6): p. e01924.
146. Abdelrahman, Y.M. and R.J. Belland, *The chlamydial developmental cycle.* FEMS Microbiol Rev, 2005. **29**(5): p. 949-59.

147. Belland, R.J., et al., *Genomic transcriptional profiling of the developmental cycle of Chlamydia trachomatis.* Proc Natl Acad Sci U S A, 2003. **100**(14): p. 8478-83.
148. Newhall, W.J.t., *Biosynthesis and disulfide cross-linking of outer membrane components during the growth cycle of Chlamydia trachomatis.* Infect Immun, 1987. **55**(1): p. 162-8.
149. Nicholson, T.L., et al., *Global stage-specific gene regulation during the developmental cycle of Chlamydia trachomatis.* J Bacteriol, 2003. **185**(10): p. 3179-89.
150. Shaw, E.I., et al., *Three temporal classes of gene expression during the Chlamydia trachomatis developmental cycle.* Mol Microbiol, 2000. **37**(4): p. 913-25.
151. Cho, S.H., et al., *A New Family of Membrane Electron Transporters and Its Substrates, Including a New Cell Envelope Peroxiredoxin, Reveal a Broadened Reductive Capacity of the Oxidative Bacterial Cell Envelope.* mBio, 2012. **3**(2): p. e00291-11-e00291-11.
152. Mukhopadhyay, S., et al., *Identification of Chlamydia pneumoniae proteins in the transition from reticulate to elementary body formation.* Mol Cell Proteomics, 2006. **5**(12): p. 2311-8.
153. Beatty, W.L., G.I. Byrne, and R.P. Morrison, *Morphologic and antigenic characterization of interferon gamma-mediated persistent Chlamydia trachomatis infection in vitro.* Proc Natl Acad Sci U S A, 1993. **90**(9): p. 3998-4002.
154. Beatty, W.L., R.P. Morrison, and G.I. Byrne, *Immunoelectron-microscopic quantitation of differential levels of chlamydial proteins in a cell culture model of persistent Chlamydia trachomatis infection.* Infect Immun, 1994. **62**(9): p. 4059-62.
155. Chopra, I., et al., *Antibiotics, peptidoglycan synthesis and genomics: the chlamydial anomaly revisited.* Microbiology, 1998. **144 (Pt 10)**: p. 2673-8.
156. Hogan, R.J., et al., *Chlamydial persistence: beyond the biphasic paradigm.* Infect Immun, 2004. **72**(4): p. 1843-55.
157. Bavoil, P., A. Ohlin, and J. Schachter, *Role of disulfide bonding in outer membrane structure and permeability in Chlamydia trachomatis.* Infect Immun, 1984. **44**(2): p. 479-85.
158. Wyrick, P.B., *Chlamydia trachomatis persistence in vitro: an overview.* J Infect Dis, 2010. **201 Suppl 2**: p. S88-95.
159. Abromaitis, S. and R.S. Stephens, *Attachment and Entry of Chlamydia Have Distinct Requirements for Host Protein Disulfide Isomerase.* Plos Pathogens, 2009. **5**(4).
160. Conant, C.G. and R.S. Stephens, *Chlamydia attachment to mammalian cells requires protein disulfide isomerase.* Cell Microbiol, 2007. **9**(1): p. 222-32.
161. Lazarev, V.N., et al., *The role of intracellular glutathione in the progression of Chlamydia trachomatis infection.* Free Radic Biol Med, 2010. **49**(12): p. 1947-55.
162. Prevention, C.f.D.C.a., *Sexually Transmitted Diseases Treatment Guidelines.* Morbidity and Mortality Weekly report, 2015. **64**(3).

163. DeMars, R. and J. Weinfurter, *Interstrain gene transfer in Chlamydia trachomatis in vitro: mechanism and significance.* J Bacteriol, 2008. **190**(5): p. 1605-14.
164. Demars, R., et al., *Lateral gene transfer in vitro in the intracellular pathogen Chlamydia trachomatis.* J Bacteriol, 2007. **189**(3): p. 991-1003.
165. Suchland, R.J., et al., *Horizontal transfer of tetracycline resistance among Chlamydia spp. in vitro.* Antimicrob Agents Chemother, 2009. **53**(11): p. 4604-11.
166. Binet, R., et al., *Impact of azithromycin resistance mutations on the virulence and fitness of Chlamydia caviae in guinea pigs.* Antimicrob Agents Chemother, 2010. **54**(3): p. 1094-101.
167. Binet, R. and A.T. Maurelli, *Frequency of spontaneous mutations that confer antibiotic resistance in Chlamydia spp.* Antimicrob Agents Chemother, 2005. **49**(7): p. 2865-73.
168. Binet, R. and A.T. Maurelli, *Frequency of development and associated physiological cost of azithromycin resistance in Chlamydia psittaci 6BC and C. trachomatis L2.* Antimicrob Agents Chemother, 2007. **51**(12): p. 4267-75.
169. Dessus-Babus, S., et al., *Sequencing of gyrase and topoisomerase IV quinolone-resistance-determining regions of Chlamydia trachomatis and characterization of quinolone-resistant mutants obtained In vitro.* Antimicrob Agents Chemother, 1998. **42**(10): p. 2474-81.
170. Dreses-Werringloer, U., et al., *Detection of nucleotide variability in rpoB in both rifampin-sensitive and rifampin-resistant strains of Chlamydia trachomatis.* Antimicrob Agents Chemother, 2003. **47**(7): p. 2316-8.
171. Kutlin, A., et al., *Emergence of resistance to rifampin and rifalazil in Chlamydophila pneumoniae and Chlamydia trachomatis.* Antimicrob Agents Chemother, 2005. **49**(3): p. 903-7.
172. Morrissey, I., et al., *Serial passage of Chlamydia spp. in sub-inhibitory fluoroquinolone concentrations.* J Antimicrob Chemother, 2002. **49**(5): p. 757-61.
173. Suchland, R.J., et al., *Rifampin-resistant RNA polymerase mutants of Chlamydia trachomatis remain susceptible to the ansamycin rifalazil.* Antimicrob Agents Chemother, 2005. **49**(3): p. 1120-6.
174. Yokoi, S., et al., *Uncommon occurrence of fluoroquinolone resistance-associated alterations in GyrA and ParC in clinical strains of Chlamydia trachomatis.* J Infect Chemother, 2004. **10**(5): p. 262-7.
175. Jones, R.B., et al., *Partial characterization of Chlamydia trachomatis isolates resistant to multiple antibiotics.* J Infect Dis, 1990. **162**(6): p. 1309-15.
176. Mourad, A., et al., *Relative resistance to erythromycin in Chlamydia trachomatis.* Antimicrob Agents Chemother, 1980. **18**(5): p. 696-8.

177. Lefevre, J.C. and J.P. Lepargneur, *Comparative in vitro susceptibility of a tetracycline-resistant Chlamydia trachomatis strain isolated in Toulouse (France).* Sex Transm Dis, 1998. **25**(7): p. 350-2.
178. Misyurina, O.Y., et al., *Mutations in a 23S rRNA gene of Chlamydia trachomatis associated with resistance to macrolides.* Antimicrob Agents Chemother, 2004. **48**(4): p. 1347-9.
179. Somani, J., et al., *Multiple drug-resistant Chlamydia trachomatis associated with clinical treatment failure.* J Infect Dis, 2000. **181**(4): p. 1421-7.
180. Golden, M.R., *Expedited partner therapy for sexually transmitted diseases.* Clin Infect Dis, 2005. **41**(5): p. 630-3.
181. Sandoz, K.M. and D.D. Rockey, *Antibiotic resistance in Chlamydiae.* Future Microbiol, 2010. **5**(9): p. 1427-42.
182. Ondondo, B.O., et al., *Frequency and magnitude of Chlamydia trachomatis elementary body- and heat shock protein 60-stimulated interferon gamma responses in peripheral blood mononuclear cells and endometrial biopsy samples from women with high exposure to infection.* J Infect Dis, 2009. **199**(12): p. 1771-9.
183. Aiyar, A., et al., *Influence of the tryptophan-indole-IFNgamma axis on human genital Chlamydia trachomatis infection: role of vaginal co-infections.* Front Cell Infect Microbiol, 2014. **4**: p. 72.
184. Wyrick, P.B. and S.T. Knight, *Pre-exposure of infected human endometrial epithelial cells to penicillin in vitro renders Chlamydia trachomatis refractory to azithromycin.* J Antimicrob Chemother, 2004. **54**(1): p. 79-85.
185. Kutlin, A., P.M. Roblin, and M.R. Hammerschlag, *Effect of prolonged treatment with azithromycin, clarithromycin, or levofloxacin on Chlamydia pneumoniae in a continuous-infection Model.* Antimicrob Agents Chemother, 2002. **46**(2): p. 409-12.
186. Kutlin, A., P.M. Roblin, and M.R. Hammerschlag, *In vitro activities of azithromycin and ofloxacin against Chlamydia pneumoniae in a continuous-infection model.* Antimicrob Agents Chemother, 1999. **43**(9): p. 2268-72.
187. Donati, M., et al., *Chlamydia trachomatis serovar distribution and other concurrent sexually transmitted infections in heterosexual men with urethritis in Italy.* Eur J Clin Microbiol Infect Dis, 2009. **28**(5): p. 523-6.
188. Stamm, W.E., et al., *Chlamydia trachomatis urethral infections in men. Prevalence, risk factors, and clinical manifestations.* Ann Intern Med, 1984. **100**(1): p. 47-51.
189. Ravel, J., et al., *Vaginal microbiome of reproductive-age women.* Proc Natl Acad Sci U S A, 2011. **108 Suppl 1**: p. 4680-7.

190. Kaewsrichan, J., K. Peeyananjarassri, and J. Kongprasertkit, *Selection and identification of anaerobic lactobacilli producing inhibitory compounds against vaginal pathogens.* FEMS Immunol Med Microbiol, 2006. **48**(1): p. 75-83.
191. Nardini, P., et al., *Lactobacillus crispatus inhibits the infectivity of Chlamydia trachomatis elementary bodies, in vitro study.* Sci Rep, 2016. **6**: p. 29024.
192. Wunderlich, M., R. Jaenicke, and R. Glockshuber, *The redox properties of protein disulfide isomerase (DsbA) of Escherichia coli result from a tense conformation of its oxidized form.* J Mol Biol, 1993. **233**(4): p. 559-66.
193. Newman, L., et al., *Global Estimates of the Prevalence and Incidence of Four Curable Sexually Transmitted Infections in 2012 Based on Systematic Review and Global Reporting.* PLoS One, 2015. **10**(12): p. e0143304.
194. Haggerty, C.L., et al., *Risk of sequelae after Chlamydia trachomatis genital infection in women.* J Infect Dis, 2010. **201 Suppl 2**: p. S134-55.
195. Shouldice, S.R., et al., *Structure and function of DsbA, a key bacterial oxidative folding catalyst.* Antioxid Redox Signal, 2011. **14**(9): p. 1729-60.
196. Tusnady, G.E. and I. Simon, *Principles governing amino acid composition of integral membrane proteins: application to topology prediction.* J Mol Biol, 1998. **283**(2): p. 489-506.
197. Tusnady, G.E. and I. Simon, *The HMMTOP transmembrane topology prediction server.* Bioinformatics, 2001. **17**(9): p. 849-50.
198. Nugent, T. and D.T. Jones, *Transmembrane protein topology prediction using support vector machines.* BMC Bioinformatics, 2009. **10**: p. 159.
199. Studier, F.W., *Protein production by auto-induction in high-density shaking cultures.* Protein Expression and Purification, 2005. **41**(1): p. 207-234.
200. Evans, J.C. and G.L. Ellman, *The ionization of cysteine.* Biochim Biophys Acta, 1959. **33**(2): p. 574-6.
201. Holmgren, A., *Thioredoxin catalyzes the reduction of insulin disulfides by dithiothreitol and dihydrolipoamide.* J Biol Chem, 1979. **254**(19): p. 9627-32.
202. Lee, K., et al., *De novo designed peptidic redox potential probe: linking sensitized emission to disulfide bond formation.* J Am Chem Soc, 2004. **126**(42): p. 13616-7.
203. Vivian, J.P., et al., *Structure and function of the oxidoreductase DsbA1 from Neisseria meningitidis.* J Mol Biol, 2009. **394**(5): p. 931-43.
204. Guzman, L.M., et al., *Tight regulation, modulation, and high-level expression by vectors containing the arabinose PBAD promoter.* J Bacteriol, 1995. **177**(14): p. 4121-30.
205. Vonrhein, C., et al., *Data processing and analysis with the autoPROC toolbox.* Acta Crystallogr. D Biol. Crystallogr., 2011. **67**(Pt 4): p. 293-302.

206. Kabsch, W., *XDS.* Acta Crystallogr. D Biol. Crystallogr., 2010. **66**(Pt 2): p. 125-132.
207. Evans, P., *Scaling and assessment of data quality.* Acta Crystallogr. D Biol. Crystallogr., 2006. **62**(Pt 1): p. 72-82.
208. Afonine, P.V., et al., *Towards automated crystallographic structure refinement with phenix.refine.* Acta Crystallogr. D Biol. Crystallogr., 2012. **68**(Pt 4): p. 352-367.
209. Emsley, P. and K. Cowtan, *Coot: model-building tools for molecular graphics.* Acta Crystallographica Section D: Biological …, 2004.
210. Chen, V.B., et al., *MolProbity: all-atom structure validation for macromolecular crystallography.* Acta Crystallogr. D Biol. Crystallogr., 2010. **66**(Pt 1): p. 12-21.
211. Dailey, F.E. and H.C. Berg, *Mutants in disulfide bond formation that disrupt flagellar assembly in Escherichia coli.* Proc Natl Acad Sci U S A, 1993. **90**(3): p. 1043-7.
212. Chivers, P.T., K.E. Prehoda, and R.T. Raines, *The CXXC motif: a rheostat in the active site.* Biochemistry, 1997. **36**(14): p. 4061-4066.
213. Quan, S., et al., *The CXXC motif is more than a redox rheostat.* J. Biol. Chem., 2007. **282**(39): p. 28823-28833.
214. Holm, L. and P. Rosenstrom, *Dali server: conservation mapping in 3D.* Nucleic Acids Res, 2010. **38**(Web Server issue): p. W545-9.
215. Lin, T.Y. and P.S. Kim, *Urea dependence of thiol-disulfide equilibria in thioredoxin: confirmation of the linkage relationship and a sensitive assay for structure.* Biochemistry, 1989. **28**(12): p. 5282-5287.
216. Krause, G., et al., *Mimicking the active site of protein disulfide-isomerase by substitution of proline 34 in Escherichia coli thioredoxin.* J. Biol. Chem., 1991. **266**(15): p. 9494-9500.
217. Robert, X. and P. Gouet, *Deciphering key features in protein structures with the new ENDscript server.* Nucleic Acids Res, 2014. **42**(Web Server issue): p. W320-4.
218. Guddat, L.W., J.C. Bardwell, and J.L. Martin, *Crystal structures of reduced and oxidized DsbA: investigation of domain motion and thiolate stabilization.* Structure, 1998. **6**(6): p. 757-767.
219. Ruddock, L.W., T.R. Hirst, and R.B. Freedman, *pH-dependence of the dithiol-oxidizing activity of DsbA (a periplasmic protein thiol:disulphide oxidoreductase) and protein disulphide-isomerase: studies with a novel simple peptide substrate.* Biochem J, 1996. **315 (Pt 3)**: p. 1001-5.
220. Drozdetskiy, A., et al., *JPred4: a protein secondary structure prediction server.* Nucleic Acids Res, 2015. **43**(W1): p. W389-94.
221. McMahon, R.M., et al., *Virulence of the Melioidosis Pathogen Burkholderia pseudomallei Requires the Oxidoreductase Membrane Protein DsbB.* Infect Immun, 2018. **86**(5).

222. Kobayashi, T., et al., *Respiratory chain is required to maintain oxidized states of the DsbA-DsbB disulfide bond formation system in aerobically growing Escherichia coli cells.* Proc Natl Acad Sci U S A, 1997. **94**(22): p. 11857-62.
223. Lehrer, S.S., *Fluorescence and absorption studies of the binding of copper and iron to transferrin.* J Biol Chem, 1969. **244**(13): p. 3613-7.
224. Carepo, M.S., et al., *Mo-Cu metal cluster formation and binding in an orange protein isolated from Desulfovibrio gigas.* J Biol Inorg Chem, 2014. **19**(4-5): p. 605-14.
225. Koropatkin, N., et al., *The structure of the iron-binding protein, FutA1, from Synechocystis 6803.* J Biol Chem, 2007. **282**(37): p. 27468-77.
226. Regeimbal, J., et al., *Disulfide bond formation involves a quinhydrone-type charge-transfer complex.* Proc Natl Acad Sci U S A, 2003. **100**(24): p. 13779-84.
227. Collins, M.D. and D. Jones, *Distribution of isoprenoid quinone structural types in bacteria and their taxonomic implication.* Microbiol Rev, 1981. **45**(2): p. 316-54.
228. Okada, K., et al., *Biological significance of the side chain length of ubiquinone in Saccharomyces cerevisiae.* FEBS Lett, 1998. **431**(2): p. 241-4.
229. Soballe, B. and R.K. Poole, *Requirement for ubiquinone downstream of cytochrome(s) b in the oxygen-terminated respiratory chains of Escherichia coli K-12 revealed using a null mutant allele of ubiCA.* Microbiology, 1998. **144 (Pt 2)**: p. 361-73.
230. Takahashi, Y.H., K. Inaba, and K. Ito, *Characterization of the menaquinone-dependent disulfide bond formation pathway of Escherichia coli.* J Biol Chem, 2004. **279**(45): p. 47057-65.
231. Fontaine, E., F. Ichas, and P. Bernardi, *A ubiquinone-binding site regulates the mitochondrial permeability transition pore.* J Biol Chem, 1998. **273**(40): p. 25734-40.
232. Edlund, C., et al., *Ubiquinone-10 protects neurons from virus-induced degeneration.* J Neurochem, 1994. **63**(2): p. 634-9.
233. Stephens, R.S., et al., *Genome sequence of an obligate intracellular pathogen of humans: Chlamydia trachomatis.* Science, 1998. **282**(5389): p. 754-9.
234. Barta, M.L., et al., *Structural and biochemical characterization of Chlamydia trachomatis hypothetical protein CT263 supports that menaquinone synthesis occurs through the futalosine pathway.* J Biol Chem, 2014. **289**(46): p. 32214-29.
235. Guddat, L.W., et al., *Structural analysis of three His32 mutants of DsbA: support for an electrostatic role of His32 in DsbA stability.* Protein Sci, 1997. **6**(9): p. 1893-900.
236. Otzen, D.E., *Protein unfolding in detergents: effect of micelle structure, ionic strength, pH, and temperature.* Biophys J, 2002. **83**(4): p. 2219-30.

237. Nielsen, M.M., et al., *Unfolding of beta-sheet proteins in SDS.* Biophys J, 2007. **92**(10): p. 3674-85.

238. Booth, P.J., et al., *Intermediates in the folding of the membrane protein bacteriorhodopsin.* Nat Struct Biol, 1995. **2**(2): p. 139-43.

239. Dong, M., et al., *Complete removal and exchange of sodium dodecyl sulfate bound to soluble and membrane proteins and restoration of their activities, using ceramic hydroxyapatite chromatography.* Anal Biochem, 1997. **247**(2): p. 333-41.

240. Lund, S., et al., *Detergent structure and associated lipid as determinants in the stabilization of solubilized Ca2+-ATPase from sarcoplasmic reticulum.* J Biol Chem, 1989. **264**(9): p. 4907-15.

241. VanAken, T., et al., *Alkyl glycoside detergents: synthesis and applications to the study of membrane proteins.* Methods Enzymol, 1986. **125**: p. 27-35.

242. Fleming, K.G., A.L. Ackerman, and D.M. Engelman, *The effect of point mutations on the free energy of transmembrane alpha-helix dimerization.* J Mol Biol, 1997. **272**(2): p. 266-75.

243. Riske, K.A., et al., *Biophysical approaches in the study of biomembrane solubilization: quantitative assessment and the role of lateral inhomogeneity.* Biophys Rev, 2017. **9**(5): p. 649-667.

244. Seddon, A.M., P. Curnow, and P.J. Booth, *Membrane proteins, lipids and detergents: not just a soap opera.* Biochim Biophys Acta, 2004. **1666**(1-2): p. 105-17.

245. Esmann, M., J.C. Skou, and C. Christiansen, *Solubilization and molecular weight determination of the (Na+ + K+)-ATPase from rectal glands of Squalus acanthias.* Biochim Biophys Acta, 1979. **567**(2): p. 410-20.

246. Esmann, M. and J.C. Skou, *Kinetic properties of C12E8-solubilized (Na+ + K+)-ATPase.* Biochim Biophys Acta, 1984. **787**(1): p. 71-80.

247. Zhang, H., et al., *A defined protein-detergent-lipid complex for crystallization of integral membrane proteins: The cytochrome b6f complex of oxygenic photosynthesis.* Proc Natl Acad Sci U S A, 2003. **100**(9): p. 5160-3.

248. Dijkman, P.M. and A. Watts, *Lipid modulation of early G protein-coupled receptor signalling events.* Biochim Biophys Acta, 2015. **1848**(11 Pt A): p. 2889-97.

249. Yao, J., et al., *Chlamydia trachomatis Relies on Autonomous Phospholipid Synthesis for Membrane Biogenesis.* J Biol Chem, 2015. **290**(31): p. 18874-88.

250. Hackstadt, T., et al., *Chlamydia trachomatis interrupts an exocytic pathway to acquire endogenously synthesized sphingomyelin in transit from the Golgi apparatus to the plasma membrane.* EMBO J, 1996. **15**(5): p. 964-77.

251. Hackstadt, T., M.A. Scidmore, and D.D. Rockey, *Lipid metabolism in Chlamydia trachomatis-infected cells: directed trafficking of Golgi-derived sphingolipids to the chlamydial inclusion.* Proc Natl Acad Sci U S A, 1995. **92**(11): p. 4877-81.
252. Hatch, G.M. and G. McClarty, *Phospholipid composition of purified Chlamydia trachomatis mimics that of the eucaryotic host cell.* Infect Immun, 1998. **66**(8): p. 3727-35.
253. Wylie, J.L., G.M. Hatch, and G. McClarty, *Host cell phospholipids are trafficked to and then modified by Chlamydia trachomatis.* J Bacteriol, 1997. **179**(23): p. 7233-42.
254. Carabeo, R.A., D.J. Mead, and T. Hackstadt, *Golgi-dependent transport of cholesterol to the Chlamydia trachomatis inclusion.* Proc Natl Acad Sci U S A, 2003. **100**(11): p. 6771-6.
255. Elwell, C.A., et al., *Chlamydia trachomatis co-opts GBF1 and CERT to acquire host sphingomyelin for distinct roles during intracellular development.* PLoS Pathog, 2011. **7**(9): p. e1002198.
256. Soupene, E., D. Wang, and F.A. Kuypers, *Remodeling of host phosphatidylcholine by Chlamydia acyltransferase is regulated by acyl-CoA binding protein ACBD6 associated with lipid droplets.* Microbiologyopen, 2015.
257. Denisov, I.G. and S.G. Sligar, *Nanodiscs for structural and functional studies of membrane proteins.* Nat Struct Mol Biol, 2016. **23**(6): p. 481-6.
258. Bayburt, T.H. and S.G. Sligar, *Membrane protein assembly into Nanodiscs.* FEBS Lett, 2010. **584**(9): p. 1721-7.
259. Abreu, I.C., et al., *Hypercholesterolemic diet induces hepatic steatosis and alterations in mRNA expression of NADPH oxidase in rat livers.* Arq Bras Endocrinol Metabol, 2014. **58**(3): p. 251-9.
260. Vogel, H. and C.W. Wheat, *Accessing the transcriptome: how to normalize mRNA pools.* Methods Mol Biol, 2011. **772**: p. 105-28.
261. Heuer, D., et al., *Tackling the intractable - approaching the genetics of Chlamydiales.* Int J Med Microbiol, 2007. **297**(7-8): p. 569-76.
262. Tam, J.E., C.H. Davis, and P.B. Wyrick, *Expression of recombinant DNA introduced into Chlamydia trachomatis by electroporation.* Can J Microbiol, 1994. **40**(7): p. 583-91.
263. Binet, R. and A.T. Maurelli, *Transformation and isolation of allelic exchange mutants of Chlamydia psittaci using recombinant DNA introduced by electroporation.* Proc Natl Acad Sci U S A, 2009. **106**(1): p. 292-7.
264. Gong, S., et al., *Characterization of Chlamydia trachomatis plasmid-encoded open reading frames.* J Bacteriol, 2013. **195**(17): p. 3819-26.
265. Bauler, L.D. and T. Hackstadt, *Expression and targeting of secreted proteins from Chlamydia trachomatis.* J Bacteriol, 2014. **196**(7): p. 1325-34.

266. Agaisse, H. and I. Derre, *A C. trachomatis cloning vector and the generation of C. trachomatis strains expressing fluorescent proteins under the control of a C. trachomatis promoter.* PLoS One, 2013. **8**(2): p. e57090.

267. Johnson, C.M. and D.J. Fisher, *Site-specific, insertional inactivation of incA in Chlamydia trachomatis using a group II intron.* PLoS One, 2013. **8**(12): p. e83989.

268. Nguyen, B.D. and R.H. Valdivia, *Virulence determinants in the obligate intracellular pathogen Chlamydia trachomatis revealed by forward genetic approaches.* Proc Natl Acad Sci U S A, 2012. **109**(4): p. 1263-8.

269. Tippin, B., P. Pham, and M.F. Goodman, *Error-prone replication for better or worse.* Trends Microbiol, 2004. **12**(6): p. 288-95.

270. Kokes, M., et al., *Integrating chemical mutagenesis and whole-genome sequencing as a platform for forward and reverse genetic analysis of Chlamydia.* Cell Host Microbe, 2015. **17**(5): p. 716-25.

271. Kari, L., et al., *Generation of targeted Chlamydia trachomatis null mutants.* Proc Natl Acad Sci U S A, 2011. **108**(17): p. 7189-93.

272. Sega, G.A., *A review of the genetic effects of ethyl methanesulfonate.* Mutat Res, 1984. **134**(2-3): p. 113-42.

273. Till, B.J., et al., *Mismatch cleavage by single-strand specific nucleases.* Nucleic Acids Res, 2004. **32**(8): p. 2632-41.

274. Huston, W.M., et al., *The temperature activated HtrA protease from pathogen Chlamydia trachomatis acts as both a chaperone and protease at 37 degrees C.* FEBS Lett, 2007. **581**(18): p. 3382-6.

275. Huston, W.M., et al., *Expression and characterisation of a major c-type cytochrome encoded by gene kustc0563 from Kuenenia stuttgartiensis as a recombinant protein in Escherichia coli.* Protein Expr Purif, 2007. **51**(1): p. 28-33.

276. Huston, W.M., et al., *Chlamydia trachomatis responds to heat shock, penicillin induced persistence, and IFN-gamma persistence by altering levels of the extracytoplasmic stress response protease HtrA.* BMC Microbiol, 2008. **8**: p. 190.

277. Ong, V.A., *Determination of the effect of JO146, a CtHtrA inhibitor, on the chlamydial developmental cycle and persistence*, in *Queensland University of Technology*. 2015.

278. Cousins, M.M., D. Donnell, and S.H. Eshleman, *Impact of mutation type and amplicon characteristics on genetic diversity measures generated using a high-resolution melting diversity assay.* J Mol Diagn, 2013. **15**(1): p. 130-7.

279. Schirmer, M., et al., *Illumina error profiles: resolving fine-scale variation in metagenomic sequencing data.* BMC Bioinformatics, 2016. **17**: p. 125.

280. Laehnemann, D., A. Borkhardt, and A.C. McHardy, *Denoising DNA deep sequencing data-high-throughput sequencing errors and their correction.* Brief Bioinform, 2016. **17**(1): p. 154-79.

281. Ouellette, S.P., *Feasibility of a Conditional Knockout System for Chlamydia Based on CRISPR Interference.* Front Cell Infect Microbiol, 2018. **8**: p. 59.

282. Ize, B., V. Viarre, and R. Voulhoux, *Cell fractionation.* Methods Mol Biol, 2014. **1149**: p. 185-91.

283. Tinsley, C.R., et al., *Three homologues, including two membrane-bound proteins, of the disulfide oxidoreductase DsbA in Neisseria meningitidis: effects on bacterial growth and biogenesis of functional type IV pili.* J Biol Chem, 2004. **279**(26): p. 27078-87.

284. Allan, I., T.P. Hatch, and J.H. Pearce, *Influence of cysteine deprivation on chlamydial differentiation from reproductive to infective life-cycle forms.* J Gen Microbiol, 1985. **131**(12): p. 3171-7.

285. Davey, L., et al., *Functional analysis of paralogous thiol-disulfide oxidoreductases in Streptococcus gordonii.* J Biol Chem, 2013. **288**(23): p. 16416-29.

286. Franchi, L., et al., *NLRC4-driven production of IL-1beta discriminates between pathogenic and commensal bacteria and promotes host intestinal defense.* Nat Immunol, 2012. **13**(5): p. 449-56.

287. Lebeer, S., J. Vanderleyden, and S.C. De Keersmaecker, *Host interactions of probiotic bacterial surface molecules: comparison with commensals and pathogens.* Nat Rev Microbiol, 2010. **8**(3): p. 171-84.

288. Nelson, J.W. and T.E. Creighton, *Reactivity and ionization of the active site cysteine residues of DsbA, a protein required for disulfide bond formation in vivo.* Biochemistry, 1994. **33**(19): p. 5974-83.

289. Hamman, J.H., P.H. Demana, and E.I. Olivier, *Targeting receptors, transporters and site of absorption to improve oral drug delivery.* Drug Target Insights, 2007. **2**: p. 71-81.

290. Zhang, H., et al., *Identification of a strong and specific antichlamydial N-acylhydrazone.* PLoS One, 2017. **12**(10): p. e0185783.

291. Hybiske, K., *Expanding the Molecular Toolkit for Chlamydia.* Cell Host Microbe, 2015. **18**(1): p. 11-3.

292. Grauschopf, U., et al., *Why is DsbA such an oxidizing disulfide catalyst?* Cell, 1995. **83**(6): p. 947-55.

293. Feher, V.A., et al., *A 3-dimensional trimeric beta-barrel model for Chlamydia MOMP contains conserved and novel elements of Gram-negative bacterial porins.* PLoS One, 2013. **8**(7): p. e68934.

294. Motohashi, K., et al., *Comprehensive survey of proteins targeted by chloroplast thioredoxin.* Proc Natl Acad Sci U S A, 2001. **98**(20): p. 11224-9.

295. Denoncin, K., et al., *The protein-disulfide isomerase DsbC cooperates with SurA and DsbA in the assembly of the essential beta-barrel protein LptD.* J Biol Chem, 2010. **285**(38): p. 29425-33.